VOLUME 38 JUNE 1960 NUMBER 6

Canadian Journal of Physics

Published by THE NATIONAL RESEARCH COUNCIL

OTTAWA CANADA

CANADIAN JOURNAL OF PHYSICS

Under the authority of the Chairman of the Committee of the Privy Council on Scientific and Industrial Research, the National Research Council issues THE CANADIAN JOURNAL OF PHYSICS and five other journals devoted to the publication, in English or French, of the results of original scientific research. Matters of general policy concerning these journals are the responsibility of a joint Editorial Board consisting of: members representing the National Research Council of Canada; the Editors of the Journals; and members representing the Royal Society of Canada and four other scientific societies.

Manuscripts for publication should be submitted to Dr. H. E. Duckworth, Editor, Canadian Journal of Physics, Hamilton College, McMaster University, Hamilton, Ontario.
For instructions on preparation of copy, see **NOTES TO CONTRIBUTORS** (back cover).

Proof, correspondence concerning proof, and orders for reprints should be sent to the Manager, Editorial Office (Research Journals), Division of Administration and Awards, National Research Council, Ottawa 2, Canada.

Subscriptions, renewals, requests for single or back numbers, and all remittances should be sent to Division of Administration and Awards, National Research Council, Ottawa 2, Canada. Remittances should be made payable to the Receiver General of Canada, credit National Research Council.

The journals published, frequency of publication, and subscription prices are:

Canadian Journal of Biochemistry and Physiology	Monthly	$9.00 a year
Canadian Journal of Botany	Bimonthly	$6.00 a year
Canadian Journal of Chemistry	Monthly	$12.00 a year
Canadian Journal of Microbiology	Bimonthly	$6.00 a year
Canadian Journal of Physics	Monthly	$9.00 a year
Canadian Journal of Zoology	Bimonthly	$5.00 a year

The price of regular single numbers of all journals is $2.00.

CORRECTIONS

Volume 35, 1957

Page 572. In equation (6), "$+2(a_1+a_2)\{-a_1(a_1+a_2)\}^{-\frac{1}{2}}Ht \sin \chi$" should read "$+2(a_1+a_2)\{-a_1(a_1+1)\}^{-\frac{1}{2}}Ht \sin \chi$".

Volume 38, 1960

Page 332. In line 15 up "(Wilson, Rose, and Pomerantz 1959)" should read "(Wilson, Rose, and Pomerantz 1960)".

Page 333. In line 8 up "Wilson, B. G., Rose, D. C., and Pomerantz, M. A. 1959. Can. J. Phys. **38**, 328." should read "Wilson, B. G., Rose, D. C., and Pomerantz, M. A. 1960. Can. J. Phys. **38**, 328."

Canadian Journal of Physics

Issued by THE NATIONAL RESEARCH COUNCIL OF CANADA

VOLUME 38 JUNE 1960 NUMBER 6

SPECTROSCOPIC TEMPERATURE MEASUREMENTS IN A SHOCK TUBE USING CN AS A THERMOMETRIC MOLECULE[1]

W. H. PARKINSON[2] AND R. W. NICHOLLS[3]

ABSTRACT

Rotational intensity measurements on the CN spectrum, excited through shock excitation of a powdered mixture of NH_4Cl, KNO_2, and C by helium-driven shock waves in argon have been used to infer "rotational temperatures" of the gas between 6350° K and 8750° K. The measured values agree well with gas kinetic temperatures inferred from simple gas dynamic theory and shock-wave velocity measurements.

INTRODUCTION

Temperature is a parameter of great importance in gas dynamics, particularly in the study of transient luminous phenomena associated with shock waves. It therefore became necessary to determine, spectroscopically if possible, the temperature of the luminous gas behind the reflected shock wave during a series of experiments upon shock excitation of powdered solids (Nicholls 1959; Parkinson and Nicholls 1959*a*, *b*; Nicholls and Parkinson 1957, 1958; Nicholls, Parkinson, and Van der Laan 1959; Nicholls, Watson, and Parkinson 1959).

Spectroscopic temperature measurements using line reversal methods (Clouston, Gaydon, and Glass 1958; Clouston, Gaydon, and Hurle 1959) have been employed with success by some workers for temperatures up to about 3600° K. In the work described below, rotational temperatures (in the range 6000–9000° K) of CN radicals introduced into the reflected shock wave in argon have been measured (Parkinson and Nicholls 1959*b*; Nicholls 1959) and compared with gas kinetic temperatures inferred, by means of one-dimensional theory (Glass 1958), from initial pressures, temperatures, and gas composition on either side of the diaphragm and also from velocity measurements. The gas behind the reflected rather than the incident shock wave was studied because of the limitations in the bursting strength of the high pressure section of the tube.

[1]Manuscript received January 11, 1960.
Contribution from the Molecular Excitation Group, Department of Physics, University of Western Ontario, London, Ont.
[2]Now at Department of Chemical Technology, Imperial College, London, S.W.7, England.
[3]Temporarily on leave of absence at the National Bureau of Standards, Washington, D.C.

METHOD

It is well known (Johnson 1949; Herzberg 1950; Gaydon and Wolfhard 1953) that the intensity distribution $I_{J'J''}$ of lines in a molecular band is given by

$$I_{J'J''} = C\,\lambda^{-4}_{J'J''} S_{J'} N_{v'J'} \tag{1}$$

and further that if a Boltzmann energy distribution exists in the rotational energy levels of the molecules, i.e.

$$N_{v'J'} = N_{v'}/Q_{\text{rot}} \exp\,(-E_{\text{rot}}/kT_{\text{rot}}) \tag{2}$$

then

$$I_{J'J''} = C/Q_{\text{rot}}\,\lambda^{-4}_{J'J''} N_{v'} S_{J'} \exp\,(-E_{\text{rot}}/kT_{\text{rot}}). \tag{3}$$

The notation is conventional and defined in the above references. The Boltzmann energy distribution in rotational levels implies that thermal equilibrium exists between translational and rotational degrees of freedom.

From equation (3) it is seen that a plot of $\log I\,\lambda^4/S$ versus E_{rot} for lines of a band should lead to a straight line of slope $1/kT_{\text{rot}}$ if thermal equilibrium obtains. The rotational temperature T_{rot} may thereby be measured from intensity distributions within bands. The bands should preferably be of simple, well-resolved structure such as of the CN violet ($B^2\Sigma^+ — X^2\Sigma^-$) system.

In an attempt to introduce CN into the hot gas of the reflected shock wave, a series of survey experiments involving shock excitation of powdered metallic cyanides and other CN containing compounds were first performed (Parkinson and Nicholls 1959*a*). In all cases the CN violet system was easily excited, as were the C_2 Swan bands, and an underlying carbon-particle blackbody continuum which prevented accurate intensity measurement of the CN lines. Shock excitation of solids appears to ablate atoms (Nicholls 1959) which recombine into diatomic molecules if the environment is cool enough. This suggests that the carbon-particle continuum and C_2 bands can then be reduced, relative to CN bands, by reducing the C:N ratio in the gas. This was successfully achieved by shock-exciting a solid mixture which gave rise to a hot luminous gas containing C and N with a small C:N ratio. After a series of trials with various molar proportions the mixture $NH_4Cl + KNO_2 + 1/20$ C was found to behave very satisfactorily in producing CN bands, a few C_2 bands, and no carbon-particle continuum.

EXPERIMENTAL

The powdered mixture was made into a paste with acetone and painted on the center of a mylar membrane. After evaporation of the acetone, the membrane, coated with dry powder, was clamped near the window end of the shock tube (Parkinson and Nicholls 1959*a*) with the powder towards the window so as to intercept the reflected shock wave. It had previously been established that the luminosity from shock excitation of mylar involved only the *D* lines of sodium at 5893 Å, and the 4227-Å line of calcium. Spectra were recorded upon Kodak Royal Pan film using an ARL *f*/3.5 Raman spectrograph with a reciprocal dispersion of 12 Å/mm at 4200 Å and a free spectral range of 4000 Å – 6500 Å.

The response curve of the emulsion was obtained by using a calibrated step wedge mounted at the spectrograph slit. Homochromatic photometry was sufficient for the CN violet (0,1) band at λ 4216 Å which only extends over about 17 Å. The relative intensities of 15 of the best resolved lines ($J' = 45$–59 inclusive) of the P branch of the band were measured at incident Mach numbers of 5.7, 5.9, and 6.3. Adequate spectra could not be photographed below Mach 5.7 with one exposure, as band intensities decrease significantly with decrease in Mach number.

RESULTS

Plots of log $I\lambda^4/S$ vs. $J(J+1)$ yielded straight lines in each case. A rotational temperature could be inferred from the slope of each line. The plots and best "least squares" lines are shown respectively in Figs. 1*a*, 1*b*, 1*c*. In Table I,

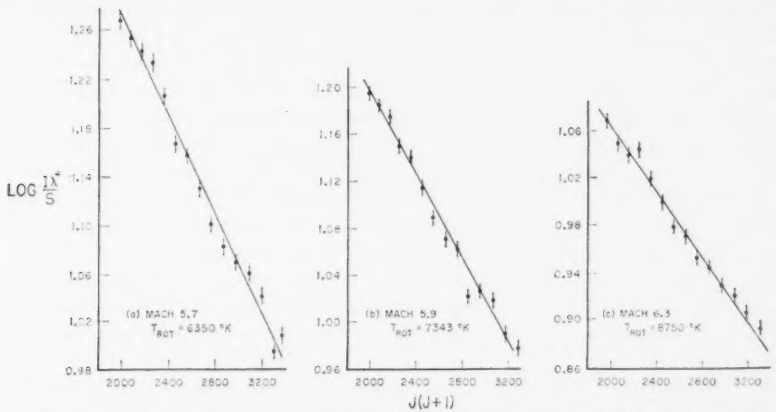

FIG. 1. Plots of log $I\lambda^4/S$ versus $J(J+1)$ of P-branch lines of the CN violet (0,1)λ 4216-Å band produced by shock excitation of KNO_2+NH_4Cl + 1/20 C in argon.

the inferred rotational temperature is compared with a gas kinetic temperature derived from one-dimensional shock wave theory (Glass 1958) and the initial conditions of pressure temperature and gas composition on each side of the membrane prior to initiation of the shock wave for a number of typical cases.

TABLE I

Comparison between measured rotational temperature and calculated gas kinetic temperature

Mach number	Calculated gas kinetic temperature, °K	Measured rotational temperature, °K	
6.3	9000	8750 8300	±5%
5.9	8200	7340 6850 6800	±5%
5.7	7650	6350	±5%

DISCUSSION

It will be noticed in Table I that the measured rotational temperatures are 10–15% lower than the ideal calculated temperatures based on one-dimensional theory and the assumption of a perfect gas. This is consistent with the results of other experiments (Parkinson and Nicholls 1959*a*) in which shock-wave velocities were measured while making time-resolved spectroscopic studies of MgO. The measured velocities were about 5% lower than the calculated velocities, which was equivalent to about a 10% reduction in the effective gas kinetic temperature below that predicted by one-dimensional perfect gas theory. Thus the measured rotational temperature is probably a reasonable measure of the actual translational temperature of the real gas of the reflected shock wave.

It is well known that a most prevalent source of error in measurement of rotational temperature is self-absorption. This can be especially significant when the source is at high pressures ($\sim$ 100 p.s.i.a. as is the gas behind the reflected shock wave). The effect of self-absorption on the semilogarithmic plots is to reduce the slope of the straight lines, which gives rise to a higher apparent temperature. Thus the obtaining of a straight line in the conventional semilogarithmic plots such as Fig. 1 does not necessarily imply that self-absorption is absent (Marr 1957). However, the isointensity method of spectroscopic temperature measurement of Knauss and McCay (1939) treats pairs of band lines of equal intensity and is therefore independent of self-absorption artifacts. This method was used to obtain estimates of rotational temperature for several pairs of *P*-branch lines in each case, and the temperatures obtained agreed well with those given in Table I derived from the slopes. Thus self-absorption did not appear to play a significant role in affecting our measurements.

It is therefore apparent that, under suitable conditions, the CN molecule is a good spectroscopic thermometer for indication of the transient temperature of the hot luminous gas behind reflected shock waves in argon over the approximate temperature range of 6000° K to 9000° K. Cooling of the luminous gas by ablation from the powder particles was probably minimized and compensated for by the exothermic nature of the KNO_2 and NH_4Cl mixture used.

While this paper was in preparation, a recent paper by Sobolev *et al.* (1959) became available. They describe attempts to measure temperatures of shock waves in air spectroscopically by: (*a*) comparison of relative intensities of lines of sodium (and also of potassium) excited by shock excitation following dusting of the shock tube walls with the respective chlorides, (*b*) measurement of spectral intensity distributions in CN violet bands excited when dicyanogen $(CN)_2$ was introduced into the shock-excited air.

In the experiments with alkali metal lines, which also require a knowledge of appropriate oscillator strengths, poor agreement between measured excitation temperatures and theoretically predicted gas kinetic temperatures was attributed to self-absorption effects, and they conclude that the method is

not useful for studying the "state of the air behind a shock wave". They also point out that agreement between their spectroscopic rotational temperatures from CN line intensities and gas kinetic temperatures inferred from velocity measurements was not good. They attribute this to the effects of finite vibrational relaxation times required to dissociate $(CN)_2$ into 2CN and to equilibrate it with the hot gas.

Evidently, in our experiments, the exothermic nature of $NH_4Cl + KNO_2$ together with the most likely formation of CN from an atomic gas (Parkinson and Nicholls 1959; Nicholls, Watson, and Parkinson 1959) make the experimental environment more favorable for spectroscopic temperature measurement of the hot argon with which the CN was mixed.

REFERENCES

CLOUSTON, J. G., GAYDON, A. G., and GLASS, I. I. 1958. Proc. Roy. Soc. A, **248**, 429.

CLOUSTON, J. G., GAYDON, A. G., and HURLE, I. R. 1959. Proc. Roy. Soc. A, **252**, 143.

GAYDON, A. G. and WOLFHARD, H. G. 1953. Flames, their structure, radiation and temperature (Chapman & Hall, Ltd., London).

GLASS, I. I. 1958. University of Toronto Institute of Aerophysics Review, No. 12, Part 1.

HERZBERG, G. 1950. Spectra of diatomic molecules (D. Van Nostrand Co., Inc., New York).

JOHNSON, R. C. 1949. An introduction to molecular spectra (Methuen & Co., Ltd., London).

KNAUSS, H. D. and MCCAY, N. S. 1939. Phys. Rev. **52**, 1147.

MARR, G. V. 1957. Can. J. Phys. **35**, 1270.

NICHOLLS, R. W. 1959. J. Roy. Astron. Soc. Can. **53**, 109.

NICHOLLS, R. W. and PARKINSON, W. H. 1957. J. Chem. Phys. **26**, 423.

——— 1958. Can. J. Phys. **36**, 625.

NICHOLLS, R. W., PARKINSON, W. H., and VAN DER LAAN, H. 1959. J. Appl. Phys. **30**, 797.

NICHOLLS, R. W., WATSON, M. D., and PARKINSON, W. H. 1959. J. Roy. Astron. Soc. Can. **53**, 223.

PARKINSON, W. H. and NICHOLLS, R. W. 1959*a*. Shock tube spectroscopy I. Scientific Report No. 1, Contract AF 19(604)-4560, Department of Physics, University of Western Ontario.

——— 1959*b*. Shock tube spectroscopy II. Scientific Report No. 3, Contract AF 19(604)-4560, Department of Physics, University of Western Ontario.

SOBOLEV, N. N., POTAPOV, A. V., KITAEVA, V. F., FAIZULLOV, F. S., ALIAMOVSKII, V. N., ANTROPOV, E. T., and ISAEF, I. L. 1959. Optika i Spektroskopiya (Optics and Spectroscopy, Optical Society of America, translation **3**, 185).

A COMPTON-ELECTRON γ-SPECTROMETER WITH TWO-DIRECTIONAL FOCUSING[1]

G. E. LEE-WHITING

ABSTRACT

Improvements in the design of one type of Compton-electron spectrometer for γ-rays are proposed. The design requires a magnetic field of cylindrical symmetry and of slow radial variation, a simply curved radiator, and a system of apertures. Electrons are accepted only if they are ejected from the radiator with small components of momentum in two orthogonal directions perpendicular to the incident γ-ray. Since the magnetic field can also be used to measure the momentum of the selected electrons, the instrument can function as a γ-ray spectrometer. Higher-order aberrations are discussed, and a method of calculating the values of the various spectrometer parameters corresponding to maximum efficiency is given. Calculations of the intrinsic line-width, caused by the motion of the electron within the atom before collision with the photon, are carried out.

1. INTRODUCTION

Consider a parallel beam of finite cross section of monoenergetic γ-rays incident upon a thin sheet of some light material such as cellophane. Measurement both of the energy of an electron which has been set in motion by Compton scattering and of its angle of ejection with respect to the γ-beam enables one to calculate the energy of the incident photon. An apparatus which selects the electrons recoiling in a particular direction and measures their energies will thus serve as a γ-ray spectrometer. In the sort of device to be considered in this paper the electrons ejected in the forward direction are utilized; their momenta are measured in a β-spectrometer of the type in which the electron motion is predominantly perpendicular to the magnetic field, i.e. the "flat" type of Siegbahn (1955, Chap. III).

As an example of the class of instrument to be discussed, let us take the spectrometer described by Groshev *et al.* (1956). A well-collimated beam of neutron-capture γ-rays from an extended source in a reactor is incident upon a curved sheet of polystyrene (to be called the radiator) marked R in Fig. 1. The magnetic field of the β-spectrometer is axially symmetric about a perpendicular raised at O, and has mirror symmetry in the plane of the figure; the field in this plane is perpendicular to it. Within the circle of radius r_0 the magnetic field is uniform. The radiator, which lies entirely in the uniform field, is so shaped that forward Compton electrons produced by photons of the correct energy will move in circular orbits which pass through the focus F_1, after turning through approximately 90°. After passing F_1 the electrons, now outside the circle of radius r_0, are in a region where the field falls off radially in such a manner as to produce an improved radial focus at F_2, 180° beyond F_1. Though Groshev *et al.* do not say so, the field is presumably shaped in accordance with the theory of Beiduk and Konopinski (1948); in this case there is also a small amount of axial focusing outside the circle of

[1]Manuscript received January 7, 1960.
Contribution from the Theoretical Physics Branch, Chalk River, Ontario.
Issued as A.E.C.L. No. 1002.

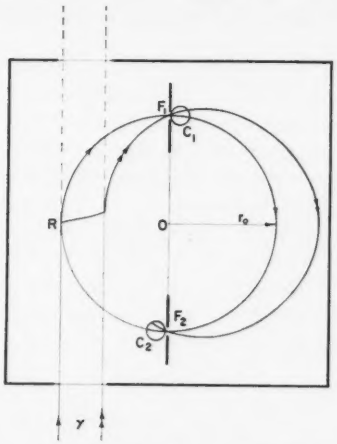

FIG. 1. Sketch showing the principle of the type of instrument used by Groshev *et al.* (1956). The thin radiator, R, lies in the uniform field region within the circle of radius r_0. The orbits of electrons ejected by the extreme rays of the well-collimated γ-beam are labelled with one or two arrow-heads.

radius r_0. It should be clear that the combination of curved radiator and two slits selects those electrons of the desired energy having initially a zero component of momentum in the direction perpendicular to the γ-beam and in the plane of the figure. The only limitation placed upon the component of initial momentum perpendicular to this plane results from the finite heights of the radiator and of the slits at F_1 and F_2. In order to reduce the background, coincidences are recorded between the counters C_1 and C_2 placed behind the slits at F_1 and F_2 respectively.

The principle of the extended radiator used by Groshev *et al.* was first suggested by Dzhelepov and Orbeli (1948), and was employed in the design of the "ritron" (see Dzhelepov *et al.* 1954). A discussion of the use of a curved radiator in a uniform magnetic field has been given by Dzhelepov (1951).

Great improvement was effected in the performance of β-spectrometers of the "flat" type when it was realized that radially varying magnetic fields could be used and that the focus need not be at 180° (see Siegbahn (1955, Chap. III) for discussion and references). The improvement resulted from a first-order focus in the axial direction, allowing the use of shorter detectors, and from higher-order focusing in the radial direction, producing a sharper line at a given transmission. Can one obtain similar benefits with a spectrometer of the general type illustrated by Fig. 1 by permitting the use of an inhomogeneous magnetic field and by allowing the designer to choose the relative positions of the radiator and slits? It turns out, as we shall show in Section 2, that with this extra freedom one can arrange to select electrons with zero initial momentum in the axial direction; the length of detector needed is also decreased. It is also possible to employ higher-order radial focusing to sharpen the spectral line of the instrument.

Before going into the detailed discussion of the various components of the line-width of a Compton spectrometer, as we do in Section 4, it is desirable to have some estimate of the intrinsic width caused by the motion of the electrons within the target atoms before the scattering takes place. In Section 3 calculations of this effect are presented; they are more complete than those which have already been given by Dzhelepov (1955). A few observations on the shape of the pole pieces of an iron-cored magnet designed to produce the required field are made in Section 5.

In discussing the Compton process we shall take formulae from the Chapter by Davisson in Seigbahn's handbook (1955). Energies will be measured in units of m_0c^2, momenta in units of m_0c, m_0 being the electron's rest mass. Let α be the energy of the photon and let E be the *kinetic* energy of an electron recoiling in the forward direction. Then

$$E = 2\alpha^2(2\alpha+1)^{-1}. \tag{1}$$

Now since the relative half-width of the momentum line of a β-spectrometer is independent of the momentum, it is usually more convenient to work with momentum instead of energy. If p is the momentum of a forward recoiling electron, then

$$p = 2\alpha(\alpha+1)(2\alpha+1)^{-1}. \tag{2}$$

It will also be useful to have an expression for the cross section per target electron for the ejection of a Compton electron per unit solid angle in the forward direction, viz.

$$[d\sigma/d\Omega]_0 = r_c^2 S(\alpha), \tag{3a}$$

$$S(\alpha) = 4(\alpha+1)^2(2\alpha^2+2\alpha+1)(2\alpha+1)^{-3}; \tag{3b}$$

here $r_c^2 \doteqdot 7.94\times10^{-26}$ cm^2 is the square of the classical radius of the electron. Note that although the total cross section for Compton scattering decreases as the photon energy is increased, the differential cross section in the forward direction increases sharply. As α is increased from 2 to 20, $d\sigma/d\Omega$ rises from 2.97×10^{-25} to 17.1×10^{-25} cm^2. Thus, for energies at which the half-angle of the cone of electrons accepted by a Compton spectrometer is small compared to the width of the forward lobe of the differential cross section, the efficiency of the instrument will improve as the photon energy is increased.

Although it is customary to quote the relative half-width of the line profile plotted against electron momentum as a measure of the resolution of a Compton spectrometer, the quantity which is relevant to the resolving of γ-rays is the relative half-width of the line profile plotted against the corresponding photon energy. By differentiation of (2) we obtain

$$\Delta\alpha/\alpha \doteqdot U(\alpha)\Delta p/p \tag{4a}$$

$$U(\alpha) = (\alpha+1)(2\alpha+1)(2\alpha^2+2\alpha+1)^{-1}. \tag{4b}$$

The function $U(\alpha)$ falls monotonically from 1.2 to 1 as α is increased from 1 to ∞. Hence we may use the electron momentum resolution instead of the photon energy resolution and not be seriously misled.

2. PRINCIPLES OF FOCUSING

The general arrangement of the spectrometer under consideration in this section, shown in Fig. 2, is very similar to that of Fig. 1. The magnetic field

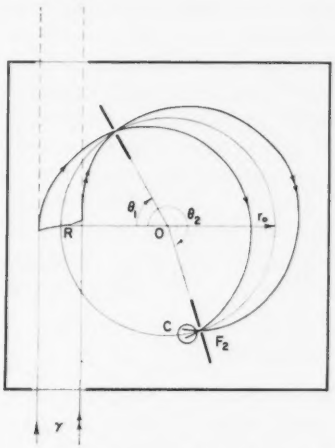

FIG. 2. Sketch of the instrument discussed in this paper. The radiator lies astride the optic circle. The magnetic field varies radially in all regions.

is axially symmetric about the perpendicular erected at O, and has mirror symmetry in the plane of the page. The two slits at F_1 and F_2 are situated on a circle (to be called the optic circle) of radius r_0, centered at O, and lying in the plane of symmetry. In describing the position of an electron it is convenient to use the radial and axial departures from the optic circle, expressed in units of r_0:

$$\eta = (r-r_0)/r_0, \qquad \tau = Z/r_0. \tag{5}$$

The third co-ordinate will be the angle θ, as in cylindrical co-ordinates, measured in a clockwise sense from the line OR.

As is well known, the properties of the magnetic field in the neighborhood of the optic circle are completely determined by the radial variation of the magnetic field in the plane of symmetry; thus the coefficients a_n in the expansion

$$H_Z(r,0) = H_0 \sum_{n=0}^{\infty} a_n \eta^n \tag{6}$$

specify the field. A full discussion of the expansion parameters of the field components and of a method of calculating the electron orbits is given by Lee-Whiting and Taylor (1957).

In Fig. 2 a well-collimated beam of γ-rays is incident upon a radiator placed roughly symmetrically astride the optic circle. The beam of forward-ejected electrons is to be brought to a first radial focus at F_1 for $\theta = \theta_1$, and

to a second focus at F_2, for $\theta = \theta_2$. The symmetric arrangement of the radiator gives the minimum aberration at F_2 (and hence the sharpest line) for a given width of radiator. In discussing the general principles of focusing, as we do in this section, it is permissible to imagine perfectly parallel γ-beams and slits of zero width. The effects of finite slit-widths on resolution are discussed in Section 4.

The first problem is to show how to design the radiator surface to ensure that particles of the desired momentum pass through the slit at F_1. Since it would be extremely difficult to construct a rigid warped surface out of thin cellophane, the radiator is assumed to be a portion of the right cylinder erected on the curve in the plane of symmetry. The calculation is performed only for those photons incident in the plane of symmetry. Estimates of the aberrations caused by this approximation are made in Section 4.

Let us assume that $\eta = f(\theta)$ describes an orbit passing through F_1, and let P (see Fig. 3) be a point on this orbit. If ψ is the angle between the tangent

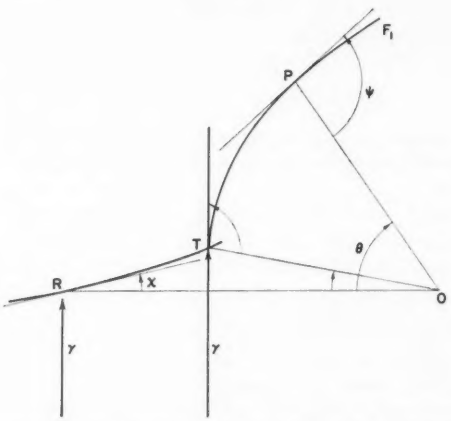

FIG. 3. Illustration of the angles involved in the derivation of the equation of the radiator surface, RT; P is a general point on the orbit TPF_1.

to the orbit at P and the line PO, the condition that the tangent be parallel to the incident γ-direction is

$$\psi - \theta = \tfrac{1}{2}\pi. \tag{7}$$

Now from elementary geometry we have

$$\begin{aligned} \tan(\psi - \tfrac{1}{2}\pi) &= r^{-1}\,dr/d\theta \\ &= (1+\eta)^{-1}\,d\eta/d\theta. \end{aligned} \tag{8}$$

Thus the θ co-ordinate of the point T common to the orbit TPF_1 and the radiator RT may be found by solving the equation

$$\tan\theta = [1+f(\theta)]^{-1}\,df(\theta)/d\theta; \tag{9a}$$

the η co-ordinate may be obtained, of course, from

$$\eta = f(\theta). \tag{9b}$$

Now let us consider a one-parameter family of orbits passing through F_1; for the parameter it is convenient to take the maximum departure of the orbit in question from the optic circle, H. Then, replacing $f(\theta)$ by $g(\theta,H)$, we obtain a parametrization of the required radiator curve from the equations (9).

A good first approximation to the radiator shape may be obtained by using the first-order solutions of the orbit equation. By adapting (1*a*) of Lee-Whiting (1957) we find

$$\eta = g(\theta,H) \equiv H \sin [\omega_1(\theta-\theta_1)], \tag{10a}$$

$$\omega_1 = (1+a_1)^{\frac{1}{2}}; \tag{10b}$$

(see Fig. 2 for the definition of θ_1.) The resulting radiator curve is easily shown to be

$$\eta = -\{1+\omega_1 \cot\theta \cot [\omega_1(\theta_1-\theta)]\}^{-1}. \tag{11}$$

In practical cases the arc of the curve defined by (11) is nearly a straight line. The position of this line can be specified by giving the value of the angle, χ, between the tangent to the curve at R and the radius OR.

$$\cot\chi = -\left[\frac{d\eta}{d\theta}\right]_{\theta=0} = -\lim_{\theta\to 0} \eta/\theta = \omega_1^{-1} \tan(\omega_1\theta_1). \tag{12}$$

Calculations of the radiator shape can, of course, be carried out using orbit equations of a higher order of approximation, though a formula as simple as (11) should not be expected. The second-order term which should be added to the η of (10*a*) can be calculated by the methods used by Lee-Whiting (1957); it is

$$\{[\tfrac{1}{2}-\tfrac{1}{8}(1+a_1)^{-1}(2a_2+5a_1+3)][1-\cos\omega_1(\theta-\theta_1)] + \tfrac{1}{8}(1+a_1)^{-1}(2a_2+5a_1+3)\sin^2\omega_1(\theta-\theta_1)\}H^2. \tag{10c}$$

Calculation of the radiator shape for a line source is considered briefly in an Appendix.

Having got the electrons as far as the slit F_1 we may now think of the second focus as F_2. The condition for the first-order radial focus at F_2 of electrons emitted by a point source at F_1 is well known; in the present notation it is

$$\omega_1(\theta_2-\theta_1) = \pi. \tag{13}$$

The two radial foci have been arranged at the cost of only one constraint, equation (13), on the three disposable parameters θ_1, θ_2, and a_1. We may thus approach the question of focusing in the axial direction with the knowledge that there is still considerable freedom available. In the $\pi\sqrt{2}$ spectrometer particles emitted from one point in the source at different angles to the plane of symmetry pass through one point (in the first approximation) of the exit slit. This is the opposite of the behavior required in a Compton

spectrometer. Here we wish to select only those orbits which are initially parallel to the plane of symmetry. If the axial variation in the $\pi\sqrt{2}$ spectrometer is described as "half-wave", that required for the Compton spectrometer is "quarter-wave". Note also that the selection of orbits should be independent of the axial co-ordinate of the point of ejection in the radiator.

For the moment we shall treat only those points in the radiator lying upon the generator erected upon the optic circle; the defocusing for other radiator points will be treated as an aberration in Section 4. In the first order the orbits under consideration lie on the cylinder containing the optic circle. From Lee-Whiting (1957) one obtains

$$\tau = T \sin(\omega_2\theta) + t \cos(\omega_2\theta) \tag{14a}$$

$$\omega_2 = (-a_1)^{\frac{1}{2}} \tag{14b}$$

for this case; t is the value of τ at the point of ejection, T is proportional to the initial slope of the orbit. To bring about the desired selection of orbits one should satisfy the equation

$$\omega_2\theta_2 = \tfrac{1}{2}\pi, \tag{15}$$

and place an aperture of infinitesimal height, as well as width, at F_2. Then only those orbits for which T is zero pass through the final aperture, and, furthermore, the value of t does not affect the selection. Sketches of the development of the cylinder containing the orbits are given in Fig. 4.

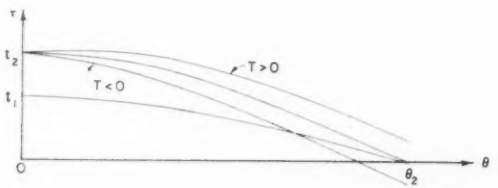

FIG. 4. Development showing orbits originating from points on the central generator of the radiator. Electrons ejected horizontally at different heights, i.e. t_1 and t_2, pass through F_2, where $\theta = \theta_2$. Electrons ejected at an angle to the plane of symmetry, i.e. with $T \neq 0$, do not pass through F_2.

Remembering that both ω_1 and ω_2 are functions of a_1 alone, we see that the desired two-directional focusing imposes two constraints, (13) and (15), on the three disposable parameters θ_1, θ_2, and a_1. One can find values of θ_1 and θ_2 satisfying (13) and (15) for a range of values of a_1 from the equations

$$\theta_1 = \pi[\tfrac{1}{2}(-a_1)^{-\frac{1}{2}} - (1+a_1)^{-\frac{1}{2}}] \tag{16}$$

and

$$\theta_2 = \tfrac{1}{2}\pi(-a_1)^{-\frac{1}{2}}. \tag{17}$$

Clearly we must have $-1 < a_1 < 0$ to get real values for the angles. If θ_1 is to be greater than zero we must have $-1/5 < a_1$; if θ_2 is to be less than 2π we must have $a_1 < -1/16$. For $a_1 = -1/10$ one finds that $\omega_1\theta_1$ is equal to

$\frac{1}{2}\pi$, and one gets the greatest radiator width for a given maximum radial departure from the optic circle. When $|a_1|$ is decreased below 1/10, θ_2 approaches 2π and the detector is too near the γ-beam. There can be little point in using values of $|a_1|$ less than 1/10. Curves of θ_1 and θ_2, as well as of χ, for the useful range of a_1 are given in Fig. 5.

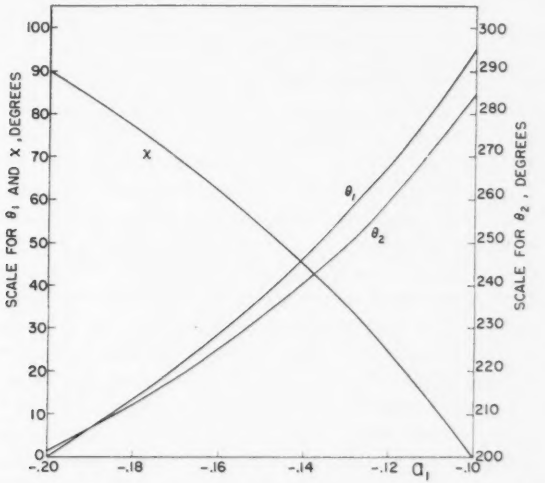

FIG. 5. Graphs of θ_1, θ_2, and χ versus a_1 for a Compton spectrometer with two-directional focusing.

For the $\pi\sqrt{2}$ β-spectrometer the two-directional first-order focusing requires the fixing of the parameter a_1, leaving but one degree of freedom, a_2, to be used in eliminating second-order aberrations. In the present case, however, we approach the question of second-order focusing with two free parameters, a_1 and a_2.

Formulae for the important second-order aberrations may be adapted from the work of Lee-Whiting (1957). Since in that paper the symbols t and T refer to the value and slope of the orbit at the source of the β-spectrometer, i.e. at F_1, we must replace them by t_1 and T_1 respectively, where

$$t_1 = t\cos\omega_2\theta_1 + T\sin\omega_2\theta_1 \tag{18a}$$

and

$$T_1 = -t\sin\omega_2\theta_1 + T\cos\omega_2\theta_1. \tag{18b}$$

Note that $\omega_2\theta_1 = \frac{1}{2}\pi - A$, if $A = [-a_1(1+a_1)^{-1}]^{\frac{1}{2}}\pi$. Thus, after some simplification, one finds:

$$\eta(\theta_2) = C_1H^2 + C_2t^2 + C_3T^2 + C_4Tt + \ldots \tag{19}$$

$$C_1 = -(1+a_1)^{-1}(1+7a_1/3+4a_2/3) \tag{20a}$$

$$C_2 = (1+a_1)^{-1}(a_1+\mu a_2) \tag{20b}$$

$$C_3 = (1+a_1)^{-1}[a_1+(2-\mu)a_2] \tag{20c}$$

$$C_4 = a_2(1+5a_1)^{-1}\sin 2A, \tag{20d}$$

$$\mu = (1+5a_1)^{-1}[(1+a_1)\sin^2 A+4a_1], \tag{21}$$

$$\tau(\theta_2) = T+B_1Ht+B_2HT+\ldots \tag{22}$$

$$B_1 = 2(-a_1)^{-\frac{1}{2}}(1+a_1)^{\frac{1}{2}}C_2 \tag{23a}$$

$$B_2 = (-a_1)^{-\frac{1}{2}}(1+a_1)^{\frac{1}{2}}C_4. \tag{23b}$$

The terms depending upon the width of the slit at F_1 have been omitted, since this width should be small enough to be of importance in the first order only.

Our next task is to try to choose the four C_i of (19) in such a way as to minimize the total second-order radial aberration. There is no point in eliminating the term C_3T^2, since, as we shall see in Section 4, a larger term proportional to T^2 arises from the dependence of the electron energy on angle of ejection. It is possible to choose a value of a_2, for any value of a_1 in the range -0.2 to -0.1, in such a way as to make any one of C_1, C_2, or C_4 zero. For no value of a_1 in the specified range, however, can one make more than one of the three coefficients vanish. If one arranges to have C_1 equal to zero, then (since H occurs only in the first term), a larger value of H, and hence a wider radiator, can be used. In principle one could continue to cancel the coefficients of higher and higher powers of H in $\eta(\theta_2)$, increasing the permissible width of the radiator at each stage. A theoretical limit on the degree of useful cancellation arises when terms such as Ht^2, HT^2, and HtT become appreciable. Let us assume that the first $(n-1)$ powers of H in $\eta(\theta_2)$ have zero coefficients; if H is small enough that the power series is rapidly convergent, then the only H-dependent term that must be retained in $\eta(\theta_2)$ is CH^n.

In the case of the β-spectrometer it was possible, by arranging to cancel either of two coefficients, to have a wide-aperture or a high-aperture instrument (Lee-Whiting and Taylor 1957). For the Compton spectrometer, as we have just seen, the wide-radiator type of instrument corresponds to the choice $C_1 = 0$; the high-radiator type, which would require the simultaneous vanishing of both C_2 and C_4, is not possible.

Returning to the wide-radiator spectrometer, we see that the condition that C_1 should be zero enables us to calculate a_2, C_2, C_3, and C_4 for a given value of a_1. Curves of the numerical values so calculated for a_1 in the range -0.2 to -0.1 are given in Fig. 6.

Since it has been decided to design the spectrometer in such a way that the coefficients of the second-order term in H is zero, a knowledge of the H-dependent third-order aberrations is useful. The most important of these terms, C_5H^3, has been evaluated:

$$C_5 = -2^{-4}\pi(1+a_1)^{-1}[6a_3+2a_2-7a_1-3+3(1+a_1)^2-20/3 \times\{(1+a_1)^{-1}(a_1+a_2)\}^2]. \tag{24}$$

Though it might not be possible to design the pole pieces to produce a desired value of a_3, it is still useful to be able to estimate the size of this aberration.

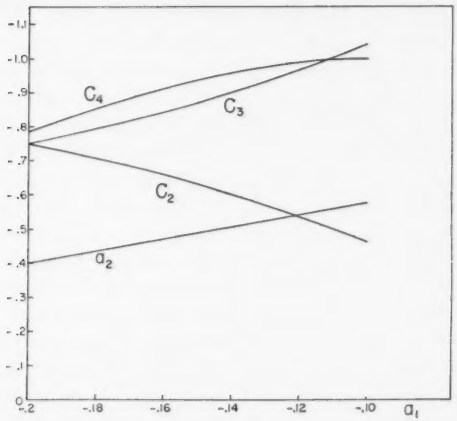

FIG. 6. Graphs of a_2, C_2, C_3, and C_4 against a_1 for a "wide-radiator" spectrometer.

In the Compton-electron spectrometers which have been built to study γ-rays the resolution achieved (2.5% to 5%) has not been good enough to make the failure to restrict the axial momentum of the electrons selected an important source of line broadening. If Compton spectrometers are to compete with other types of instrument, however, an improvement of the resolution by an order of magnitude is desirable. At such resolutions the improved form of focusing becomes almost a necessity.

For resolutions of the order of 0.3% it will not always be possible to use a counter behind the first slit, because of the energy loss and change of direction caused by multiple scattering in the counter windows. A counter could probably be constructed to give a tolerable spread for the electrons ejected by photons of energy 1 Mev, though the deterioration of the axial focusing caused by the change of electron direction of motion might be serious. Because the amount of multiple scattering decreases rapidly as the energy is increased, there should be no difficulty at photon energies greater than 2 or 3 Mev. When the two-counter mode of operation cannot be used, however, one of the great advantages of the Compton spectrometer, its low background counting rate, is in danger of being lost. An alternative method of minimizing the background which might be effective is to use a counter telescope behind the final aperture of the system. Since, in the first-order theory of orbits, the desired electrons are focused at a point at the exit aperture of the spectrometer we are discussing, the size of this aperture will be relatively small. The smaller exit aperture admits fewer stray electrons and permits the use of a smaller detector, which would be less affected by environmental background. The background can certainly be much decreased by recording coincidences between the selected electrons and the backscattered photons (Motz 1956; Motz *et al.* 1959), but the counting rate will be reduced appreciably.

3. INTRINSIC LINE-WIDTH

In the previous sections we have assumed that the electrons taking part in the Compton scattering are initially at rest; in this case all electrons ejected in the forward direction have precisely the same value of energy or momentum. When one takes into account the motion of the electron within the target atom before the collision, the sharp spectral line is replaced by one of finite width. This intrinsic width is, of course, the minimum width attainable with any Compton spectrometer using that particular material in the radiator.

The idea that the atomic motion of the electrons could cause a broadening of the energy line of the scattered photons was first suggested by Jauncey (1925), who performed his calculation using the classical Bohr orbits. Wave-mechanical calculations of this same effect were carried out and compared with experiment by Du Mond (1933). Dzhelepov (1955) calculated the width of the energy line of forward recoiling electrons for two values of the energy of the incident photon. The purpose of the present computation is to extend the range of photon energies, and to examine the effect of using better atomic wave functions.

For the case of electrons scattered in the forward direction the conservation equations are much simpler than those of the general case treated by Du Mond. Let us work, for the moment, with the electrons in one atomic shell, and let Δ be their binding energy in units of m_0c^2. The conservation of energy yields the equation

$$\alpha+1-\Delta = \alpha'+1+E; \tag{25}$$

here α and α' are the photon energies before and after scattering and E is again the kinetic energy of the ejected electron. Let the magnitude of the linear momentum vector of the electron before the collision be q (in units of m_0c), and let the angle between this vector and the direction of the incident photon be ω. Then conservation of momentum gives

$$\alpha+q\cos\omega = \alpha'\cos\theta+p \tag{26a}$$

$$q\sin\omega = \alpha'\sin\theta; \tag{26b}$$

here p is the momentum of the electron after collision (entirely in the direction of the incident γ-ray), and θ is the angle of scattering of the photon. The equations (25) and (26) determine the quantities α', θ, and p as functions of the parameters q, ω, α, and Δ.

The distribution of values of q can be calculated with the aid of quantum mechanics. Following Dzhelepov we select nitrogen as a suitable "average" cellulose atom. It will be assumed that the system consists of an isolated atom; the effects of molecular binding should be considerably smaller than those of atomic binding. For each atomic orbital we shall assume a spatial wave function of the form

$$\psi_{nl}^{m}(\mathbf{r}) = R_{nl}(r)\,Y_l^m(\theta,\phi). \tag{27}$$

The corresponding momentum wave function is

$$\phi_{nl}^{m}(\mathbf{q}) = (2\pi\alpha_0)^{-3/2} \int e^{-i\alpha_0^{-1}\mathbf{q}\cdot\mathbf{r}} \psi_{nl}^{m}(\mathbf{r})\, d\mathbf{r}, \tag{28}$$

if it assumed that the unit of length is the first Bohr radius; α_0 is the fine-structure constant. Now the quantity

$$\Phi_{nl}(q) = 2 \sum_{m} |\phi_{nl}^{m}(\mathbf{q})|^2 \tag{29}$$

is clearly the momentum density appropriate to a full shell of electrons. For the incomplete p-shell of nitrogen we shall use $\frac{1}{2}\Phi_{2p}(q)$. Then the angular dependence of the momentum density is averaged out, i.e. the probability of a photon encountering an electron with momentum specified by (q,ω) is made independent of ω. We shall use the symbol $\Phi(q)$ for the total momentum density function for all the electrons of the nitrogen atom.

Radial wave functions for the nitrogen atom have been calculated by Hartree and Hartree (1948) by the method of the self-consistent field with exchange. It was convenient to fit these wave functions with analytical formulae of the form suggested by Lowdin and Appel (1956), viz.

$$R_{1s} = \sum_{i=1}^{2} A_i e^{-\alpha_i r} \tag{30a}$$

$$R_{2s} = (r_0 - r) \sum_{i=1}^{3} A_i' e^{-\alpha' i r} \tag{30b}$$

$$R_{2p} = r \sum_{i=1}^{3} A_i'' e^{-\alpha'' i r}. \tag{30c}$$

A set of parameters yielding a fit (to about 0.1% where the wave functions were appreciable) was found with the aid of a program for a Burroughs 205 computer developed by Pope and Kennedy (1959) for another problem. The numerical values are given in Table I.

TABLE I

Parameters for Lowdin fit to Hartree wave functions for nitrogen

	r_0	A_1	A_2	A_3	α_1	α_2	α_3
$1s$	—	21.56	13.41	—	6.016	8.358	—
$2s$	0.3181	3.191	14.23	6.752	1.657	3.030	6.465
$2p$	—	1.195	5.128	3.405	1.295	2.411	5.468

When hydrogenic wave functions are used the integration of (28) and the summation of (29) are easily carried out for the states required; indeed, a formula for the general case has been given by Podolsky and Pauling (1929). For wave functions of the Lowdin type the calculation is more tedious, but it is still elementary. In Fig. 7 the radial momentum distribution $q^2\Phi(q)$

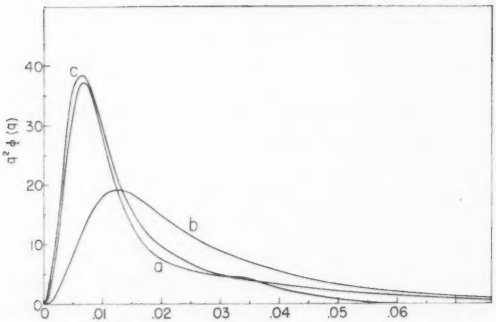

FIG. 7. Radial distributions of electron momenta for the nitrogen atom; the abscissa is momentum in units of m_0c. Curve (*a*) is computed for Hartree wave functions and curve (*b*) for unscreened hydrogenic wave functions; curve (*c*) is taken from the paper by Dzhelepov (1955).

calculated from the Hartree nitrogen wave functions is given. For the sake of comparison the same distribution calculated for unscreened hydrogenic wave functions is also plotted; because of the stronger resultant binding forces, the latter distribution falls off more slowly for large values of q than does the former. The satisfaction to reasonable accuracy of the normalization condition

$$4\pi \int_0^\infty q^2\Phi(q)dq = 7 \tag{31}$$

was used as a check on the calculated distributions. In his calculation of intrinsic line-widths Dzhelepov used the screened hydrogenic wave functions for carbon computed by Du Mond (1933) (obtained via Compton and Allison 1934), and made adjustments for the extra $2p$ electron of nitrogen. The values of the function $q^2\Phi(q)$ so obtained are also shown in Fig. 7.

Having seen how to compute the initial momentum probability density, we turn our attention again to the solution of the conservation equations (25) and (26). The dependence of p upon the small quantities q and Δ may be represented with sufficient accuracy by McLaurin expansions as far as the linear terms. Partial derivatives at $\Delta = 0$, $q = 0$ may be obtained by solving the pair of simultaneous equations arising from the differentiation of (25) and (26*a*); recall that $\theta = \pi$ for $q = 0$. Thus

$$\partial p/\partial q = (2\alpha^2+2\alpha+1)(2\alpha+1)^{-2}\cos\omega \tag{32}$$

$$\partial p/\partial \Delta = -(2\alpha^2+2\alpha+1)(2\alpha+1)^{-2}. \tag{33}$$

In this section it is convenient to use the symbol p_0 for the momentum after collision of an electron initially at rest, i.e. for the p of expression (2). The truncated series for p may now be written as

$$p = p_0\{1+\zeta(\alpha)[q\cos\omega-\Delta]\}, \tag{34}$$

$$\zeta(\alpha) = (2\alpha^2+2\alpha+1)[2\alpha(\alpha+1)(2\alpha+1)]^{-1}. \tag{35}$$

Because the peak in the distribution $q^2\Phi(q)$ of Fig. 7 occurs at about $q = 0.01$, the error resulting from the omission of higher powers of q should not be large.

The magnitude of Δ for the K electrons in nitrogen can be calculated from the critical absorption wavelength for X rays; using a value of 31.1 A° for this wavelength (Compton and Allison 1934) one gets $0.78\times10^{-3}\, m_0c^2$ for Δ. To the accuracy required in this problem there is no need to distinguish between the values of Δ for the $2s$ and $2p$ electrons. From the value 14.5 ev for the first ionization potential of nitrogen (Handbook of Chemistry and Physics 1946) one finds $0.28\times10^{-4}\, m_0c^2$ as a representative value of Δ for the L shell. First note that the values of Δ for both shells are sufficiently small to justify the retention of only the first power of Δ in (34). The effect of the presence of Δ is to shift the spectral line toward smaller values of momentum. This shift would have no effect on the line-width were it not for the fact that the magnitude of the shift is different for different shells. Compared to the effect of values of q of the order of 0.01, the shift is completely negligible for the L shell. For the K electrons the shift is about 10% of the effect of the important values of q in (34). However, since only two of the seven electrons are in the K shell, the effect of Δ may be ignored without fear of serious error, i.e. we shall put Δ equal to zero in equation (34). In his treatment of the conservation of energy Dzhelepov assumed that the electron was initially free; this is equivalent to replacing Δ in (34) by a negative function of q. Since Dzhelepov also retained terms of order q^2, it is not easy to distinguish the effect of his different treatment of the conservation of energy. The combined effect of his additional terms appears to affect the line-width only very slightly; the line is made asymmetric with the steeper side in the lower-momentum region. In a more correct calculation, i.e. one using suitable values of Δ for the different shells, the steeper side would lie in the region of higher momentum. The calculations of this paper should be more correct with regard to the conservation of energy than those of Dzhelepov, though the difference is probably negligible.

Now we are ready to derive an expression for the relative number, $N(p)$, of electrons with momenta after collision in the range p to $p+dp$. Let us assume for the present that the probability of scattering is independent of the values of q and ω. Then the number of collisions in which q is in the range q to $q+dq$ and ω is in ω to $\omega+d\omega$ is proportional to the number of electrons having their momenta initially in this range, i.e. to $2\pi q^2\Phi(q)\sin\omega\, dq\, d\omega$. We shall find $N(p)$ by transforming one of the variables of integration in

$$2\pi\int_0^{\pi}\int_0^{\infty} q^2\Phi(q)\sin\omega\, aq\, d\omega = 7 \tag{36}$$

The integration over ω will be eliminated in favor of an integration over p. A sufficiently good approximation to the relation between p and ω is obtained by using (34) with $\Delta = 0$; note that p is a monotonic function of ω in the range 0 to π. Let p_+ and p_- be the maximum and minimum values respectively attained by p for fixed q and variable ω.

$$p_{\pm} = p_0(1 \pm \zeta q) \tag{37}$$

Noting that $dp/d\cos\omega = p_0\zeta q$, we find that

$$2\pi \int_0^{\infty} q^2\Phi(q)dq \int_{p-}^{p+} (d\cos\omega/dp)dp = 2\pi(p_0\zeta)^{-1} \int_0^{\infty} q\Phi(q)dq \int_{p-}^{p+} dp = 7. \tag{38}$$

A suitable parameter to use in describing the line-shape is the fractional departure of the momentum from its nominal value, i.e. $x \equiv (p-p_0)/p_0$; it is convenient also to define the function

$$F(y) \equiv \int_y^{\infty} q\Phi(q)dq. \tag{39}$$

Upon changing the order of integration in (38) one finds

$$2\pi(p_0\zeta)^{-1} \int_{-\infty}^{\infty} F(\zeta^{-1}|x|)dp = 7. \tag{40}$$

Thus the line shape, or the dependence of the relative number of electrons in an interval dp upon x, is given by $N(p) = F(\zeta^{-1}|x|)$.

The function $F(y)$ has been evaluated for the Hartree and for the unscreened hydrogenic momentum densities by numerical integration by the Runge–Kutta process. The results are shown in Fig. 8. It is also possible, by a small number

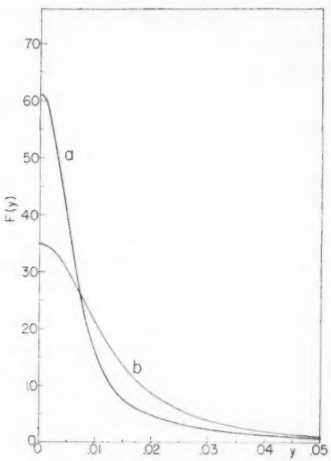

FIG. 8. The function $F(y)$ for Hartree, (a), and for unscreened hydrogenic, (b), wave functions. This function gives the number of electrons against fractional departure from the mean momentum for an incident photon of energy $0.420\ m_0c^2$.

of elementary integrations, to evaluate $F(y)$ analytically for the hydrogenic density:

$$F(y) = 2^3\pi^{-2}\{\tfrac{1}{3}\beta_1{}^5(\beta_1{}^2+y^2)^{-3}+2\beta_2{}^5[15(\beta_2{}^2+y^2)^5]^{-1}[10y^4+5y^2\beta_2{}^2+7\beta_2{}^4]\}, \tag{41}$$

with $\beta_1 = \alpha_0 Z$ and $\beta_2 = \frac{1}{2}\alpha_0 Z$; Z is the atomic number and α_0 is again the fine-structure constant. The part of (41) depending upon β_1 arises from the

K shell, the part depending upon β_2 from the L shell; different effective values of Z could be used for the two shells. Similar, but much more complex, results could be obtained for the momentum density calculated from the Lowdin formulae fitted to the Hartree wave functions. Instead the method of numerical integration was tested by comparing its values of $F(y)$ for the hydrogenic case with those obtained from (41). Another check is afforded by the normalization condition inherent in (40), viz.

$$4\pi \int_0^\infty F(y)dy = 7. \tag{42}$$

All checks were satisfied to three or four significant figures in the regions of importance.

There are two qualitative features of the spectral function $F(\zeta^{-1}|x|)$ which should be noted. Firstly, the line is symmetric about $p = p_0$, i.e. about the momentum value corresponding to an electron initially at rest. Secondly, the line-shape is the same at all photon energies, if suitable changes of scale in the abscissa are made. These two properties of the line are valid, it should be understood, only because of the assumptions that the final electron momentum is a linear function of initial electron momentum and that the binding energy can be ignored.

The graph of the function $F(y)$ given in Fig. 8 is, of course, half the line profile for the photon energy at which $\zeta(\alpha)$ is equal to unity, i.e. for $\alpha = 0.420$; the relative width at half the maximum height for the Hartree case is 1.30%. The percentage line-width w at any other sufficiently large photon energy may be calculated from formula (43).

$$w = 1.30\,\zeta(\alpha)\% \tag{43}$$

The function $w(\alpha)$ defined by (43) is plotted in Fig. 9. Also shown are the two

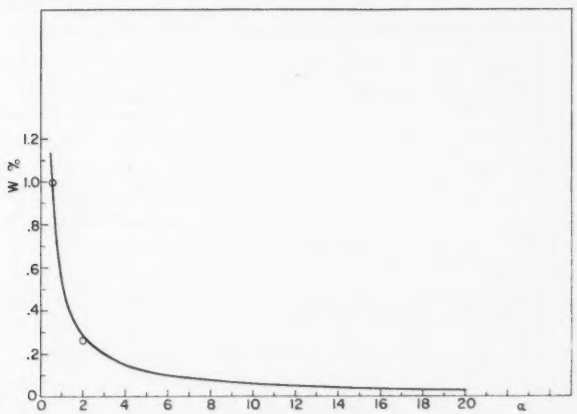

FIG. 9. The intrinsic half-width of the momentum line, w, is plotted against the energy of the photon in units of m_0c^2.

points computed by Dzhelepov (1955). Note that because Dzhelepov quotes the relative width of the line plotted against the electron kinetic energy, w', our results are not directly comparable; one must use

$$w = (2\alpha^2+2\alpha+1)[2(\alpha+1)^2]^{-1}w'. \tag{44}$$

Because the momentum density used by Dzhelepov is so similar to the one calculated from the Hartree wave functions, it is not surprising that the results are in good agreement.

Before drawing any conclusions from the results shown in Fig. 9, it is desirable to discuss the validity of the approximation that the probability of the Compton process is independent of the initial state of the electron. The effect of the atomic binding forces on the electron during the scattering has been discussed by Heisenberg and Bewilogua (1931); numerical results have been supplied by Nelms (1953). The scattering cross section differs appreciably from the free electron value only for small values of the scattering angle θ. Thus in our case the electron can be considered to be free when the cross section is being calculated. The Klein–Nishina formula for the Compton cross section as usually quoted is applicable to the case in which the electron is initially at rest. Before using this formula we must, therefore, carry out a Lorentz transformation from the laboratory co-ordinate system to one in which the electron is initially at rest. In the new co-ordinate system the energy of the photon, α^*, will differ slightly from α, and the path of the electron after collision will be inclined at a small angle, ϕ^*, to the incident γ-direction. Since the changes in α and ϕ are small, we shall calculate the effects of these changes independently. If v is the initial velocity of the electron in units of c, one finds

$$\alpha^* = \alpha(1-v\cos\omega)(1-v^2)^{-\frac{1}{2}}. \tag{45}$$

To the first order in q (45) becomes

$$\Delta\alpha \equiv \alpha^*-\alpha = -\alpha q\cos\omega. \tag{46}$$

The fractional change of the forward scattering cross section for a small change in α may be estimated with the aid of the logarithmic derivative of expression (3*a*)

$$[d\sigma/d\Omega|_0]^{-1}\Delta\left(\frac{d\sigma}{d\Omega}\right)_0 \doteqdot S^{-1}(dS/d\alpha)\Delta\alpha \tag{47}$$

$$\doteqdot -V(\alpha)q\cos\omega$$

$$V(\alpha) = 2\alpha(2\alpha^3+2\alpha^2-1)[(\alpha+1)(2\alpha+1)(2\alpha^2+2\alpha+1)]^{-1}. \tag{48}$$

The modulus of $V(\alpha)$ is less than unity for all positive values of α. Now, since the most probable value of $\cos\omega$ is zero, the average value of $q\cos\omega$ for value of q near the peak of the distribution should be considerably less than 0.01. Hence the change in cross section induced by the change in the value of α under the Lorentz transformation is negligible.

In estimating the magnitude of the departure from collinearity of the ejected electron and the incident γ-ray, it is convenient to introduce the angle of

scattering in the transformed co-ordinate system, θ^*. Starting from formulae quoted by Davisson (Siegbahn 1955), one can show that

$$\tan \phi^* = (\alpha+1)^{-1}[(1+\cos\theta^*)/(1-\cos\theta^*)]^{\frac{1}{2}}. \tag{49}$$

Because of the simple relation between energy and momentum for a photon, the conservation of the scalar product of the momentum–energy four vectors for the incident and scattered photons yields

$$\alpha\alpha'(1-\cos\theta) = \alpha^*\alpha'^*(1-\cos\theta^*). \tag{50}$$

The relation between α^* and α has already been given in (45); similarly

$$\alpha'^* = \alpha'[1-v\cos(\theta-\omega)](1-v^2)^{-\frac{1}{2}}. \tag{51}$$

The expansion of $\cos\theta$ in powers of q can be obtained from equations (25) and (26) by differentiation; we shall need only the first two terms.

$$\cos\theta = -1+\tfrac{1}{2}(\alpha'^{-1}q\sin\omega)^2+\ldots \tag{52}$$

Substitution of (51) and (52) in (49) leads to

$$\phi^* \doteqdot \tfrac{1}{2}[\alpha(\alpha+1)]^{-1}q\sin\omega \text{ radians}. \tag{53}$$

When $q = 0.01$ and $\omega = \frac{1}{2}\pi$, the values for ϕ^* at $\alpha = 0.5$ and $\alpha = 20$ are 0.4 degree and 0.7×10^{-3} degree respectively. To see that the differential cross sections at these values of energy and ϕ^* differ from the values at $\phi^* = 0$ by negligible amounts, one has only to inspect the curves of computed values given by Nelms (1953).

The only remaining errors of importance in the values of w of Fig. 9 arise from the approximate nature of the Hartree wave functions. From the curves of Fig. 8 one learns that the width for unscreened hydrogenic wave functions is about double that for Hartree wave functions. (The greater width in the hydrogenic case occurs because the stronger resultant binding forces give rise to larger kinetic energies.) Since the Hartree wave functions are believed to be considerably more accurate than unscreened hydrogenic wave functions, it would be surprising if the error in the calculated values of w were greater than 20%. Such accuracy is certainly adequate for a discussion of the role of intrinsic width in determining the resolution of existing spectrometers.

The measured relative half-widths are considerably greater than the intrinsic half-width in all energy regions. Below 1 Mev there is a rapid deterioration of the resolution of a Compton spectrometer, attributable to multiple scattering of electrons in the radiator, and, in some cases, to scattering by the residual gas in the instrument; this deterioration masks the increase in w below $\alpha = 2$. At higher energies the measured resolution is roughly constant, e.g. in the spectrometer of Groshev *et al.* (1956) the measured resolution for photon energies between 1.5 and 8.5 Mev was about 2.3% compared with an intrinsic width of the order of 0.1%.

4. TRANSMISSION AND RESOLUTION

In this section we examine the problem of choosing the parameters of a Compton spectrometer in such a way that its efficiency is maximized for operation at a given resolution. In order to handle the analysis with reasonable

facility it is necessary to make sufficiently bold approximations that the various functions involved can be obtained in simple algebraic form. Thus the relationship derived among efficiency, resolution, and photon energy, though it is believed to be accurate enough for design purposes, is not intended to be used as an intensity calibration.

Let the transmission, $\mathfrak{T}$, be defined as the fraction of the photons incident upon the radiator which eject an electron which passes through the slit at F_1 (see Fig. 2) and through the axial aperture at F_2; the effect of the radial width of the slit at F_2 will be considered separately. The transmission can be approximated by the product of three factors. The first of these, the differential cross section for the production of a Compton electron in the forward direction, has been given in formula (3). The second is the average solid angle, $\bar{\Omega}$, defined at a point in the radiator by the width of the slit at F_1, $2sr_0$, and by the height of the aperture at F_2, $2Tr_0$. Let ϕ_r be the angle between the γ-direction and the projection on the plane of symmetry of the initial velocity vector of an electron whose orbit passes through either edge of the slit at F_1; let ϕ_Z be the angle between the γ-direction and the projection (on a plane perpendicular to the plane of symmetry and containing the γ-direction) of the initial velocity of an electron whose orbit touches the upper or lower edge of the aperture at F_2. Then

$$\phi_r \doteqdot \omega_1 \operatorname{cosec} (\omega_1\theta_1)s \tag{54}$$

and

$$\phi_Z \doteqdot \omega_2 T. \tag{55}$$

Also

$$\bar{\Omega} \doteqdot (2\phi_r)(2\phi_Z) = 4\omega_1\omega_2 \operatorname{cosec} (\omega_1\theta_1)sT. \tag{56}$$

The third factor is the projected superficial density of radiator electrons in a plane perpendicular to the γ-beam. To calculate this density we shall assume that a mean radiator atom has the atomic number 7 and the atomic weight 14. Let ξ represent the thickness, measured perpendicularly to its surface, of the radiator, in mg/cm^2. The projected electron density is then approximately $3.01\times10^{20}\xi$ sec χ electrons per cm^2, if the curvature of the radiator is not too great; χ is the angle between the central normal to the radiator and the γ-direction (see relation (12)). Collecting all the factors one finds

$$\mathfrak{T} = 9.56\times10^{-5}S(\alpha)\,\omega_1\omega_2\,\xi sT \operatorname{cosec} (\omega_1\theta_1) \sec \chi. \tag{57}$$

Now the efficiency of the spectrometer also depends upon the component, A, of the area of the radiator projected in the γ-direction. If a well-collimated beam of γ-rays of sufficient cross-sectional area is available, the counting rate will be proportional to the product of A and $\mathfrak{T}$, a quantity which we shall term the luminosity, L. If t is the maximum value of the parameter τ corresponding to an irradiated point in the radiator, then the effective height of the radiator is $2tr_0$. We shall assume that the effective width of the radiator

is defined by baffles between the two slits which limit the radial departure of orbits from the optic circle; let the magnitude of the maximum permitted departure be H. If the value of H is not too large, and if the angle χ is not too large, a good approximation to the effective width of the radiator is $2Hr_0 \sin(\omega_1\theta_1)$; this distance is the width of the electron beam in the direction OR of Fig. 2. Thus

$$A = 4r_0^2 \sin(\omega_1\theta_1)Ht \tag{58}$$

and

$$L = 3.82\times10^{-4} r_0^2 S(\alpha)\, \omega_1\omega_2\, \xi Ht\, sT \sec\chi. \tag{59}$$

The central problem of spectrometer design is to choose values of the five parameters ξ, H, t, s, and T in such a way as to maximize L for a given line-width. As may be seen, the line-width increases when any of the five parameters is increased. Our next task is to derive a simple approximate formula relating line-width to these parameters. In most of this section line-width may be assumed to mean instrumental line-width, the intrinsic line-width of Section 2 being added in at the end of the calculation. Imagine a detector of height $2Tr_0$ and of infinitesimal width placed at F_2. If the magnetic field is varied while the instrument is receiving a well-collimated beam of monoenergetic photons, then the total "area" under the observed line is equal to the product of the luminosity L and the flux density of photons at the radiator. For convenience we shall refer to the line observed with an infinitesimal exit slit as the image, reserving the term line for the case of an exit slit of finite dimensions. The symbol 2σ will be used for the total basal width of the image, relative to the magnetic field which causes the electrons of maximum momentum to move in a circle of radius r_0.

The sources of image broadening fall into two classes: the ordinary aberrations of a β-spectrometer, and those resulting from the greater curvature of the orbits of the lower-energy electrons emitted at an angle to the γ-direction. We shall begin by calculating the contribution of the former class to the basal width of the image; relative momentum is, of course, equivalent to relative magnetic field strength. The contribution to 2σ from the ordinary aberrations is

$$\tfrac{1}{2}\omega_1{}^2[2s+|D|H^n+|C_2|t^2+|C_3|T^2+2|C_4|tT]. \tag{60}$$

The factor $\frac{1}{2}\omega_1{}^2$ relates relative radial displacement in the focal plane to relative changes of momentum (Lee-Whiting 1957). The first term in the bracket of (60) is the result of the finite width of the slit at F_1. The remaining terms correspond to higher-order aberrations; formulae for the coefficients C_i are listed in Section 2.

The 2 multiplying the term in tT is present because, with a symmetrically situated radiator, the contribution to the basal width of an aberration which is odd in t is twice as large as one that is even in t. The factor D before H^n is either C or $2C$, depending on whether n is even or odd, where C is the coefficient of H^n in $\eta(\theta_2)$.

By manipulating formulae given by Davisson (Siegbahn 1955), one can show that for an electron emitted at a small angle ϕ to the γ-direction the fractional change in momentum is given by

$$(\Delta p)/p \doteqdot -\tfrac{1}{2}(E+1)\phi^2; \tag{61}$$

recall that E is the kinetic energy of the electron in units of m_0c^2. In terms of the angles ϕ_r and ϕ_Z defined earlier in this section, the maximum value of ϕ^2 permitted by the geometry of the system is $\phi_r^2 + \phi_Z^2$. Since the term in ϕ_r^2 is proportional to s^2, and since we have already a term in 2σ proportional to s, we may discard the ϕ_r^2. Note that ϕ_Z depends only upon the height of the aperture at F_2, and not upon the height of the radiator; this result is a consequence of the first-order orbit theory.

The geometrical limit on ϕ^2 described above can be exceeded for those electrons which undergo appreciable scattering in the radiator. This effect is the principal reason for limiting the thickness of the radiator. The distribution of scattering angles as calculated in the simpler theories of multiple scattering is proportional to the scattering angle and to a Gaussian function of this angle (see Bethe and Ashkin in Segre (1953)). The mean value of the square of the scattering angle for an electron which has passed through X mg/cm^2 of material with $A = 14$ and $Z = 7$ is given by

$$\langle\Theta^2\rangle \doteqdot 6.0\times10^{-3}\, X\, p^{-4}(p^2+1) \text{ (radians)}^2. \tag{62}$$

In deriving (62) a slowly varying logarithmic factor has been approximated by a mean value appropriate to $X = 1$ mg/cm^2 and to photon energies in the range 1 to 10 Mev. Since the electrons can be assumed to be produced uniformly throughout the radiator, and since the normal to the radiator makes an angle χ approximately with the initial electron direction, we have

$$X = \tfrac{1}{2}\xi \sec\chi. \tag{63}$$

In order to get an effective basal width to add to (60), we shall approximate the shape of the distribution function for scattering angle by a triangle with the same initial slope, the same area, and the same value of the mean of the square of the scattering angle. For such a distribution function the square of length of the base, Θ_b, is related to the mean of the square of the scattering angle by

$$[\Theta_b^2/\langle\Theta^2\rangle] = \tfrac{1}{2}[5+(21)^{\frac{1}{2}}] \doteqdot 4.79. \tag{64}$$

Using the Θ_b calculated from (62) and (64), we shall assume that the ϕ^2 of expression (61) may be approximated by $\phi_Z^2 + \Theta_b^2$. The total contribution to the basal image width resulting from the acceptance of electrons ejected at an angle to the γ-direction is thus

$$\tfrac{1}{2}(E+1)[\omega_2^2T^2+1.4\times10^{-2}p^{-4}(p^2+1)\xi \sec\chi]. \tag{65}$$

The thickness of the radiator also affects the image width through the reduction of the energy of the electron in multiple scattering. Using approxima-

tions similar to those of the preceding paragraphs, one can show that the fractional reduction in momentum at the most probable energy loss (Segre 1953, page 256) is given by

$$p^{-2}(E+1)(0.8\times10^{-3})\xi \sec\chi. \tag{66}$$

Our estimate of the importance of this term is probably too small, because the most probable energy loss has been used instead of some effective maximum value. Since (66) is always much smaller than the ξ term of (65), the error should not be serious.

The discussion of the preceding paragraphs enables us to express the basal width of the image, 2σ, as a function of the five parameters to which the luminosity is proportional. Thus

$$2\sigma = K_1 s + K_2 \xi \sec\chi + K_3 H^n + K_4 t^2 + K_5 T^2 + 2K_6 tT \tag{67}$$

with

$$K_1 = 1+a_1 \tag{68a}$$

$$K_2 = p^{-2}(E+1)[7p^{-2}(p^2+1)+0.8]\times10^{-3} \tag{68b}$$

$$K_3 = \tfrac{1}{2}(1+a_1)|D| \tag{68c}$$

$$K_4 = \tfrac{1}{2}(1+a_1)|C_2| \tag{68d}$$

$$K_5 = \tfrac{1}{2}|(E+1)(-a_1)-(1+a_1)\,C_3| \tag{68e}$$

$$K_6 = \tfrac{1}{2}(1+a_1)|C_4|. \tag{68f}$$

As a first step in our program of maximizing the counting rate for given resolution, we shall maximize the luminosity (59), holding the basal width of the image (67) fixed. It is not difficult to show that a maximum is attained for the following values of the parameters:

$$s = [2n/(3n+1)]K_1^{-1}\,\sigma \tag{69a}$$

$$\xi = [2n/(3n+1)]K_2^{-1}\,\sigma\cos\chi \tag{69b}$$

$$H = [2/(3n+1)]^{1/n}K_3^{-1/n}\sigma^{1/n} \tag{69c}$$

$$t = [n/(3n+1)]^{\frac{1}{2}}(K_5/K_4)^{\frac{1}{2}}[K_6+(K_4K_5)^{\frac{1}{2}}]^{-\frac{1}{2}}\sigma^{\frac{1}{2}} \tag{69d}$$

$$T = [n/(3n+1)]^{\frac{1}{2}}(K_4/K_5)^{\frac{1}{2}}[K_6+(K_4K_5)^{\frac{1}{2}}]^{-\frac{1}{2}}\sigma^{\frac{1}{2}}. \tag{69e}$$

The corresponding formula for the maximized luminosity, which we shall call L_0, is

$$L_0 = 1.91\times10^{-4}r_0^2S(\alpha)\omega_1\omega_2n^3[2/(3n+1)]^{3+1/n}K_1^{-1}K_2^{-1/n}[K_6+(K_4K_5)^{\frac{1}{2}}]^{-1}\sigma^{3+1/n}. \tag{70}$$

At this point let us return to a consideration of the best choice of the field parameter a_1. The product $\omega_1\omega_2 = [-a_1(1+a_1)]^{\frac{1}{2}}$ varies only from 0.3 to 0.4 as $-a_1$ is increased from 0.1 to 0.2. Figure 6 shows one that C_2 and C_4, and hence K_4 and K_6, do not vary enormously rapidly with a_1. The two terms in

(68e) vary in opposite ways; at low values of E their effects tend to cancel; at very high values of E the resulting variation tends to counteract that of $\omega_1\omega_2$. The coefficient K_2 does not depend upon a_1. The only remaining factor, $K_3^{-1/n}$, depends upon higher field-expansion coefficients as well as upon a_1, and is not likely to be at the designer's disposal; the fact that an nth root is involved decreases the probability of any great variation. Our conclusion then is that, as far as known factors in the luminosity are concerned, there is no significantly best value of a_1.

One should bear clearly in mind that the conclusion of the last paragraph depends upon the assumption that r_0 is fixed and that well-collimated beams of γ-rays are available with cross sections as large as required. For a given value of H, it is true, the width of the radiator increases when θ_1 is increased. But, on the other hand, the solid angle in which electrons are accepted decreases as θ_1 is increased, since the width of the slit at F_1 is fixed by a first-order aberration. These two effects cancel approximately in the circumstances we have assumed.

If for a given instrument the cross section of the available beam is smaller than the optimum size for a given value of a_1, then it is advantageous to increase the solid angle in which electrons are collected by decreasing the value of θ_1, i.e. by increasing $|a_1|$. One must not, however, make θ_1 so small that the second-order aberration caused by the acceptance of lower-energy electrons ejected at an angle to the γ-direction is greater than the first-order aberration due to finite slit-width at F_1. There are, however, other reasons more pressing for preventing θ_1 from becoming too small.

As θ_1 becomes very small the angle between the central radiator normal and the γ-direction approaches 90°; in fact, $\chi \doteq \frac{1}{2}\pi - \theta_1$ when θ_1 is small (see formula (12)). Since the optimum value of the radiator thickness is proportional to $\cos\chi$, the radiator will become very thin, and hence difficult to make, as χ approaches $\frac{1}{2}\pi$. More careful shaping and positioning of the radiator would also be required for smaller values of θ_1.

Another point to be considered in the choice of a_1 is the necessity to keep the background from scattering as low as possible. One way to do this is to keep the detector as far from the γ-beam as possible; this is accomplished by allowing θ_2 to be as close to π as possible. On the other hand, one must ensure a reasonable clearance between the γ-beam and the slit at F_1 to reduce scattering; this necessity argues against too small values of θ_1.

As a reasonable compromise in the face of all the effects discussed, the value $a_1 = -0.14$ is suggested. The corresponding value of χ is 44.8°. For values of a_1 closer to -0.20, the optimum radiator thickness begins to decrease rapidly.

Our discussion of the criteria for fixing the various spectrometer parameters is based upon the assumption that the beam of γ-rays is perfectly collimated and is of adequate cross section. In practice the idealized beam is simulated by inserting a system of longitudinal baffles between the radiator and a broad source; the cross section of the source should cover the projection of the radiator. Let us suppose that only those γ-rays whose directions lie within a

cone of half-angle δ about the nominal γ-direction are permitted to fall upon the radiator. Then the fraction of the photons leaving the source which are accepted by the spectrometer is approximately $\frac{1}{4}\delta^2$. Thus, ignoring the absorption of γ-rays in the source, the current of electrons arriving at the final slit of the spectrometer is $S(\frac{1}{4}\delta^2)L$, if S is the specific activity of the source in photons per unit area. The divergence of the γ-beam will also affect the resolution. One can approximate this effect by adding the term $\frac{1}{2}(E+1)\delta^2$ to the right side of equation (67). If the design of the collimating system is included in that of the spectrometer, then one should maximize $\delta^2 L$, instead of L, and add δ to the list of parameters to be chosen. Because δ^2 and s appear in the function being maximized and in the constraint in the same way, the best value of δ may be obtained from the relation

$$K_1 s = \tfrac{1}{2}(E+1)\delta^2. \tag{71}$$

The ratios of the terms in (67) may still be calculated from the relations (69), but the normalization must be altered.

So far we have ignored the influence of the radial aperture at F_2. Let the width of this slit be $2s'r_0$. Using our knowledge of the dispersion of a β-spectrometer, we can compute the relative change of momentum, 2ϵ, corresponding to a change of $2s'$ in the value of η in the focal plane.

$$\epsilon = \tfrac{1}{2}\omega_1{}^2 s'$$

It should be clear that an increase of the momentum width of the exit slit beyond the basal width of the image (i.e. making $\epsilon > \sigma$) does not result in any increase in the counting rate. The best value of ϵ for a given value of σ depends, of course, upon the distribution of intensity in the image, i.e. upon the line-shape observed with a detector of infinitesimal width. If the distribution of intensity in the image is uniform, the best slit-width is that corresponding to $\epsilon = \sigma$, the width of the line at half the peak height is 2σ, and the peak counting rate for unit incident flux density is equal to the luminosity. In an actual spectrometer the distribution in the image is almost certainly strongly peaked, since most of the broadening arises from quadratic terms.

For present purposes it is not unreasonable to assume that the graph of the intensity distribution in the image is an isosceles triangle, with a base length 2σ. Let w be the half-width of the line observed with an exit slit equivalent to a fractional change of momentum of 2ϵ, and let C be the counting rate at the peak of the line for a γ-beam of unit flux density. We shall use the symbol x for the ratio ϵ/σ. An elementary calculation leads to

$$\begin{aligned} w &= \sigma(1+\tfrac{1}{2}x) && \text{for } 0 \leqslant x \leqslant 2/5 \\ &= 2\sigma\{1+x-[x(2-x)]^{\frac{1}{2}}\} && \text{for } 2/5 \leqslant x \leqslant 1, \end{aligned} \tag{72a}$$

$$C = Lx[2-x]. \tag{72b}$$

In maximizing C for fixed w, we assume that L has already been maximized for fixed σ. Thus L in (72b) is to be replaced by L_0, which is proportional to σ^λ, with $3 > \lambda \geqslant 7/2$. Now, if w is held constant, (72a) defines σ as a function

of x, and C can be regarded as a function of x alone. It is not difficult to show, by examining dC/dx, that in the region $0 \leqslant x \leqslant 2/5$ the function $C(x)$ increases monotonically for all values of λ of interest. If $0 \leqslant \lambda \leqslant 9/2$, a maximum exists for a value of x in the range $2/5 \leqslant x \leqslant 1$; this value of x, say x_0, may be obtained by solving the equation

$$\lambda = 2(1-x_0)(1+2x_0^2)\{2x_0^2(2-x_0)-(1-2x_0)[x_0(2-x_0)]^{\frac{1}{2}}\}^{-1}. \tag{73}$$

Recall that $\lambda = 3+n^{-1}$, and that $n \geqslant 2$. With these restrictions the solution of (73), to an accuracy of better than 1%, is

$$x_0 \doteqdot 0.442-0.034\, n^{-1}. \tag{74}$$

Combining (69*a*) with the definitions of x and ϵ, we find that the best value for the ratio of the widths of the slits at F_2 and F_1 is

$$s'/s = (3+n^{-1})x_0; \tag{75}$$

the corresponding value of C may be calculated by substituting x_0 of (74) in (72*b*).

As an example of the use of the various criteria that have been developed, let us work out the parameters for a spectrometer with $a_1 = -0.14$ having an instrumental half-width of 0.2% for a perfectly collimated γ-beam. From equations (16) and (17) one can compute the angles specifying the positions of the slits: $\theta_1 = 46.42°$ and $\theta_2 = 240.5°$. The value of a_2 for which C_1 is zero is -0.505. Let us assume that no other field expansion coefficients are at the disposal of the designer, i.e. that $n = 3$. The optimum value of the ratio $x = \epsilon/\sigma$ is $x_0 = 0.431$, and the corresponding value of the parameter σ is 1.64×10^{-3}. The half-widths of the first and second slits may be found from (69*a*) and (75): $s = 1.1\times10^{-3}$ and $s' = 1.6\times10^{-3}$.

The optimum value for H depends upon K_3, which in turn depends upon the unknown parameters a_3. Making use of (24) one finds $K_3 = |0.793-1.18a_3|$. We shall assume that the field variation is essentially quadratic in the region of the optic circle, i.e. that a_3 is small, and put K_3 equal to unity; since it is the cube root of K_3 that enters into the calculation, it is probable that no large error has been made here. The resulting value of H is 0.069.

The best values of t, T, and ξ depend upon the photon energy at which the optimization is carried out; let us assume $\alpha = 4$, or a photon energy of about 2 Mev. Then $t = 0.031$, $T = 0.019$, and $\xi = 0.37$ mg/cm^2. If a density of 1.5 g/cm^3 is assumed for the material of the radiator, a thickness of 2.5 μ is obtained; since a radiator as thin as 5 μ has been used in a Compton spectrometer (Dzhelepov and Shestopalova 1956), our calculated value is not impossibly small.

The values of the effective radiator area and of the transmission for the parameters corresponding to an optimization carried out at $\alpha = 4$ and at an instrumental half-width of 0.2% are:

$$A = 5.8\times10^{-3}r_0^2 \text{ and } \mathfrak{T} = 3.1\times10^{-9} \text{ electrons per photon.}$$

The instrumental half-width w depends upon photon energy, because of the dependence of K_2 and K_5 upon the electron energy. In curve (*a*) of Fig. 10

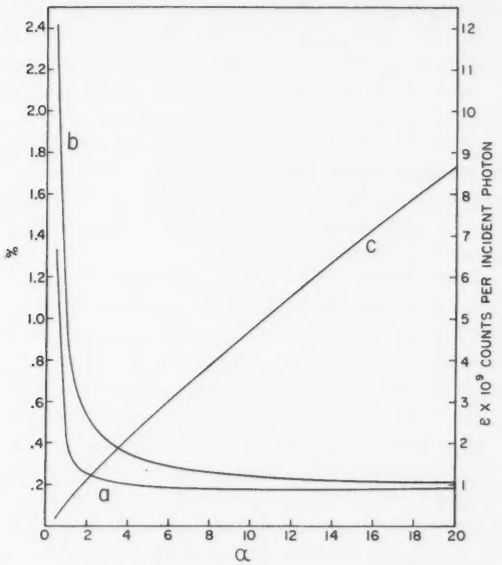

FIG. 10. The variation with photon energy of the resolution and efficiency of a Compton spectrometer optimized at $\alpha = 4$. Curve (*a*) shows the "instrumental" relative half-width of the momentum line, curve (*b*) the sum of the "instrumental" and intrinsic half-widths. In (*c*) is shown the efficiency $\mathfrak{E}$, the number of electrons passing through the exit slit per incident photon at the peak of the line.

the variation of the instrumental half-width with α is displayed. Also shown is the sum of the intrinsic and instrumental half-widths; this sum is an upper bound to the combined effect of the two types of broadening. Note that in the range 2 to 10 Mev of photon energy the effective resolution falls from 0.35% to 0.2%; the intrinsic width makes an appreciable contribution. The sharp rise in curve (*a*) as α is decreased below 2 is chiefly caused by the increasing amount of change of direction for electrons multiply scattered in the radiator; the slow rise in (*a*) for larger values of α originate in the increasing relative departure from the maximum momentum for electrons ejected at a fixed angle to the γ-direction.

The quantity usually quoted as a measure of the efficiency, $\mathfrak{E}$, of a Compton spectrometer is the number of electrons counted at the peak of the line per incident photon. If one assumes that the electron detector is 100% efficient, $\mathfrak{E}$ is related to $\mathfrak{T}$ just as C is related to L in (72*b*). Now assuming that the spectrometer parameters are maintained at their optimum values for $\alpha = 4$, $\mathfrak{E}$ will vary with α because of the variation of the forward Compton cross section, and because of the dependence of line-shape upon energy; curve (*c*) of Fig. 10 shows the dependence of $\mathfrak{E}$ upon photon energy.

The curves of Fig. 10 will be somewhat modified when the divergence of the incident γ-beam is taken into account. An estimate of the optimum value of

the half-angle of the cone of divergence can be made from equation (71). For our example $\delta \doteqdot 1.2°$, and the fraction of γ-rays leaving the source which get through the collimating slits is about 10^{-4}. The curve of half-width against photon energy shown in Fig. 10 should be moved slightly upward, if a divergence as large as 1° is assumed. The neglect of this effect is at least partly compensated by the fact that the intrinsic and instrumental half-widths have been combined additively to get the result of Fig. 10.

The normal to the radiator at the central point is, in the example we have been discussing, inclined at an angle of 44.8° to the γ-beam. No very great curvature of the radiator is needed; the normal to the inner end of the radiator is more inclined to the γ-beam than the central normal by about 13°. The exact value of the effective width which the radiator presents to the γ-beam agrees within 1% with the value of this width calculated by means of the approximation, $2H \sin(\omega_1\theta_1)$, used in deriving the expression for the luminosity.

One of the approximations made in Section 2 was to apply the axial focusing condition only to points lying on the central generator of the radiator. Electrons originating at other points will arrive at F_2 after having been turned through an angle slightly different from θ_2. Electrons emitted from such points with a zero axial component of momentum will not have $\tau = 0$ at F_2; this error is equivalent to an effective increase in the height of the aperture at F_2. Now the radiator lies within the sector defined by the lines $\theta = \pm 3°$. The corresponding increase in effective slit height is $2t \sin(\omega_2 3°) = 0.0012$. Since the increase is less than 4% of the height of the aperture at F_2, it should not lead to any serious additional line broadening.

The second-order axial aberrations also contribute to an increased effective aperture height at F_2. Substituting numerical values in the formulae (23), one finds

$$\tau(\theta_2) = \ldots -2.98\,Ht - 2.38\,HT + \ldots . \tag{76}$$

This effect is equivalent to a 50% increase in the effective aperture height, but only for one quarter of the electrons emitted from the extreme ends of the upper and lower edges of the radiator at the maximum permitted angle to the plane of symmetry.

Another approximation of Section 2 was that the radiator surface could be a section of a cylinder, instead of a piece of a warped surface. Because of this approximation, orbits originating above or below the plane of symmetry, will not pass through F_1. Another aberration at F_1 occurs for those electrons which are ejected at a small angle to the plane of symmetry; for the moment we shall ignore the effect of the change of energy. The relevant terms in $\eta(\theta_1)$, calculated by the methods used by Lee-Whiting (1957), are:

$$\begin{aligned}\eta(\theta_1) = \ldots\ & (1+a_1)^{-1}(a_1+a_2)(1-\cos\omega_1\theta_1)t^2 \\ & +\{(1+a_1)^{-1}[\tfrac{1}{2}a_1+2a_1a_2(1+5a_1)^{-1}](1-\cos\omega_1\theta_1) \\ & +a_2(1+5a_1)^{-1}\sin^2\omega_2\theta_1\}(T^2-t^2) \\ & +a_2(1+5a_1)^{-1}[\sin 2\omega_2\theta_1 - 2\omega_1^{-1}\omega_2\sin\omega_1\theta_1]tT + \ldots .\end{aligned} \tag{77}$$

Inserting the numerical values for the special case that we have been discussing, we find $\eta(\theta_1) = \ldots -0.18t^2 - 0.025T^2 - 0.034Tt$. For the worst combination of t and T, the change in $\eta(\theta_1)$ is only -0.2×10^{-3}, less than 10% of the width of the slit at F_1. The effect of this aberration is to cause a small decrease in the probability that electrons emitted from the extreme upper and lower edges of the radiator will pass through the slit at F_1.

There is yet another aberration affecting the focus at F_1. An electron leaving the radiator with its momentum decreased by a fraction ϵ below the nominal value will have at F_1 an additional aberration given by

$$\eta(\theta_1) = \ldots . + \omega_1^{-2}(1-\cos\omega_1\theta_1)\epsilon. \tag{78}$$

For the special case under consideration the aberration is 0.313ϵ. The quantity ϵ may be calculated from (65); at $\alpha = 4$ we find $\epsilon = 1.0\times10^{-3}$. The resulting radial shift is about 14% of the width of the slit at F_1. Note that this effect applies almost entirely to electrons which have undergone the maximum amount of multiple scattering, and may therefore be beneficial.

In deriving the equation for the shape of the radiator the first-order orbit equation was used. The effect of the second-order correction term, (10*c*), is to produce a shift in $\eta(\theta_1)$ of 0.55×10^{-3}. Though this is not large compared to the width of the slit at F_1, 2.3×10^{-3}, it would probably be desirable to include (10*c*) in the $f(\theta)$ of equation (9*a*).

Albeit that the design that we have been considering is intended for high resolution, where the axial focusing is necessary, a comparison with the instrument of Groshev *et al.* (1956) is not without interest. These authors achieved a peak counting rate of 2.5×10^{-7} electrons per incident photon at a resolution of 2.7% for a photon of 1.33 Mev; the area of the radiator was 20 cm² and the radius of the spectrometer was 6 in. Scaling up from the numerical example that has been discussed and using $r_0 = 6$ in. we find $A = 12$ cm² and $\mathfrak{E} = 13\times10^{-7}$ electrons per photon at 2.7% resolution. Thus the estimated efficiency of an instrument of the design suggested in this paper is about three times the measured efficiency of the spectrometer of Groshev *et al.* under comparable conditions; a large part of the improvement is probably caused by the symmetric position of the radiator on the optic circle (compare Fig. 1 and Fig. 2).

5. REALIZATION OF THE MAGNETIC FIELD

The value of a_1 for the proposed Compton spectrometer, -0.14, lies between the values for the 180° and the $\pi\sqrt{2}$ β-spectrometers, 0 and $-\frac{1}{2}$ respectively. Since fields for both the latter spectrometers have been obtained without much difficulty, there is no apparent reason why the field for the Compton spectrometer should not be realized. Indeed, the problem should be even easier than that of the $\pi\sqrt{2}$ spectrometer, since any value of a_1 in a fairly wide range is satisfactory.

The method used by Lee-Whiting and Taylor (1956) for calculating the parameters of a system of pairs of air-cored coils producing a desired field variation should also be applicable in this case. The use of air-cored coils has

the advantage that calculations of high accuracy are possible, and the disadvantage that the field expansion coefficients a_n sometimes become undesirably large for higher values of n. In the case of a Compton spectrometer which is to be used in the neighborhood of a reactor, there is the further difficulty that the earth's magnetic field, distorted by nearby iron, would be difficult to cancel.

In designing the pole pieces of an iron spectrometer one can usually assume that the permeability of the iron is sufficiently large that the magnetostatic potential is constant on the pole faces. If the exciting coil and the outer edge of magnet are sufficiently remote from the region of interest, the problem reduces to one of finding the shape of two symmetrically placed, equipotential surfaces giving a desired field distribution in the plane of symmetry. In the remainder of this section we discuss a simple method of finding these equipotential surfaces.

Consider a finite magnetic dipole lying in the axis of symmetry of the spectrometer, with one pole of strength Q_i at a distance b_i above the plane of symmetry, the other of strength $-Q_i$ at a distance $-b_i$ below. The potential of a system of such dipoles is

$$\phi = \sum_i Q_i[(1/R_i^-)-(1/R_i^+)], \tag{79}$$

$$(R_i^{\pm})^2 = r^2+(Z \pm b_i)^2. \tag{79a}$$

The magnetic field in the plane of symmetry is given by

$$H = -\sum_i (2b_iQ_i)(b_i^2+r^2)^{-3/2}. \tag{80}$$

The quantities which one wishes to fix in spectrometer design are the expansion coefficients of H about the point $r = r_0$, as defined in (6); the first few of these coefficients are:

$$a_1 = -3\Lambda^{-1}\sum_i Q_i\beta_i\lambda_i^{5/2} \tag{81a}$$

$$a_2 = \frac{3}{2}\Lambda^{-1}\sum_i Q_i\beta_i\lambda_i^{5/2}(5\lambda_i-1) \tag{81b}$$

$$a_3 = -\frac{5}{2}\Lambda^{-1}\sum_i Q_i\beta_i\lambda_i^{7/2}(7\lambda_i-3) \tag{81c}$$

$$\Lambda = \sum_i Q_i\beta_i\lambda_i^{3/2} \tag{82}$$

with $\beta_i = b_i/r_0$, $\lambda_i = (1+\beta_i^2)^{-1}$.

If a_1 and a_2 only are to have given values, it is sufficient to use only two dipoles; let Q stand for the ratio Q_2/Q_1. We have three variables, β_1, β_2, and Q, to choose in such a way as to satisfy two equations, (81a) and (81b). Let us hold β_1 fixed and seek solutions for β_2 and Q. Define

$$Y = (1+\beta_1^2)^{-1}[(3+a_1)+a_1\beta_1^2]^{-1}[2(6-a_2)-(3+4a_2)\beta_1^2-2a_2\beta_1^4]. \tag{83}$$

After eliminating Q one gets a quadratic equation in β_2^2. Using the fact that β_1^2 satisfies the same equation, one finds that

$$\beta_1^2\beta_2^2 = (2a_2+a_1Y)^{-1}[(3+a_1)Y-2(6-a_2)]\,. \tag{84}$$

The corresponding value of Q is

$$Q = -[3\beta_1\lambda_1^{5/2}+a_1\beta_1\lambda_1^{3/2}][3\beta_2\lambda_2^{5/2}+a_1\beta_2\lambda_2^{3/2}]^{-1}. \tag{85}$$

Solutions to the problem exist for all values of a_1 and a_2 for which the right side of (84) is positive. A good choice for β_1 is one which does not give large values to higher derivatives. One can guard against this danger by calculating the value of a_3, and by plotting the resulting field in the region of interest.

To obtain the equipotential surface return to (79) and calculate ϕ at some point through which it is desired to have the surface pass. Other points may be found by the numerical solution of an algebraic equation; the process is simple and rapid, though somewhat tedious. It is necessary to check that the free poles on the axis do not lie between the equipotential surfaces chosen.

A good fit to the field form of the example that we discussed in Section 4 —$a_1 = -0.14$ and $a_2 = -0.505$—is obtained with:

$$\beta_1 = 0.7 \qquad \beta_2 = 2.448 \qquad Q_2/Q_1 = -18.84$$

The corresponding value of a_3 is 0.47.

It is probably necessary to make an approximate correction for the fact that the permeability of the iron is not infinite. The magnitude of this correction will depend upon the dimensions of the magnet, as well as upon the magnitude of the permeability. Because of the uncertainty in the calculated value of a_3 it is probably unwise to rely on the possibility of cancelling out the third-order aberration proportional to H^3.

6. SUMMARY

In Section 2 the principle of two-directional focusing in a Compton-electron spectrometer is developed, and the required form of the magnetic field is derived. An equation is obtained for the shape of the radiator. The intrinsic line-width caused by the initial motion of the atomic electrons, which limits the ultimate resolution attainable with a Compton spectrometer, is calculated as a function of photon energy in Section 3. The relationship between transmission and resolution is considered in Section 4, and an attempt is made to calculate the optimum values of various spectrometer parameters. In Section 5 a method of calculating the shapes of iron pole pieces which would produce the desired magnetic field is described.

ACKNOWLEDGMENTS

The author is greatly indebted to Dr. G. A. Bartholomew, who first suggested to him the possible advantages of a Compton spectrometer with an inhomogeneous magnetic field, for many helpful discussions, with particular reference to Section 4. Dr. G. Manning brought to his attention the necessity of including a discussion of the intrinsic line-width. Acknowledgment is also due to Drs.

N. K. Pope and J. M. Kennedy for making available the data of Table I, to Drs. T. D. Newton and L. G. Elliott for reading the manuscript, and to Mrs. R. B. Tomlinson for drawing the figures.

APPENDIX

It is possible to set up an equation for the radiator shape for the case of a point source located at a large distance, L, from the center of the radiator. Then the γ-ray incident on radiator at T (see Fig. 3) will make an angle β with the direction of the γ-ray incident at R;

$$\tan \beta = (r_0 - r \cos \theta)\ (L + r \sin \theta)^{-1}, \tag{A1}$$

if r and θ are the co-ordinates of T. The condition for the selection of forward-ejected electrons which replaces (7) is

$$\psi - \theta = \tfrac{1}{2}\pi - \beta, \tag{A2}$$

leading to the equations

$$\tan (\theta - \beta) = [1 + f(\theta)]^{-1} df/d\theta \tag{A3a}$$

$$r = r_0[1 + f(\theta)] \tag{A3b}$$

for the co-ordinate of a point on the radiator. Equations (A3) must be solved numerically, even for the first-order form of $f(\theta)$.

The heights of the radiator and of the source may be increased considerably, if a system of slits is provided to prevent the γ-rays from striking the radiator at too large an angle to the plane of symmetry.

REFERENCES

Beiduk, F. M. and Konopinski, E. J. 1948. Rev. Sci. Instr. **19**, 594.

Compton, A. H. and Allison, S. K. 1934. X-rays in theory and experiment (D. Van Nostrand Co., Inc., New York).

Du Mond, J. W. M. 1933. Revs. Modern Phys. **5**, 1.

Dzhelepov, B. S. 1951. Doklady Akad. Nauk S.S.S.R. **77**, 389.

——— 1955. Doklady Akad. Nauk S.S.S.R. **101**, 825.

Dzhelepov, B. S. and Orbeli, M. L. 1948. Doklady Akad. Nauk S.S.S.R. **62**, 615. English translation NRC TT-630.

Dzhelepov, B. S. and Shestopalova, S. Z. 1956. Izvest. Akad. Nauk S.S.S.R. Ser. Fiz. **20**, 328. Bull. Acad. Sci. U.S.S.R. Phys. Ser. **20**, 302.

Dzhelepov, B.S., Zhukovski, N. N., and Khol'nov, Iu. V. 1954. Izvest. Akad. Nauk S.S.S.R. Ser. Fiz. **18**, 599; Bull Acad. Sci. U.S.S.R. Phys. Ser. **18**, 285.

Groshev, L. V., Adyasevich, B. P., and Demidov, A. M. 1956. Proceedings of the International Conference on the Peaceful Uses of Atomic Energy, Geneva, 2, 39.

Handbook of Chemistry and Physics, 1947. 30th ed. (Chemical Rubber Publishing Co., Cleveland, Ohio).

Hartree, D. R. and Hartree, W. 1948. Proc. Roy. Soc. A, **193**, 299.

Heisenberg, W. and Bewilogua, L. 1931. Physik. Z. **32**, 737, 740.

Jauncey, G. E. M. 1925. Phys. Rev. **25**, 314, 723.

Lee-Whiting, G. E. 1957. Can. J. Phys. **35**, 570.

Lee-Whiting, G. E. and Taylor, E. A. 1956. Atomic Energy of Canada Limited Report CRT-668.

——— 1957. Can. J. Phys. **35**, 1.

Lowdin, P. O. and Appel, K. 1956. Phys. Rev. **103**, 1746.

Motz, H. T. 1956. Phys. Rev. **104**, 1353.

Motz, H. T., Carter, R. E., and Fisher, P. C. 1959. Bull. Am. Phys. Soc. II, **4**, 246.

Nelms, A. T. 1953. Natl. Bur. Standards, Circular 542.

Podolsky, B. and Pauling, L. 1929. Phys. Rev. **34**, 109.

Pope, N. K. and Kennedy, J. M. (1959). Private communication.

Segre, E. (*Editor*). 1952. Experimental nuclear physics (John Wiley & Sons, Inc., New York).

Seigbahn, K. (*Editor*). 1955. Beta- and gamma-ray spectroscopy (North-Holland Pub. Co., Amsterdam).

THE THERMAL NEUTRON CAPTURE CROSS SECTION AND RESONANCE CAPTURE INTEGRAL OF PROTACTINIUM-233[1]

T. A. EASTWOOD AND R. D. WERNER

ABSTRACT

The thermal neutron capture cross section and resonance capture integral of Pa^{233} to form the 1.2-minute and 6.7-hour isomeric states of Pa^{234} have been measured using activation methods. The results are as follows:

	$Pa^{233}(n,\gamma)Pa^{234}$ (1.2 minute)	$Pa^{233}(n,\gamma)Pa^{234}$ (6.7 hour)
Thermal neutron capture cross section, barns	20±4	19±3
Resonance integral, including $1/v$ part, 0.5 ev to ∞, barns	470±90	460±100
s_0	27±5	27±5
Effective cross section in NRX lattice position, ($r\sqrt{T/T_0} = 0.023$), barns	32±5	31±5
Total effective cross section in NRX lattice position, barns	63±7	

Irradiations made with different thicknesses of cadmium cover show the absence of a major resonance for the formation of the 6.7-hour state in the region of the cadmium cutoff. The results are compared with earlier values and some reasons for discrepancies have been studied experimentally.

INTRODUCTION

Protactinium-233 is an intermediate in the conversion of Th^{232} to U^{233} by neutron irradiation. It is well known that this conversion has great significance in the development of nuclear power because by this means natural thorium is converted to a useful reactor fuel, U^{233}. The important nuclear reactions which occur during neutron irradiation of thorium are given in Fig. 1 and the relevant nuclear properties of the nuclides are given in Table I. Figure 1 shows that Pa^{233} is consumed by two processes in a nuclear reactor. The first, β-decay, leads to fissile U^{233} and is governed by the half-life for radioactive decay. The second process is neutron capture which leads to Pa^{234} and thence by β-decay to U^{234}, a non-fissile isotope of uranium. It is governed by the capture cross section of Pa^{233} and the conditions of neutron irradiation. The first process leads to a useful product, while the second not only leads to a non-fissile product but also wastes neutrons. A knowledge of the cross section of Pa^{233} for neutron capture is therefore important to the reactor designer.

The significance of this cross section was recognized when U^{233} was shown to be fissile and several measurements have been reported. The first of these was by Katzin and Hagemann (1952). In 1946 they compared uranium produced from thorium irradiated in high and low neutron fluxes and observed

[1]Manuscript received January 4, 1960.
Contribution from the Research Chemistry Branch, Atomic Energy of Canada Limited, Chalk River, Ontario.
Issued as A.E.C.L. No. 1007.

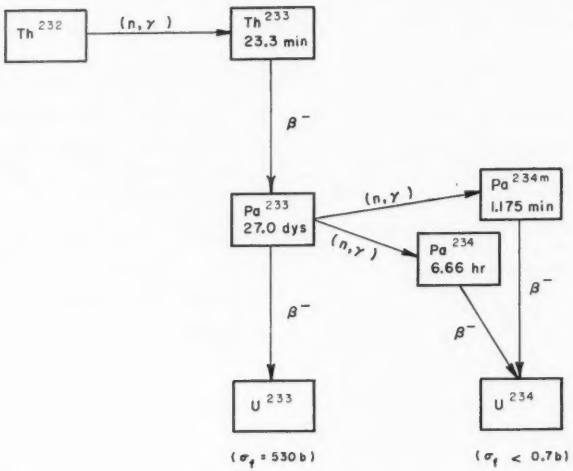

FIG 1. Important nuclear reactions in the Th^{232}–U^{233} chain in a nuclear reactor.

TABLE I

Radiations of protactinium and thorium isotopes as summarized by Strominger *et al.* (1958)

	Pa^{233}	Pa^{234m}	Pa^{234}	Th^{234}
Half-life	27.0 days	1.175 min	6.66 hr	24.10 days
Max. β-particle energies (Mev) and abundances (%)	0.15 (37%) 0.257 (58%) 0.568 (5%)	0.58 (1%) 1.50 (9%) 2.31 (90%)	0.16 (28%) 0.32 (32%) 0.53 (27%) 1.13 (13%)	0.100 (35%) 0.191 (65%)
γ-Ray energies (Mev) and relative abundances	0.016 0.028 0.040 0.058 0.075 0.086 0.140 0.272 0.301 (22) 0.313 (150) 0.341 (6) 0.376 0.400 0.417 0.476	0.043 (2.5) 0.230 0.255 (0.10) 0.770 (0.87) 0.803 (0.16) 0.807 1.01 (1.5) 1.24 1.44 (0.09) 1.69 (0.07) 1.83 (0.11)	0.043 (20) 0.099 (14) 0.125 (15) 0.153 (7) 0.225 (13) 0.293 0.333 0.368 (3.5) 0.566 (7) 0.603 0.732 (9) 0.803 (0.2) 0.887 (14) 0.924 (25) 1.24 1.43 (3.5) 1.68 (2.5)	0.029 0.063 0.091

the ratio of α-particle emission to the fission rate in a thermal neutron beam. The α-particle emission rate reflects the U^{234} content and the fission rate gives the U^{233} content. They obtained an effective neutron capture cross section of 37 ± 14 barns for Pa^{233} in a graphite-moderated reactor. According to Halperin *et al.* (1955; 1956) and Stoughton and Halperin (1959) the same uranium product was mass-analyzed at a later date and a value of 55 ± 6 barns was obtained. Apparently the integrated neutron flux for this experiment was obtained from the reactor operators and the uncertainty in this datum is not included in the error given for the effective cross section.

Halperin *et al.* (1955; 1956) irradiated thorium for varying lengths of time in the Low Intensity Test Reactor and also in an unspecified graphite reactor and deduced the effective cross section of Pa^{233} from the 233–234 mass ratio of the uranium produced. The yield of U^{233} gave the integrated neutron flux and the effective capture cross section of Th^{232} was taken to be 8.0 barns. The values obtained were 151 and 129 for the LITR and graphite reactor respectively. The average effective cross section for thermal reactor neutrons was given as 140 ± 20 barns.

This completes the information available at the time when the present investigation was begun. Recently the results of another investigation have become available. Smith and co-workers at the MTR have determined the cross section of Pa^{233} to form both isomeric states of Pa^{234} and their measurement is described in U.S. Atomic Energy Commission Report IDO-16226 (1955). Their method is very similar to the one used in the present investigation. They used an activation method in which samples of Pa^{233} were irradiated for a suitable time in the reactor and the yields of the isomeric states of Pa^{234} were determined by counting methods. Irradiations were made with and without 0.040-in. cadmium covers so that epithermal neutron effects could be separated from thermal effects. The thermal cross sections for formation of the 1.2-minute and 6.7-hour states were found to be 43 ± 5 and 25 ± 4 barns respectively, and the corresponding resonance capture integrals were 400 and 270 barns.

Smith and co-workers employed 0.03 in. diameter cobalt–aluminum alloy wires containing 0.52% cobalt to measure the cadmium ratio for cobalt in the irradiation positions they used. The thermal neutron capture cross section and resonance capture integral of Co^{59} were taken to be 37.0 barns and 41 barns respectively. Recent investigations of Johnston *et al.* (1960) and Eastwood and Werner (1959) have shown that there is a large amount of self-shielding in cobalt for neutrons of the resonance energy. It appears that adequate allowance for this effect was not made in early measurements of the cobalt resonance integral and therefore the results were too low. A more accurate value for dilute cobalt alloys of the type used by Smith *et al.* has been found to be 75 barns. It would appear that the resonance integrals obtained by Smith *et al.* should be increased by the factor 75/41. Self-shielding should also be considered in reactor neutron irradiations made without cadmium covers but Smith *et al.* made allowance for this so that their thermal neutron values are unaltered. The adjusted values of Smith *et al.* have been summarized in Table II.

TABLE II

Summary of the results of Smith *et al.* (1955), corrected for the change in the resonance integral of cobalt

	Reaction $Pa^{233}(n,\gamma)Pa^{234}$ (1.2 min)	Reaction $Pa^{233}(n,\gamma)Pa^{234}$ (6.7 hr)
Thermal neutron capture cross section, barns	43±5	25±4
Resonance capture integral, including $1/v$ part, barns	740	470

EXPERIMENTAL

As pointed out earlier the method used in the present investigation was very similar to that used by Smith and his associates. The rates of the Pa^{233} (n,γ) Pa^{234} (1.2 minute) and Pa^{233} (n,γ) Pa^{234} (6.7 hour) reactions were measured by determining the Pa^{234}–Pa^{233} disintegration-rate ratio in Pa^{233} samples irradiated for measured periods. This method has the advantage that the chemical processing of the irradiated protactinium need not be quantitative because by using suitable counting techniques the disintegration rates of both Pa^{233} and Pa^{234} can be determined in the same sample. Therefore chemical yields do not enter the calculation of the cross section. In order to separate the thermal neutron and resonance neutron effects some irradiations were made under cadmium. Cobalt was used as a flux monitor.

Irradiations

All irradiations were made in an empty lattice position of the NRX reactor at Chalk River (Hurst 1955) using a pneumatic "rabbit" to move the samples into and out of the reactor. About 0.01 μg (10^7 disintegrations per second) of Pa^{233} in the form of protactinium nitrate was evaporated in the bottom of a small sample capsule which was enclosed in a "super-pure" iron carrier capsule. A cobalt wire monitor, 0.005-in. diameter, 0.5-in. long, wrapped in aluminum foil, was placed in the carrier capsule beside the sample capsule. Subsidiary experiments showed that the spatial variation in flux in the irradiation position was less than 1%.

In the 1.2-minute Pa^{234} experiments irradiations without cadmium covers were made in nylon sample capsules because, in a short irradiation followed by a short decay period, nylon produces less interfering radioactivity than most container materials. Nylon capsules could not be used for irradiations under cadmium owing to the high temperature reached in these irradiations. Quartz capsules were therefore used and to minimize breakage they were packed in the carrier capsule with a little powdered graphite. Aluminum sample capsules were used for the 6.7-hour Pa^{234} irradiations.

The irradiations for the measurement of the 1.2-minute isomer were about two minutes long and the uncertainty in the length of irradiation had to be considered. As the capsule entered the reactor it was detected by a photocell which started an electric timer. On its return journey it passed the photocell again and stopped the timer. From the design of the apparatus and the speed at which the capsule travels it was estimated that about one second elapses

between the starting of the timer and the arrival of the capsule in the high flux position. A similar period elapses on the return trip. The length of the irradiation was therefore taken to be 2 seconds less than the reading on the timer and an uncertainty of one second in the length of irradiation was included in the estimates of the errors.

The decay time following the irradiation was measured by a timer which started when the capsule passed the photocell on the return journey.

The irradiations for the measurement of the 6.7-hour isomer were about 22 hours long and so timing was not an important source of error.

Preparation of Pa^{233}

The Pa^{233} used for the irradiation was prepared by the neutron irradiation of thorium and was purified by ion exchange. Dried $Th_2(CO_3)_3$ powder was irradiated for about two days and then after a suitable decay period it was dissolved in boiling concentrated HNO_3. After conversion to chloride it was dissolved in 8 *N* HCl and applied to an anion exchange column. The thorium was removed by washing with 8 *N* HCl and, to obtain a separation from uranium, the protactinium was eluted with redistilled 3.8 *N* HCl. After evaporation to dryness the product was metathesized to nitrate form with concentrated, redistilled HNO_3 and a stock solution 3 *N* in HNO_3 was prepared. Suitable amounts of the stock solution were taken for irradiation and evaporated to dryness in carefully washed sample capsules.

Purification of 1.2-minute Pa^{234}

The irradiated protactinium was separated from fission products and other impurities emitting β-particles by solvent extraction using 2-thenoyltrifluoroacetone (TTA). The separation was made in the sample capsule using 0.5 ml 0.4 *M* TTA in benzene and 0.5 ml 4 *N* HNO_3. Preliminary experiments showed that some Al^{28} and Zr^{97} was extracted with the protactinium into the organic phase but in the experiments reported here this was kept to a minimum by adding aluminum and zirconium holdback carriers to the HNO_3. The TTA–HNO_3 mixture was agitated for 40 seconds using a pipette. The mixture was then transferred to a small test-tube and, after the phases had separated, the organic layer was transferred to a preheated standard aluminum counting tray. The solution was evaporated to dryness and the tray was heated until decomposition of the organic matter was complete. After cooling the source was ready for counting. The time from the end of the irradiation to the beginning of counting was $2\frac{1}{4}$–$2\frac{1}{2}$ minutes.

When an irradiation was made in a quartz sample capsule a specially constructed stainless steel mortar and pestle were used to crush the capsule after irradiation. The extraction with TTA–HNO_3 was made in the mortar. The mixture was then transferred to a test tube for processing as described above.

Purification of 6.7-hour Pa^{234}

The protactinium from the longer irradiations was also purified by solvent extraction with TTA, but because the half-life of the product was longer greater care could be taken to obtain a good purification. The protactinium

was dissolved from the sample capsule using 1 ml of 5 N HNO_3 containing Na, Zr, and Cu holdback carriers. The protactinium was then extracted into 1 ml of 0.4 M TTA in benzene by mixing the two solutions vigorously with a pipette for 3 minutes. The phases were allowed to separate and the organic phase was transferred to a standard aluminum counting tray where the benzene was evaporated. The tray was heated to destroy the organic material. After cooling it was covered with paper tape and counted.

Measurement of Pa^{233}

In outline, the method consisted of counting the Pa^{233}, after the Pa^{234} had decayed, using an end-window proportional β-counter the efficiency of which was determined using sources of Pa^{233} made from a solution standardized by 4π β-counting.

Sources used for the measurement of the cross section for formation of the 1.2-minute isomer were covered with paper tape after the 1.2-minute isomer had decayed and were allowed to decay for at least 18 hours before the first measurement of Pa^{233}. They were then counted with an end-window methane-flow proportional β-counter. The decay of Pa^{233} was observed for 10 half-lives to be sure that it was radiochemically pure and the decay rate at the end of the irradiation was obtained by extrapolation of the decay curve. To allow for minor day-to-day variations in the efficiency of the counter a standard was counted after the Pa^{233} and the Pa^{233} count was corrected accordingly.

The efficiency of the end-window counter was determined using sources made from a Pa^{233} solution prepared as described in an earlier section and counted in a 4π methane-flow proportional counter. Redistilled reagents were used to minimize source thickness. Four aliquots of the Pa^{233} solution, ranging in size from 2 to 20 μl, were evaporated on gold-coated VYNS films with a total thickness of about 25 $\mu g/cm^2$ (Pate and Yaffe 1955). The aliquots were made to cover about the same area so that the source thickness varied, although the variation would not be a factor of 10 because dissolved material agglomerates on evaporation. It was found that the counting rate per unit volume of solution was independent of sample size. This is not an unusual observation and indicates that the sources are thin. Merritt *et al.* (1959), for example, found that with Nb^{95}, the maximum β^- energy of which is close to that of the main β^- group of Pa^{233}, the amount of self-absorption is constant at mean superficial thicknesses below 6 $\mu g/cm^2$.

To obtain the disintegration rate from the 4π counter data, self-absorption corrections must be considered. This subject has been discussed in several papers, the most pertinent of which is by Merritt *et al.* They have established a relationship between the amount of self-absorption and the maximum β^- energy for sources about 2 $\mu g/cm^2$ mean superficial density prepared by evaporation. The correction obtained for the self-absorption of the Pa^{233} β^- radiations is about 17% using this relationship. Considerable internal conversion follows the β^- decay of Pa^{233} and the conversion electrons have sufficient energy to be detected with high efficiency by the 4π counter. Also, they are in coincidence with the β^- particles. The presence of these conversion electrons reduces the self-absorption correction to about 4%. The reduction

cannot be estimated exactly because the decay of Pa^{233} is poorly understood. Fortunately, the uncertainty in the amount of self-absorption is not carried directly into the cross section result because it is the Pa^{234}–Pa^{233} disintegration rate ratio which enters the calculation. Nevertheless, as will be indicated in a later section in which all the errors are considered, the uncertainties in the 4π β-counting account for most of the error in the rate of reaction shown in Tables VI and XII.

Absorption of the β-particles of Pa^{233} in the VYNS film was studied by adding a second layer of gold-coated VYNS to the back of each source. No change in counting rate was observed and it was concluded that absorption in the source mount was negligible.

Five aliquots of the Pa^{233} solution were also evaporated on standard aluminum counting trays. The sources were covered with paper tape just as were the irradiated protactinium sources, and the counting rates were measured with the end-window counter. Because a total of about 10 mg/cm^2 of absorber was present in this counting arrangement differences in the thicknesses of the sources used for calibration and the irradiated protactinium sources themselves were considered to be unimportant.

The efficiency of the end-window counter for detecting Pa^{233} was thus found to be 0.231%. The standard deviation of this result was 2%.

Measurement of 1.2-minute Pa^{234}

The Pa^{234} content of the irradiated protactinium was determined using an anthracene crystal detector. The bias of the amplifier was adjusted so that pulses from the high energy β-particles of Pa^{234} were accepted and smaller pulses from Pa^{233} were rejected. The efficiency of the detector was determined using sources of 1.2-minute Pa^{234} in equilibrium with 24-day Th^{234} prepared from solutions standardized by 4π β-counting.

The detector was an anthracene crystal $1\frac{1}{2}$ in. diameter, 3/16 in. thick coupled to a DuMont 6292 photomultiplier tube using Silicone oil. The crystal and tube were covered with 0.0003 in. thick aluminum foil. In order to be certain that the source, crystal, and photomultiplier tube were coaxial, a brass positioning ring was placed over the assembly.

Standard aluminum trays were used for counting; they are 1 5/16 in. diameter and have a turned-up lip about 3/32 in. high. The lip served to confine the protactinium to a circle of diameter 1 3/16 in. The sources after they had been prepared as described earlier were turned upside down on top of the detector. The lip determined the source-to-anthracene distance and positioning ring placed the source over the center of the anthracene. A few tests showed that the efficiency of the detector was independent of the location of the protactinium on the tray, probably because the anthracene was larger than the area of the counting tray. This is essential because the protactinium could not be confined to a particular area on the tray owing to time limitations.

The output of the photomultiplier, after passing a cathode follower, went to a Franklin Electronic Company DD-2 linear amplifier and pulses above a certain bias were recorded on a scaler. The counting intervals were measured with a stop watch and in most experiments 15-second intervals were used

followed by 15 seconds for recording the counts and resetting the apparatus. Considerable care was taken to select the bias used to discriminate between the high energy Pa^{234} pulses and the less energetic ones from Pa^{233} so that changes in gain of the apparatus did not have a large effect on the efficiency. Corrections for minor day-to-day variations in efficiency were made by counting a standard source of 1.2-minute Pa^{234} in equilibrium with 24-day Th^{234} before and after each sample of irradiated protactinium.

The efficiency of the anthracene counter was determined by comparison with a 4π β-counter. Sources prepared from a solution of Pa^{234} in equilibrium with its parent Th^{234} were used. The Th^{234} was separated from natural uranium using solvent extraction and ion exchange methods (Dyrsseen 1950) and care was taken to minimize the solid content of the solution. The 4π counter detected β-particles from the decay of both Th^{234} and Pa^{234} but the anthracene counter recorded only the pulses from Pa^{234} decay; the electronic bias was such that the low energy pulses from Th^{234} were rejected. Furthermore, less than 1% of the 1.2-minute isomeric state decays to 6.7-hour Pa^{234} (Zijp *et al.* 1954). Therefore the Pa^{234} disintegration rate was taken to be one-half the corrected counting rate observed with the 4π β-counter.

Four aliquots of a Pa^{234}–Th^{234} solution were counted with the anthracene counter. A set of 5 aliquots was also evaporated on gold-coated VYNS films and counted in a 4π methane-flow proportional counter. The aliquots in the set of 5 were of different sizes varying by more than a factor of 20 and were made to cover about the same area of film. They were therefore of different superficial thickness although, as pointed out earlier, the actual thickness of source material would not be expected to vary by a factor of 20. The disintegration rate per unit volume of solution was found to be independent of sample size and it was concluded that the sources were thin. The correction for self-absorption given by Merritt *et al.* for such sources is about 15% if conversion electrons from Th^{234} are ignored or about 11% if the rather inadequate information on conversion electron abundance is used. This uncertainty is considered in the estimation of errors (Table VI).

Loss by absorption of β-particles in the VYNS film was investigated in the manner described for Pa^{233} and it was found that tripling the thickness of the film had no detectable effect on the counting rate and no correction was therefore made.

A second solution of Pa^{234}–Th^{234} was made and 4 equal-size aliquots were taken for 4π β-counting and 4 for measurement with the anthracene detector. The average value of the two efficiency determinations was $17.7 \pm 1.1\%$. The error shown is the deviation from the mean.

To compare this method of efficiency determination with that employed by Smith and his associates, their method was also used. Weighed amounts of finely ground natural U_3O_8 with Pa^{234} in equilibrium were spread on aluminum and platinum counting trays with the aid of a little ether. The superficial thickness ranged from 1 to 2 mg/cm^2. These were measured with the anthracene counter and a comparison of the results will be given in a later section.

Measurement of 6.7-hour Pa^{234}

The decay of the 6.7-hour isomer of Pa^{234} yields several γ-rays of energy greater than the highest γ-ray energy of Pa^{233} at 476 kev (Table I). It was therefore possible to use a NaI (Tl) crystal spectrometer to differentiate between Pa^{233} and 6.7-hour Pa^{234} in the irradiated protactinium. Because the large amounts of less energetic radiation from Pa^{233} saturate an unshielded NaI (Tl) crystal a lead absorber was interposed between the source and the crystal. The efficiency of the spectrometer for Pa^{234} was determined using sources prepared from a solution of 6.7-hour Pa^{234} which had been standardized by 4π β-counting.

A NaI (Tl) detector $1\frac{1}{4}$ in. $\times 1\frac{1}{4}$ in. diameter was used in conjunction with an RCA 5819 photomultiplier tube. After amplification the pulses from the photomultiplier were displayed on a 24-channel pulse height analyzer. The counts obtained in a measured counting period were plotted to give a spectrum and the sum of the counts in the energy range 0.80 to 1.03 Mev was taken to be the Pa^{234} count. To correct for small changes in gain and in efficiency of the apparatus a standard was counted before and after each measurement of irradiated protactinium. The 6.7-hour isomeric state of Pa^{234} in equilibrium with Th^{234} could not be used as a standard because the gamma rays from the decay of the 1.2-minute isomeric state are in the same energy range as those from the 6.7-hour state and are much more abundant. Therefore a Sc^{46} source was used as a standard. It has an 83.9-day half-life and gamma rays at 0.885 and 1.119 Mev. The position of the Sc^{46} γ-rays was used to determine the energy scale and the counting rate of Sc^{46} in the energy range 0.80 to 1.25 Mev was used to monitor the detector efficiency.

The major γ-activity in the irradiated protactinium after chemical purification was Pa^{233}. It has a prominent γ-ray of 313 kev energy and the source strengths were such that this radiation saturated the NaI (Tl) detector. Lead absorbers, usually 9 or 18 g/cm^2 (5/16 or 5/8 in. thick) were therefore used to attenuate the Pa^{233} γ-rays. The Pa^{233} γ-ray peak was still a prominent feature of the spectrum but contributed less than 5% of the initial Pa^{234} count rate in the 0.83–1.03 Mev region. Allowance for this and the counter background was made from the Pa^{234} decay curve.

The efficiency of the NaI crystal detector for 6.7-hour Pa^{234} was determined using sources standardized by the 4π β-counting method. Solutions of Pa^{234} were separated from parent Th^{234} by anion exchange using a method based on the work of Kraus and Moore (1950). The Th^{234} was obtained from natural uranium as described for the 1.2-minute isomer. A known fraction of each solution was evaporated on a gold-coated VYNS film and the counting rate was measured with a 4π methane-flow proportional β-counter. Care was taken to minimize the solid content of the sources and they were assumed to be thin. From Merritt *et al.* the self-absorption correction would be about 7% if the presence of conversion electrons is ignored or about 4% if the scanty information on the decay of Pa^{234} is used. The uncertainty thus introduced into the rate of reaction was included with the other errors (Table XII). Auxiliary

experiments similar to those described for Pa^{233} and 1.2-minute Pa^{234} were made and it was found that absorption of β-particles in the film was negligible. The remainder of each Pa^{234} solution was evaporated to dryness on standard aluminum trays and counted with the NaI detector. The Sc^{46} standard was counted with each Pa^{234} measurement and the decay of Pa^{234} was observed with both the 4π and the NaI counter in order to correct for the presence of a few per cent Th^{234} contamination.

The efficiency determination was made in triplicate and the average efficiency obtained using the 9 g/cm^2 absorber was found to be $(3.89\pm0.11)\times10^{-3}$%. The error given is the maximum deviation from the mean.

Flux Measurements

Cobalt wires, 0.005 in. diameter, 1/2 in. long were used as flux monitors for these experiments. The yield of Co^{60} from the short irradiations used for the 1.2-minute Pa^{234} experiments was measured with a NaI (Tl) crystal counter and the yield from the longer irradiations in the 6.7-hour Pa^{234} experiments was measured with a high pressure ionization chamber. The thermal neutron capture cross section of Co^{59} was taken to be 36.65 barns, the average of the activation and absorption values given in the summary by Hughes and Schwartz (1958) and the resonance integral was taken to be 75 barns (Johnston *et al.* 1960; Eastwood and Werner 1959). The Co^{60} half-life used for decay corrections was 5.28 years.

After a decay period of about a week the cobalt flux monitors used in the 1.2-minute Pa^{234} irradiations were weighed and the Co^{60} content was measured. A well-type NaI (Tl) crystal coupled to a DuMont 6292 photomultiplier tube served as the detector and a conventional cathode follower, linear amplifier, and scaler completed the apparatus. The bias of the amplifier was adjusted so that only pulses from γ-rays of energy greater than 570 kev were accepted for counting. The efficiency of the apparatus for Co^{60} was determined using two sources of Co^{60} prepared from a solution which had been standardized by 4π β-, γ-coincidence counting.

The cobalt monitors from the 6.7-hour Pa^{234} irradiations were also allowed to decay for at least a week before their weight and Co^{60} content were determined. The Co^{60} content of these wires was too high to be measured with the NaI counter and a high-pressure ionization chamber was used instead. The measurements were made by placing the cobalt monitor in a well which entered the chamber and the current produced was compared with that from a radium standard. The Co^{60} equivalent of the radium standard was determined using sources standardized by 4π β- and β-, γ-coincidence counting techniques. Further details of this method of measurement are given by Jervis (1957).

The self-shielding corrections to be applied to the observed $Co^{59}(n,\gamma)Co^{60}$ reaction rate in 0.005 in. diameter cobalt wire have been determined by Eastwood and Werner (1959). They are 1.06 ± 0.03 and 1.64 ± 0.05 for thermal and epithermal neutrons respectively. These corrections have been applied to the observed rates and give the corrected rates which appear in Tables III and VIII.

RESULTS

The thermal neutron capture cross section and the resonance integral were calculated from experimental observations using the convention proposed by Westcott (1958) and Westcott *et al.* (1958). The application of this convention to activation cross section methods has been discussed in detail elsewhere (Eastwood *et al.* 1958; Roy and Roy 1959). The symbols used in these references have been retained in the present work. The rate of the $Pa^{233}(n,\gamma)Pa^{234}$ reaction is:

$$R = \frac{(dN/dt)_{234}\lambda_{233}}{(dN/dt)_{233}(1-e^{-\lambda_{234}t})} \tag{1}$$

where $(dN/dt)_{234}/(dN/dt)_{233}$ is the ratio of disintegration rates of Pa^{234} and Pa^{233} at the end of the protactinium irradiation (destruction of Pa^{233} during the irradiation is negligible in these experiments), λ_{233} and λ_{234} are the decay constants of Pa^{233} and Pa^{234} respectively, and t is the length of irradiation. The effective cross section, $\hat{\sigma}$, is defined by the equation:

$$\hat{\sigma} = R/nv_0 \tag{2}$$

and is related to the thermal (2200 m/sec) cross section by the equation:

$$\hat{\sigma} = \sigma_0(g+r\sqrt{(T/T_0)}s_0). \tag{3}$$

The value of s_0 for infinitely dilute cobalt was taken to be 1.77 (Eastwood and Werner 1959). In cadmium ratio experiments the factor $r\sqrt{(T/T_0)}$ is related to the cadmium ratio, R_{Cd}, as follows:

$$r\sqrt{(T/T_0)} = \frac{1}{R_{Cd}(s_0+1/K)-s_0}. \tag{4}$$

The coefficient K depends on the thickness of cadmium used and the appropriate values were taken from Westcott *et al.* (1958).

The resonance integral excluding the $1/v$ part is given as:

$$\Sigma' = \sqrt{(\pi/4)}\, s_0\sigma_0 \tag{5}$$

and to obtain Σ, the total resonance integral which is usually quoted, the $1/v$ part equal to 0.44 σ_0, is added to Σ'.

In these experiments it is assumed that the Pa^{233} cross section follows the $1/v$ law in the thermal neutron region and therefore $g = 1$. Furthermore, it is assumed that the epithermal neutron flux per unit energy interval is proportional to $1/E$ in the irradiation position used.

Cross Section for the Production of 1.2-minute Pa^{234}

Four groups of measurements were made and the reactor was in steady operation during each group. There may have been minor changes in operating conditions between the groups. Each group consisted of one irradiation with cadmium cover and one without cadmium. The results of these experiments are

given in Tables III to V. The estimated errors are given in Table VI and a summary of the important conclusions appears in Table XIII. Comments on certain aspects of the results follow.

TABLE III

Flux measurements with cobalt for the $Pa^{233}(n,\gamma)Pa^{234}$ (1.2 min) reaction

Group	Uncovered $Co^{59}(n,\gamma)Co^{60}$ reaction rate $\times 10^{10}$ (sec^{-1})	Cadmium-covered $Co^{59}(n,\gamma)Co^{60}$ reaction rate $\times 10^{10}$ (sec^{-1})	Cadmium ratio for cobalt	$r\sqrt{(T/T_0)}$ $\times 10^2$	σ for cobalt $\times 10^{24}$ (cm^2)	$nv_0 \times 10^{-13}$ (cm^{-2} sec^{-1})
I	31.0_1	1.46_4	21.1_8	2.08_3	38.0_1	8.15_8
II	29.7_0	1.43_9	20.6_4	2.19_3	38.0_8	7.79_9
III	33.5_7	1.50_4	22.3_2	2.02_8	37.9_7	8.84_1
IV	31.9_7	1.54_8	20.6_4	2.19_8	38.0_8	8.39_5

TABLE IV

Rates of $Pa^{233}(n,\gamma)Pa^{234}$ (1.2 min) reaction

Group	Pa^{233} disint. rate $\times 10^{-5}$ (sec^{-1})	Pa^{234} (1.2 min) disint. rate $\times 10^{-3}$ (sec^{-1})	$1-e^{-\lambda_{234}t}$	Rate $\times 10^{10}$ (sec^{-1})
		Uncovered		
I	7.83_2	4.47_9	0.686_2	24.7_4
II	5.16_6	3.18_6	0.686_5	26.6_7
III	8.18_0	5.19_2	0.686_2	27.4_7
IV	13.0_7	7.19_0	0.686_8	23.7_8
		Covered		
I	24.3_2	5.18_9	0.684_7	9.24_9
II	46.1_1	10.6_5	0.685_0	10.0_1
III	47.6_2	8.51_1	0.685_9	7.73_5
IV	41.7_8	8.82_8	0.685_3	9.15_3

TABLE V

Cross sections for the $Pa^{233}(n,\gamma)Pa^{234}$ (1.2 min) reaction

Group	$\hat{\sigma}$ for Pa^{233} $\times 10^{24}$ (cm^2)	Cadmium ratio for Pa	s_0 for Pa^{233}	σ_0 for Pa^{233} $\times 10^{24}$ (cm^2)	Σ' for Pa^{233} $\times 10^{24}$ (cm^2)	Σ for Pa^{233} $\times 10^{24}$ (cm^2)
I	30.3	2.68	29.5	18.8	491	499
II	34.2	2.66	28.1	21.1	527	536
III	31.1	3.55	20.0	22.1	392	402
IV	28.3	2.60	29.3	17.2	448	455
Averages	31.0		26.7	19.8	464	473

The decay of irradiated protactinium from uncovered irradiations was resolved graphically into three components with half-lives in the ranges 1.03–1.20 minutes, 3.4–5.9 minutes, and 40–150 minutes. The first period was taken to be Pa^{234} and the counting rate at the end of the irradiation was obtained by extrapolation of this component. It accounted for 70–80% of the activity at the end of the irradiation. The other periods could not be assigned definitely to particular nuclides.

The Pa^{234} counting rate at the end of the irradiation was also obtained by fitting three components, one of which had the accepted half-life of Pa^{234} (1.175 minutes), to the decay data using the method of least squares. A Datatron digital computer was used for this calculation. The results obtained agreed with those obtained graphically to within 10% and there was no systematic variation in the two methods. The average of the results obtained by the two methods was used.

The decay of the protactinium from irradiations under cadmium showed only two components, one with a half-life in the range 1.08 to 1.25 minutes and the other longer than 150 minutes. Because the decay data were simpler only the graphical method of analysis was used. The short-lived component which was taken to be Pa^{234} accounted for 22–88% of the total activity.

A summary of the estimated errors in the measurements is given in Table VI. Errors are considered to be of two types: first, random or non-systematic errors which are reflected in the deviation of the individual measurements

TABLE VI

Errors in the cross sections of the $Pa^{233}(n,\gamma)Pa^{234}$ (1.2 min) reaction

(*a*) Errors in σ_0		
Non-systematic errors (2×std. dev. of average σ_0)		11%
Systematic errors in rate of reaction		13%
Systematic errors in nv_0		6%
Systematic errors in $(1+rs)$		2%
	Quadrature sum	18%
(*b*) Errors in Σ'		
Non-systematic errors (2×std. dev. of average Σ')		13%
Systematic errors in σ_0		14%
Systematic errors in s_0		5%
	Quadrature sum	20%

from the mean and second, systematic errors which may affect all measurements in the same direction. We have taken the non-systematic error in the average value of σ_0 and Σ' to be twice the standard deviation calculated from the results of the individual measurements given in Tables IV and V.

The most important systematic error is in the determination of the efficiency of the counters for Pa^{234} and Pa^{233}. These determinations rest upon the standardization of Pa^{233} and Pa^{234}–Th^{234} solutions by 4π β-counting. As mentioned earlier, contributions from conversion electrons make the self-absorption corrections uncertain but they are about the same for Pa^{233} and Pa^{234}. They have therefore been taken to be equal and, because of the uncertainty thus introduced, an error of 10% has been assigned to the disintegration rate ratio. This, together with systematic errors of 4, 6, and 1% in the reproducibility of the efficiencies of the Pa^{233} and Pa^{234} counters and the saturation factor, $1-\exp(-\lambda_{234}t)$, when added in quadrature gives a total systematic error of 13% in the rate of reaction.

The systematic error in nv_0 includes a 1.5-barn uncertainty in the Co^{59} cross section, 3% uncertainty in the self-shielding corrections for cobalt, and

1% error in measuring the duration of the irradiation. The largest part of the systematic error in $(1+rs)$ and s_0 listed in Table VI is connected with the uncertainty about the direction of incidence of neutrons on the cadmium-shielded samples and the proper value of Westcott's coefficient K to use for the calculations.

It will be observed that the capture cross section and resonance integral for the formation of the 1.2-minute state of Pa^{234} are about one half the values reported by Smith *et al.* summarized in Table II. Two possible reasons for this discrepancy have been studied. The first is the loss of Pa^{234} by recoil into, or "hot atom" reaction with, the nylon walls of the sample capsule. In order to determine the magnitude of this effect four additional measurements were made with the protactinium in a different environment. In the first of these 500 μg of $Ca(NO_3)_2$ was dissolved in the Pa^{233} solution before irradiation. The solution was evaporated to dryness in a nylon sample capsule and then irradiated. The second and third irradiations were the same except that in these the Pa^{233}–$Ca(NO_3)_2$ solution was evaporated on 1 mg $CaCO_3$ and then irradiated in a nylon capsule. In the fourth irradiation Pa^{233} solution, with $Ca(NO_3)_2$, was evaporated in a quartz capsule and sealed. After the irradiation the capsule was crushed in the stainless steel mortar and pestle and the fragments were treated with the usual TTA–HNO_3 mixture. In these experiments recoil protactinium atoms would be expected to dissolve with the bulk of the protactinium and calcium salts. Isotope fractionation should be minimized although the possibility that the Pa^{234} is in a chemical form which is not extracted by TTA under the conditions of our experiments is not eliminated. It was observed that protactinium from these irradiations was less pure than protactinium from the irradiations in nylon mentioned earlier. Nevertheless, a component with half-life 0.9–1.2 minutes was resolved in each experiment and it accounted for 17–60% of the total activity. The results obtained are shown in Table VII. Since the effective cross sections agree

TABLE VII

Cross section for the $Pa^{233}(n,\gamma)Pa^{234}$ (1.2 min) reaction on various substrates

Substrate	n_0v_0 from cobalt monitor $\times 10^{-13}$ (cm^{-2} sec^{-1})	Pa^{233} disint. rate $\times 10^{-5}$ (sec^{-1})	Pa^{234} (1.2 min) disint. rate $\times 10^{-3}$ (sec^{-1})	$1-e^{-\lambda t}$	Rate of Pa reaction $\times 10^{10}$ (sec^{-1})	$\hat{\sigma}$ for Pa $\times 10^{24}$ (cm^2)
$Ca(NO_3)_2$	7.78	3.57	1.37	0.686	16.6	21.4
$Ca(NO_3)_2+CaCO_3$	7.62	46.9	26.8	0.686	24.8	32.5
$Ca(NO_3)_2+CaCO_3$	7.67	41.6	21.1	0.686	21.9	28.6
$Ca(NO_3)_2$ in quartz	7.40	86.9	18.7	0.686	9.29	12.6

reasonably well with the values in Table V and are at any rate no larger it was concluded that a preferential loss of Pa^{234} during irradiation was not a significant source of error. The data from these auxiliary experiments using different substrates were not included in the calculation of the final results.

The other reason for the discrepancy may be in the measurement of the efficiency of the Pa^{234} detector. Smith *et al.* used the 1.2-minute Pa^{234} in

equilibrium with a weighed amount of natural uranium as a standard whereas Pa^{234}–Th^{234} equilibrium mixture was used in the present work. The Pa^{234}–U^{238} sources used by Smith *et al.* were thick compared to the irradiated protactinium sources. However, they argued that scattering and absorption effects should be small for the energetic electrons emitted by 1.2-minute Pa^{234}. Platinum mounts were used by Smith *et al.* and differences in the number of backscattered electrons detected from sources of different thicknesses might be expected to be more important when platinum is the backing than when aluminum is used, although here again the difference might be small owing to the high average energy of the Pa^{234} β-particles. Smith *et al.* allow for 10% uncertainty in the determination of the Pa^{234} disintegration rate but an experimental foundation for this allowance seemed desirable and therefore an intercomparison of the methods was made.

Measurements of the efficiency of our anthracene counter were made using Pa^{234}–U^{238} and Pa^{234}–Th^{234} equilibrium sources prepared and standardized as described in an early section. It was found that for sources mounted on aluminum the detection efficiency obtained using Pa^{234}–Th^{234} sources was about 6% higher than that obtained using Pa^{234}–U^{238} equilibrium sources of the type used by Smith *et al.* It was also found that the increase in the contribution of backscattered electrons to the counting rate on going from aluminum- to platinum-backed sources was greater for the thinner Pa^{234}–Th^{234} sources by about 2%. These observations confirm the estimates of Smith *et al.* and show that these factors are not responsible for the discrepancy.

Cross Section for the Production of 6.7-hour Pa^{234}

Nine experiments were made, five without cadmium and four with 0.025-in. cadmium covers. The results obtained from individual experiments are given in Tables VIII to X. The method of obtaining σ_0 and Σ' is shown together with the results in Table XI. A summary of the estimated errors is given in Table XII and, finally, the important conclusions are presented in Table XIII. Comments about certain aspects of the measurements are given in the paragraphs which follow.

TABLE VIII

Flux measurements with cobalt for $Pa^{233}(n,\gamma)Pa^{234}$ (6.7 hr) reaction

Expt. number	Uncovered $Co^{59}(n,\gamma)Co^{60}$ rate $\times 10^{10}$ (sec^{-1})	Cadmium thickness (in.)	Cadmium-covered rate $\times 10^{10}$ (sec^{-1})	Cadmium ratio for cobalt	$r\sqrt{(T/T_0)}$ $\times 10^2$	$\hat{\sigma}$ for cobalt $\times 10^{24}$ (cm^2)	$n v_0$ $\times 10^{-13}$ (cm^{-2} sec^{-1})
1	26.9_2	0.025	1.45_0	18.5_7	2.47_6	38.2_6	7.03_6
2	28.8_4	0.025	1.42_7	20.2_1	2.20_4	38.0_8	7.57_4
3	25.0_9	0.025	1.35_2	18.5_6	2.47_3	38.2_6	6.55_8
4	25.9_7	0.025	1.24_7	20.8_2	2.13_8	38.0_4	6.82_7
5	24.6_9	0.025	1.41_8	17.4_1	2.56_2	38.3_0	6.44_6
6	27.0_8	0.025	1.39_7	19.3_6	2.37_0	38.1_9	7.08_2
7	27.9_8	0.025	1.49_6	18.7_8	2.37_6	38.1_9	7.32_0
8	25.5_4	0.025	1.40_7	18.1_8	2.53_6	38.3_0	6.66_2
9	26.4_5	0.030	1.33_1	19.8_8	2.25_0	38.1_2	6.94_0
10	24.9_4	0.025	1.33_8	18.6_4	2.39_2	38.1_9	6.53_2
11	23.9_0	0.040	1.20_2	19.8_7	2.34_0	38.1_7	6.26_1

TABLE IX

Effective cross section for $Pa^{233}(n,\gamma)Pa^{234}$ (6.7 hr) reaction

Expt. number	Pa^{233} disint. rate $\times 10^{-6}$ (sec^{-1})	Pa^{234} (6.7 hr) disint. rate $\times 10^{-4}$ (sec^{-1})	$1-e^{-\lambda_{234}t}$	Uncovered $Pa^{233}(n,\gamma)Pa^{234}$ rate $\times 10^{10}$ (sec^{-1})	$\hat{\sigma}$ for Pa^{233} $\times 10^{24}$ (cm^2)
1	5.11_1	3.42_0	0.898_7	22.1_1	31.4
3	4.28_5	2.03_8	0.670_7	21.0_5	32.1
5	7.28_5	3.80_2	0.898_7	17.2_3	26.7
8	3.09_7	1.97_8	0.887_6	21.3_6	32.0
10	3.13_2	1.83_5	0.892_2	19.4_0	29.8
					Average 30.4

TABLE X

Cadmium ratios and s_0 values for the $Pa^{233}(n,\gamma)Pa^{234}$ (6.7 hr) reaction

Expt. number	Pa^{233} disint. rate $\times 10^{-6}$ (sec^{-1})	Pa^{234} (6.7 hr) disint. rate $\times 10^{-2}$ (sec^{-1})	$1-e^{-\lambda_{234}t}$	Cadmium-covered Pa rate $\times 10^{10}$ (sec^{-1})	Calculated uncovered rate $\times 10^{10}$ (sec^{-1})	Cadmium ratio	s_0	$1+r$ $\sqrt{(T/T_0)}s_0$
2	1.10_8	3.09_2	0.898_7	9.20_7	23.0	2.50	29.4	1.65
4	86.3_8	205.8	0.898_7	7.87_9	20.8	2.64	29.8	1.64
6	2.48_1	4.56_8	0.757_3	7.21_9	21.5	2.98	20.5	1.49
7	20.6_4	44.6_0	0.706_4	9.08_1	22.3	2.45	28.2	1.67
						Averages	27.0	1.61
9	10.9_2	21.8_6	0.899_7	6.60_1	21.1	3.20	19.5	1.44
11	9.49_1	19.6_2	0.886_6	6.92_6	19.0	2.75	23.7	1.55

It was found that the radiochemical purity of the Pa^{234} was excellent. In all but one irradiation without cadmium, Pa^{234} was the only short-lived nuclide present and accounted for more than 99% of the counting rate observed at the end of the irradiation. In the exception, Mn^{56} was present to the extent of 60%. In irradiations under cadmium 90–99% of the activity observed at the end of the irradiation was Pa^{234} in three of the four experiments. An unidentified short-lived activity was present to the extent of 45% in one experiment. A graphical analysis of the decay data was therefore entirely satisfactory.

The irradiations were usually 22 hours long and required careful planning to fit them into the irradiation program of the Branch. Furthermore observations of the decay of Pa^{234} occupied the counting apparatus for several days after each irradiation. For these reasons the irradiations were made at intervals of a week or more and the reactor operating conditions were usually different for each experiment. This necessitated a somewhat different approach to the analysis of the results than that used for the 1.2-minute Pa^{234} measurements. In order to characterize the neutron spectrum for each experiment an auxiliary cobalt monitor was irradiated after each protactinium irradiation. If the protactinium sample and the monitor which accompanied it were cadmium-covered the auxiliary monitor was not covered during its irradiation and vice versa. The rates of the reaction in uncovered irradiations were calculated using equation (1) and from this the effective cross section for each individual experiment and the average for all five was obtained (Tables VIII and IX).

In order to arrive at the thermal neutron cross section and the resonance integral a knowledge of the cadmium ratio for protactinium is required. Normally this would be obtained from irradiations made under similar reactor conditions but since this was not possible the observed rate of the $Pa^{233}(n,\gamma)Pa^{234}$ (6.7-hour) reaction under cadmium was compared with the rate without cadmium calculated using the observed nv_0 and average value of the effective cross section. The factors s_0 and $(1+rs)$ for each covered irradiation were then obtained (Table X). An average value of σ_0 was then deduced by dividing the average $\hat{\sigma}$ by the average $(1+rs)$ and similarly an average Σ' was calculated from the average σ_0 and average s_0. These manipulations are shown in Table XI.

TABLE XI

Calculation of the average σ_0 and Σ values for the $Pa^{233}(n,\gamma)Pa^{234}$ (6.7 hr) reaction

Average value $\hat{\sigma}$ (Table IX) and std. dev. of average = 30.4±1.0 barns
Average value s_0 (Table X) and std. dev. of average = 27.0±2.2
Average value $(1+rs)$ and std. dev. of average = 1.61±0.04
σ_0 = average $\hat{\sigma}$/average $(1+rs)$ = 18.9±0.8 barns
Σ'(resonance integral, excess over $1/v$ part, from 0.5 ev to ∞)
$= \sqrt{(\pi/4)}$ (average s_0) (average σ_0) = 452±41 barns
Σ (resonance integral including $1/v$ part, from 0.5 ev to ∞)
$= 0.44\,\sigma_0+\Sigma'$ = 460±41 barns

In a second approximation the rate of the uncovered reaction in the individual experiments was calculated from the measured nv_0 and $r\sqrt{(T/T_0)}$ values and the s_0 values obtained from the first approximation. The average σ_0 and Σ' values deduced from the second approximation agreed with those from the first.

A summary of the estimated errors is given in Table XII. Here again it is seen that a major source of systematic error is in the determination of the rate

TABLE XII

Errors in the cross section of the $Pa^{233}(n,\gamma)Pa^{234}$ (6.7 hr) reaction

(*a*) Errors in σ_0 (= average $\hat{\sigma}$/average $(1+rs)$)	
Non-systematic errors in $\hat{\sigma}$ (2×std. dev. of average $\hat{\sigma}$)	7%
Non-systematic errors in $1+rs$ (2×std. dev. of average $1+rs$)	5
Systematic errors in rate of reaction	12
Systematic errors in nv_0	6
Systematic errors in $(1+rs)$	2
Quadrature sum	16%
(*b*) Errors in Σ' (= $\sqrt{(\pi/4)}$×average s_0×average σ_0)	
Non-systematic errors in s_0 (2×std. dev. of average s_0)	16%
Systematic errors in s_0	5
Total errors in σ_0	16
Quadrature sum	23%

of reaction. As pointed out in an earlier section a large fraction of this error is associated with the determination of the disintegration rate of Pa^{233} and Pa^{234}. The systematic error in nv_0 includes the uncertainty in the capture cross

section of Co^{59} and in the self-shielding corrections for cobalt. The error in s_0 is connected with the uncertainty in the choice of K just as was the case with the 1.2-minute Pa^{234} measurements.

In order to investigate the position of the resonance or resonances responsible for the large resonance integral two additional experiments were made with 0.03 and 0.04 in. thick cadmium covers, the effective cutoff energies of which are about 0.5 and 0.55 ev respectively. The results are shown for experiments 9 and 11 in Tables VIII and X. The values for σ_0 and Σ' determined from these experiments agree, within experimental error, with the values obtained using 0.025-in. cadmium. It is concluded therefore that there is no large resonance near 0.5 ev.

SUMMARY AND DISCUSSION

The results obtained for the neutron capture cross section and resonance capture integral of Pa^{233} in the reactions $Pa^{233}(n,\gamma)Pa^{234}$ (1.2 minute) and $Pa^{233}(n,\gamma)Pa^{234}$ (6.7 hour) are summarized in Table XIII. The convention

TABLE XIII

Summary of results

	Reaction $Pa^{233}(n,\gamma)Pa^{234}$ (1.2 min)	Reaction $Pa^{233}(n,\gamma)Pa^{234}$ (6.7 hr)
Thermal neutron capture cross section, σ_0, barns	20±4	19±3
Resonance capture integral, excess over $1/v$ part, 0.5 ev to ∞, Σ', barns	460±90	450±100
Resonance capture integral, including $1/v$ part, 0.5 ev to ∞, Σ, barns	470±90	460±100
s_0	27±5	27±5
Effective cross section in NRX lattice position ($r\sqrt{(T/T_0)} = 0.023$), barns	32±5	31±5
Effective cross section ($r\sqrt{(T/T_0)} = 0.05$), barns	47±9	45±9

proposed by Westcott has been used to analyze the experimental data. In this treatment it is assumed that Pa^{233} is a $1/v$ absorber in the thermal energy region (i.e. $g = 1$) and that the epithermal neutron flux is proportional to $1/E$ per unit energy interval.

Experiments using different thicknesses of cadmium cover indicate that there is no large resonance for the formation of the 6.7-hour isomeric state of Pa^{234} near the cadmium cutoff (0.5 ev).

The results for the 6.7-hour Pa^{234} agree with those of Smith *et al.* but differ from theirs by a factor of 2 for the 1.2-minute isomer. It has been shown experimentally that the discrepancy between our results and those of Smith *et al.* cannot be ascribed to differences in the method of measuring the Pa^{234} produced nor to the loss of Pa^{234} by recoil or "hot atom" reactions although the possibility that the Pa^{234} is in a chemical form which is not extracted by TTA has not been eliminated. The reason for the discrepancy remains unresolved.

A comparison of our results with the earlier results of Halperin *et al.* or Katzin and Hagemann is difficult because the neutron spectra in which they made their irradiations are not known. If we assume a value of 0.05 for $r\sqrt{(T/T_0)}$ for their experiments, which is not unreasonable for a graphite-moderated reactor, the effective cross section for formation of both states of Pa^{234} calculated from the results in Table XIII is 92 ± 13 barns. This result is lower than the value obtained by Halperin *et al.* (140 ± 20 barns) but higher than the value of Katzin and Hagemann (55 ± 6 barns). The presence of such a large resonance means that the effective cross section is very dependent on the neutron spectrum and therefore the lack of agreement between the various effective cross sections is not surprising.

ACKNOWLEDGMENTS

We are grateful to Mrs. J. Merritt and Dr. P. J. Campion, who provided standardized Co^{60} sources, and to Dr. J. M. Kennedy, who made the Datatron analysis of the 1.2-minute Pa^{234} decay data.

REFERENCES

Dyrsseen, D. 1950. Svensk Kem. Tidskr. **62**, 153.
Eastwood, T. A., Baerg, A. P., Bigham, C. B., Brown, F., Cabell, M. J., Grummitt, W. E., Roy, J. C., Roy, L. P., and Schuman, R. P. 1958. International Conference on the Peaceful Uses of Atomic Energy, A/Conf. 15/P/203.
Eastwood, T. A. and Werner, R. D. 1959. Atomic Energy of Canada Limited Report CI-207. Unpublished.
Halperin, J., Stoughton, R. W., Ellison, C. V., and Ferguson, D. E. 1956. Nuclear Sci. and Eng. **1**, 1.
Halperin, J., Stoughton, R. W., Ferguson, D. E., Ellison, C. V., Overholt, D. C., and Stevens, C. M. 1955. Proceedings of the International Conference on the Peaceful Uses of Atomic Energy, **7**, 258.
Hughes, D. J. and Schwartz, R. B. 1958. U.S. Atomic Energy Commission Report BNL-325, 2nd ed.
Hurst, D. G. 1955. Proceedings of the International Conference on the Peaceful Uses of Atomic Energy, **5**, 111.
Jervis, R. E. 1957. Atomic Energy of Canada Limited Report CRDC-730.
Johnston, F. J., Halperin, J., and Stoughton, R. W. 1960. J. Nuclear Energy. A. Reactor Science, **11**, 95.
Katzin, L. I. and Hagemann, F. 1952. U.S. Atomic Energy Commission Report TID-5223, Part 2, p. 543.
Kraus, K. A. and Moore, G. E. 1950. J. Am. Chem. Soc. **72**, 4293.
Merritt, J. S., Taylor, J. G. V., and Campion, P. J. 1959. Can. J. Chem. **37**, 1109.
Pate, B. D. and Yaffe, L. 1955. Can. J. Chem. **33**, 15.
Roy, J. C. and Roy, L. P. 1959. Can. J. Phys. **37**, 907.
Smith, R. R., Passell, T. O., Reeder, S. D., Alley, N. P., and Heath, R. L. 1955. U.S. Atomic Energy Commission Report-IDO 16226.
Stoughton, R. W. and Halperin, J. 1959. Nuclear Sci. and Eng. **6**, 100.
Strominger, D., Hollander, J. M., and Seaborg, G. T. 1958. Revs. Modern Phys. **30**, 585.
Westcott, C. H. 1958. Atomic Energy of Canada Limited Report No. 670.
Westcott, C. H., Walker, W. H., and Alexander, T. K. 1958. International Conference on the Peaceful Uses of Atomic Energy, A/Conf. 15/P/202.
Zijp, W. J., Tom, Sj., and Sizoo, G. J. 1954. Physica, **20**, 727.

THE DISTRIBUTION OF RADIO-AURORA IN CENTRAL CANADA[1]

P. A. Forsyth, F. D. Green, and W. Mah

ABSTRACT

Five bistatic v.h.f. radio systems were operated in central Canada during the I.G.Y. for the purpose of detecting auroral ionization. Consistent records were obtained for a period of 5 months and these records have now been analyzed. Two types of events were detected. The nighttime (*A*) events occur most frequently in the auroral zone and characteristically are observed simultaneously at two points separated by about 300 kilometers. The daytime (*S*) events occur simultaneously over a much larger area. The time of maximum occurrence of *A* events becomes later with decreasing latitude whereas the reverse is true for *S* events. The variation with latitude of the occurrence of *A* events is similar to that of other auroral phenomena.

INTRODUCTION

The term "radio-aurora" has been used to indicate the ionospheric ionization, associated with auroral disturbances, that gives rise to radio reflections in the very-high and ultra-high frequency ranges. The degree of association between the radio-aurora and the visible or optical aurora is still uncertain. Some of the early work (see, for example, Currie, Forsyth, and Vawter 1953) did suggest a very close association for certain specific instances but recently Gadsden (1959) has concluded, on the basis of statistical studies, that no such association exists. It is clearly of some importance to establish the statistical characteristics of the radio-aurora in order to compare them with those of the optical aurora. While most observations of radio-aurora have been carried out with radar (backscatter) systems in which the radio transmitter and receiver are situated at the same station, some studies have been made recently using bistatic systems in which the transmitter and receiver are separated by a distance of about 1000 kilometers (Forsyth and Vogan 1957; Collins and Forsyth 1959). These studies were started in an effort to provide a simple method of studying radio-aurora that might be free from some of the observational bias that may operate in the case of backscatter observations. As part of the Canadian program for the International Geophysical Year the existing network of bistatic systems was extended to include five new circuits operating at a frequency of 38.07 Mc/s and five operating at a frequency of 49.99 Mc/s. The transmitters were located at Yellowknife, N.W.T., and the receivers were located at Baker Lake, Churchill, The Pas, Saskatoon, and Sulphur Mountain (near Banff, Alberta). The technical details of these circuits, together with examples of the records and a discussion of the method of analysis have been given in the earlier paper (Collins and Forsyth 1959), but for convenience a map of central Canada showing the location of the various stations is given in Fig. 1 and some details of the paths are given in

[1]Manuscript received March 21, 1960.
Contribution from the Institute of Upper Atmospheric Physics, University of Saskatchewan, Saskatoon, Saskatchewan. This work was supported in part under DRB Contract No. 700121 with the Defence Research Telecommunications Establishment.

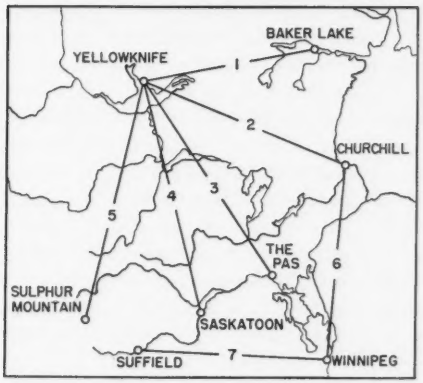

FIG. 1. Map showing the location of the transmission paths in central Canada.

Table I. Several changes were made in the equipment during the I.G.Y., some because of instrumental difficulties and some in an effort to examine more carefully particular features of the scattered signals. As a result, the longest

TABLE I

The radio circuits used for the I.G.Y. study

Path No.	Receiver location		Path length, km
1	Baker Lake	64.3° N., 96.2° W.	900
2	Churchill	58.8° N., 94.0° W.	1120
3	The Pas	53.8° N., 101.3° W.	1180
4	Saskatoon	52.2° N., 106.6° W.	1200
5	Sulphur Mountain	51.2° N., 115.6° W.	1200

NOTE: Common transmitters located at Yellowknife (62.5° N., 114.5° W.); frequencies, 38.07 Mc/s and 49.99 Mc/s; radiated power, 700 watts.

continuous period for which consistent recordings are available is one of about 5 months starting 1 December, 1957. The purpose of this paper is to record some of the results revealed by analysis of these recordings.

ANALYSIS OF THE RECORDINGS

The earlier work (Collins and Forsyth 1959) established the occurrence of two classes of events, designated as '*A*' and '*S*' events, that appeared to increase in frequency of occurrence as the auroral zone was approached. Each of these events was indicated on the signal record by a period of strong enhancement of the received signal strength. The *S* events occurred primarily during the daylight hours and were not associated with magnetic disturbances. The principal reason for suggesting that they might properly be included with the other forms of radio-aurora was the increase of occurrence with increasing geomagnetic latitude. The *A* events occurred primarily at night and were associated with magnetic disturbance. Three subclasses of *A* events, designated

A_1, A_2, and A_3 were distinguishable on the records, of which A_2 events seemed to be most closely associated with visible aurora, A_1 events, always short-lived, with the earlier stages, and A_3 events with the later stages of the auroral occurrence.

For the 5-month period covered by the present analysis the bistatic systems were intentionally operated at very low sensitivity in order that only the major events would be recorded. A preliminary analysis revealed that for this mode of operation very few A_3 events were detected. As was expected from the earlier work, only one or two, doubtful, A_1 events were detected. In consequence, it was decided to retain only the A and S designations in the analysis although it should be borne in mind that nearly all, if not all, of the A events were actually of the A_2 type. In addition, presumably because of the reduced sensitivity, very few events were detected at the higher frequency. The detailed analysis was restricted therefore to the lower frequency (38.07 Mc/s).

The available records were divided into 15-minute intervals and the presence or absence of an event for each path for each interval was noted. This initial record scaling was carried out for the most part by one of the authors who had no previous experience with records of this type. It is encouraging to note that working only from the descriptions and illustrations of the earlier paper, he was able to recognize the various events and classify them without difficulty. The total number of recording intervals for which the records could be scaled is given for each path in Table II, together with the percentage occurrence of A and S events. It may be noted from the table that while the first four paths each yielded some 11,000 useful recording intervals, the fifth path (Yellowknife–Sulphur Mountain) yielded only about 5000 intervals. This was because of local difficulties with equipment and interference at the receiving station.

VARIATION WITH GEOMAGNETIC LATITUDE

The variation of occurrence of S events with latitude is indicated in Table II. There is a slight decrease of occurrence for path 2 (Yellowknife–Churchill)

TABLE II

The relative occurrence of events for each of the paths

		% occurrence	
Path No.	Recording intervals	A	S
1	11,712	7.8	16.9
2	11,808	12.1	12.7
3	11,712	9.3	18.7
4	11,808	7.1	17.9
5	5,232	2.1	4.0

the mid-point of which lies close to the maximum of the auroral zone. It is hard to decide on the basis of the present evidence if this decrease is significant. It may be that the high occurrence of both A and S events for this path has

caused some of the *S* events to be masked by *A* events but this seems unlikely. Alternatively, there may be a higher incidence of daytime absorption for path 2 than for the other paths which would reduce the apparent rate of occurrence of *S* events. Until further confirmation of this latitudinal distribution is obtained it is probably not wise to attempt any further interpretation of the observed variation.

The *A* events are more likely to behave in a manner that is similar to other auroral phenomena. It is interesting to compare the observed latitudinal variation of occurrence of *A* events with that derived by Vestine (1944) from optical and magnetic measurements. The relative occurrence of auroral phenomena found by Vestine for longitudes close to that of Saskatoon is plotted against geomagnetic latitude as the solid line in Fig. 2. In the same

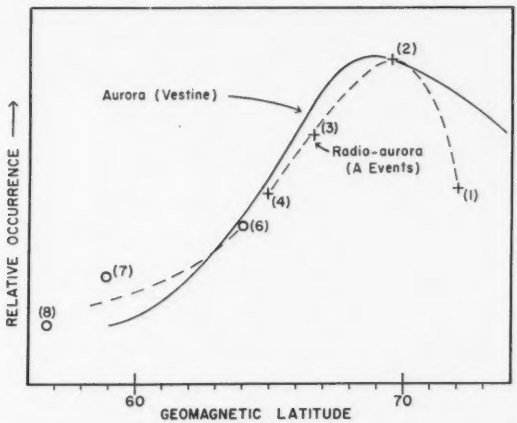

FIG. 2. The relative occurrence of radio-aurora (*A* events) and visible aurora (after Vestine) as a function of geomagnetic latitude.

figure the relative occurrence of *A* events for each of the four most northerly paths is plotted (as a cross) against the geomagnetic latitude of the path midpoint. The value for path 5 (Yellowknife–Sulphur Mountain) is omitted because of its doubtful validity. In order to fill in the diagram for lower latitudes the relative occurrence for three of the paths used in the earlier investigation, Churchill–Winnipeg (6), Suffield–Winnipeg (7), and Greenwood–Ottawa (8) are included. Because of the different sensitivities and the different periods of observation the absolute values of occurrence for these paths can not be compared directly with those observed on the northern paths. For this reason a scaling factor was introduced to adjust the occurrence rates on paths 6, 7, and 8 such that the value for path 6 was in reasonable agreement with the values for paths 3 and 4.

There seems to be no doubt that the general trend of the occurrence of *A* events as a function of geomagnetic latitude is similar to that deduced by Vestine. The observations were made over a period of only 5 months and the

values plotted in Fig. 2 might be changed substantially in any long-time average. In addition, the previous work has shown that the scattered signals do not originate exclusively from ionization near the path mid-points. Particularly for east–west paths, the scattering may take place in regions located two or three hundred kilometers to the north of the path mid-point. This argument might be used to justify the movement on the graph of Fig. 2 of the points (1), (7), and (8) as much as two or three degrees toward higher latitudes. If this were done the agreement with Vestine's curve would be much better. In any case, these particular measurements could hardly be used to establish, or to verify, the precise position of the auroral zone; however, it does seem likely that the zone of maximum occurrence of radio-aurora is closely associated with that for optical aurora.

DIURNAL VARIATIONS

The diurnal variation of occurrence for each of the five paths is shown separately for the A and S events in Fig. 3. Also included are the histograms

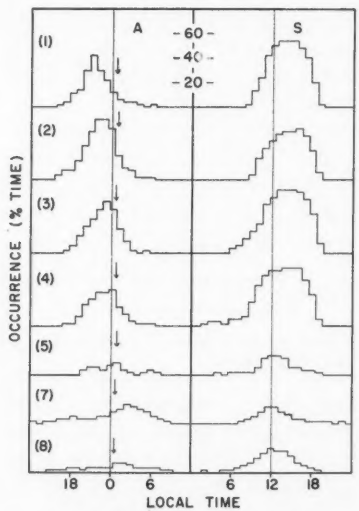

FIG. 3. Histograms showing the diurnal variation of occurrence of A events and S events for each of seven paths arranged from top to bottom in order of decreasing latitude.

found earlier by Collins and Forsyth for paths 7 and 8. Each histogram is plotted with respect to local (mean) time at the path mid-point, but in the left-hand column the time of occurrence of magnetic midnight is indicated by an arrow. Clearly, for all paths the A events tend to concentrate near midnight and the S events near noon. For each class of event there seems to be a systematic shift in time of maximum occurrence with latitude. For the A events the maximum occurs at progressively later times with decreasing latitude and for the S events, at progressively earlier times with decreasing

latitude. Unfortunately, for the range of latitudes and longitudes involved, it is not clear if the variation of time of maximum occurrence would be more systematic if measured with respect to magnetic time rather than solar time. In the earlier work, Collins and Forsyth were led by the symmetrical distribution of *S* events about noon (particularly for path 7) to believe that the *S* events were subject to strong solar control. Although solar control may operate, some further mechanism is required to explain the high-latitude observations.

The observed variation of time of maximum occurrence with latitude is reminiscent of that found by other workers for magnetic and ionospheric phenomena. In Fig. 4 the times of maximum occurrence for the *A* and *S*

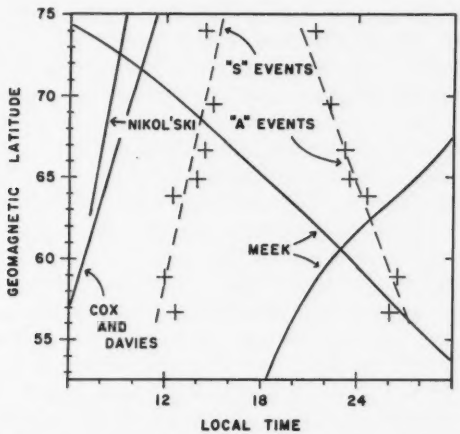

FIG. 4. Graph showing the time of maximum occurrence of *A* events and *S* events as a function of geomagnetic latitude. Also shown is the latitudinal dependence of time of maximum occurrence for each of three other investigations (by Nikol'ski, Cox and Davies, and Meek) of possibly related events.

events are plotted against geomagnetic latitude. Instead of the time of maximum occurrence, the time corresponding to the "center of mass" of the distribution may be used. When this is done the latitudinal variation seems somewhat more systematic but hardly enough to justify this refinement of presentation. In studying the time of maximum occurrence of ionospheric "blackout", Cox and Davies (1954) found the latitudinal variation indicated in the diagram of Fig. 4. Nikol'ski (1956) suggested a latitudinal variation in time of maximum occurrence of magnetic disturbance. The approximate variation that he found for longitude 105° west is also indicated in Fig. 4. Meek (1955) found that when times of maximum magnetic disturbance were plotted on a polar diagram of geomagnetic time vs. geomagnetic latitude, two opposing spirals were produced. In Fig. 4 the relevant portions of these two spirals have been replotted without correction for differences between solar and magnetic time.

The points representing the A and the S events in Fig. 4 may be fairly represented by the two straight broken lines. In drawing the lines, it may be appropriate to attach less importance to the points representing the data from path 8 because this path is located more than 35 degrees of longitude to the east of the other paths. While there seems to be little relation between the present results and those of the other workers mentioned, it is interesting to note that the line representing the S events and that representing the results of Cox and Davies, although displaced by about five hours, have nearly the same slope.

GEOGRAPHICAL EXTENT OF THE DISTURBANCES

In any consideration of the nature of radio-aurora it is important to have some indication of the geographical extent of a single occurrence. The data from the I.G.Y. network may be used to estimate the size of the area affected by each class of event (A and S). By assuming once again that the path mid-points are representative of the regions in which the signals are scattered, the distances between the various scattering regions can be calculated. Leaving out path 5 (because of the very poor statistics of the data from this path) the remaining four paths provide a range of separations from 200 to 730 kilometers. For each type of event the percentage time of simultanous occurrence of the event on each pair of adjacent paths was determined. Then the percentage time of simultaneous occurrence was determined for three adjacent paths and finally for all four paths. These figures were taken as a measure of the occurrence of the event simultaneously over the whole area represented by the distance between the corresponding path mid-points. In order to calculate the probability, $P(0,x)$, that an event would occur simultaneously on two paths having mid-points x kilometers apart, given that the event occurs on one of them, the percentage times of simultaneous occurrence were divided by the mean percentage time of occurrence of the event for the paths involved.

In Fig. 5 the probability, $P(0,x)$ is plotted as a function of the dimension x

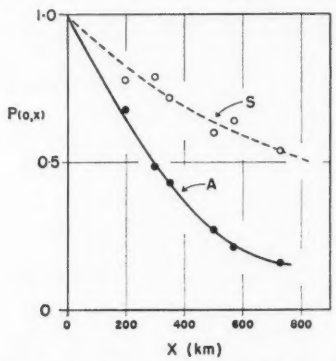

FIG. 5. The probability of simultaneous occurrence of an event at two points separated by a distance x, as a function of x, shown separately for A events and S events.

for the A and S events independently. A reasonable estimate of the size of the area affected by a single occurrence of each type of event may be obtained from the value of x where P falls to 0.5. On this basis a single A event characteristically affects an area having a diameter of about 300 kilometers. Similarly, the S events affect a much larger area, possibly having a diameter greater than 800 kilometers. There is little justification for assuming a circular area for each event but, at least for the A events, the apparent consistency of the plotted points in Fig. 5 for widely differing directions of mid-point separation suggests that there is no great systematic departure from circular symmetry. The use of the path mid-point separation as a measure of the diameter of the affected area may be somewhat misleading. Since the area of sensitivity of each path is quite large the actual disturbance area may be somewhat smaller than that indicated in Fig. 5. This effect should be more pronounced for the A events, but even for these events it would be largely offset by the aspect sensitivity of the scatterers. Thus, in spite of the approximations involved, this method of measurement should give quite a good estimate of the size of the affected area.

In Fig. 5 there is much more scatter in the points representing the S events than in those representing the A events. This may be due in part to the very large size of the area affected by an S event. The S events may in fact tend to be more widespread at higher latitudes and more localized at lower latitudes. Certainly, in Fig. 5, the two points that lie above the broken line were derived from the most northerly combinations of paths and the two points that lie below the line were derived from the most southerly combinations of paths.

DISCUSSION

The very limited period of time covered by the present analysis makes it impossible to draw firm conclusions relating to the long-time behavior of radio-aurora. On the other hand, a large number of events were observed and the coverage was virtually continuous in both space and time for the area and period concerned. It seems likely, therefore, that the results give an accurate picture of the actual behavior of radio-aurora over this limited time span.

It is unfortunate that there is not available, at the present time, optical evidence of a similar nature covering the same period. The characteristics of the A events seem to show no marked dissimilarities to those of optical aurora generally. Certainly, the diurnal variations and distributions in latitude are similar. The geographic extent of a single optical auroral display is still the subject of some disagreement. There is some suggestion that optical displays tend to occur simultaneously over very large areas. The alternative view is that while the very largest displays do occur simultaneously over large areas, most displays are quite localized and may even move systematically in latitude or longitude or both. The evidence presented in Fig. 5 seems to support the latter view in that, on the average, the radio-auroral A events are quite localized.

In the earlier paper (Collins and Forsyth 1959) the S events were tentatively associated with the recurrent daytime absorption observed at high latitudes

and which is now known as "polar-cap absorption". The present evidence concerning the diurnal variation and geographic extent of the *S* events is in accord with this tentative association. It is interesting to note that Little and Leinbach (1958) found that daytime absorption measurements at stations separated by 800 kilometers produced a correlation coefficient of 0.57 while nighttime absorption measurements produced a lower value.

The latitudinal variation of the time of maximum occurrence for both *A* events and *S* events seems to be real but not easily understood.

For the *S* events the operation of solar control is not completely excluded by the present measurements. Assuming solar control, there are at least two possible explanations of the high-latitude lag in the time of maximum occurrence. If the morning absorption observed by Cox and Davies is a fairly regular occurrence (see Fig. 4) then at high latitudes the morning occurrences of *S* events would be masked and the apparent time of maximum occurrence would be displaced to the afternoon. Alternatively, the delay in maximum occurrence after local noon may be due to an increase at high latitudes of what Appleton (1953) has called the "sluggishness" of the ionosphere. According to this latter suggestion the observed results could come about through a decrease in recombination coefficient with increasing latitude or, more probably, a slight decrease in the height of the scattering region with increasing latitude. Appleton has shown that the "relaxation time" of the ionosphere falls off very rapidly with height in the lower ionosphere. Any description of the basic nature of the auroral phenomenon must include an explanation of the diurnal and latitudinal variation of occurrence as well as an explanation of the variation of the time of maximum occurrence with latitude. It would be valuable, therefore, to extend the present study to another period in time and perhaps over a larger geographic area.

ACKNOWLEDGMENTS

The bistatic auroral scatter network was operated by a number of co-operating agencies under the direction of the Radio Physics Laboratory of the Defence Research Board as part of the Canadian program for the International Geophysical Year. The authors are indebted to the present Superintendent of the Radio Physics Laboratory, Dr. C. O. Hines, for making the records available for analysis. A valuable discussion regarding the behavior of the *S* events was held with Mr. C. Collins.

REFERENCES

APPLETON, E. V. 1953. J. Atmospheric and Terrest. Phys. **3**, 282.
COLLINS, C. and FORSYTH, P. A. 1959. J. Atmospheric and Terrest. Phys. **13**, 315.
COX, J. W. and DAVIES, K. 1954. Can. J. Phys. **32**, 743.
CURRIE, B. W., FORSYTH, P. A., and VAWTER, F. E. 1953. J. Geophys. Research, **58**, 179.
FORSYTH, P. A. and VOGAN, E. L. 1957. J. Atmospheric and Terrest. Phys. **10**, 215.
GADSDEN, M. 1959. Ann. géophys. **15**, 403.
LITTLE, C. G. and LEINBACH, H. 1958. Proc. Inst. Radio Engrs. **46**, 334.
MEEK, J. H. 1955. J. Atmospheric and Terrest. Phys. **6**, 313.
NIKOL'SKI, A. P. 1956. Doklady Akad. Nauk S.S.S.R. **109**, 939 (Defence Research Board Translation T232R).
VESTINE, E. H. 1944. Terrestrial Magnetism and Atmospheric Elec. **49**, 77.

THE GROUP VELOCITY OF PLANE SURFACE WAVES[1]

A. G. MUNGALL AND D. MORRIS

ABSTRACT

The velocity of transmission of a modulated microwave signal over a dielectric-covered plane conductor has been measured over a range of dielectric thicknesses for which the first order *TM* surface wave mode is known to propagate. An exact theoretical treatment of plane surface wave group velocity for both *TM* and *TE* surface wave modes of any order has been developed and calculations carried out for the first two orders. The experimentally determined signal velocities are in good agreement with the group velocities calculated for the first order *TM* mode. Effects of possible surface wave propagation on the accuracy of microwave distance-measuring methods are discussed.

INTRODUCTION

During the past few years a number of papers dealing with the propagation of plane surface waves over dielectric-covered metal surfaces have been written (Attwood 1951; Barlow and Cullen 1953; Brown 1953; Cullen 1954; Rich 1955; Mungall and Morris 1959). However, apart from a theoretical discussion by Smorgonskiy (1955), very little attention seems to have been paid to the question of the speed at which information can be transmitted by means of modulated surface waves. Smorgonskiy has shown theoretically that the group velocity of surface waves, which defines the speed at which a modulated wave travels, can be very different from the phase velocity. This paper will describe experimental measurements of the velocity of transmission of frequency-modulated waves over a surface wave structure, and will show that this velocity is in good agreement with the theoretically predicted group velocity.

Practically, the group velocity can be of importance in the field of precise radio distance measurement. In this application, the velocity at which a signal travels between the two measuring stations must be known to a few parts per million if the distance between them is to be determined to a similar accuracy. The experimental case dealt with in this paper, that of a layer of sand covering a conducting surface, is one which might be encountered in practical field conditions.

THEORETICAL

A previous paper (Mungall and Morris 1959) dealt with the experimental measurement of surface wave phase velocity over a sand-covered conducting surface and outlined the theoretical treatment of the problem. The relation between the group velocity and the phase velocity over such a structure will now be discussed. For the *TM* and *TE* cases, the phase velocity v of surface

[1]Manuscript received February 18, 1960.
Contribution from the Division of Applied Physics, National Research Council, Ottawa, Canada.
Issued as N.R.C. No. 5673.

wave propagation over a dielectric-covered perfectly conducting metal surface was given by the following expressions:

(1) *TM* and *TE* $$v = \omega\left[\frac{\omega^2}{c^2}\kappa_2' - \beta_2^2\right]^{-\frac{1}{2}}$$

(2) *TM* $$\beta_2 \tan \beta_2 l = \kappa_2'\left[\frac{\omega^2}{c^2}(\kappa_2' - 1) - \beta_2^2\right]^{\frac{1}{2}}$$

(3) *TE* $$\beta_2 \cot \beta_2 l = -\left[\frac{\omega^2}{c^2}(\kappa_2' - 1) - \beta_2^2\right]^{\frac{1}{2}}$$

where all symbols are the same as in the previous paper;

ω = angular frequency,
c = velocity of electromagnetic waves in free space,
κ_2' = dielectric constant of the dielectric, assumed loss-less,
l = thickness of the dielectric,
β_2 = a phase constant of wave propagation in the dielectric.

The group velocity v_g may in general (Slater 1950) be defined by

(4) $$v_g = \frac{1}{(d\beta/d\omega)}$$

where β is the phase constant. The phase velocity v is given by

(5) $$v = (\omega/\beta).$$

The group velocity v_g can be determined approximately in the manner followed by Smorgonskiy for the first *TM* mode. This involves replacing the exact expression for the relations between v, l, and ω by a simpler, approximate algebraic expression giving v explicitly as a function of l and ω. The derivation of v_g then involves a differentiation of this expression. It is possible, however, to derive an exact solution for all modes, both *TM* and *TE*, as follows.

From (4) and (5) it follows that

(6) $$v_g = \frac{v}{1 - \frac{\omega}{v}\frac{dv}{d\omega}}.$$

This can be expressed in dimensionless terms, using the relative surface wave phase velocity $V = v/c$ and the relative dielectric depth in wavelengths $L = l/\lambda_0$ where λ_0 is the free space wavelength. Thus equation (6) becomes

(7) $$V_g = \frac{V}{1 - \frac{L}{V}\frac{dV}{dL}}$$

where $V_g = v_g/c$, the relative surface wave group velocity. Substitution of (1) in equations (2) and (3) yields the following expressions for L in terms of V

(8) *TM*: $$L = \frac{V}{2\pi(\kappa_2' V^2 - 1)^{\frac{1}{2}}} \tan^{-1}\left[\kappa_2'\left(\frac{1 - V^2}{\kappa_2' V^2 - 1}\right)^{\frac{1}{2}}\right]$$

(9) TE: $$L = \frac{V}{2\pi(\kappa_2' V^2 - 1)^{\frac{1}{2}}} \cot^{-1}\left[-\left(\frac{1-V^2}{\kappa_2' V^2 - 1}\right)^{\frac{1}{2}}\right].$$

By differentiation dL/dV may be determined and hence V_g obtained, using equation (7).

For TM modes:

(10) $$V_g = V\frac{1+\frac{C_1}{V^2}}{1+\kappa_2' C_1}$$

where

$$C_1 = \left[\frac{1+\kappa_2'(1-V^2)}{\kappa_2'}\right]\left(\frac{1-V^2}{\kappa_2' V^2 - 1}\right)^{\frac{1}{2}} \tan^{-1}\left[\kappa_2'\left(\frac{1-V^2}{\kappa_2' V^2 - 1}\right)^{\frac{1}{2}}\right]$$

and for the TE modes

(11) $$V_g = V\frac{1+\frac{C_2}{V^2}}{1+\kappa_2' C_2}$$

where

$$C_2 = V^2\left(\frac{1-V^2}{\kappa_2' V^2 - 1}\right)^{\frac{1}{2}} \cot^{-1}\left[-\left(\frac{1-V^2}{\kappa_2' V^2 - 1}\right)^{\frac{1}{2}}\right].$$

Since these equations express V_g in terms of V rather than L, it is necessary to determine V_g as a function of L by simultaneous solution of either (8) and (10), or (9) and (11) for various values of V.

As in the previous paper, calculations were carried out for both TM and TE modes for $\kappa_2' = 3.0$, a value representative of dry sand. These results are shown in Fig. 1, where both the relative phase and group velocities are plotted

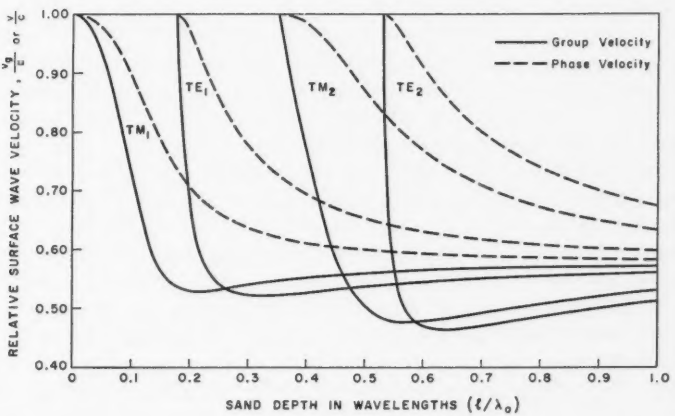

FIG. 1. Relative surface wave phase velocity v/c and group velocity v_g/c as functions of the sand depth in wavelengths. Only the first two TM and TE modes are shown.

as functions of the relative dielectric depth, L. For the sake of clarity, only the first two TM and TE modes are shown.

Examination of this figure shows that the group velocity is always less than the phase velocity. For example, in the case of the TE_2 mode it assumes a value of only 0.51 of the phase velocity for a value of l/λ_0 of 0.59. For all modes the group velocity passes through a minimum before increasing slightly to approach asymptotically the value $c/\sqrt{\kappa_2'}$. Both group and phase velocities tend toward this same value for large values of l/λ_0.

EXPERIMENTAL

The group velocity was measured by determining the transit time of frequency-modulated waves over the surface wave structure. This consisted of a copper gauze sheet about 28 feet long and 10 feet wide covered with a layer of dry sand, the thickness of which was varied as required. This structure was completely surrounded by walls of microwave absorber 3 feet high to eliminate reflections from objects in the laboratory. At each end openings in the walls were made for the transmitting and receiving antennas. Each consisted of an 18 in. diameter parabolic reflector with a double dipole feed.

The transit time was measured by a pair of Tellurometer sets. These instruments employ both frequency modulation and pulse techniques at carrier frequencies near 3000 Mc/sec. A signal is transmitted from one, the master, to the other, the remote, where it is received and retransmitted at a slightly different carrier frequency back to the master. Directions of polarization of the outgoing and returning microwave beams are at 90° to each other and at 45° to the horizontal. Accuracy of measurement is approximately $\pm 10^{-9}$ sec.

Successful launching of the surface waves using the parabolic reflectors required adjustment of the antennas relative to the surface and shaping of the surface in their vicinity. It was not possible to launch a surface wave whose amplitude exceeded that of the free space component which always accompanies it unless the sand layer was tapered gradually from the full thickness several feet from the antenna to zero thickness immediately in front of it. It was also found, as mentioned in the previous paper, that the launching efficiency (power transmitted as a surface wave relative to total power emitted) decreased with decreasing surface wave velocity.

The surface waves were launched by two different methods. The first and simplest required only that the reflector be tilted so as to direct the beam downward onto the surface. An angle of incidence of about 60° to the surface normal was found satisfactory. This technique (Fig. 2*a*) was only applicable for surface waves whose group velocity did not differ from c by more than about 10%. For slower waves the surface wave launching efficiency deteriorated and transmission between the antennas was due predominantly to free space propagation.

A second, somewhat more complicated technique (Fig. 2*b*) was found to excite surface waves in such a way that the free space component was relatively small even for very slow waves ($v_g = .55c$). This involved surrounding the antennas completely with microwave absorber on both sides, back and top,

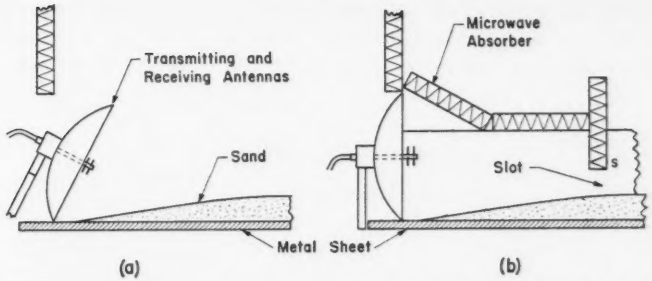

FIG. 2. Diagram showing positioning of antennas relative to the surface wave structure and placing of absorbing panels.

and allowing radiation to leave this enclosure only through a narrow horizontal rectangular slot aperture above the sand surface several feet in front of the antenna. This aperture was bounded below by the sand surface, above by the lower edge of the absorbing sheet, *s*, shown in Fig. 2*b*, and at each side by other absorbing sheets. The slot width was varied by raising or lowering sheet *s*. It was found that both the slot width and the distance between antenna and slot affected the relative power in the surface wave and free space wave components. If the slot was made sufficiently narrow, less than a wavelength, the free space component was apparently absorbed, leaving the surface wave component effectively undisturbed. This did not occur if the absorbing panel was placed too close to the antenna.

In most of the experiments described in the present paper the slot technique was used with a slot width of about 7.5 cm ($3\lambda_0/4$). This width appeared to be a satisfactory compromise between the ideal situation with the entire absence of a free space component, attainable only for a very narrow slot, and the presence of a relatively strong one resulting from an unlimited reflector aperture.

The measurement of the transit time between the two antennas by means of the Tellurometer requires further explanation. This instrument measures effectively the phase shift in a 10-Mc/sec frequency modulation, superimposed on a 3000-Mc/sec carrier, due to the time taken for the signal to travel from one set, the master, to the other, the remote, and back. The exact system of measurement has been discussed in another paper (Wadley 1958) and will not be described in detail here. It is essentially a phase comparison system, and as a result, interference between the wave train of interest and any other results in an unwanted phase shift. It can be shown that this alteration of phase due to reflected waves, or to any other interfering waves whose amplitude is independent of frequency over a small frequency range, varies cyclically with carrier frequency alternately positive and negative. To a first approximation, the resultant phase measured over several cycles of variation can be averaged to yield a value close to the true phase.

In the present experiment, interference occurs between the surface waves and free space waves, whether direct or reflected. This results in a variation

of the measured transit time; the variation may be small as shown by the solid curve in Fig. 3, for only slight interference, or quite large as in the dashed curve when there is a free space signal of the same order as the surface wave.

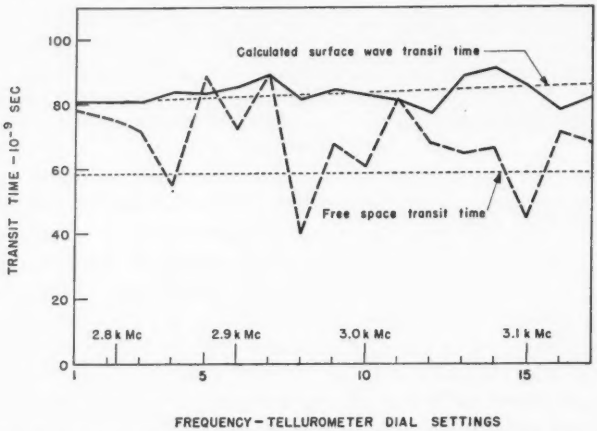

FIG. 3. Transit time as a function of carrier frequency: solid curve, amplitude of surface wave greatly exceeds that of the free space wave; dashed curve, amplitude of surface wave about equal to that of free space wave.

Both curves in this figure represent transit times for a sand depth of about 11.5 mm. The first was obtained with a 7.5-cm slot and the second with a 15-cm slot. The solid curve follows very closely the calculated surface wave transit time, which increases slightly with frequency over the range of measurement. The dashed curve is very erratic, but tends to oscillate near the free space value.

Measurements of transit time were carried out over sand depths up to 25 mm, the range over which previous work on the phase velocity had shown that the first TM mode was easily measurable. The surface wave signal strengths for thin sand layers tended to be similar to those occurring in direct free space transmission over the bare metal sheet. As the layer was increased in thickness, however, the signals received at each antenna decreased sharply until at 25 mm thickness they were near to noise level. The velocity of signal propagation was calculated from the transit times measured and the values are shown in Fig. 4 in relation to the theoretical curve for the group velocity of the first order TM mode. All experimental transit times incorporate approximate corrections for the different velocities over the short tapered portion of the sand. The experimental points tend to fall below the curve in the upper portion of it and above in the lower. These deviations result from the fact that the depth plotted is simply the arithmetic mean of 20 to 30 measurements taken along a line between the two antennas. Since at the upper end of the curve depths greater than the average tend to affect the velocity more than

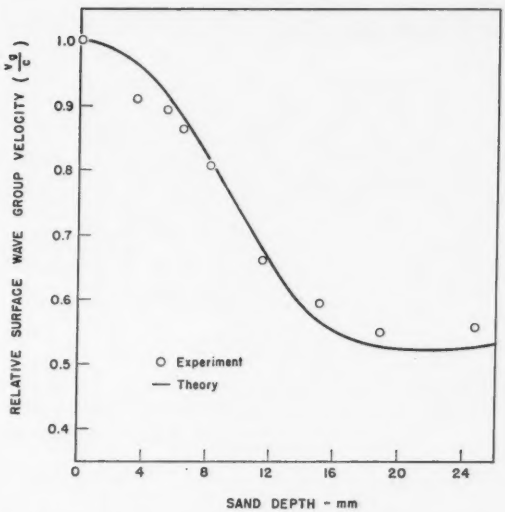

FIG. 4. Comparison between theoretical and experimental variation of surface wave group velocity with sand depth.

those less than the average, variation in sand depth will tend to make the experimental points drop below the curve. The reverse holds true for the lower part of the curve. Despite the irregularity of the sand depth, however, the experimental points fall quite close to the theoretical curve and demonstrate that the velocities measured approximate the theoretically predicted group velocities.

Although it was difficult to ascertain the depth with any degree of accuracy, several measurements for sand depths in the vicinity of 40 to 45 mm were made. These indicated that a surface wave with a group velocity of about $0.55c$ propagated between the antennas at a power level similar to that found for a depth of 11.5 mm. Since the power transmitted in the first TM mode had decreased nearly to noise level for depths greater than 19 mm, the relatively large power transmission at 40 to 45 mm depth suggests the existence of the second order TM mode. Equipment designed to provide greater uniformity in sand depth is now being constructed in order to make possible investigation of the higher order TM and TE modes.

The fact that it was possible to excite surface waves simply by directing the microwave antennas downward toward the sand-covered metal surface indicates that these waves may also be excited in any microwave methods of distance measurement in the field. If such waves are excited, it is clear that the transit times arising from surface wave propagation can be very different from those due to free space propagation, as indicated in Fig. 3. Large errors in the measured distance could result.

REFERENCES

ATTWOOD, S. S. 1951. J. Appl. Phys. **22**, 504.
BARLOW, H. M. and CULLEN, A. L. 1953. Proc. Inst. Elec. Engrs. (London), III, **100**, 329.
BROWN, J. 1953. Proc. Inst. Elec. Engrs. (London), III, **100**, 363.
CULLEN, A. L. 1954. Proc. Inst. Elect. Engrs. (London), IV, **101**, 225.
MUNGALL, A. G. and MORRIS, D. 1959. Can. J. Phys. **37**, 1349.
RICH, G. J. 1955. Proc. Inst. Elec. Engrs. (London), B, **102**, 237.
SLATER, J. C. 1950. Microwave electronics (D. Van Nostrand Co. Inc., New York).
SMORGONSKIY, V. Y. 1955. Radiotekhnika, **10**, No. 5, 25.
WADLEY, T. L. 1958. Trans. S. African Inst. Elec. Engrs. **49**, 143.

AN IMPROVED ELECTROSTATIC ELECTRON SELECTOR[1]

PAUL MARMET AND LARKIN KERWIN

ABSTRACT

A cylindrical electrostatic electron selector is described which provides a 10^{-7} ampere beam of electrons whose energy may be varied from 0 to 50 ev and whose energy spread is less than 100 mv. Space-charge problems involved in the construction of the device were overcome by the use of grids for focusing electrodes with exterior electron traps, and a non-reflecting surface for electrons made from a network of tiny tubes. The selector is provided with an energy analyzer. When used to determine the appearance potential curve of argon, the selector resolved the $2P_{3/2}$ and $2P_{1/2}$ states separated by 0.18 ev, and indicated the formation of A_2^+ at an energy of 0.8 ev below the threshold for A^+.

1. INTRODUCTION

A few years ago, Father Ernest Clarke (1954) reported from this laboratory the use of an electron selector to measure ionization probability curves. Some details of the instrument are shown in Fig. 1.

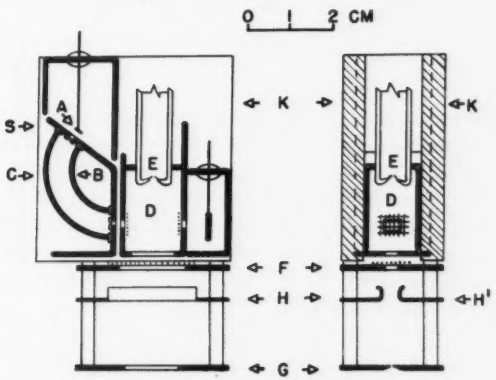

FIG. 1. Electrostatic electron selector (Clarke 1954).

Electrons from a filament A are accelerated to about 3-volt energy and enter the selector through a slit in plate S. There the electrostatic field maintained between C (1.5 v) and B (4.5 v) caused the 3-volt electrons to describe a circular path so as to emerge from the exit slit of S. They were then further accelerated to any desired energy by means of a voltage applied to the ionization chamber D. Here they were used to bombard gas molecules entering the chamber from E. The resulting ions were then analyzed by a mass spectrometer whose accelerating slit system is shown at F, H, and G.

[1]Manuscript received February 29, 1960.
Contribution from the Centre de Recherches en Physique, Université Laval, Quebec, Que.

The 127° selector used will not pass electrons of other energies than those for which it is adjusted, to a good approximation. It also produces direction focusing (Hughes and McMillan 1929), which is necessary for useful beam intensity. In Fig. 2 is shown the energy distribution obtained from this selector.

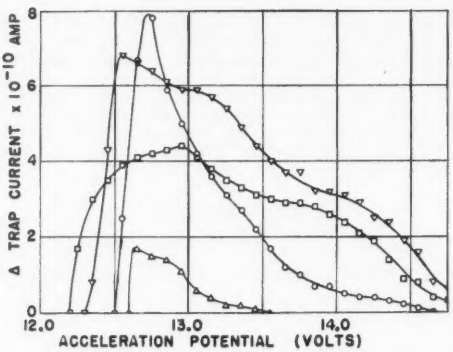

FIG. 2. Energy spread of electron beam in selector. Outer deflection plate potential: (*a*) 1.1 volt —□—; (*b*) 1.2 volt —▽—; (*c*) 1.3 volt —○—; (*d*) 1.4 volt —△—.

Under typical operating conditions an effective energy distribution of 300 mv at half-height was obtained. This stems from the measured distribution (Fig. 2*c*) modified by the fact that the low-energy electrons are less effective in producing ions. The electron beam current was about 10^{-8} amp, and could be used from about 7-ev to 60-ev energy. With this instrument measurements were made leading to the determination of the dissociation energy of nitrogen (9.79 ev), the electron affinity of oxygen (1.5 ev), and other data.

It would have been desirable to increase the electron beam current and to reduce its lower energy limit as well as the energy spread. These are opposed desiderata and the above characteristics represent the optimum conditions obtainable under the circumstances. The principal block to improvement was the formation of space charge by reflection from surfaces and scattering in the gas atmosphere of the mass spectrometer ion source.

2. IMPROVEMENTS

Grid Construction

Since the space charge results in part from the reflection of electrons from surfaces, it was thought to prevent this by making the surfaces transparent and capturing the space-charge-creating electrons on charged plates when they left the selector region. This was tried on a large scale selector model, where the long paths favored space-charge formation. As shown in Fig. 3, the selector was constructed of 90% transparent wolfram mesh grids (G_1 and G_2) beyond which were outer plates (P_1 and P_2). In one experiment the electrodes were connected in circuit as shown with G_1 connected to G_2 and P_1 to P_2. The following readings were obtained:

		Setting A	Setting B	Setting C
Total emission,	I_t	500 μamp	500 μamp	500 μamp
Slit voltage,	V_s	3 v	3 v	3 v
Slit current,	I_s	500 μamp	500 μamp	470 μamp
Grid voltage,	V_g	0 v	0 v	3 v
Grid current,	I_g	0.0 μamp	<0.5 μamp	~0 μamp
Plate voltage,	V_p	0 v	50 v	50 v
Plate current,	I_p	0 μamp	0 μamp	30 μamp

Comparing settings A and B it is seen that in the first case no appreciable current reached the grids, the electrons which passed through the slit being reflected back to the slit by the space charge created at A. In the second case the voltage on the plates resulted in very little field penetration through the grids as may be seen from the small grid current. In setting C, the grid voltage attracts electrons, which are captured by the plates as they pass through the grids, preventing space-charge build-up. The 30-μamp current previously reflected to the slit now continues to the plates.

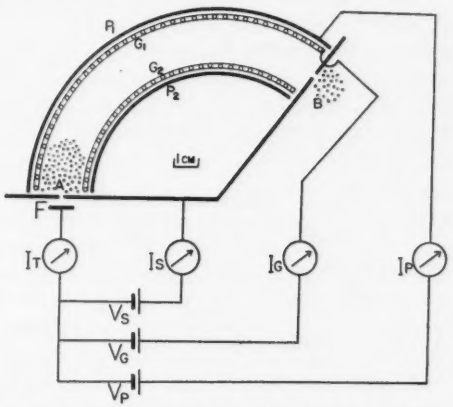

Fig. 3. Grid construction of selector electrodes.

With the plates grounded, no electron beam could be passed through the selector. With the plates at 50 volts, the removal of space charge resulted in a current of about 10^{-9} amp with an energy spread of about 200 mv. It was also found that the selector could be operated at very low electron energies (about 0.5 ev), which is important, since the theoretical spread in energy is proportional to the energy ($\Delta E/E = \Delta R/R$ (Hughes and McMillan 1929)).

Focusing

The cylindrical electrostatic lens provides direction focusing in the planes normal to the cylindrical walls. A certain focusing in the surfaces concentric with these walls was achieved by adding electrodes at the top and bottom of the selector. These were of wolfram mesh and were provided with exterior plates for the removal of space charge as in the case of the selector grids. The use of this focusing always increased the beam intensity by at least a factor of 3. These electrodes and plates may be seen in the photograph of the complete selector in Fig. 7.

The large selector constructed for these experiments would not operate well at high (10^{-3} mm Hg) pressures because of the long electron trajectories. Its relatively small height also limited the beam strength, which was found experimentally to vary inversely as the volume of the selector.

Electron Velvet

When a small electron selector was made using the above-mentioned improvements, its characteristics were measured by means of a second "selector" (the "analyzer") and a beam of about 10^{-7} amp was obtained. However, when the mass spectrometer ionization chamber was located at the selector exit slit, space-charge limitation was encountered anew in region B (Fig. 3) as the electrons scattered from the ionization chamber walls. The solution of grid walls could not be applied here, as ions would be formed in regions between the grid walls and plates by electrons whose energy was undetermined. Another possibility lay in the finding of a surface which would absorb electrons rather than reflect them. In practice these surfaces would not be physically "clean", as, in the atmosphere of the mass spectrometer source, surface layers of gas molecules and products of catalysis at the filament would always be present.

Measurements were carried out on a number of surfaces as shown in Fig. 4. Electrons from the selector were directed onto a surface M whence, if reflected,

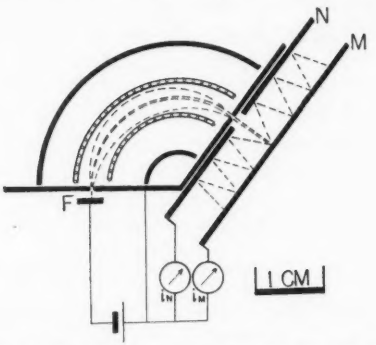

FIG. 4. Apparatus for measuring reflection coefficients.

they proceeded to a surface N, then back to M, etc. Currents at M and N were measured as shown. The experiment was made at low pressure (10^{-5} mm Hg) to avoid the effects of gas-scattering.

If R_m is the percentage of electrons reflected from M and R_n that from N, then when i is the current from the selector:

$$i_m = i(1-R_m)+R_mR_ni(1-R_m)+R_m^2R_n^2i(1-R_m)+R_m^3R_n^3i(1-R_m)+\ldots$$

$$i_n = R_mi(1-R_n)+R_m^2R_ni(1-R_n)+R_m^3R_n^2i(1-R_n)+\ldots$$

whence

$$\frac{i_n}{i_m} = R_m\frac{(1-R_n)}{(1-R_m)}. \tag{1}$$

When M and N are identical, this simplifies to

$$\frac{i_n}{i_m} = R_m \,. \tag{2}$$

As a result of these measurements, the following results were obtained for electrons of 1 ev:

Surface	Coefficient of reflection R_m, ±5%
Iron, polished	72
Platinum	68
Copper, etched	66
Iron	66
Gold	65
Cadmium	60
Palladium	59
Copper	58
Iron, etched	40
Soot on metal	21
Finned copper	16

The high reflectivities obtained here are not at variance with the low values obtained by other workers (e.g. Fowler and Farnsworth 1958) for similar metals when the surface conditions are taken into account. Thus no attempt was made to degas the surfaces for our measurements, and it is obvious that the reflectivities obtained are characteristic of the gross texture and of surface conditions ordinarily met at high pressures in a mass spectrometer source rather than of the metals used.

From these results it was clear that no simple surface lent itself to the absorption of slow electrons. Soot (deposited from a flame) was relatively good. A stainless steel ionization chamber coated with soot was used with the selector, and the space-charge problem at Y (Fig. 3) immediately reduced to practical proportions. However, this surface could not be tolerated in the spectrometer. The low reflectivity of a surface bristling with many small fins suggested that this be seriously considered.

After many attempts, a good surface was obtained as follows. Fine aluminum wire (0.5 mm) is cleaned and plated with 0.01 mm copper. Thousands of 3- or 6-in. lengths of plated wire are inserted in an aluminum cylinder of the same length and about 4 cm in diameter. The whole is compressed to approximately oval sections with a pressure of about 600 kg/cm^2, squeezing the wires tightly together. The end of the cylinder is then worked flat and polished, when the fine network of copper plating may be seen on the aluminum surface formed by the ends of the squeezed wires. This surface is placed for a few seconds in sodium hydroxide, which dissolves a little aluminum and leaves the copper plating (tubes) in slight relief. The surface is then heavily plated with copper (0.5 mm). This end of the cylinder is then sliced off to form a plate about 2 mm thick which is ground and polished on both sides to a thickness of about 1 mm. It is then immersed in sodium hydroxide until all of the aluminum has been dissolved, leaving the fine copper tubes, about 1 mm long and 0.5 mm in diameter anchored to their plated copper base. The sheet

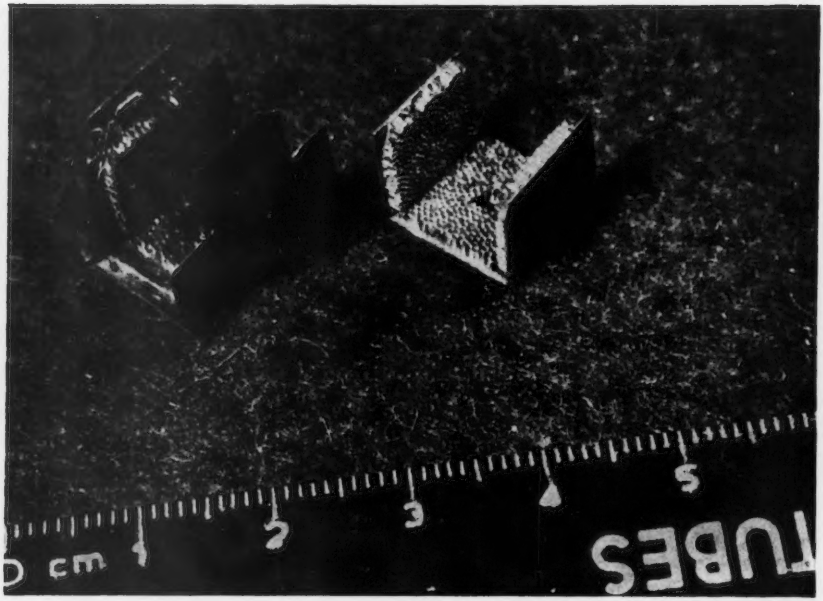

FIG. 5. Electron velvet ionization chamber.

is then plated with gold. The appearance of this material (named "electron velvet" by Dr. Clarke) is shown in Fig. 5, where it has been hand-worked into the shape of an ionization chamber. Its coefficient of reflection measured as in Fig. 4 is 20%.

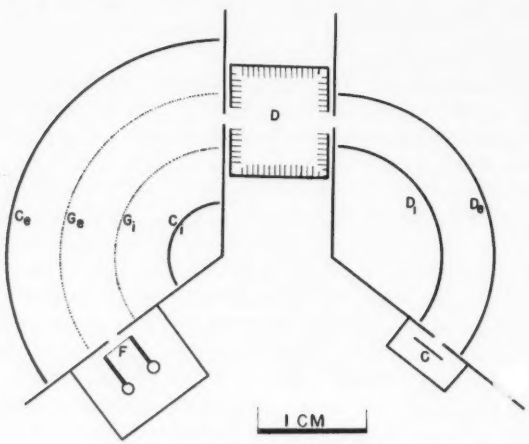

FIG. 6. Plan of selector and analyzer.

In Fig. 7 is seen a photograph of a complete selector, together with an analyzer. In this picture the ionization chamber has been replaced by an analog

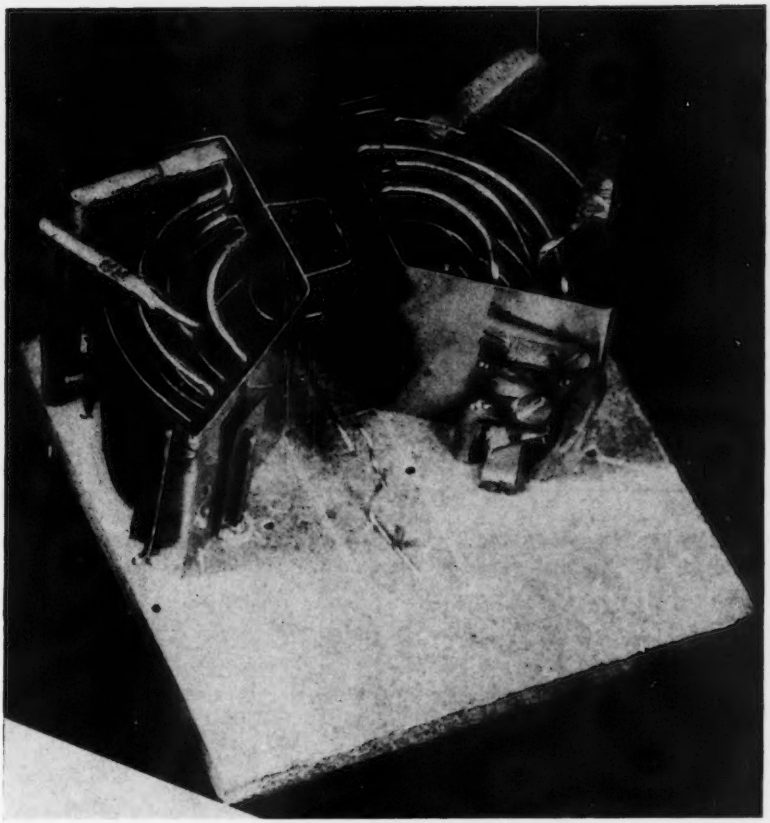

FIG. 7. Complete electron selector and analyzer.

mesh structure. In the final model of the selector described below the space-charge-capturing plates outside of the mesh grids were also constructed of electron velvet.

3. CHARACTERISTICS

All potentials are referred to mid-filament potential, and should be corrected for contact potential as indicated by measurements made on the appearance potentials of gases and the use of negative potentials on some electrodes. A strip filament placed about one millimeter from the selector entrance was used. Shields were placed about the filament, the selector, the ion chamber, the analyzer, and the beam detector to eliminate stray-reflected electrons.

Because of the difficulty of knowing the precise value of V_1 (in addition to contact potential there was a voltage drop along the filament and penetration of fields), V_e was calibrated in practice.

The electron energy was set at 1 ev, so as not to mask the energy spread of the selector beam by the resolution of the analyzer. The current to the

TABLE I

Electron selector data

		Selector	Analyzer
Radius of inner plate,	r_1	5 mm	—
inner grid,	r_2	10 mm	10 mm
outer grid,	r_3	15 mm	15 mm
outer plate,	r_4	20 mm	—
Mean trajectory radius,	r_5	12.5 mm	12.5 mm
Entrance slit width	s_1	0.5 mm	0.5 mm
Exit slit width	s_2	0.5 mm	0.5 mm
Height of slits		4 mm	4 mm
Height of selector		25 mm	25 mm
Initial electron energy,	V_1	1 ev	$V_1+V_5=V_e$
Potential of inner grid,	V_2	0 ev	$V_e-1.0$ ev
outer grid,	V_3	−1.4 ev	$V_e-1.5$ ev
all plates,	V_4	45 ev	—
vertical focusing grids	—	−1 ev	—
Potential of ionization chamber	V_5	Variable	—
beam trap	V_6	—	7.5 ev

ionization chamber was about 10^{-7} amp, and that emerging from the analyzer was about 10^{-9} amp. A sweep of the analyzer voltage produced the curve shown in Fig. 8.

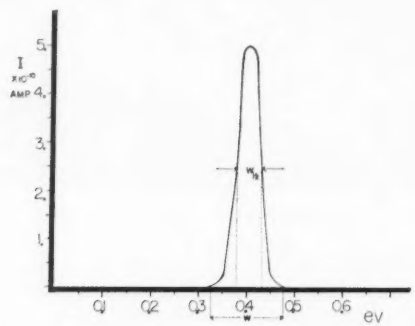

FIG. 8. Measured energy distribution of the selector–analyzer.

The measured energy distribution is seen to be about 0.05 ev at half-height. A portion of this width is contributed by the resolving power of the analyzer, so that we may infer that the electron beam traversing the ionization chamber had an energy spread at half-height of not more than about 0.04 ev. This is of

the order of the thermal agitation of gas molecules at ordinary source temperatures, and so probably represents a practical lower limit beyond which it would not be very useful to proceed.

Measurements of appearance potentials, as described in the next section, confirm the attainment of this narrow energy spread.

4. APPLICATION

The electron selector was placed in a bell jar which was evacuated, outgassed, and filled with argon at various pressures. The ions formed in this gas as the energy of the electron beam provided by the selector was increased were collected on an electrode placed a few millimeters from the ionization chamber and maintained at a few volts positive with respect to it. The resulting "ionization curves" are shown in Fig. 9, which abstracts the salient features of many runs.

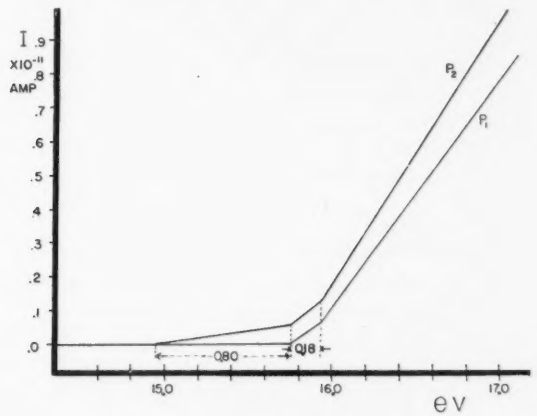

FIG. 9. Ionization curves for argon.

At relatively low pressure (5×10^{-4} mm Hg) curves as indicated at P_1 were obtained. The break following the appearance potential appeared at an average value for 50 runs of $0.18_1 \pm 0.01$ ev. This agrees well with the 0.178-ev difference in levels between the $2P_{3/2}$ and the $2P_{1/2}$ states of argon known from spectroscopy (Moore 1949). This break has been mentioned by Fox (1956) and recently by Fineman (1960). The resolution of these two levels by the electron selector is considered to be a creditable performance.*

At relatively higher pressures (5×10^{-3} mm Hg), the appearance potential curve appeared as at P_2. We ascribe the process appearing at 0.8 ± 0.1 ev below the threshold for A^+ (average of 12 runs) to the formation of A_2^+. Horn-

*Following a visit to our laboratory to inspect the selector, Dr. R. L. Conrod, of the M.I.T. Department of Aeronautics and Astronautics, has just advised us that they have successfully duplicated it.

beck and Molnar (1951) have reported the formation of this ion at these pressures in considerable abundance, and report its appearance potential as being $0.7\ ^{+0.7}_{-0.2}$ ev below the threshold for A^+.

ACKNOWLEDGMENTS

This research was carried out at the Centre de Recherches en Physique of Laval University with the assistance of National Research Council Grant-in-aid BT-45. The help of the Council is acknowledged with pleasure. Messrs. William McGowan and Jean-Denis Carette of the mass spectrometry laboratory contributed an indispensable running commentary and assistance.

6. REFERENCES

CLARKE, E. M. 1954. Can. J. Phys. **32**, 764.
FINEMAN, M. A. and BOUFFARD, R. 1960. Bull. Am. Phys. Soc. Ser. II, **5**, 15.
FOX, R. E. 1956. Westinghouse Electric Corp. Research Report 60-94439-4-R2.
FOWLER, H. A. and FARNSWORTH, H. E. 1958. Phys. Rev. **111**, 103.
HORNBECK, J. A. and MOLNAR, J. P. 1951. Phys. Rev. **84**, 621.
HUGHES, A. L. and MCMILLAN, J. H. 1929. Phys. Rev. **34**, 291.
MOORE, CHARLOTTE. 1949. Atomic Energy Levels, Bureau of Standards Circular No. 467, U.S. Gov't. Printing Office, Washington.

ANALYSE DE LA BANDE 1–0 DU SYSTÈME $^3\Pi_i$–$^3\Sigma^-$ DE PH[1]

F. LEGAY[2]

ABSTRACT

The (1,0) band of the $^3\Pi_i$–$^3\Sigma^-$ system of PH has been photographed in absorption under high dispersion. Values for the rotational constants, the spin-coupling constant, and the vibrational interval $\Delta G'_{\frac{1}{2}}$ of the $^3\Pi_i$ state have been obtained. A study of the Λ-doubling shows the existence of a perturbation in the $^3\Pi_0$ state; it is not possible, however, to determine unambiguously the nature of the perturbing state.

1. INTRODUCTION

La bande 0–0 à 3400 Å appartenant à la transition $^3\Pi_i$–$^3\Sigma^-$ de PH est connue depuis longtemps et a été photographiée en émission à haute dispersion par Pearse (1930), puis par Ishaque et Pearse (1936, 1939). Ces derniers ont également photographié la bande correspondante de PD et l'analyse de ces deux bandes leur a permis de déterminer les constantes des deux états de la transition pour le plus bas niveau de vibration. Jusqu'à présent on ne possédait aucune information relative aux autres niveaux de vibration.

Le présent travail est consacré à l'analyse de la bande 1–0 à 3200 Å qui a pu être photographiée en absorption avec une intensité suffisante. Les constantes de l'état $^3\Pi_i$, $v' = 1$ ont été déterminées et un effet de perturbation a été mis en évidence.

2. TECHNIQUE EXPÉRIMENTALE

Les bandes 0–0 et 1–0 de PH ont été observées par le Dr. J. W. C. Johns et le Dr. D. A. Ramsay au cours d'expériences de photolyse par éclair ("flash-photolysis") sur le phosphure d'hydrogène.

Les conditions expérimentales peuvent se décrire brièvement comme suit:

Longueur du parcours d'absorption: 12 traversées d'une cuve de 1 mètre.

Lampe de photolyse: 1 mètre de long, alimentée par une batterie de condensateurs de 250 μf chargée à 8 kv. Durée de l'éclair: 80 μsec environ.

Lampe source: lampe capillaire en quartz alimentée par un condensateur de 3 μf chargé à 15 kv. Durée de l'éclair: 10 μsec environ.

Pression du phosphure d'hydrogène: 5 mm de Hg. Gaz renouvelé après chaque éclair.

Retard de temps: 25 μsec environ, d'un pic à l'autre.

Les bandes ont été photographiées dans le troisième ordre à l'aide d'un spectrographe à réseau concave de 21 pieds, sur des plaques Eastman Kodak I-O. L'étalonnage des longueurs d'onde a été réalisé au moyen d'une cathode

[1]Manuscrit reçu le 8 janvier 1960.
Contribution du Département de Physique Pure, Conseil National de Recherches, Ottawa, Canada.
Publication N.R.C. No. 5675.
[2]Boursier 1959 du Conseil National de Recherches. Adresse actuelle: Laboratoire d'infrarouge, 12 rue Cuvier, Paris 5, France.

creuse en fer dont les longueurs d'onde ont été prises dans les tables M.I.T. (Harrison 1939) et rapportées au vide à l'aide des corrections d'Edlén (1953). Les positions des raies sur la plaque photographique de la bande 1–0 ont été mesurées à l'aide d'un comparateur équipé d'un viseur photoélectrique du type décrit par Tomkins et Fred (1951). Il n'a pas été jugé utile de mesurer de nouveau la bande 0–0.

3. ANALYSE ROTATIONNELLE

L'identification des raies de la bande 1–0 ne présente aucune difficulté puisque l'état de base $^3\Sigma^-$ est connu par l'analyse de la bande 0–0 due à Ishaque et Pearse. Les nombres d'ondes et la numération des raies des différentes branches sont portés dans le Tableau I et une reproduction du spectre est donnée sur la Fig. 1.

Sur les 27 branches prévues par la théorie pour une transition $^3\Pi_i$–$^3\Sigma^-$, 23 ont été observées. L'allure générale de la bande 1–0 est très semblable à celle de la bande 0–0. Notons simplement que les premières raies de la branche R_3 et de ses satellites sont très serrées et se chevauchent fortement, comme dans une branche du type Q. Au contraire, les raies des branches Q_3 et $^OP_{32}$ sont très espacées. Ces deux effets sont plus marqués ici que dans la bande 0–0.

L'analyse de la bande 1–0 a confirmé entièrement l'identification des raies de la bande 0–0 par Ishaque et Pearse.

La structure théorique de l'état $^3\Pi_i$ de PH a été décrite par ces auteurs qui donnent le schéma des niveaux et des transitions permises avec l'état $^3\Sigma^-$. Nous reprenons les mêmes notations à l'exception du nombre quantique K qui sera désigné par N, conformément à l'usage actuel. On trouvera également dans une étude du spectre de NH par Dixon (1959) un schéma très clair de ce type de transition.

A. Constantes B′ et D′

En utilisant des relations de combinaisons entre les raies de la bande 1–0, il est possible de déterminer directement les constantes B'_1 et D'_1. Mais Ishaque et Pearse ont obtenu les constantes B'_0 et D'_0 avec vraisemblablement une précision supérieure à celle que l'on peut obtenir sur B'_1 et D'_1, car, par rapport à la bande 1–0, la bande 0–0 est plus intense, les raies se chevauchent moins et ne sont pas déplacées par un effet de perturbation. Il est donc préférable d'utiliser les différences entre les nombres d'ondes des raies de la bande 1–0 et ceux des raies correspondantes de la bande 0–0, ce qui permet d'obtenir les différences entre les constantes des deux états de vibration:

$$\alpha' = -(B'_1 - B'_0),$$

$$\beta' = D'_1 - D'_0,$$

$$\Delta G'(\tfrac{1}{2}) = G'(1) - G'(0).$$

En effet, à l'aide d'une formule donnée par Gilbert (1936), la différence entre les sommes des termes pour l'état $^3\Pi_i$ des deux bandes s'écrit:

$$(1) \qquad \sum_i T'_i(J)_{v'=1} - \sum_i T'_i(J)_{v'=0} = \Delta G'(\tfrac{1}{2}) - \alpha'[3J(J+1)-1] - \beta'[3J^2(J+1)^2 + 12J(J+1)+5].$$

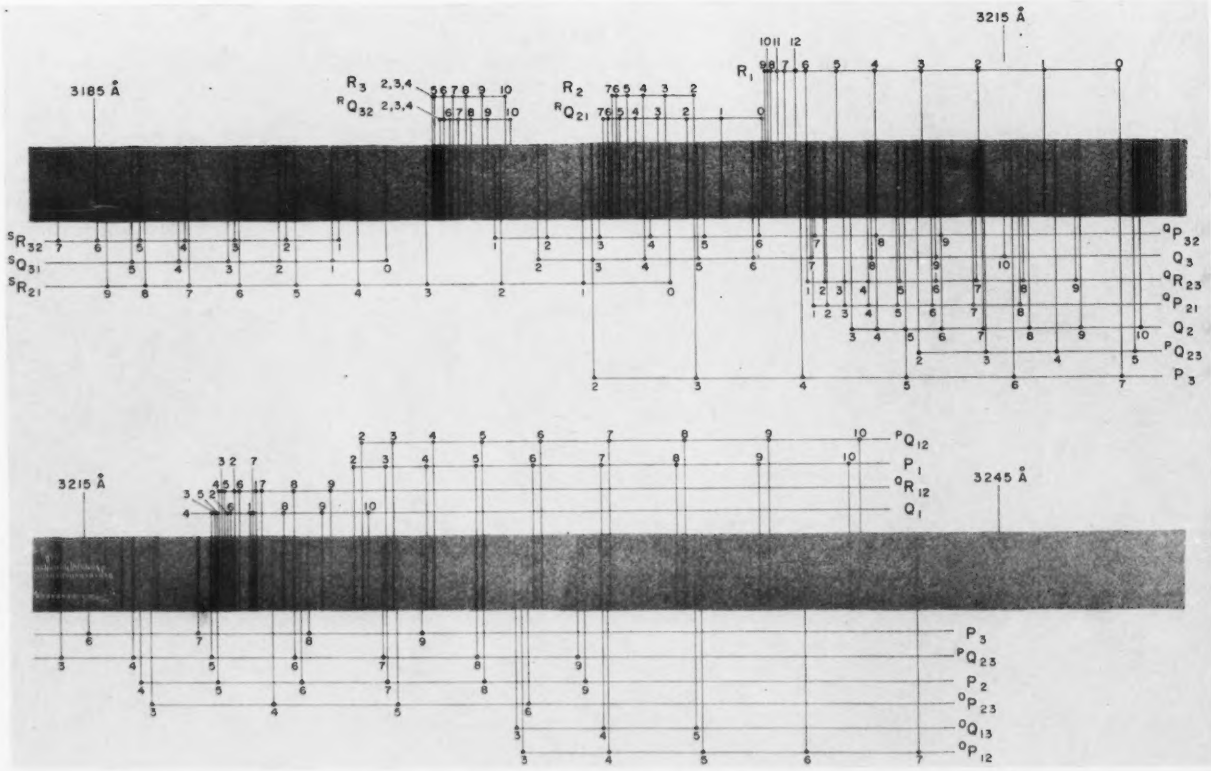

FIG. 1. Spectre de PH observé en absorption et montrant la bande 1–0 du système $^3\Pi_r$–$^3\Sigma^-$ et l'identification des raies.

TABLEAU I

Nombres d'ondes dans le vide et identification des raies de la bande 1–0 de PH

N	$^OP_{12}$	$^OQ_{12}$	$^PQ_{12}$	P_1	$^QR_{12}$	Q_1	R_1		
0							31058.76		
1					31040.42	31042.22	082.91		
2			31006.57	31009.38	047.25	049.44	103.81		
3	30956.18	30958.58	30996.82	30999.18	051.23	053.49	121.74		
4	929.68	931.43*	984.05	986.35	052.29	054.63*	136.76*		
5	900.16	902.19	968.34	970.65*	050.29	052.80	148.98		
6	867.77		949.83	952.49	045.69	048.32	158.70*		
7	832.71		928.76	931.43	038.54	041.22	165.55		
8			905.08	907.84	028.28*	031.54	169.92		
9			878.94	881.93	016.49	019.32	171.70		
10			850.67	853.50		004.76	171.22		
11							167.99		
12							162.28		
N	$^OP_{23}$	P_2	$^PQ_{23}$	Q_2	$^QP_{21}$	$^QR_{23}$	R_2	$^RQ_{21}$	$^SR_{21}$
0								31172.85	31202.58
1					31156.44	31158.70*		185.98	230.64
2			31123.45		152.72	153.14	31194.75*	196.97	256.65
3	31072.79		102.32	31144.60	146.94*	146.94*	203.72	206.02	280.78
4	035.06	31077.19	079.35	136.76*	139.11*	139.11*	210.79*	213.26	302.97
5	30995.57	052.80*	054.63*	127.10*	129.69	129.31	216.17	218.64	323.26
6	954.39	026.66	028.28*	116.03	118.65	117.70*	219.56	222.18	341.65
7		30998.42	000.13	102.98	105.69	104.89	221.11*	224.07	358.17
8		968.34*	30970.65*	088.22	091.00	089.85			372.26
9		937.35	939.07	071.42		072.79			384.42
10				052.80*					
11				032.26					
12				009.38					
N	P_3	$^QP_{32}$	Q_3	$^RQ_{32}$	R_3	$^SR_{32}$	$^SQ_{21}$		
0							31293.84		
1		31258.33				31309.33	311.31		
2	31227.61	241.73	31244.51	31276.04*	31278.21*	326.12	328.35		
3	193.69*	225.25	227.61	276.04*	278.21*	342.78	345.05		
4	160.71	208.60	210.79*	276.04*	278.21*	358.64	361.09		
5	127.10*	191.65	193.69	275.02*	277.12	373.53	376.09		
6	093.39	174.11	176.03	273.19	275.02*	387.37			
7	058.70*	155.83	157.63	270.32	272.13	399.83			
8	024.00	136.76*	138.22	266.23	267.97				
9	30987.99	116.03*	117.70*	260.66	262.31				
10			095.55						

*Raies fortement recouvertes.

Le premier membre est determiné en prenant la moyenne entre les niveaux c et d des états $^3\Pi_1$ et $^3\Pi_2$ et en n'utilisant que les niveaux d de l'état $^3\Pi_0$, car il sera vu plus loin que les niveaux c de cet état sont assez fortement perturbés. Les valeurs des constantes ont été alors obtenues par la méthode des moindres carrés et ont été portées dans le Tableau III, ainsi que les valeurs de B'_e et D'_e calculées à partir des valeurs de B'_0 et D'_0 données par Ishaque et Pearse.

Afin de se rendre compte de la différence du comportement des niveaux c et d, la variation du premier membre de l'équation (1) en fonction $J\ (J+1)$ est montrée sur la Fig. 2 séparément pour les niveaux c et d. La courbe a été calculée avec les valeurs du Tableau III.

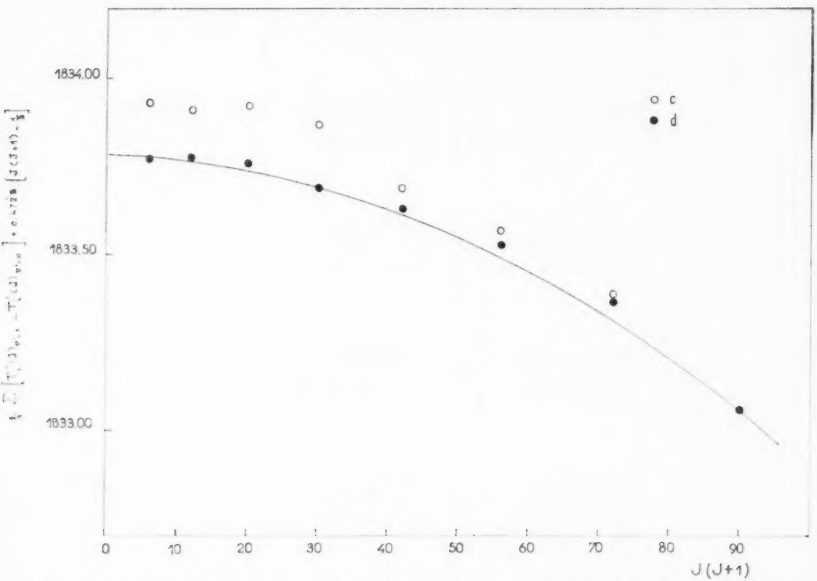

FIG. 2. Différence entre les sommes des termes $\Sigma_i T'_i(J)$ pour $v' = 1$ et pour $v' = 0$ en fonction de $J(J+1)$, séparément pour chacune des composantes c et d.

B. Constante de couplage A

La constante de couplage spin-orbite A a été déterminée à l'aide de l'équation suivante, due à Gilbert:

$$(2)\qquad \frac{3}{4B_v^2}(F_3-F_1)^2+\frac{1}{4B_v^2}[(F_3-F_2)-(F_2-F_1)]^2$$

$$= 3(Y_v-2)^2-8+12J(J+1)-24J(J+1)[2J(J+1)+1]$$

$$\frac{D_v}{B_v}+12[2J(J+1)-1]\frac{D_v}{B_v}Y_v+48J^2(J+1)^2[J(J+1)+1]\left(\frac{D_v}{B_v}\right)^2$$

où $$Y_v = \frac{A_v}{B_v}.$$

Les différences entre les termes rotationnels qui apparaissent au premier membre se déterminent à l'aide de combinaisons de différences entre les nombres d'ondes des raies. La moyenne de ces différences pour les niveaux c et d a été portée dans cette équation, mais les valeurs correspondant aux niveaux perturbés $F'_{3c}(J)$ ont été remplacées par des valeurs obtenues en supposant les niveaux F'_{3c} séparés des niveaux F'_{3d} par le même intervalle que dans la bande 0–0, ce qui revient à supposer la perturbation absente et le dédoublement Λ identique dans les deux bandes. Les valeurs de A portées en fonction de $J(J+1)$ sont montrées sur la Fig. 3, courbe 1. À titre indicatif,

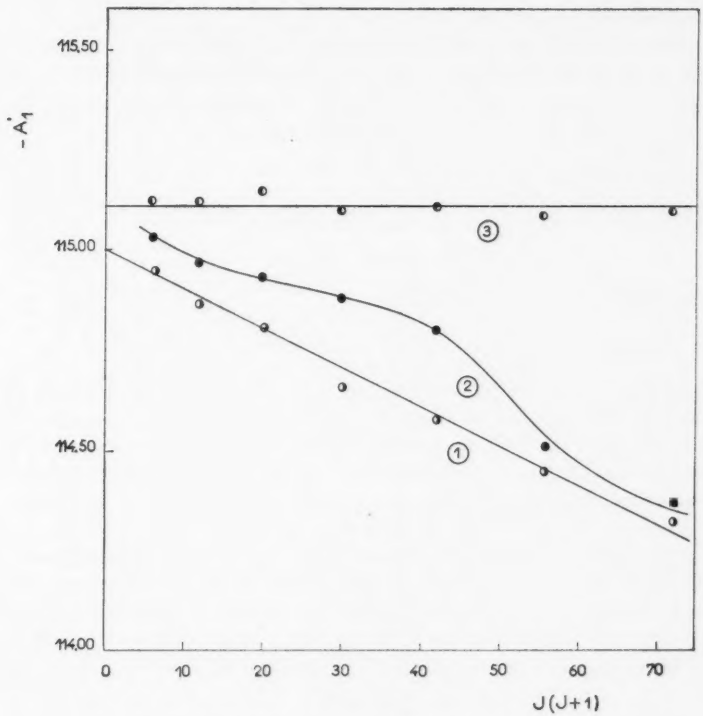

FIG. 3. Variation de la constante de couplage A'_1 avec J déterminée:
(1) Sans γ'_1 et en excluant les niveaux F_{3c}.
(2) Sans γ'_1 et avec les niveaux F_{3c}.
(3) Avec γ'_1 et en excluant les niveaux F_{3c}.

on a porté également les valeurs de A'_1 déterminées en utilisant les niveaux F'_{3c} réels (courbe 2). On remarquera que A'_1 n'est pas constant, mais varie régulièrement avec J. Dixon, étudiant les bandes de NH appartenant au

système correspondant, a montré qu'il était nécessaire de tenir compte de termes supplémentaires prévus par Mulliken (1930):

$$f_1'(N) = \gamma_v' N,$$
$$f_2'(N) = -\gamma_v',$$
$$f_3'(N) = -\gamma_v'(N+1).$$

En corrigeant les termes F_1', F_2', F_3' à l'aide de ces relations et en ajustant convenablement la constante γ_1', on obtient une valeur A_1' indépendante de J. Ceci est atteint pour

$$\gamma_1' = 0.065$$

comme le montre la courbe 3 de la Fig. 3.

Les valeurs de A_1' et de γ_1' sont portées dans le Tableau III ainsi que les valeurs de A_0' et γ_0' relatives à la bande 0–0 et qui ont été recalculées d'après les mesures de Ishaque et Pearse. Ces auteurs, n'ayant pas introduit la constante γ_0', trouvent une valeur un peu inférieure pour A_0'.

C. Dédoublement du type Λ

Chaque niveau $F_i'(J)$ est dédoublé en sous-niveaux c et d dont l'écartement

$$\delta_{cd}(N)_i = F_{ic}'(N) - F_{id}'(N)$$

peut se déterminer à l'aide des relations

$$2\delta_{cd}(N+\tfrac{1}{2})_i = R_i(N) - Q_i(N) - Q_i(N+1) + P_i(N+1)$$

et des relations analogues qui se trouvent aisément à l'aide du schéma de transition. Hebb (1936) a calculé théoriquement cet effet en fonction de trois constantes C_0, C_1, et C_2. À partir de ces résultats, Gilbert a pu ajuster les trois constantes de manière à rendre compte des résultats expérimentaux pour la bande 0–0. Par contre, le dédoublement dans la bande 1–0 s'écarte considérablement des prévisions théoriques; pour les états $^3\Pi_1$ et $^3\Pi_2$ le dédoublement est très peu différent d'une bande à l'autre, mais l'écart est considérable pour l'état $^3\Pi_0$ et l'ajustement des trois constantes est impossible. Ceci suggère que l'un au moins des deux ensembles de niveaux c et d est perturbé dans l'état $^3\Pi_0$; $v' = 1$. Ce phénomène peut s'étudier avec plus de précision en utilisant les différences entre les raies correspondantes des deux bandes. On a, par exemple,

$$[\delta_{cd}(J = N+1-i)_i]_{v'=1} - [\delta_{cd}(J = N+1-i)_i]_{v'=0}$$
$$= [R_i(N-1)]_{v'=1} - [R_i(N-1)]_{v'=0} - [Q_i(N)]_{v'=1} + [Q_i(N)]_{v'=0}$$

ainsi que d'autres relations du même type. Les valeurs obtenues sont portées dans le Tableau II. L'importance de l'écart dans l'état $^3\Pi_0$ est frappante.

TABLEAU II

Variation du dédoublement Λ entre la bande 1–0 et la bande 0–0

	$(\delta_{cd})_{v'=1}-(\delta_{cd})_{v'=0}$, cm^{-1}		
J	$^3\Pi_0$	$^3\Pi_1$	$^3\Pi_2$
0	0.04*		
1	−0.12*	0.07*	
2	0.43	−0.01	0.05
3	0.41	−0.02	0.03
4	0.56	0.04	−0.09
5	0.43	0.18	−0.12
6	0.34	−0.07	−0.10
7	0.26	−0.09	−0.04
8	0.26	−0.12	−0.10
9	0.37*		−0.08
10			−0.08
11			−0.27*

*Détermination douteuse.

D. Perturbation de l'état $^3\Pi_0$

Afin de confirmer l'hypothèse d'une perturbation de l'état $^3\Pi_0$ et de voir dans quelle mesure les deux niveaux *c* et *d* sont également affectés par celle-ci, les différences des termes rotationnels $F_i'(J)$ entre les deux bandes ont été calculées en utilisant les formules de Budó (1936) qui s'écrivent (Herzberg 1950, p. 235)

$$F_1(J) = B_v[J(J+1)-\sqrt{Z_1}-2Z_2]-D_v(J-\tfrac{1}{2})^4,$$

$$F_2(J) = B_v[J(J+1)+4Z_2]-D_v(J+\tfrac{1}{2})^4,$$

$$F_3(J) = B_v[J(J+1)+\sqrt{Z_1}-2Z_2]-D_v\left(J+\frac{3}{2}\right)^4,$$

où

$$Z_1 = \Lambda^2 Y_v(Y_v-4)+\frac{4}{3}+4J(J+1),$$

$$Z_2 = \frac{1}{3Z_1}\left[\Lambda^2 Y_v(Y_v-1)-\frac{4}{9}-2J(J+1)\right].$$

Ces formules ne sont qu'approchées et ne tiennent pas compte du dédoublement Λ. Néanmoins elles ont le mérite d'une simplicité relative et donnent une bonne approximation pour les faibles valeurs de J. Le calcul a été fait en utilisant les valeurs des constantes rotationnelles et de A_0' données dans le Tableau III. Plusieurs valeurs de Y_1' ont été essayées de façon à représenter

TABLEAU III

Constantes de l'état $^3\Pi_i$

$B_1' = 8.261_9$ cm^{-1}	$\Delta G'(\tfrac{1}{2}) = 1833.78\pm0.02$ cm^{-1}
$B_0' = 8.025$ cm^{-1}*	$A_0' = -115.67\pm0.02$ cm^{-1}
$\alpha' = 0.4728\pm0.0005$ cm^{-1}	$A_1' = -115.11\pm0.03$ cm^{-1}
$D_1' = 5.2_3\times10^{-4}$ cm^{-1}	$\gamma_0' = 0.050\pm0.005$ cm^{-1}
$D_0' = 5.7\times10^{-4}$ cm^{-1}*	$\gamma_1' = 0.065\pm0.005$ cm^{-1}
$\beta' = 0.85\pm0.03\times10^{-4}$ cm^{-1}	

*D'après Ishaque et Pearse (1939).

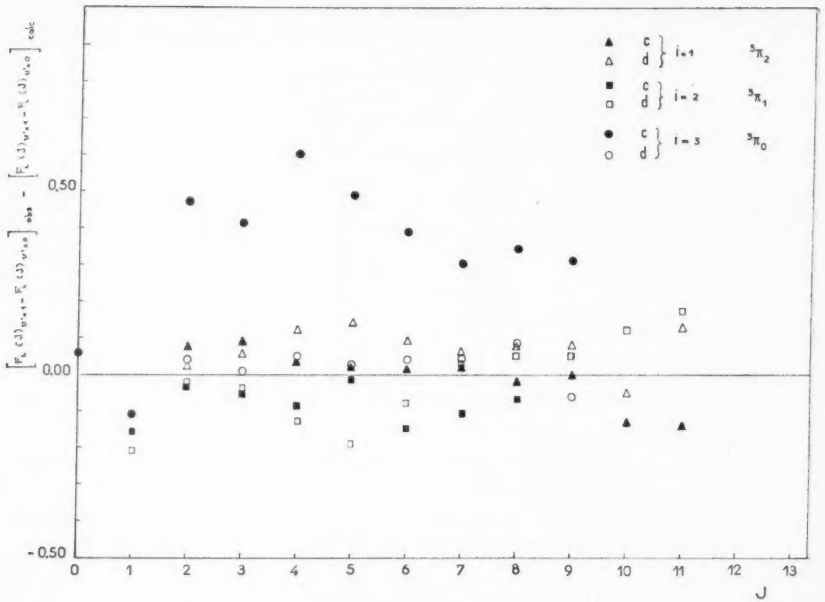

FIG. 4. Valeurs observées moins valeurs calculées de la différence entre les termes rotationnels F_i pour $v' = 1$ et $v' = 0$ portées en fonction de J, séparément pour chacune des composantes c et d.

au mieux les résultats expérimentaux. Pour

$$Y_1' = -15.257 \tag{3}$$

on obtient le résultat représenté sur la Fig. 4 où les valeurs observées moins les valeurs calculées des différences,

$$F_i'(J)_{v'=1} - F_i'(J)_{v'=0},$$

ont été portées en fonction de J pour les niveaux c et d pris séparément. Les points se groupent assez bien autour de l'axe d'ordonnée nulle, excepté ceux relatifs aux niveaux F_{3c}' qui s'en écartent considérablement pour la plupart. Toute autre valeur de Y_1' donne une dispersion plus importante. La valeur (3) est différente de la valeur $Y_1' = -15.241$ calculée à partir des valeurs du Tableau III. Cependant cette différence reste dans la marge d'erreur possible, si l'on tient compte du fait que les coefficients γ_0' et γ_1' n'ont pas été introduits dans les formules de Budó.

L'existence d'une perturbation des niveaux c de l'état $^3\Pi_0$ semble donc assez fermement établie. La perturbation des autres niveaux est, sinon nulle, du moins assez faible et il est difficile de prouver son existence avec certitude. En effet la faible variation du dédoublement quand on passe de la bande 0–0 à la bande 1–0 pour les états $^3\Pi_1$ et $^3\Pi_2$ peut s'expliquer aussi bien par une perturbation que par le changement des valeurs des constantes intervenant dans

la théorie de Hebb. La précision des mesures n'est pas suffisante pour décider. La dispersion autour de l'axe d'ordonnée zéro des points autres que ceux appartenant aux niveaux F_{3e} peut également s'interpréter par les raisons précédentes et aussi par le fait que l'approximation des formules de Budó n'est peut-être pas suffisante.

Il est difficile de déduire des résultats précédents la nature de l'état perturbateur. Si l'on admet que seule une des composantes des doublets de $^3\Pi_0$ est perturbée, parmi tous les états donnés par les deux premières configurations électroniques de PH (voir Herzberg, p. 341), seuls sont possibles les états $^3\Sigma^-$ et $^1\Sigma^+$, d'après les règles de sélection des perturbations. Cependant une perturbation par l'état de base $^3\Sigma^-$ semble peu probable, car le nombre quantique de vibration v'' devrait atteindre des valeurs trop élevées. Une perturbation par l'état $^1\Sigma^+$ reste une hypothèse plausible, mais il est difficile de l'établir fermement en l'absence de données expérimentales plus complètes.

REMERCIEMENTS

Je désire exprimer ma gratitude au Dr Herzberg et au Dr Ramsay pour leurs suggestions et conseils. Je remercie également ce dernier, ainsi que le Dr Johns, pour avoir mis à ma disposition les plaques photographiques du spectre de PH.

BIBLIOGRAPHIE

BUDÓ, A. 1936. Z. Physik, **98**, 437.
DIXON, R. N. 1959. Can. J. Phys. **37**, 1171.
EDLÉN, B. 1953. J. Opt. Soc. Am. **43**, 339.
GILBERT, C. 1936. Phys. Rev. **49**, 619.
HARRISON, G. R. 1939. M.I.T. wavelength tables (John Wiley & Sons, Inc., New York).
HEBB, M. H. 1936. Phys. Rev. **49**, 610.
HERZBERG, G. 1950. Spectra of diatomic molecules (D. Van Nostrand Co., Inc., New York).
ISHAQUE, M. et PEARSE, R. W. B. 1936. Proc. Roy. Soc. A, **156**, 221.
——— 1939. Proc. Roy. Soc. A, **173**, 265.
MULLIKEN, R. S. 1930. Revs. Modern Phys. **2**, 107.
PEARSE, R. W. B. 1930. Proc. Roy. Soc. A, **129**, 328.
TOMKINS, F. S. and FRED, M. 1951. J. Opt. Soc. Am. **41**, 641.

FORBIDDEN TRANSITIONS IN DIATOMIC MOLECULES

V. THE ROTATION–VIBRATION SPECTRUM OF THE HYDROGEN-DEUTERIDE (HD) MOLECULE[1]

R. A. DURIE[2] AND G. HERZBERG

ABSTRACT

The 1–0, 2–0, and 3–0 rotation–vibration bands of HD have been observed with a PbS infrared grating spectrometer and the 3–0 and 4–0 bands have been photographed with a 21-ft concave grating spectrograph. From these spectra precise values of the vibrational and rotational constants of HD in its electronic ground state have been determined. The variation of B_v and ΔG with v is similar to that recently established for H_2, that is, the values for $v = 0$ and 1 are markedly above the values corresponding to a linear extrapolation of the subsequent points. This leads to an uncertainty in the ω_e and B_e values which is much greater than that of the ΔG and B_v values. The (very low) intensity of the rotation–vibration spectrum of HD is in close agreement with that predicted. The decrease of intensity in going from 1–0 to 4–0 is strikingly slow, far slower than in a normal series of fundamental and overtone bands. This also is in qualitative agreement with theoretical expectation for a molecule like HD which does not have a dipole moment in its equilibrium position.

A. INTRODUCTION

The rotation–vibration spectrum of a homonuclear diatomic molecule is one of the most strongly forbidden transitions. It is forbidden as dipole radiation on account of (1) the absence of a permanent dipole moment of the molecule, (2) the selection rule that electronic states of the same parity cannot combine with one another ($g \leftrightarrow g$), ($u \leftrightarrow u$), (3) the selection rule that symmetric rotational levels do not combine with antisymmetric ones. The spectrum can occur in the free molecule only as quadrupole radiation which is many orders of magnitude weaker than dipole radiation. This is particularly so at long wavelengths since the intensity is inversely proportional to λ^3 rather than λ. The intensity of the quadrupole spectrum of H_2 was predicted to be of the order of 10^{-9} of the normal dipole intensity of infrared spectra of heteronuclear molecules. In spite of this low intensity, by using extremely long paths (up to 50 km atm), it has been observed as described in paper I of this series (Herzberg 1949, 1950*a*).

In a homonuclear molecule the three selection rules just given are not independent. But in a heteronuclear molecule consisting of two isotopes of the same atomic number, such as HD, while the rules (1) and (3) are no longer applicable, the electronic selection rule (2) still applies and may be considered as the reason for the extremely low intensity of the rotation–vibration spectra of such isotopic molecules. However, rule (2) when not supported by (3) is not an absolute rule because of the interaction of electronic motion and

[1]Manuscript received March 14, 1960.
Contribution from the Division of Pure Physics, National Research Council, Ottawa, Ontario.
Issued as N.R.C. No. 5681.

[2]National Research Council Postdoctorate Fellow 1954–55. Present address: C.S.I.R.O. Coal Research Section, Chatswood, Australia.

rotation and vibration. On account of this interaction, dipole transitions contradicting rule (2) will occur with small intensity. Alternatively, one may ascribe the occurrence of these transitions to the presence of a small dipole moment which arises when the molecule is vibrating (i.e. on account of interaction of vibration and electronic motion) but is absent in the equilibrium position. These transitions belong therefore to the group of forbidden transitions which occur because the particular selection rule holds only in a certain approximation [type (1) of I (Herzberg 1950*a*)]. They are of the same type as for example Σ^+–Σ^- transitions which are forbidden by the electronic selection rules but which can occur very weakly on account of the interaction of rotation and electronic motion.

The simplest spectrum of the type here considered is that of the HD molecule. An estimate of the intensity of this spectrum was first made by Wick (1935) and it was first observed in this laboratory (Herzberg 1950*b*) by means of the second and third overtone in the photographic infrared. Since then, measurements of the fundamental and first and second overtone have been made with a high resolution infrared spectrometer. In the present paper all the measurements from 3450 to 13,680 cm^{-1} are collected and evaluated.

B. EXPERIMENTAL

In order to obtain the photographic infrared spectrum a White multiple reflection cell similar to, but smaller than, that used in earlier papers (Bernstein and Herzberg 1948) was used. This cell was made of a glass tube 5 m long and 10 cm wide and was fitted with a set of mirrors of 5 m radius of curvature. With up to 200 traversals the intensity was still sufficient to obtain spectra with a 21-ft concave grating spectrograph. The absorbing paths were thus up to 1000 m at a pressure of 1 atm.

For the studies in the "lead-sulphide" region a similar absorption tube of 3 m length and 10 cm diameter but made of brass was used. With photoelectric detection and electronic recording the number of traversals that can be used is limited by the fall in the signal-to-noise ratio. The optimum number of traversals is dependent on the reflectivity of the mirrors and for the tube used was found to be 40 traversals. Pressures up to 3 atm were used, permitting a maximum path of 360 m atm.

The light sources used were a zirconium concentrated arc in the photographic infrared and a tungsten filament lamp in the "lead-sulphide" region.

The photographic infrared spectrum was obtained in the first order of the N.R.C. 21-ft grating spectrograph on I-N and I-M Eastman Kodak infrared plates. Exposure times ranged from ½ to 16 hours. An iron arc was used as the source of a comparison spectrum.

The "lead-sulphide" spectrum was obtained with the infrared spectrometer described by Douglas and Sharma (1953), with a 7200 lines/inch grating in first, second, and third orders and with a 15,000 lines/inch grating in first order using suitable filters to isolate the orders. Interferometrically determined Hg, Ne, Ar, and Xe lines (Burns and Adams 1953; Burns, Adams, and Longwell 1950; Meggers and Humphreys 1934) were used in higher orders as standards

for the lower-order infrared spectra. Interference fringes produced by a Fabry–Perot etalon in a continuous spectrum were used to interpolate between these standards. The vacuum corrections of Edlén (1953) were applied. Calibration and HD spectrum scans were recorded simultaneously (with photomultiplier detector for the former) by illuminating different sections of the entrance slit. Careful corrections were made for the shift produced by the curvature of the entrance slit image of the spectrometer at the exit slit (see Minkowski 1942).

Measurements on different plates in the photographic infrared and on different recordings in the lead-sulphide region show agreement within a given band to ± 0.02 cm^{-1}. The possibility of slight systematic errors remains due to very slight deviations from the integral relations between different orders, or in the photographic region due to a slight shift between comparison and absorption spectrum on account of temperature or barometric pressure changes. Thus there is a systematic difference of -0.04 cm^{-1} between the photographic and lead-sulphide wave numbers in the 3–0 band. The absolute accuracy therefore is estimated to be of the order ± 0.04 cm^{-1}.

The hydrogen deuteride (HD) was prepared by the action of heavy water on lithium–aluminum hydride ($LiAlH_4$) according to the method of Wender, Friedel, and Orchin (1949) as modified by Fookson, Pomerantz, and Rich (1951). Mass spectrometric analyses of several samples showed from 85 to 95% HD. In measurements with the brass tube it was necessary to prepare fresh HD frequently since H_2O and HDO lines gradually came up and interfered with the measurements of the HD lines. Preferential adsorption of HD on the metal wall and exchange reactions with the H_2O already present probably account for the appearance of H_2O and HDO vapor in the tube.

C. OBSERVED SPECTRA

In each of the 1–0, 2–0, and 3–0 bands seven lines were observed, in the 4–0 band six lines. The region of the 4–0 band is freest from H_2O lines. A spectrogram of this band is reproduced in Fig. 1. As can be seen, the lines form a clear R and P branch with a zero gap in between, i.e. as expected the band has the same structure as that of an ordinary infrared band of a heteronuclear diatomic molecule. In Fig. 2 part of a recording of the 2–0 band is shown including the $R(0)$, $R(1)$, $R(2)$, and $R(3)$ lines as well as a number of H_2O lines. In these regions where many H_2O lines are present the HD lines can only be recognized by comparison with spectra taken with no HD in the absorption tube. Even so some of the observed HD lines are blends with H_2O and possibly HDO lines.

In Table I the results of the measurements of the four bands are listed. For the 3–0 band the mean of the measurements from the photographic infrared plates and from the infrared recordings is given. These measurements are given separately in Table II in order to show the slight systematic difference between them.

The sharpness of the HD absorption lines on all plates and recordings even at pressures of 3 atm indicates that the slit width used was the limiting factor.

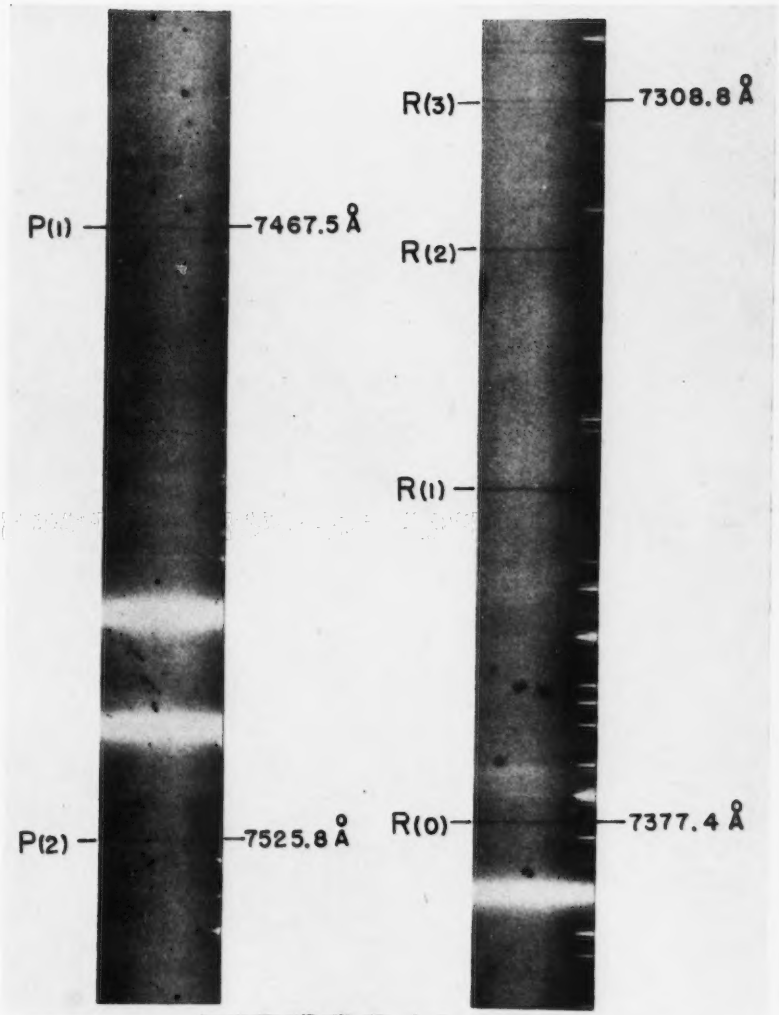

FIG. 1. 4–0 band of HD.
Absorbing path 1000 m atm. First order of 21-ft grating.

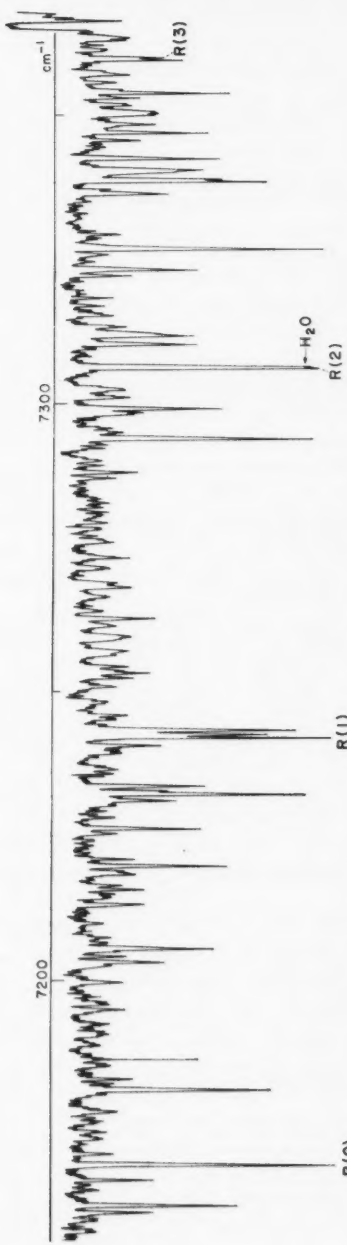

FIG. 2. *R* branch of 2–0 band of HD.
Absorbing path 200 m atm. Rapid scan in 2nd order of 7200 lines/inch grating. The unmarked absorption lines are due to H_2O.

TABLE I

Wave numbers of lines in observed HD bands

	1–0 band				2–0 band			
J	$R(J)$	o−c	$P(J)$	o−c	$R(J)$	o−c	$P(J)$	o−c
0	3717.527	−0.006			7168.428*	−0.036		
1	3798.471	+0.009	3542.934	+0.017	7241.818	0.000	6997.666	+0.016
2	3874.374*	+0.009	3450.440	−0.023	7306.541*	+0.100	6901.403	+0.010
3	3944.718	−0.008			7361.911	−0.001	6798.787	+0.011
4	4009.096	+0.002						
	3–0 band				4–0 band			
J	$R(J)$	o−c	$P(J)$	o−c	$R(J)$	o−c	$P(J)$	o−c
0	10445.466	+0.005			13551.066	+0.002		
1	10511.462	+0.016	10278.373	+0.044	13609.650	−0.006	13387.652	+0.009
2	10564.987	−0.006	10178.382	−0.009	13652.205	+0.009	13283.982	−0.011
3	10605.657	+0.001	10068.395	−0.008	13678.330	−0.003		

*Blends of doubtful accuracy.

TABLE II

Comparison of infrared and photographic infrared measurements of 3–0 band (in cm^{-1})

Line	Infrared	Phot. infrared	Average
$P(3)$		10068.408	10068.395
$P(2)$	10178.365	178.400	178.382
$P(1)$	278.362	278.384	278.373
$R(0)$	445.455	445.478	445.466
$R(1)$	511.455	511.468	511.462
$R(2)$	564.965	565.009	564.987
$R(3)$		605.670	605.657

Any pressure broadening of the HD lines is below the detectable limit. This result is similar to that for the quadrupole spectrum of H_2 for which no broadening was detectable up to 10 atm (Herzberg 1950*a*). Any collision induced dipole and quadrupole moments in H_2 and HD are clearly extremely small.

D. BAND ANALYSIS AND MOLECULAR CONSTANTS OF HD

As already mentioned, the observed band structure agrees with the expectation for dipole radiation. Because of the absence of the distinction between symmetric and antisymmetric rotational levels, transitions with $\Delta J = \pm 1$ can occur and in fact are the only ones occurring, just as for ordinary heteronuclear molecules. Consequently, the analysis of the band structure proceeds in much the same way as for the spectra of HCl, HF, CO, and others except that here, because of the high B value, the branches are very short and therefore at one place or another the standard method must be slightly modified.

If the line positions are calculated from the preliminary constants based on the 3–0 and 4–0 bands and the Raman data of Teal and MacWood (1935) systematic deviations from the present data (−0.7 for the 1–0 and −0.3 cm^{-1}

for the 2–0 band) are found. The present data allow a much more precise evaluation in themselves and can also be compared and combined with the more recent accurate Raman data of Stoicheff (1957).

Since all the branches are very short it is not possible to obtain a reliable value for the rotational constant H_v. We have therefore adopted for all vibrational levels the value $H_v = 2.2\times10^{-5}$ cm^{-1} obtained by Stoicheff for the $v = 0$ level from the rotational Raman spectrum.

Unfortunately, only two Δ_2F'' values (for $J = 1$ and $J = 2$) are available. Subtracting $12H_v(J+\frac{1}{2})^5$ from these values they give

$$(4B_0-6D_0+27/4H_0)\,(J+\tfrac{1}{2})-(8D_0-34H_0)\,(J+\tfrac{1}{2})^3$$

for $J = 1$ and $J = 2$. Therefore B_0 and D_0 can just be determined. For this purpose the average Δ_2F'' for all four bands were used. The B' and D' values obtained in the same way from the Δ_2F' are much less accurate since only one set is available for each v' and no averaging is possible. Therefore for the upper states, in order to take account of all observed lines, the constants B' and D' were determined directly from the observed line frequencies by adding $F''(J)$ as obtained from the constants just determined and making a least squares solution for ν_0, B', and D'. The results are presented in Tables III and IV. In Table III, for comparison, the rotational constants for $v = 0$ and 1

TABLE III

Rotational constants (in cm^{-1})

	Present work		Stoicheff	
v	B_v	D_v	B_v	D_v
0	44.668_7	0.0263_0	44.667_8	0.0259_2
1	42.742_7	0.0254_4	42.741_4	0.0255_3
2	40.838_5	0.0241_0		
3	38.998_8	0.0244_3		
4	37.140_1	0.0231_1		

TABLE IV

Band origins and vibrational quanta (in cm^{-1})

v	ν_0	$\Delta G(v+\frac{1}{2})$
0	0	
		3632.14_9
1	3632.14_9	
		3454.73_4
2	7086.88_3	
		3280.68_0
3	10367.56_2	
		3109.31_3
4	13476.87_6	

obtained by Stoicheff from Raman spectra are given. It is seen that the agreement is most satisfactory.

As a final check the wave numbers of the band lines were calculated back from the constants. The deviations (o−c) obtained in this way are included in Table I. These are well within ±0.02 for non-blended lines in the 1–0, 2–0, and 4–0 bands. The only larger deviation in the case of the 3–0 band is probably due to an unrecognized blending with lines of the H_2O band at 9400 Å.

In Figs. 3*a* and 3*b* the values of B_v and B_v less a linear term are plotted against v. Just as in the case of H_2 (Herzberg and Howe 1959) it is clearly seen that the first two points are appreciably above the (straight) line representing the remaining points. On account of this effect a representation of the B_v

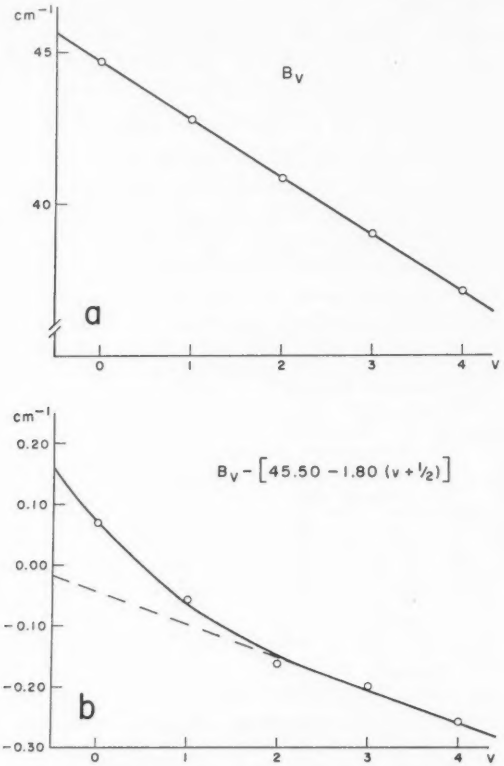

FIG. 3. B_v curve of the ground state of HD.
(*a*) Plotted directly. (*b*) Plotted after subtraction of a linear term.

values by a formula is somewhat ambiguous. A three-parameter formula through the first three B_v values is

$$B_v = 45.639_9 - 1.9478(v+\tfrac{1}{2}) + 0.0109(v+\tfrac{1}{2})^2. \tag{1}$$

But it yields deviations (o−c) for B_3 and B_4 of +0.0427 and +0.0446 cm^{-1} while a four-parameter formula using the first four B_v values is

$$B_v = 45.626_5 - 1.9069(v+\tfrac{1}{2}) - 0.02112(v+\tfrac{1}{2})^2 + 0.00712(v+\tfrac{1}{2})^3 \tag{2}$$

yielding a deviation of -0.126_2 for B_4.

If all five B_v values are used for a five-parameter solution one finds

$$B_v = 45.5920 - 1.7912(v+\tfrac{1}{2}) - 0.13418(v+\tfrac{1}{2})^2 + 0.04918(v+\tfrac{1}{2})^3 - 0.005258(v+\tfrac{1}{2})^4 \quad (3)$$

while a least squares solution with four parameters yields

$$B_v = 45.662_7 - 2.0034(v+\tfrac{1}{2}) + 0.03972(v+\tfrac{1}{2})^2 - 0.003400(v+\tfrac{1}{2})^3 \quad (4)$$

with residuals -0.0018, $+0.0072$, -0.0108, $+0.0072$, -0.0018. The B_e values following from the last two equations are rather different, showing, as did the work on H_2, that the representation of the B_v curve by a polynomial is not very satisfactory. It seems clear from the shape of the curve in Fig. 3*b* that the B_v curve is concave upwards near $v = 0$ and therefore is likely to lead to a B_e value that is higher than that which is obtained by linear extrapolation from B_0 and B_1, that is, higher than 45.6317 cm^{-1}. This would eliminate the B_e value from (3) and suggests that the B_e from (4) i.e.

$$B_e = 45.663 \text{ cm}^{-1}$$

is close to the true value although it must be realized that the other B_e values represent the observed B_v values just as well or even better.

The D_v values are plotted against v in Fig. 4. Their accuracy is not sufficient to distinguish the resulting curve from a straight line

$$D_v = 0.0266_7 - 0.0007_8(v+\tfrac{1}{2}). \quad (5)$$

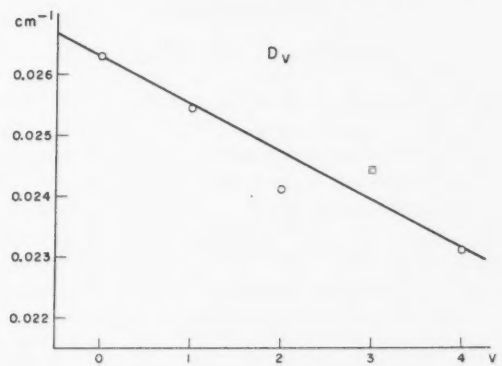

FIG. 4. D_v curve of the ground state of HD.

It is probable that for higher v values the D_v curve has a minimum with a subsequent steep rise as does the corresponding curve for H_2.

The band origins ν_0 as determined from the least squares solution for each band are given in Table IV together with the first differences, i.e. the ΔG values. The first ΔG value, $\Delta G(\frac{1}{2})$, may be compared with the value obtained by Stoicheff from the 1–0 Raman band: 3632.05_3 cm^{-1}. Our value is higher

TABLE V

Rotational and vibrational constants in the ground state of HD

B_0	44.668_7	cm^{-1}	D_e	0.0266_7	cm^{-1}
B_e	45.663	cm^{-1}	β_e	-0.0007_8	cm^{-1}
α_e	2.003_4	cm^{-1}	H_e	0.000022	cm^{-1}[a]
γ_e	0.03972	cm^{-1}	$\Delta G(\frac{1}{2})$	3632.14_9	cm^{-1}[b]
δ_e	-0.003400	cm^{-1}	ω_e	3812.29_2	cm^{-1}
r_e	0.74151	Å	$\omega_e x_e$	90.908	cm^{-1}
r_e^*	0.74119	Å	$\omega_e y_e$	0.504	cm^{-1}

[a] From Stoicheff (1957).
[b] Stoicheff gives 3632.05_4.

by 0.096 cm^{-1}. When this discrepancy was first found it amounted to 0.125 cm^{-1}. Subsequently the whole process of determining the wavelengths was carefully scrutinized but no error was detected in the infrared measurements. Fortunately a number of H_2O lines are present on the recordings of the 1–0 band which have recently been measured independently under high resolution by Plyler and Tidwell (1957). When these H_2O lines were measured on our recordings, wave numbers were found for them which differed only by $+0.029\pm0.010$ cm^{-1} from those of Plyler and Tidwell. Even though the absolute accuracy of Plyler and Tidwell's data is not known we have corrected our data of the 1–0 band by the amount given. Such a correction could be ascribed to the breakdown of the integral relation between overlapping orders. The remaining discrepancy with Stoicheff is still well outside the probable error of each determination. It is independent of either our or Stoicheff's least squares solution. This can be seen by the following combination relation

$$Q(J-1)+Q(J) = R(J-1)+P(J) \tag{6}$$

which must hold rigorously between the Q lines of the Raman band and the R and P lines of the infrared band as can readily be verified. However, one finds for $J = 1$ and $J = 2$ for the left-hand side from the Raman data 7260.252 and 7248.708 and for the right-hand side from the infrared data 7260.461 and 7248.911 cm^{-1}, that is, for both cases the left-hand side is 0.20 cm^{-1} lower than the right-hand side, which means a difference of 0.10 for ν_0. The reason for this discrepancy is not clear. The following vibrational formulae are based on the infrared measurements. If the Raman value for $\Delta G(\frac{1}{2})$ should turn out to be the correct one, ω_e will have to be reduced by approximately 0.1 cm^{-1}.

Figure 5 shows the ΔG values as a function of v after subtraction of a linear term. While the four points are not sufficient to establish the shape of the curve at higher v values, in the region investigated there is again a strong similarity to H_2, that is the first two ΔG values are appreciably above the straight line which represents the next ΔG values. For the same reasons as for H_2 it is again difficult to find unambiguous vibrational constants.

A three-parameter formula representing the first three ΔG values is

$$\Delta G(v+\tfrac{1}{2}) = 3722.11_7-180.77_6(v+\tfrac{1}{2})+1.680_5(v+\tfrac{1}{2})^2. \tag{7}$$

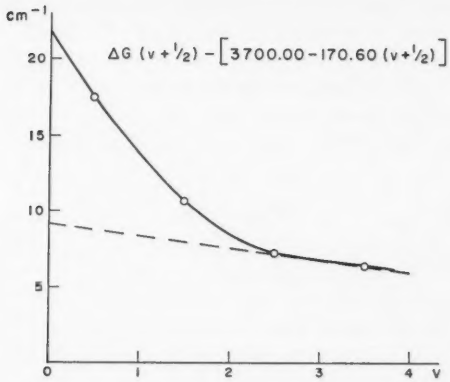

FIG. 5. $\Delta G(v+\frac{1}{2})$ curve of the ground state of HD.

It yields $\Delta G(3\frac{1}{2}) = 3109.99$ cm^{-1}, that is o−c = −0.67 cm^{-1} which is far outside any possible error. A four-parameter formula derived from all four observed ΔG values is

$$\Delta G(v+\tfrac{1}{2}) = 3722.32_8 - 181.42_2(v+\tfrac{1}{2}) + 2.186_0(v+\tfrac{1}{2})^2 - 0.1123(v+\tfrac{1}{2})^3. \quad (8)$$

Finally a three-parameter expression obtained by the least squares method from the four-observed values is

$$\Delta G(v+\tfrac{1}{2}) = 3721.88_9 - 180.30_4(v+\tfrac{1}{2}) + 1.512(v+\tfrac{1}{2})^2 \quad (9)$$

leading to residuals +0.034, −0.101, +0.101, and −0.034 cm^{-1}. The differences between these formulae point up the degree of ambiguity in the resulting ω_e, $\omega_e x_e$, ... values, an ambiguity that is not likely to be removed when higher ΔG values become known. It may be removed only when the initial curvature is understood from theory. It must be emphasized, however, that except for the very small discrepancy between Raman and infrared values of $\Delta G(\frac{1}{2})$ there is no ambiguity in the relative position of the energy levels. The ambiguity exists only with respect to their absolute position with regard to the potential minimum (i.e. the value of the zero-point energy).

Transforming equation (9) to the vibrational energy levels we obtain

$$G(v) = 3812.29_3(v+\tfrac{1}{2}) - 90.908(v+\tfrac{1}{2})^2 + 0.504(v+\tfrac{1}{2})^3. \quad (10)$$

In Table V the rotational and vibrational constants of HD in the ground state are collected. The value of r_e has been obtained from B_e neglecting the mass of the two electrons while r_e^* has been obtained from a corrected B_e^* in the way indicated by Stoicheff (1957), and may be compared with his results. These two values may be compared with the corresponding values for H_2 which are, according to Herzberg and Howe (1959), $r_e = 0.74158$, $r_e^* = 0.74116$ Å. It is gratifying to note that the two r_e^* values agree even

better than the r_e, the differences being well within the accuracy of the determinations. The corrections included in going from B_e to B_e^* are such that they should make r_e^* identical for isotopic molecules. Stoicheff (1957) on the basis of less complete data found a greater difference between the r_e^* than between the r_e. The improvement here obtained is due to the availability of data for higher vibrational levels and the recognition of the anomaly of the B_v curves at low v.

E. INTENSITIES

Wick (1935) has predicted an approximate value for the absolute intensity of the fundamental of HD in the infrared. From this figure a path of 30 m atm has been estimated as the minimum to observe this band. The actual path used here for the observation of seven lines of the 1–0 band was 200 m atm. The strongest line $R(1)$ was also observed at 50 m atm and had then an intensity which suggested that the minimum was probably 20 m atm in good qualitative agreement with Wick's prediction.

It is a striking fact that, although the maximum path used was only 50 times the minimum required for the 1–0 band, overtone bands up to 4–0 were observable. In other words the intensity of the overtone bands falls off far more slowly in HD than in ordinary heteronuclear diatomic molecules like HCl, HF, CO. In CO, for example, the 4–0 band requires a path of about 100 m atm (Herzberg and Rao 1949) while the 1–0 band can be obtained with a path of less than 0.1 cm atm, that is, the intensity ratio is greater than 100,000:1.

We have attempted a rough determination of the relative intensities of three of the HD bands 1–0, 2–0, 3–0 by measuring the integrated intensities of selected lines of these bands, selected on the basis of intensity and freedom from blends. These were $R(3)$ and $R(4)$ of the 1–0 band, $P(1)$ and $P(2)$ of the 2–0 band, and $R(1)$ of the 3–0 band. Assuming that for these low intensities the equivalent width (i.e. the integrated intensity) is proportional to the true intensity and transforming by means of the theoretical intensity ratios to $R(1)$ in each band one should obtain the same ratio independent of whether $R(3)$ or $R(4)$ of 1–0 and $P(1)$ or $P(2)$ of 2–0 are used. The considerable scatter that is actually found (up to $\pm 20\%$) may be due either to errors in placing the base line of 100% absorption or to failure of proportionality of equivalent width and true intensity. As average ratio we find, adding the estimate of the intensity ratio of the 3–0 and 4–0 bands given by Herzberg (1950*b*):

$$I_{1-0}:I_{2-0}:I_{3-0}:I_{4-0} = 1:1.9:0.24:0.08.$$

In view of the large scatter just mentioned it is not certain whether or not the initial rise of the intensity in going from the 1–0 to the 2–0 band is real. At any rate the numbers given clearly demonstrate that the intensity decrease is anomalously slow. Qualitatively this anomaly can be understood by the fact that in HD, unlike ordinary molecules like CO, the dipole moment is produced only by the vibration and increases with it. In the equilibrium position it is negligibly small. To illustrate this point Fig. 6 shows four phases

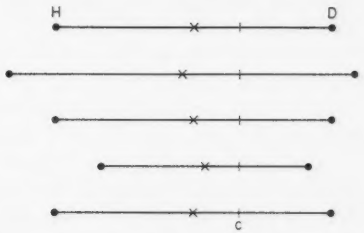

FIG. 6. Motion of center of positive (and negative) charges during vibration of HD.

of the vibration of HD: The center of mass C is of course fixed; the center of the positive charges is halfway between the H and D nuclei (indicated by x) and therefore oscillates with the frequency of vibration and with an amplitude that increases with the amplitude of the vibration. If the electrons were following instantaneously the motion of the nuclei their center would coincide with that of the positive charges, but in actual fact the electrons lag slightly behind the nuclei and therefore a dipole moment arises. The magnitude of this moment increases with the amplitude of vibration since the velocity of the nuclei increases and therefore the lagging-behind of the electrons becomes more pronounced. A quantum theoretical formulation was given a few years ago by Wu (1952). According to him the intensity ratio depends on a constant ξ whose square is essentially the ratio of intensity of Raman and Rayleigh scattering. Using the observed ratio for H_2, that is $\xi = 0.065$ one finds from Wu's diagram

$$I_{1-0}^{\text{pred.}} : I_{2-0}^{\text{pred.}} : I_{3-0}^{\text{pred.}} : I_{4-0}^{\text{pred.}} = 1:0.55:0.16:0.04$$

while for $\xi = 0.2$ one finds

$$I_{1-0}^{\text{pred.}} : I_{2-0}^{\text{pred.}} : I_{3-0}^{\text{pred.}} : I_{4-0}^{\text{pred.}} = 1:1:0.32:0.08.$$

Within the rather large uncertainty of the experimental intensities and the approximations made in the calculations the agreement must be considered as satisfactory.

It may perhaps be significant that if one matches the observed I_{3-0} by a suitable choice of ξ then both I_{2-0} and I_{4-0} are larger than predicted. In spite of a good deal of searching the 5–0 band was not found indicating that unlike 4–0 the intensity of 5–0 is not high compared to the predicted value. The intensity excess of the even-numbered bands may be due to a large quadratic term in the development of the dipole moment as a function of displacement.

F. CONCLUSION

The observation of an electric dipole infrared spectrum of HD establishes a qualitative distinction from H_2 which cannot have an electric dipole spectrum in any approximation, and this distinction is of course in conformity with the requirements of quantum mechanics. The intensity of this spectrum is determined by the mass difference. For HT the intensity would be appreciably

greater, roughly by a factor $(3/2)^2$. It may be noted that HD just as H_2 would also have a quadrupole absorption spectrum which would have an intensity very similar to that of H_2, that is, if path lengths 10 times those employed had been available the infrared bands would have shown in addition to the P and R branches also S, O, and Q branches whose intensities would show a different dependence on v than the P and R branches.

In spite of the ambiguities in the constants mentioned we believe that they, together with the Raman data, represent the best values at present available. The energy levels up to the $v = 4$ level are now known with considerable precision and can be used for precise calculations of thermodynamic functions. However, the B_v and ΔG_v formulae cannot safely be extrapolated to higher v values because as was found for H_2 no formula with three or four parameters will represent the whole course of the B_v and ΔG curves. In order to obtain reliable values for the higher vibrational levels of HD an analysis of the vacuum ultraviolet spectrum of HD under high resolution will be required.

ACKNOWLEDGMENTS

We are very much indebted to Dr. D. A. Ramsay for valuable help, particularly in the last stages of the experimental work, to Miss L. L. Howe for her painstaking work in the calculations, and to Dr. A. E. Douglas for critical discussion.

REFERENCES

BERNSTEIN, H. J. and HERZBERG, G. 1948. J. Chem. Phys. **16**, 30.
BURNS, K. and ADAMS, K. B. 1953. J. Opt. Soc. Am. **43**, 1020.
BURNS, K., ADAMS, K. B., and LONGWELL, J. 1950. J. Opt. Soc. Am. **40**, 339.
DOUGLAS, A. E. and SHARMA, D. 1953. J. Chem. Phys. **21**, 448.
EDLÉN, B. 1953. J. Opt. Soc. Am. **43**, 339.
FOOKSON, A., POMERANTZ, P., and RICH, E. H. 1951. J. Research Natl. Bur. Standards, **47**, 31.
HERZBERG, G. 1949. Nature, **163**, 170.
——— 1950*a*. Can. J. Research, A, **28**, 144.
——— 1950*b*. Nature, **166**, 563.
HERZBERG, G. and HOWE, L. L. 1959. Can. J. Phys. **37**, 636.
HERZBERG, G. and RAO, K. N. 1949. J. Chem. Phys. **17**, 1099.
MEGGERS, W. F. and HUMPHREYS, C. J. 1934. J. Research Natl. Bur. Standards, **13**, 293.
MINKOWSKI, R. 1942. Astrophys. J. **96**, 306.
PLYLER, E. K. and TIDWELL, E. D. 1957. Mém. soc. roy. sci. Liège, Ser. 4, **18**, 426.
STOICHEFF, B. P. 1957. Can. J. Phys. **35**, 730.
TEAL, G. K. and MACWOOD, G. E. 1935. J. Chem. Phys. **3**, 760.
WENDER, I., FRIEDEL, R. A., and ORCHIN, M. 1949. J. Am. Chem. Soc. **71**, 1140.
WICK, G. C. 1935. Atti reale accad. Lincei Ser. 2, **21**, 708.
WU, T. Y. 1952. Can. J. Phys. **30**, 291.

SOME RECENT DETERMINATIONS OF ATOMIC MASSES IN THE STRONTIUM–ZIRCONIUM REGION[1]

N. R. Isenor,[2] R. C. Barber,[3] and H. E. Duckworth

ABSTRACT

A large double-focusing mass spectrometer has been used to obtain new values for the masses of Sr^{86}, Sr^{88}, and Zr^{90}. Mass differences calculated from these values are found to be in better agreement with nuclear transmutation information than were previous mass spectroscopically derived values.

INTRODUCTION

There has existed in the past considerable disagreement between mass spectroscopic and nuclear transmutation determinations of the masses of certain nuclides. The most serious of these, that of the secondary standard of atomic mass, C^{12}, has been resolved only in the last few years. Another major discrepancy between the data from these two fields of investigation has existed in the strontium–zirconium region (Duckworth 1957). In this investigation a large double-focusing mass spectrometer, recently completed at McMaster University, was used in an attempt to resolve this discrepancy.

EXPERIMENTAL

The Instrument

The mass spectrometer used is a double-focusing instrument, similar in many respects to the type first used by Dempster (1935). Figure 1 is a schematic diagram of the experimental arrangement. Ions are formed in an electron bombardment source which was modified to provide for the evaporation of reasonably volatile solids, and are accelerated through a potential difference of 50 kilovolts between S_1 and S_2. The angular spread of the beam entering the electrostatic analyzer is limited by the slit S_3, which is 0.12 in. in width. The 90° electrostatic analyzer is a cylindrical condenser and is employed symmetrically. In this respect the arrangement differs from Dempster's original arrangement. The energy spread of the ions entering the magnetic analyzer is limited by a .05-in. slit, S_4. Ions of one particular value of specific charge are so deflected by the magnetic field that they pass through the collector slit, S_5. Those that pass through this slit emerge from the magnetic field and are detected by a 14-stage Allen-type electron multiplier.

The radius of curvature of the ion path in both magnetic and electrostatic analyzers is 9 ft. With $S_2 = 0.002$ in. and $S_5 = 0.003$ in., the instrument has

[1]Manuscript received February 16, 1960.
Contribution from the Department of Physics, McMaster University, Hamilton, Ontario. This work was supported by the U.S. Air Force through the Air Force Office of Scientific Research of the Air Research and Development Command and by the National Research Council of Canada.
[2]Now at Bishop's University, Lennoxville, Que. Holder of N.R.C. Studentship 1956–59.
[3]Holder of N.R.C. Bursary 1958–59.

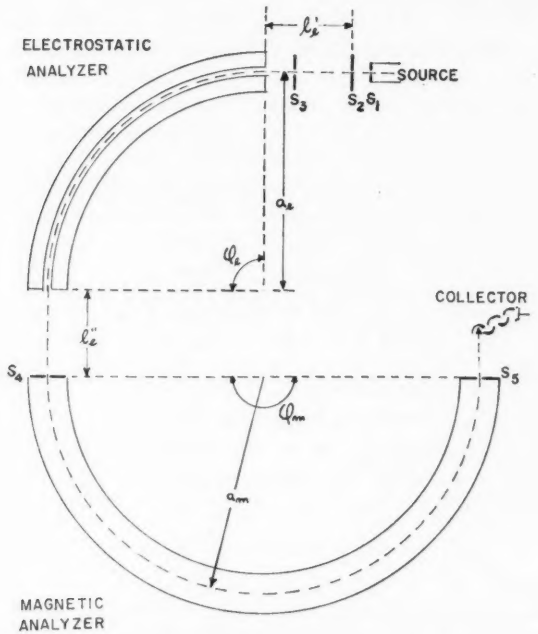

FIG. 1. Schematic diagram of the mass spectrometer. $S_1 = .006$ in., $S_2 = .002$ in., $S_3 = .12$ in., $S_4 = .05$ in. $S_5 = .003$ in., $\phi_e = 90°$, $\phi_m = 180°$, $l_e'' = l_e' = 37.8$ in., $a_e = a_m = 9$ ft.

a theoretical resolution (at the base of the peaks) of about 1 part in 20,000. The experimental resolution obtained in this investigation was about 1 part in 18,000.

The magnetic analyzer was used previously as a single-focusing instrument and its features described (Kerr, Bainbridge, Dewdney, and Duckworth 1959). When the electrostatic analyzer was added, the positions of the source and electron multiplier were changed to the positions shown in Fig. 1 and the current through the magnet coils was reversed.

Each plate of the electrostatic analyzer is made up of 11 blocks, each about 4 in. × 4 in. in cross section, fitted together and machined to give a continuously curved inner surface. The blocks are made of Armco iron, are gold-plated, and sit on alumina insulators, ground to a height of 0.625 in., which, in turn, rest on a thick steel base plate. The gap between the condenser plates is 1 in. Fringe blocks at ground potential, located 0.255 in. from the ends of the condenser plates, are used to terminate the electrostatic field (Herzog 1935). The steady deflecting voltage on the electrostatic analyzer plates is obtained from batteries.

The Peak-Matching Technique

The method of obtaining mass difference values is a variation of the now well-known peak-matching technique introduced by Smith and Damm (1956), and adapted for use in a deflection instrument by Quisenberry, Scolman, and Nier (1956).

A wave form consisting of a 30-cycle square wave (derived from batteries and a chopper relay) plus a 60-cycle sawtooth (from an oscilloscope) is imposed on the steady deflecting voltage of the electrostatic analyzer. When the amplitude of the square wave is properly adjusted, the two members of the mass spectral doublet under study are alternately transmitted by the instrument. The sawtooth component serves as a sweep voltage. In this way the doublet members are alternately swept across the collector slit and displayed as peaks on the screen of an oscilloscope (the same instrument which is supplying the 60-cycle sweep mentioned above), connected to the output of the electron multiplier by an a-c. amplifier. The square wave amplitude is adjusted carefully until the peaks appearing on the screen are superimposed. The mass difference between the doublet members is then given by the expression:

$$\Delta M = \frac{M\,\Delta V}{V+\Delta V}$$

where ΔV is the amplitude (peak to peak) of the square wave, V is the total steady voltage across the electrostatic analyzer, and M is the mass of the heavier member of the doublet. The voltages V and ΔV are measured with a differential voltmeter.

Many voltage measurements were made on each doublet, and a probable error was arrived at by combining the usual statistical error with the specified error associated with the voltmeter.

RESULTS AND DISCUSSION

Table I summarizes the mass differences obtained during this investigation. Earlier related results are included for comparison. The N_2O–CO_2 doublet

TABLE I

New mass differences (in milli-mass units) with values obtained in previous work

Doublet	This work	Previous work
N_2O–CO_2	11.2390±30	11.244 ±10 (*a*) 11.2355 ±6* (*b*) 11.23788±32 (*c*)
C_8H_7–$\frac{1}{2}Sr^{86}$	100.126 ±25	100.12 ±5† (*d*)
N_2O–$\frac{1}{2}Sr^{88}$	48.240 ±12	No previous value
CO_2–$\frac{1}{2}Sr^{88}$	36.999 ±9	37.00 ±18 (*e*)
$\frac{1}{2}Zr^{90}Cl_2^{35}$–$Kr^{80}$	4.9484±25	No previous value

*Actual doublet observed was N_2–CO.
†Actual doublet observed was C_8H_{14}–Sr^{86}.
(*a*) Kerr and Duckworth (1958).
(*b*) Scolman, Quisenberry, and Nier (1956).
(*c*) Smith (1958).
(*d*) Collins, Johnson, and Nier (1954).
(*e*) Duckworth and Preston (1951).

was used as a check on the performance of the instrument during the course of the investigation. The Sr^{++} and $ZrCl_2^{++}$ ions were obtained by evaporating strontium metal and zirconium tetrachloride into the ionization region of the source.

Table II gives the new mass values directly calculated from these differences and compares them with previous work.

TABLE II

New atomic masses (in atomic mass units) with values obtained in previous work

Nuclide	This work	Previous work
N^{14}	14.0075273±15	14.0075263 ±7 (*a*) 14.00752658±9 (*b*)
Sr^{86}	85.93667 ±5	85.93648 ±10 (*c*) 85.9362 ±8 (*d*)
Sr^{88}	87.933634 ±18	87.93396 ±11 (*c*) 87.93364 ±36 (*d*)
Zr^{90}	89.93350 ±20	89.93292 ±25 (*c*) 89.93295 ±36 (*e*)

(*a*) Scolman, Quisenberry, and Nier (1956).
(*b*) Smith (1958).
(*c*) Collins, Johnson, and Nier (1954).
(*d*) Duckworth and Preston (1951).
(*e*) Duckworth, Preston, and Woodcock (1950).

The mass values used in determining these new values were: $H^1 = 1.0081451 \pm 2$ and $C^{12} = 12.0038156 \pm 4$ (Quisenberry, Giese, and Benson 1957), $Cl^{35} = 34.9799720 \pm 22$ (Giese and Benson 1957), and $Kr^{80} = 79.94177 \pm 10$ (Duckworth 1957). Evidently, the accuracy of the new mass value of Zr^{90} is largely limited by the error in the comparison mass Kr^{90}.

Comparison with Mass Differences from Nuclear Reaction Data

The Q-values of the reactions $Sr^{86}(n,\gamma)Sr^{87}$ and $Sr^{87}(n,\gamma)Sr^{88}$ have been published (Way *et al.* 1955). These results are compared with mass spectroscopic data in Table III.

TABLE III

Sr^{88}–Sr^{86} mass difference

Transmutation data	1.99698±6	(Way *et al.* 1955)
Mass spectroscopic data	1.99748±15	(Collins, Johnson, and Nier 1954)
	1.9974±9	(Duckworth and Preston 1951)
	1.99696±5	(This work)

The results of this investigation agree very well with the transmutation data, while the best previous mass spectroscopic data disagree by about 0.5 milli-mass unit.

Two groups of values are obtained from transmutation data for the Zr^{90}–Sr^{88} mass difference, depending upon whether the $Y^{89}(\gamma,n)Y^{88}(\beta^+)Sr^{88}$ route or the $Sr^{88}(d,p)Sr^{89}(\beta^-)Y^{89}$ route is taken. The former gives a weighted mean of 1.99932±10 atomic mass units, while the latter gives 1.99971±10. The best

previous mass spectroscopic data (Collins, Johnson, and Nier 1954) give 1.99896±27 atomic mass units, while this work gives 1.99987±20.

A discrepancy of 0.39 milli-mass unit in the closed loop $Sr^{88}(d,p)Sr^{89}(\beta^-)Y^{89}(\gamma,n)Y^{88}(\beta^+)Sr^{88}$ lies at the base of the discrepancy in the transmutation data. Our work supports the $Sr^{88}(d,p)Sr^{89}(\beta^-)Y^{89}$ link. The $Y^{89}(\gamma,n)Y^{88}$ reaction (Chidley, Katz, and Kowalski 1958) seems to be a clear-cut case where the ground state of Y^{88} was definitely observed. The Q-value of the Y^{88} decay was reported (Peacock and Jones 1948) to be 3.97 milli-mass units. This value has since been estimated to be too high (Stirling and Goldberg 1956) by 0.27 milli-mass unit. Actually, the old Q-value is in better agreement with the other transmutation data and also with the mass values obtained in this investigation. This discrepancy in transmutation data deserves further attention.

REFERENCES

Chidley, B. G., Katz, L., and Kowalski, S. 1958. Can. J. Phys. **36**, 407.
Collins, T. L., Johnson, W. H., and Nier, A. O. C. 1954. Phys. Rev. **94**, 398.
Dempster, A. J. 1935. Proc. Am. Phil. Soc. **75**, 755.
Duckworth, H. E. 1957. Progress in nuclear physics, Vol. 6 (Pergamon Press Ltd., London), pp. 138–161.
Duckworth, H. E. and Preston, R. S. 1951. Phys. Rev. **82**, 468.
Duckworth, H. E., Preston, R. S., and Woodcock, K. S. 1950. Phys. Rev. **79**, 188.
Giese, C. F. and Benson, J. L. 1957. Bull. Am. Phys. Soc. II, **2**, 223.
Herzog, R. 1935. Z. Physik, **97**, 596.
Kerr, J. T., Bainbridge, G. R., Dewdney, J. W., and Duckworth, H. E. 1959. Advances in mass spectrometry (Pergamon Press Ltd., London).
Kerr, J. T. and Duckworth, H. E. 1958. Can. J. Phys. **36**, 986.
Peacock, W. C. and Jones, J. W. 1948. U.S. Atomic Energy Commission AECD-1812.
Quisenberry, K. S., Giese, C. F., and Benson, J. L. 1957. Bull. Am. Phys. Soc. II, **2**, 223.
Quisenberry, K. S., Scolman, T. T., and Nier, A. O. C. 1956. Phys. Rev. **102**, 1071.
Scolman, T. T., Quisenberry, K. S., and Nier, A. O. C. 1956. Phys. Rev. **102**, 1076.
Smith, L. G. 1958. Phys. Rev. **111**, 1606.
Smith, L. G. and Damm, C. C. 1956. Rev. Sci. Instr. **27**, 638.
Stirling, W. L. and Goldberg, N. 1956. Bull. Am. Phys. Soc. II, **1**, 291.
Way, K., King, R. W., McGinnis, C. L., and van Lieshout, R. 1955. U.S. Atomic Energy Commission TID–5300.

AN ABSOLUTE MEASUREMENT OF THE ACCELERATION DUE TO GRAVITY AT OTTAWA[1]

H. PRESTON-THOMAS, L. G. TURNBULL, E. GREEN,
T. M. DAUPHINEE, AND S. N. KALRA

ABSTRACT

An apparatus for determining the absolute value of gravity by measuring the distances through which a rule falls in discrete time intervals is described. From the data associated with 64 drops with two non-magnetic stainless steel rules in vacuum, a value of g at the absolute gravity station at Ottawa of 980.6132 cm sec^{-2} with a possible error of ± 0.0015 cm sec^{-2} has been obtained. This value is 13.7 ± 2.0 milligal less than the Potsdam value at that position.

INTRODUCTION

The determination of the acceleration due to gravity (g) is a matter of considerable importance since its value is involved in the determination of a number of derived physical, geophysical, and astronomical quantities. The value of g is both position and, to a slight extent, time dependent; however, the variations involved can be measured very accurately (to a few parts in 10^8 of g) so that in principle only a single absolute determination is required for the correct values to be assigned to the entire gravity grid of the earth. Reversible pendulums were used to make a series of such absolute determinations at Potsdam from 1898 to 1904 (Kühnen and Furtwängler 1906) and from these are derived the 'Potsdam values' of g now used throughout the world.

A number of later determinations of g have been made at various places. These have demonstrated that the Potsdam system gives values of g that are too high by an amount that is between 8 and 20 milligal (≈ 8 and 20×10^{-6} g) but the discrepancies among these measurements are such that they cannot provide an acceptable alternative to the Potsdam system, i.e. one that would be in error by an amount not substantially in excess of 1 or 2 milligal.

At the 1954 Rome meeting of the International Union of Geodesy and Geophysics it was requested that the standardizing laboratories of the participating countries attempt to complete new absolute determinations of g which would enable the Potsdam system to be superseded at the 1957 Toronto meeting of the I.U.G.G. In fact, sufficient data were not available at the 1957 meeting, and the request was renewed and emphasized with the 1960 Helsinki meeting of the I.U.G.G. being proposed for consideration of the results. The measurements reported here constitute part of this co-operative effort. The methods, results, and errors are discussed in the following sections.

[1]Manuscript received April 1, 1960.
Contribution from the Division of Applied Physics, National Research Council, Ottawa, Canada.
Issued as N.R.C. No. 5693.

Can. J. Phys. Vol. 38 (1960)

PREVIOUSLY PUBLISHED RESULTS

Although several basically different methods of determining g are available, in practice only two of them have been or are in prospect of being used: these are the determination of the periods of a reversible compound pendulum and the timing of a body in free fall. Before the Second World War, inaccuracies in the measurement of short intervals of time were such that the latter method could not compete with the former, and only compound pendulum determinations were made. From the large number of these, some few, it is commonly conceded, stand out by reason both of the care with which the determinations were made and the known corrections computed, and of the experience of the experimenters. Among these are the experiment referred to above by Kühnen and Furtwängler at Potsdam in the period 1898 to 1904, the experiment by Heyl and Cook (1936) at Washington, and the experiment by Clark (1939) at Teddington. The results of these experiments were reworked by Jeffreys (1948) to give -10.7, -17.9, and -13.1 milligal on the Potsdam system respectively. Postwar pendulum determinations by Agaletzki (1956) at Leningrad and Baglietto (1957) in Buenos Aires gave results of -12.1 milligal and -7.1 milligal from Potsdam respectively.

In 1946 Volet suggested that the timing of a rod in free fall could in principle give results that were comparable with those obtained from compound pendulums as far as accuracy was concerned, and that such measurements would not be subject to the systematic experimental errors that affected the pendulums. These errors may conceivably be quite high (of the order of milligals) and may have affected all pendulum experiments in the same sense and by approximately the same amount. By contrast it seems probable that the systematic errors of free fall experiments will be random in sense from experiment to experiment. Free fall experiments, other than a preliminary and non-definitive one by Volet (1952), have been made by Agaletzki (1956) and Martsiniak (1956) in Leningrad by two slightly different methods giving results of -7.5 and -9.3 milligal on the Potsdam system, and by Thulin (1958) at Sèvres giving -12.8 milligal on the Potsdam system. In addition, free fall experiments are underway in Brunswick, Teddington, and Washington.

It must be pointed out that the reduction of all of these results to the Potsdam system introduces the present errors in the gravity ties between the experimental stations concerned; these errors may in some instances be of the order of 1 milligal. However, it is undoubtedly possible to reduce these comparison errors to the order of half a milligal or less.

FREE FALL METHODS

One of the objects of this determination of g was the avoidance of any systematic errors that might exist in previous determinations by means of compound pendulums. The only method of measurement that did not appear as though it would probably introduce more systematic errors than it removed was the determination of the motion of a body in free fall. It was also necessary, if a satisfactory substitute for the Potsdam system was to be obtained, that errors in the experiment should be of the order of 1 or 2 parts in 10^6 or less.

The simplest free fall experiment consists of determining the time of fall (t) and the corresponding distance fallen (S) of a body that has been released from rest. The local value of g is then, of course, given by:

$$g = 2S/t^2 \tag{1}$$

and we see that if δt and δS are the errors in the time and distance measurements respectively that the error in g is given by:

$$\frac{\delta g}{g} = \frac{\delta S}{S} - \frac{2\delta t}{t}. \tag{2}$$

For purposes of comparison we will assume that S is 2 meters (giving $t \approx 0.64$ second), that lengths are measured with an uncertainty of 1 part in 5×10^6 or of 0.25×10^{-6} meter, whichever is the greater, while time intervals are measured with an uncertainty of 2×10^{-8} second. From equation (2) we then obtain a maximum possible value of δg of 0.26 milligal, 0.2 milligal arising from $\delta S/S$, and 0.06 milligal from $2\delta t/t$. This is a satisfactorily low error, but unfortunately the experiment cannot be performed in this manner. It is impracticable to release a body from rest without imparting an initial transitory acceleration to it, and it is impossible to prevent an initial relaxation of the body after its release. Position and time measurements cannot, therefore, be commenced until some time after the release.

In practice, this leaves us with two alternative methods of measurement, involving either a falling object or a rising and falling object. In the former method, adopted in this laboratory, two time intervals (t_1 and t_2) and the two corresponding length intervals (S_1 and S_2), all measured from an arbitrary point $t = 0, x = 0$, are determined, $t = 0$ being a time some tens of milliseconds after the body is released from rest. g is then given by the formula:

$$g = \left[\frac{2(S_2t_1 - S_1t_2)}{t_1t_2(t_2 - t_1)}\right]. \tag{3}$$

If, corresponding to the previous case, we consider the uncertainties of measurement to be δS_1, δS_2, δt_1, and δt_2 we obtain:

$$\frac{\delta g}{g} = \delta S_1\left[\frac{-t_2}{S_2t_1 - S_1t_2}\right] + \delta S_2\left[\frac{t_1}{S_2t_1 - S_1t_2}\right] + \delta t_1\left[\frac{S_2t_1^2 + S_1t_2^2 - 2S_1t_1t_2}{t_1(t_2 - t_1)(S_2t_1 - S_1t_2)}\right] + \delta t_2\left[\frac{S_2t_1^2 + S_1t_2^2 - 2S_2t_1t_2}{t_2(t_2 - t_1)(S_2t_1 - S_1t_2)}\right]. \tag{4}$$

If we retain the same accuracy of measurement and length of fall as before, we have thereby defined S_2, t_2, δS_2, δt_2, and δt_1. It is then necessary to select S_1 (and hence t_1), and this should be done in such a manner that the maximum value of δg is minimized. The method of doing this is shown in Appendix I, and from this and other considerations a value of ≈ 27 cm was selected for S_1, giving $\delta S_1 = 0.25$ micron and $t_1 = 0.2$ second. We then have a maximum value of δg when δS_1, δS_2, δt_1, and δt_2 all have their maximum numerical values and signs such that the errors they introduce are additive, i.e., $\delta S_1 = -0.25$ micron,

$\delta S_2 = +0.4$ micron, $\delta t_1 = +2\times10^{-8}$ second, and $\delta t_2 = -2\times10^{-8}$ second. Inserting the appropriate values of S_1, S_2, t_1, and t_2 we then obtain:

$$\delta g/g = (0.62+0.33+0.12+0.10)\ 10^{-6} = 1.2\times10^{-6} \tag{5}$$

or

$$\delta g = 1.2 \text{ milligal.}$$

Thus it can be seen that although there is no decrease in the accuracies of measurement of the time and distance intervals, yet this method has less than one quarter of the precision of the "ideal", but impracticable, first case. It is, however, sufficiently accurate for our purposes, even allowing for the effects of certain additional errors.

For completeness it should be pointed out that by throwing the free-falling body vertically upwards and timing both rise and fall (i.e. using the second of the alternative methods referred to above), it is possible to obtain the precision of the "ideal" method. If S is a fixed length in this case and t_1 and t_2 are the time intervals between the two crossings of the lower boundary and between the two crossings of the upper boundary of S respectively we have:

$$g = 8S/(t_1^2-t_2^2) \tag{6}$$

and

$$\frac{\delta g}{g} = \frac{\delta S}{S} - \frac{2t_1\delta t_1}{t_1^2-t_2^2} + \frac{2t_2\delta t_2}{t_1^2-t_2^2} \tag{7a}$$

or

$$\frac{\delta g}{g} = \frac{\delta S}{S} - \frac{2\delta t_1}{t_1} \qquad \text{for} \quad t_1 \gg t_2. \tag{7b}$$

For the same value of S and accuracy of measurement as before and the additional (and obvious) requirement that t_2 is made very small we obtain, as in the "ideal" case, a maximum value of δg of 0.26 milligal. Thus an increase in accuracy by a factor of 4.6 (for comparable geometry) will result from the substitution of the "rise and fall" for the "free fall" experiment. However, the additional complexity of the "rise and fall" experiment is considerable, and a value as high as 2 meters for S would probably be impractical in such an experiment. A ratio of 2, rather than $4\frac{1}{2}$, to 1 seems to be a more realistic appraisal of the relative accuracies. A consideration of this and the relative complexities of the experiments resulted in our selecting the "free fall" system. A "rise and fall" experiment is currently underway at Teddington.

For the equations presented above it was assumed that the local value of g was a constant over the entire experimental region; in general it is not. Above the surface of a spherically symmetrical sphere of radius r the variation in g is given by:

$$\frac{dg}{g} = -\frac{2dr}{r} \tag{8}$$

which corresponds to a gradient of about -0.3 milligal meter^{-1} for the case of the earth. Below the surface of such a sphere having a surface density of ρ we have the expression:

$$\frac{dg}{g} = -\frac{2dr}{r} + \frac{4\pi\rho G\, dr}{g}, \tag{9}$$

which for the earth gives dg/dr varying linearly with ρ from -0.23 milligal meter^{-1} to zero as ρ varies from 1 to 3.7.

It can be seen, therefore, that the variation of g will usually be significant over a vertical distance of 2 meters. However, if such variation as is present is approximately linear over the experimental apparatus (about 4 meters in the present case), the appropriate correction for g can be readily calculated (see Appendix I).

APPARATUS

As indicated above, the value of g was determined in this laboratory by measuring two vertical intervals of length and the two corresponding time intervals for a rule falling freely through these vertical intervals.

In choosing the type of rule to be dropped there are, broadly speaking, the alternatives of: (*a*) a standard meter rule carrying only two end plates, the upper one for suspension purposes, the lower one to make contact with the deceleration assembly, or (*b*) a more complicated assembly.

Alternative (*a*) has the advantages of employing a rule of 'primary standard' quality and of being so rigid in construction that movements of the graduations about the center of gravity are virtually eliminated after the initial short delay period. It is, however, limited in ultimate accuracy by its 1 meter of usable length; also it is difficult to achieve adequate uniformity of temperature along its length, while the difficulties of verifying beyond doubt that this required uniformity exists are, owing to the insulating properties of a vacuum and of metallic point contacts, almost insuperable. For these reasons we selected the second alternative (*b*); this enabled us to use a 2-meter rule, to provide a radiation shield, to measure temperatures on the rule, to measure tilt of the rule during the drop, and to provide adjustments for obtaining a truly vertical hanging position. The resulting complex construction is a considerable disadvantage, but was probably justified.

Each of the two rules used had mounted on it three semitransparent scales. These were so spaced that, as the rule fell, the scales passed the axis of a camera in synchronization with a short-duration light source activated 10 times per second. A set of fiducial cross hairs was incorporated in the camera system. The intervals between the scales were calibrated in terms of the International Metre, and the time interval between the flashes was found by photographing oscilloscope traces relating the light flashes to a standard frequency signal. At an appropriate interval before the first flash, an electrical impulse released the rule from its topmost position (see Fig. 1); it was mechanically arrested at the end of its fall. A motor-driven carriage and reset mechanism then returned the rule to its original position without the necessity of breaking the vacuum seals.

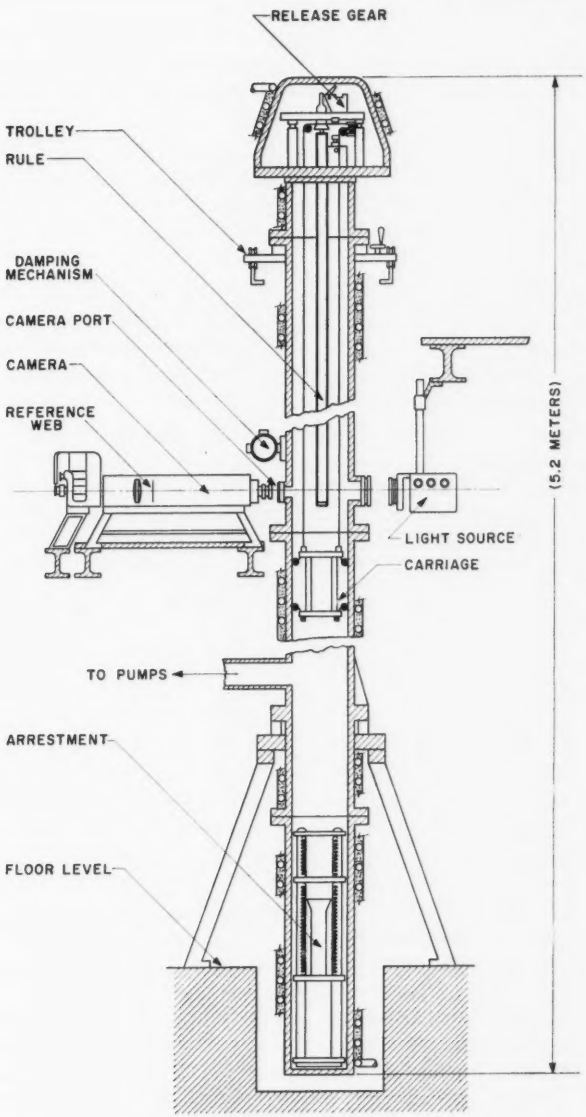

FIG. 1. General form of apparatus.

A résumé of the main points considered in the construction of the apparatus is as follows:

(*a*) Semitransparent glass scales, ruled at 0.1-mm intervals, were attached to a stainless steel rule. The relative positions of the scales, the position of each graduation on the scales, and the over-all coefficient of thermal expansion of the rule were determined.

(*b*) To reduce the effect of calibration errors, five stationary fiducial lines were used in each determination of position. The timing of the first flash, and hence the rule positions, was varied from drop to drop, and two sets (Marks I and II) of rules and scales, independently calibrated, were used in the experiment.

(*c*) Because of the high (16×10^{-6}° C^{-1}) coefficient of thermal expansion of the rule, it was desirable to know the temperature along the length of the rule to within approximately 0.005° C. This was accomplished by standard temperature stabilizing and thermometry techniques; temperatures were automatically recorded.

(*d*) Although the center of gravity of the rule assembly has an acceleration of *g*, other forces being absent, the scales can move slightly with respect to the center of gravity and so lead to erroneous determinations of *g*. The rule was assembled so as to reduce this relative movement as much as possible and to provide a high frequency of oscillation and a high degree of damping of the oscillations set up by the initial shock of release.

(*e*) The rule was dropped so as to maintain it as nearly vertical as was practicable throughout the drop. This served to reduce focussing difficulties, cosine corrections to length, and indeterminacies arising from the non-horizontality at the rule of the optical axis of the camera. Since it was not possible to maintain the rule exactly vertical, the optical axis at this point was lined up as close to the horizontal as was practicable. Determination of the angles of the fiducial lines with the horizontal were also made.

(*f*) Non-gravitational forces affecting the rule are those due to residual gases in the column and to the interaction of the rule with magnetic fields; electrostatic forces are certainly negligible. The pressure was of the order of 10^{-4} mm Hg as measured by an ionization gauge. This was high enough to impart an appreciable deceleration to the rule assembly and a correction for this effect was determined experimentally. The entire rule assembly was made of nominally non-magnetic materials so that the only effect of a magnetic field would be that arising from the introduction of eddy currents or from some ferromagnetic inclusions in the rule assembly. An approximate calculation of the upper magnitude of these effects due to the original field and field gradient suggests that they are negligible. Nevertheless, the column was wound with a series of current carrying coils which reduced the vertical component of $H(dH/dx)$ to a value of 2×10^{-4} gauss^2 cm^{-1} or less throughout the length of the column.

(*g*) Three seismographs were used to monitor the movements of the fixed camera mounting. This ensured that the position of this was not affected by

random microseisms or, more seriously, since this would constitute a systematic instead of a random error, by the release shock transmitted through the apparatus and the building walls.

(*h*) The time intervals were measured by determining the departure from the nominal 0.1-second repetition rate of the illuminating flash. This departure did not, in fact, exceed 2×10^{-8} second.

(*i*) If the rule position and the timing are to be accurately and unambiguously determined, it is necessary to have a high-contrast, fine grain photographic plate and a short period flash with a time–intensity relation that is approximately symmetrical about the peak intensity. Two types of plates and two light sources (air spark and xenon flash) were used in this experiment; these appeared to approximate sufficiently closely to the required conditions.

Details of the more important of these considerations are as follows.

Construction and Calibration of the Rules

The two rules employed were machined from No. 304 (S.A.E.) stainless steel bar stock, and differed only in minor details. Each rule (Fig. 2) is approximately 2 meters long with a channel section of about 2.3 cm^2, slotted to accommodate five scales.

The scales are aluminized to give 30% light transmission, the graduations being ruled through the aluminum. Four of these scales have a range from 14 to 20 mm, with 0.1-mm subdivisions; two longitudinal parallel lines 0.2 mm apart define the calibrated portion of the graduations while two diagonal lines serve to identify the particular graduations which are being photographed. The scales are cemented to stainless steel holders which, in turn, were fixed to the channel bar. They were aligned, using the standard optical techniques, so as to be colinear and coplanar (to within 25 μ) when the rule was unconstrained.

The fifth scale is an auxiliary focussing scale (Fig. 2). It has 12 lines ruled at 0.1-mm intervals and has its plane set at an angle of about 40 degrees to the plane of the other four scales, its graduations being parallel to their center line. When the delay circuit was adjusted so that this scale was photographed during a drop, we were able to measure the fore and aft deviation of the rule during that drop. The accuracy of this measurement depended on the depth of focus of the camera as well as on the horizontal separation of the graduations; in the system we used it was of the order of ±40 μ.

Six thermistors (Westinghouse type 14A, nominal resistance 10^5 Ω, 5000 Ωdeg^{-1}) were held in close thermal contact with the rule by inserting them into aluminum holders which were themselves cemented and clamped to the rule. The connecting wires (40 S.W.G. Tensolite cable) were cemented to the rule along its length to a point where they were brought out to the duralumin sheath, cemented to it, and attached to the 12-pole contactor shown in Fig. 2.

The radiation shield is a duralumin tube (5 cm in diameter, 210 cm long) which is clamped to the collar supporting the rule at its upper Airy point. At the lower Airy point screws project to within about 0.1 mm of the rule when the assembly is in the vertical position. These limit whip of the rule when it strikes the arrestment and provide the conventional second support for the

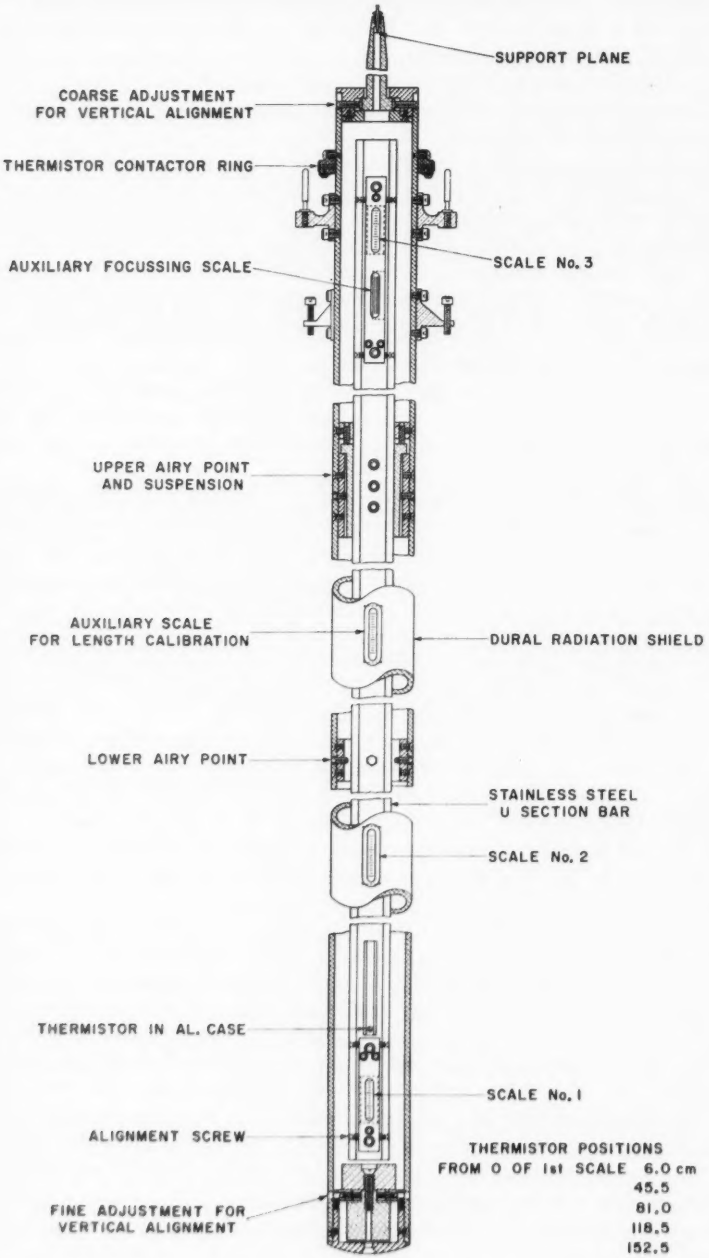

FIG. 2. Mark II rule assembly. Over-all length 210 cm, diameter 5 cm, mass ≈ 7 kg.

rule when it is being calibrated in the horizontal position. The assembly is made to hang vertically (from a 1-mm radius hemisphere resting on a plane) by means of the coarse and fine adjustments shown in Fig. 2.

Calibration

The intervals between the calibrated scales on the *g* rules were indirectly compared with the Canadian Standard Metre rule No. 306, the transfers being effected by means of two laboratory reference standards Nos. 169 and 7556, 1 and 2 meters in length respectively. Rule 306 has been compared with the standards of the International Bureau of Weights and Measures on several different occasions since its acquisition in 1921, the latest calibration being in May 1957.

The two reference standards are of invar. Rule 169 was purchased from the Société Genevoise d'Instruments de Physique in 1913; in 1951 it was sent back to the makers for refinishing and regraduating, and was received back in the National Research Council in 1953. Rule 7556, obtained expressly for the purpose of calibrating the *g* rules, was bought from the Société Genevoise in 1956. On both rules the graduations are narrow and cleanly cut—excellent for pointing operations.

The calibrations of the two principal intervals of each *g* rule were carried out immediately before and after each definitive series of drops.

Since it was impractical to immerse the *g* rules directly in the water of the comparator tank, it was necessary to encase them in specially constructed watertight (copper) tubes, with dams around the viewing ports to prevent the entrance of the water. In order that the reference rules be viewed under the same conditions, i.e. through air rather than through water, similar enclosures had to be provided for them.

The subdivisions (0.1 mm) of the scales had been previously calibrated in terms of the over-all length of each individual scale and these lengths, together with certain other principal intervals on the scales, had been compared *in situ* (by the Abbé method) with a master scale. The corresponding intervals on the master scale had been measured interferometrically and had been compared with subdivisions of rule 169. Thus in the final calculation of *g* each determination of position could be referred to the zero of the appropriate scale.

The short (i.e. the 27 cm) intervals on the *g* rules were compared with rule 169. These measurements were carried out in four steps in the following sequence:

(*a*) Four different intervals, covering practically the entire operating range of scales 1 and 2 (Fig. 2) were measured using various intervals in the region adjacent to the zero end of rule 169.

(*b*) Rule 169 was then turned end-for-end and the procedure repeated using, this time, intervals in the region adjacent to its 100-cm end.

(*c*) and (*d*) These calibrations were carried out after the series of drops had been completed; the *g* rule was turned end-for-end from its previous position and the procedures (*a*) and (*b*) repeated.

The basic short interval used in the subsequent calculations of *g* was the mean of these 16 measurements corrected to the respective zeros of their

scales. Table I gives the results of the calibrations of the short interval of the Mk II rule; the standard deviation of the 16 determinations is 0.2 μ.

TABLE I

Comparison of the 16 calibrations of various lengths in the short (27 cm) interval

Interval (cm)			Distance between scale "zeros" (20° C, cm)	
			November 1959	December 1959
Mk II	Scale No. 1 0.70	Scale No. 2 0.88	26.417 138	26.417 138
169	97.0	70.0		
Mk II	Scale No. 1 0.62	Scale No. 2 1.30	26.417 150	26.417 150
169	97.5	70.0		
Mk II	Scale No. 1 1.00	Scale No. 2 1.68	26.417 135	26.417 109
169	97.5	70.0		
Mk II	Scale No. 1 0.40	Scale No. 2 0.08	26.417 142	26.417 161
169	96.5	70.0		
Mk II	Scale No. 1 0.70	Scale No. 2 0.88	26.417 156	26.417 167
169	0.0	27.0		
Mk II	Scale No. 1 0.62	Scale No. 2 1.30	26.417 170	26.417 156
169	0.5	28.0		
Mk II	Scale No. 1 1.00	Scale No. 2 1.68	26.417 125	26.417 134
169	0.5	28.0		
Mk II	Scale No. 1 0.40	Scale No. 2 0.08	26.417 131	26.417 151
169	0.5	27.0		
Means			26.417 143	26.417 146
Mean of all			26.417 145 $^{+0.000025}_{-0.000036}$	
Standard deviation			0.16 μ	

In the measurement of the long (i.e. the 199 cm) intervals the *g* rules were compared with rule 7556 using a procedure similar to that described for the short intervals. In addition the long intervals were built up in terms of rule 169 using an intermediate scale (mid scale, Fig. 2) on the *g* rules. The differences between the direct and the built-up calibrations for these intervals were 0.1 μ for each rule.

Optical System

The optical system used to photograph the scales is illustrated in Fig. 3. Its component parts are:

(*a*) a flashing light source of very short duration which includes: a xenon discharge tube (or the air gap spark used for the Mk I rule) flashing at exactly 0.1-second intervals; a condenser system to focus the light from the flash onto the scale, and an infrared filter to prevent undue heating of the rule when it is illuminated for focussing purposes;

(*b*) a primary lens system, having a very carefully levelled optical axis,

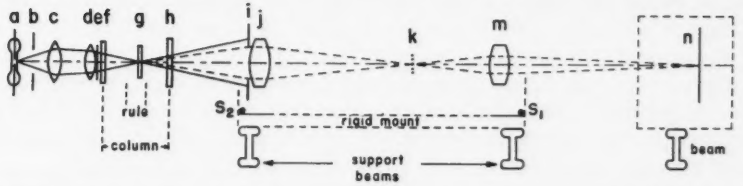

FIG. 3. Optical system. Legend: (*a*) xenon flash, (*b*) shutter, (*c*) and (*d*) condenser lenses, (*e*) heat-absorbing glass, (*f*) window, (*g*) scale, (*h*) plane parallel viewing window, (*i*) defining aperture, (*j*) primary camera lens, (*k*) fiducial cross hairs and scale image plane, (*m*) secondary camera lens, (*n*) rotating photographic plate and image plane.

which focuses an image of the scale into the plane of the set of five fiducial cross hairs; and

(*c*) a secondary lens system which focuses the combined image of scale and cross hairs onto the emulsion of a photographic plate which is rotating in such a way that the pictures from successive flashes of the drop are located in a circle without overlapping.

The xenon discharge tube and its associated circuit (see Fig. 4) are mounted on a shielded chassis just in front of the illuminating window. The tube itself

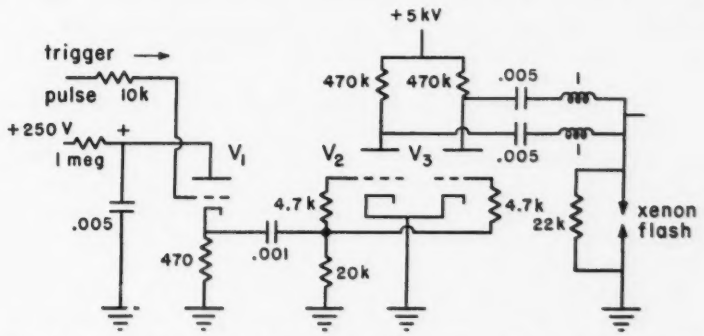

FIG. 4. Xenon flash circuit. V_1, 2D21; V_2 V_3, 3C45; resistance, Ω; capacitance, μf; inductance, μh.

has a discharge gap of about 1 mm in a 1-mm capillary which is almost filled by the electrodes so that the scrubbing action of the expanding gas will help to keep the glass clean. A xenon pressure of about 4 cm has been found to give a good intensity–time relation with little afterglow. Use of a striking voltage (3 to 5 kv) of several times the breakdown voltage of the tube produces short and accurately reproducible initiation times.

The image of the flash as it is focussed into the plane of the scale is about 2 mm high and 3 mm wide. It subtends a cone of light large enough to ensure that the transmitted beam through any used point on the scale completely fills the camera optical system. This is necessary in order that the effective

optical axis of the camera may be made and kept accurately horizontal, even though occasional slight changes are made in the position of the condenser lens so as to obtain optimum illumination.

The optical axis is defined by a circular aperture located immediately in front of the first camera lens and with its center at exactly the same level as the point in the plane of the scale which focuses on the middle one of the five cross hairs.

Aperture size was chosen at $F/5$. This value gives a depth of sharp focus of about ± 0.0040 cm and the pictures will therefore indicate immediately if the rule is not dropping straight. A larger aperture makes it difficult to illuminate the system uniformly from the flash source and could result in some loss of sharpness in the picture for tolerable horizontal shifts in the rule. The remainder of the optical system is relatively straightforward. There is an over-all magnification of about 10, equally divided between the two stages. The scale is brought into sharp focus at the plane of the cross hairs by moving the first camera lens and defining aperture in a horizontal slide (without rotation which might disturb the optical axis) after a preliminary adjustment of the rule itself by moving the whole column. Lateral adjustments can be made to sufficient accuracy by moving the column until the single vertical hairline is approximately midway between the images of the two vertical rulings on the scale. We have found that visual focussing is most convenient if the scale is under continuous illumination through a blue filter (so that the eye has the same color sensitivity as the photographic plate) and the combined image at the last focal plane is viewed with a small magnifying glass.

Before any optical alignment procedures were carried out the mechanical axis of the whole assembly was aligned and levelled. The optical axis as finally determined is, in fact, almost identical with the mechanical axis. The final adjustments for levelling the optical axis were made by means of a precisely levelled surface plate carrying a microscope. The microscope was focussed on right bisector cross hairs accurately locating the center of the aperture; it was then translated along the surface plate and sighted onto the image of the fiducial cross hairs at the scale plane. In this way it was possible to check the optical axis with all components in place except the viewing window. The optical neutrality of this window has been established separately.

The lenses and cross hairs are mounted on a heavy channel iron beam which is in turn firmly mounted on two I-beams. These I-beams are completely isolated from the main column so that the disturbances caused by release of the rule will not result in shifts of camera position. The plateholder with its motor-drive is mounted on a separate I-beam to isolate it from the rest of the optical system. As a check for possible shifts two quick response seismographs are connected at either end of the camera mounting. A further slow response seismograph is used to ensure that no long term seismic disturbances can cause an error in the measurement. These seismographs showed that no shifts greater than 0.1 μ occurred prior to the arrestment shock ($\approx 1\ \mu$) during any drop.

Light Source and Photographic Image

We are concerned with recording on a photographic plate the position of the image of a moving line that has been illuminated by a flash with some particular intensity–time relationship. In our case, three identical flashes are produced at the instants $t = 0$, t_1, and t_2, and we require that the subsequently deduced distance intervals derived from the corresponding photographs shall give us the correct value of g. This will occur only if the measured positions of the photographic images depart from some arbitrarily defined position of the optical images (e.g. that at the instant of peak intensity of the flash) by amounts δx_1, δx_2, and δx_3 such that (see equation (3)):

$$t_2\,(\delta x_2 - \delta x_1) = t_1\,(\delta x_3 - \delta x_1). \tag{10}$$

This condition is satisfied if $\delta x_n = Cv_n$ where v_n is the velocity of the rule at scale n and C is a constant.

We may assume that a photographic image is produced on the plate at all points where the intensity–time integral is equal to or greater than a certain value (K). That is to say an image will then be produced at a point distance x ($= vt$) from the position $x = 0$, $t = 0$ (corresponding to the center of the optical image at the peak intensity of the flash) if a relation of the form:

$$\int_{t+(d/2v)}^{t-(d/2v)} I_t\,dt \geqslant K \tag{11}$$

is satisfied, where d is the thickness of the optical image, v is its velocity, and $I = f(t)$.

It will be observed that the limits of development, giving the width of the photographic image, are symmetrically positioned about $x = 0$ if $I_t = I_{-t}$, i.e. if the flash is symmetrical in time. Such a flash, therefore, satisfies the conditions of equation (10) and has the additional advantage of giving equal density gradients at both limits of the photographic image, thus compensating to some extent for the non-infinite contrast of the plates. This lack of infinite contrast, even in the best of fine grain high contrast plates, makes it necessary to employ a very short duration flash so that the boundaries of the photographic image may be unequivocally determined. A short duration flash also serves to prevent undue elongation of the image.

After considerable experimental work we obtained an air spark and a xenon discharge approximating to the desired conditions of short duration

FIG. 5. Oscilloscope trace showing 100-kc reference pulse, 10-Mc timing signal, and photomultiplier output giving time–intensity relation of xenon flash.

symmetrical light flashes (see Fig. 5). The departure from symmetry consists of a comparatively long duration tail which it is impossible to eliminate entirely. It can be shown graphically that for the tails associated with our light sources there is no significant departure from the condition of equation (10) unless the peak intensities of the flashes illuminating the three scales differ by 25% or more. To guard against this possibility, the light source was always started several seconds before the drop took place, and the photographic record of the photomultiplier output showed that the intensities of the three flashes illuminating any plate were, in fact, substantially equal.

Since the flash duration is not infinitely short, there will be a difference in the appearance of the photographs of the three scales due to the differing velocities of the rule. This can be seen in the microdensitometer traces of scales 1 and 3 shown in Fig. 6.

Temperature Control and Measurement

The two stainless steel rules used for the final drops had a coefficient of thermal expansion of approximately 16×10^{-6}° C^{-1}. If temperature uncertainties were not to produce appreciable errors (0.1 milligal or more) the mean temperature of the 2-meter interval had to be known to ±0.004° C and that of the 27-cm interval to ±0.01° C. This is a fairly difficult requirement to meet for a bar that is vacuum-insulated and has the dimensions and thermal conductivity of the *g* rules. It was accomplished by controlling the temperature of the column, putting a duralumin radiation shield around the rule, and limiting the heat input to the rule.

The column was 'water-cooled' to maintain its temperature to within ±0.05° C, and the duralumin radiation shield reduced the rate of drift of temperature at any point on the rule to ±0.02° C per hour for a 1° C difference between shield and rule. The heat sources inside the column were three electric motors (for the damping mechanism, the contactor, and the setting mechanism), which were so located as to lose their heat to the column, and the arrestment, which absorbed about 150 joules of kinetic energy at each drop. In practice, this latter quantity of heat appeared not to reach the rule in an amount (≈2 joules for 0.01° C rise over 20 cm of length) sufficient to be troublesome.

Besides these heat sources, a certain amount of heat was introduced by the light source used during the damping of the oscillations of the rule and for the focussing of the camera before each drop. This heat input was reduced as far as possible by the use of heat absorbing filters and by rapid damping and focussing; however, the cumulative effect was sometimes such as to require respites from dropping during a day's operation. The gradual temperature drift evident in Fig. 7 is from this cause.

Temperature measurement was by means of six type 14A thermistors in thermal contact with the rule. These were used in conjunction with a motor-driven selector switch, a resistance bridge, and a Leeds and Northrup microvolt d-c. breaker amplifier feeding into an AZAR recorder. These last two were adjusted so as to give a sensitivity of 0.01° C per chart division, see Fig. 7. The entire unit, consisting of thermistors, switch, bridge amplifier, and

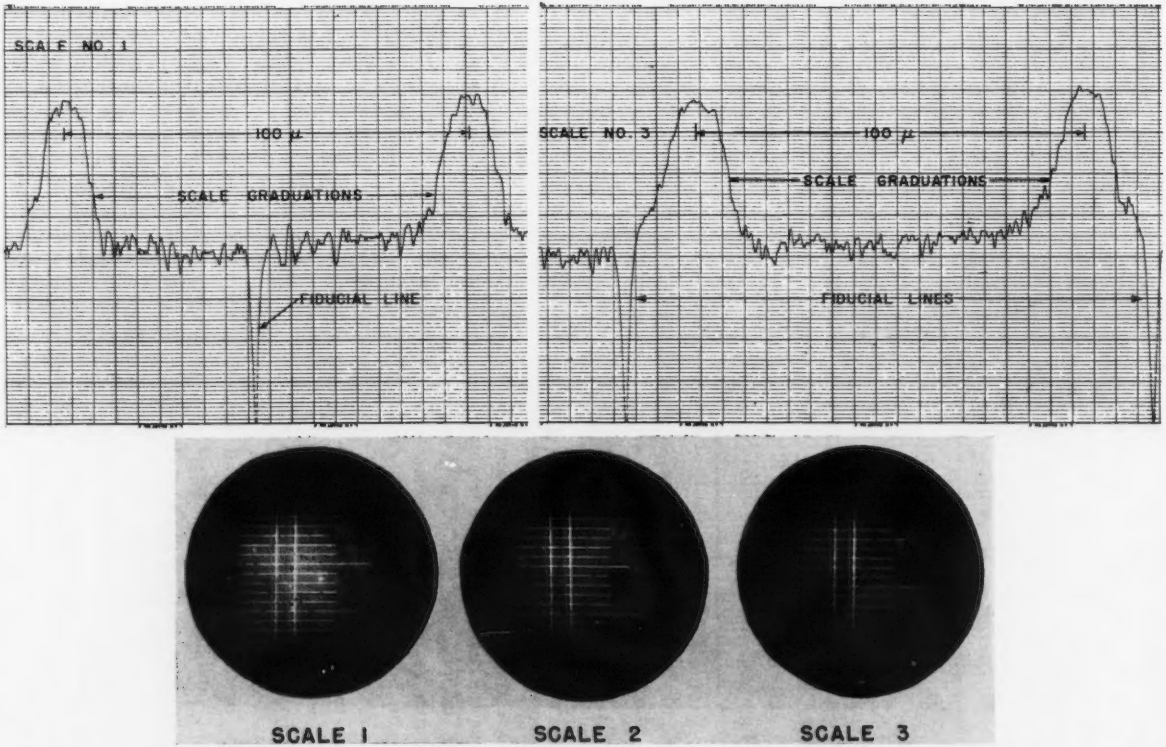

FIG. 6. Scales 1, 2, and 3 from the plate of drop 38 of rule Mk II. Microdensitometer traces from scales 1 and 3, showing effect of rule velocity and finite flash duration.

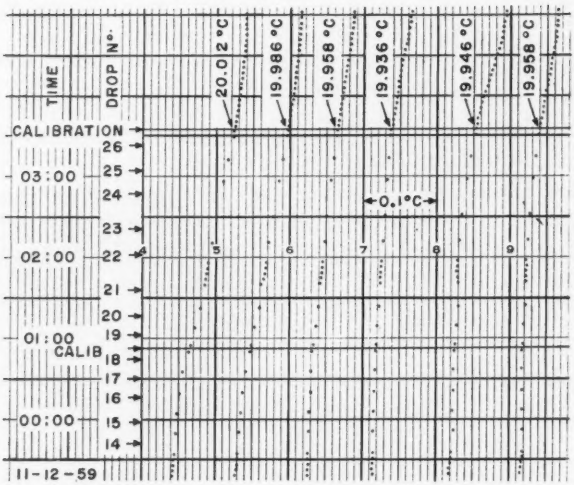

FIG. 7. Time–temperature profiles along rule Mk II.

recorder, was periodically calibrated. During four such calibrations over a period of 2 years no calibration drift greater than 0.002° C was observed. It was thus possible to determine the temperature profile along the rule with the necessary precision.

By selecting the appropriate mercury-in-glass thermostats it was possible to adjust the rule temperature to any desired value both during the calibration and in dropping the rule. The temperatures selected were such that the calibrations (excepting those used to determine the coefficient of thermal expansion, but including the calibration of the Canadian Primary Standard Metre, No. 306, at Sèvres) and all drops were made with the three standard and the two *g* rules entirely within the temperature interval of 19.7° C to 20.2° C. In any one drop, or calibration, the temperature profile of the *g* rule was within a temperature range of 0.08° C and its rate of drift of temperature did not exceed 0.05° C per hour.

These precautions resulted in all corrections for thermal expansion being very small and also made it certain that errors could not arise from uncertainties in the determination of the coefficients of thermal expansion.

Time

The accuracy of time measurement is determined by:

(i) the accuracy of measurement of cathode ray tube traces in terms of the time scale defined by a 10 Mc/s and a 100 kc/s signal;

(ii) the knowledge of the frequency of the crystal oscillator.

By measuring the timing of the light flash against the 100 kc/s pulse all trigger errors are eliminated. The pulse shapes repeat themselves with such regularity that any arbitrary point on the pulse can be measured against the

10 Mc/s signal to about 10% of the period of the latter, i.e. to 1×10^{-8} second. The time intervals t_1 and t_2 can therefore be measured to 2×10^{-8} second in terms of the time scale defined by the crystal oscillator.

The absolute frequency of this time scale, which forms part of the national frequency standard, is known to 2 parts in 10^9 through comparisons with:

(i) the time scale U.T.2 determined by the Dominion Observatory;
(ii) the caesium-beam frequency resonator standard;
(iii) the time scale U.T.2 of the other national observatories.

The maximum total error of time measurement is therefore 2×10^{-8} second or 1 part in 10^7 for the shorter time interval.

Electronic Circuits

The controls are designed to release the rule a preset interval of time before the first photograph, open the camera shutter and, after a preset number of flashes, cut off the high voltage supply from the light source. An additional function is to monitor the exact timing and shape of the light pulse. All the control and monitoring signals are obtained from a precision Essen ring type of quartz crystal oscillator. This oscillator forms a part of the national frequency standard, hence its frequency and history is known to a high accuracy.

The block diagram of Fig. 8 shows the principles of the control circuit. The fundamental frequency (100 kc/s) of the oscillator is divided down to 10 pulses

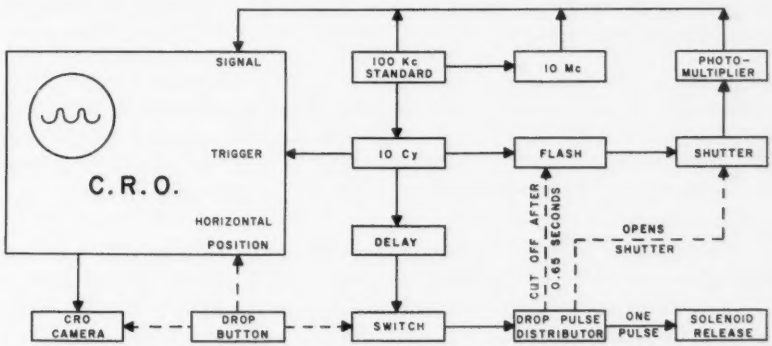

FIG. 8. Block diagram of electrical control and timing circuit.

per second which are used for control; the 100 kc/s signal is also multiplied up to a 10 Mc/s signal that is used for defining the time scale of the oscillograph trace.

A small part of the light from the spark is picked up by a photomultiplier and used to monitor the flash, and the resulting pulse is added to the 100 kc/s pulses and 10 Mc/s signals obtained from the crystal oscillator. The composite signal is displayed on the cathode ray tube, successive light flashes being automatically displaced in the vertical direction. A single photograph then shows all the light flashes for one drop. Figure 5 shows a trace due to one flash. The small amplitude sine wave is the 10 Mc/s signal, the first pulse is the

100 kc/s pulse and the second is the photomultiplier signal. Departures from the nominal values (0.2 second and 0.6 second) of t_1 and t_2 are shown as variations in this trace form.

All time measurements are made in terms of the 10 Mc/s signal and at the end a correction is applied for the departure from nominal frequency of the crystal oscillator.

Vacuum System

The column is evacuated through a 15-cm pumping line which leads directly to the water-cooled baffle of a 15-cm oil diffusion pump. This pump has a nominal 600 liter/sec pumping speed which allows us to maintain pressures below 0.1 μ, even in the presence of substantial air leaks, and ensures that other vapor pressures, e.g. of lubricants in the motors and fluid from the shock absorbers, are held to negligible values. The column pressure is measured with an ionization gauge which has been checked *in situ* by means of a Knudsen gauge.

Contactor

Electrical connections for the six thermistors are made by means of a contacting ring on the rule and a corresponding outer ring in the top of the column. This outer ring is lowered into contact position by means of a small motor before the full weight of the rule is on the support plane. Two pairs of pins and sockets position the rule on the support plane before the carriage is lowered for the next drop.

Damping

Impulses imparted to the rule during the positioning operation cause it to pendulate. The amplitude of this pendulation is reduced to the order of 25 μ by a motor-driven forked cam which is brought into contact with the assembly and then slowly withdrawn from it.

Release

The rule is released by a current pulse. The ground and lapped, hardened steel plane, on which the spherical bearing of the rule rests, is maintained in position by an electromagnet. When this is de-energized, a spring lowers the plane at an acceleration of several gravities and withdraws it from the path of the falling rule. Resetting is by means of a motor-driven cam assembly.

It was not possible to withdraw the support plane without giving a very slight lateral impulse to the top of the rule. To prevent this impulse from throwing the scales out of focus a compensating impulse was applied for the first millimeter of the drop by means of a knife-edge which pressed with constant tension against a short pin projecting from the top of the rule.

Arrestment

The arrestment mechanism consists essentially of a cage suspended by four coil springs. The falling rule assembly is received in the cage and brought to rest at an average deceleration of 8 gravities. The energy in the stretched springs is given up to two oil-filled shock absorbers which allow the cage and rule assembly to return slowly to their rest position. The initial shock of

impact, during which a high velocity is imparted to the cage, is mitigated by a sponge rubber cushion; the peak deceleration, as determined by a high-speed camera, is of the order of 60 gravities.

Rule Return

The rule is returned to its initial position by means of a motor-driven carriage. Because the motor generates a substantial amount of heat it is placed outside the column and operates through an O-ring vacuum seal.

EXPERIMENTAL PROCEDURE

The scales having been aligned on the rule, the rule was adjusted to hang vertically, using two plumb wires and travelling microscopes of short focal length to determine the relation of the upper and lower scales to the plumb wires. The rule was then given a rough preliminary calibration, inserted into the apparatus, and dropped about 20 times. This was with the intention of seeing if any gross changes in the relative positions of the scales occurred during the first few decelerations (none ever did) and of adjusting the release mechanism until the rule was dropping nearly vertically, i.e. with a rotation of 0.2 minute or less.

After this procedure the rule was removed from the apparatus, calibrated as described above, and replaced in the apparatus. Before the definitive drops began the rule was brought to within 0.1° C of the temperature at which it was calibrated and the 'degaussing' field was switched on.

The sequence of operations for each drop was:

Thermistor contactor lifted, focussing scale illuminated, rule mechanically damped, camera focussed, air conditioning switched off (to reduce vibrations), plate holder inserted and set running, pressure read, flash started (with shutter closed), amount of initial delay set, seismographs started, rule dropped. The system was then restored to the 'ready' position, the whole cycle taking about 15 minutes. When the drops were completed the rule was recalibrated.

The plates were developed, washed, and dried in the usual manner. Each plate was then read on a Zeiss 200-mm comparator by three observers. Since there were five reference marks, this meant that there were 15 determinations of position for each image.

Measurement of Photographic Plates

The distance through which the rule falls between the first and either of the two subsequent photographic exposures was computed from the measured positions of the five fiducial lines superimposed on each of the three scales, from the linear calibration of the scale itself, and from the previously determined interval between the scales concerned. The procedure adopted in measuring the photographic plates was to point on each of the fiducial lines and on the adjacent graduations.

With perfect calibrations and ideal observers we would have for any one drop the relations:

$$(12) \qquad {}^1x_{n,m} = {}^2x_{n,m} + P = {}^3x_{n,m} + Q$$

where x is the distance of a fiducial line n read by observer m from the zero of the scale designated by the superscript, and P and Q are two constants connecting scales 1 and 2 and scales 1 and 3 respectively. To assess the consistency of the readings and the accuracy of the calibrations, values of P and Q were determined for each of the 15 sets of readings made for each drop. Table II shows the results for a typical* drop (number 38 for rule Mk II). As an

TABLE II

Comparison of the results of the readings of the three observers (A, B, and C) on each of the five fiducial lines for a typical drop (drop 38, rule Mk II)

Constants of equation	12	P, mm	Q, mm
Fiducial line 1	A	8.3849	3.7231
	B	54	35
	C	48	29
Fiducial line 2	A	58	40
	B	61	33
	C	52	25
Fiducial line 3	A	47	28
	B	49	26
	C	47	26
Fiducial line 4	A	54	34
	B	50	28
	C	47	26
Fiducial line 5	A	62	34
	B	52	31
	C	54	35
Mean of all		8.3852	3.7231
Range from mean	A	$(+1.0, -0.5)\mu$	$(+0.9, -0.3)\mu$
	B	$(+0.9, -0.3)$	$(+0.4, -0.5)$
	C	$(+0.2, -0.5)$	$(+0.4, -0.6)$

additional check on the consistency of the readings, the value of g as determined from the readings of each observer for all drops was computed. These differed from the mean value by less than 0.1 milligal.

RESULTS

A preliminary set of 19 drops was made in August 1957 with the Mk I rule and gave a value for g (employing one observer only) of 980.6136 cm sec^{-2}.

A definitive series of 32 drops was made in August 1958 with the same rule (Mk I) after the scales had been realigned and minor improvements made to the apparatus. The value obtained for g was 980.6139 cm sec^{-2}. In both series for this rule an air spark light source was employed. This rule did not have an auxiliary focussing scale.

In December 1959 another definitive series of 32 drops was carried out with the Mk II rule using a xenon discharge tube as light source. The value for g obtained from these drops was 980.6124 cm sec^{-2}.

The individual values obtained from these drops are shown in Table III and Fig. 9.

*Of the 32 sets of values for P and Q obtained with this rule, half have variations greater and half have variations smaller than those of this plate.

TABLE III

Dec. 1959		Aug. 1958		Aug. 1957	
Drop No.	g, cm sec^{-2}	Drop No.	g, cm sec^{-2}	Drop No.	g, cm sec^{-2}
1	980.6122	2	980.6132	2	980.6089
3	.6130	4	.6131	5	.6122
4	.6130	6	.6154	6	.6123
6	.6124	8	.6142	8	.6189
7	.6130	9	.6118	9	.6141
8	.6124	11	.6139	12	.6131
11	.6132	12	.6133	24	.6129
12	.6124	13	.6159	25	.6162
13	.6122	15	.6148	26	.6160
14	.6116	16	.6146	28	.6131
16	.6123	17	.6144	29	.6107
17	.6106	18	.6151	30	.6138
20	.6124	20	.6143	32	.6140
21	.6128	21	.6147	33	.6156
22	.6118	22	.6140	34	.6114
23	.6123	23	.6141	35	.6157
24	.6127	24	.6145	36	.6144
26	.6127	25	.6136	38	.6140
27	.6132	26	.6136	40	.6123
28	.6135	27	.6142		
29	.6130	28	.6139		
30	.6123	29	.6139		
31	.6122	30	.6148		
33	.6118	32	.6132		
34	.6117	33	6135		
36	.6123	34	.6131		
37	.6122	35	.6136		
38	.6121	36	.6125		
40	.6121	37	.6130		
42	.6117	38	.6124		
43	.6130	39	.6139		
44	.6129	40	.6132		
Mean	980.6124		980.6139		980.6136
Std. dev.	±0.0006		±0.0009		±0.0022
Range	0.0029		0.0041		0.0100

In practice, about 25% of the drops involved some mechanical or human malfunctioning, so that position, time, and satisfactory seismograph records were not all available. No drop where all three were available has been omitted from the above table. In the two definitive sets of drops no drop had to be omitted due to unsatisfactory seismograph records. The mean of the definitive sets is 980.6132 cm sec^{-2}.

CORRECTIONS

Extension of Rule under Vacuum

This was calculated from standard data for the steel used: the correction amounted to +0.2 milligal.

Extrapolation to Vacuum Condition

The definitive drops were carried out at a pressure of about 0.07 μ of Hg. The appropriate correction to g was found experimentally. The correction was high (+0.5 milligal) and to a considerable extent indeterminate; it has therefore been discussed separately, see Appendix II.

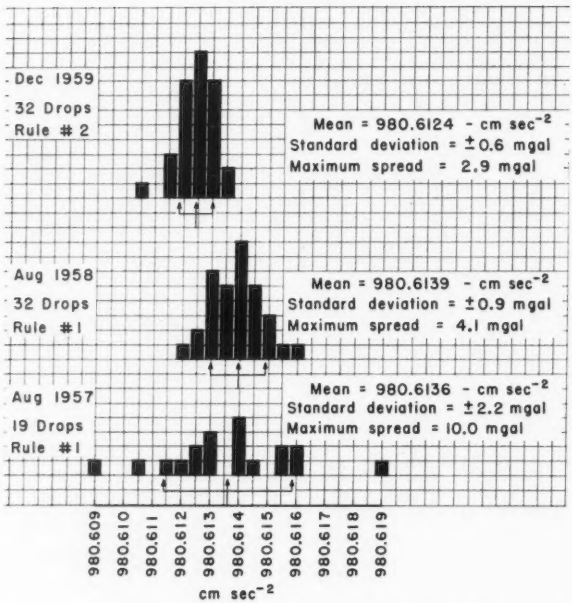

FIG. 9. Histogram of the three sets of drops with rules Mk I and II.

Non-Horizontality of the Fiducial Lines

In the drops made with the Mk II rule the fiducial lines departed significantly from horizontality. The rule was dropping with a measurable lateral shift, and an appropriate correction, averaging 0.3 milligal, was applied to each drop.

Departure of Standard Frequency from Nominal

This was -8 parts in 10^8 for the drops of the Mk I rule and -9.5 parts in 10^8 for Mk II rule (-0.16 and -0.19 milligal).

Correction for Gravitational Gradient

The values of g obtained from equation (3) apply to a position in space approximately 55 cm below the center of gravity of the rule assembly at the start of the time and distance intervals (see Appendix I). The local vertical gradient of g has been measured and found to be 2.6×10^{-6} cm sec^{-2} cm^{-1}. The appropriate correction to reduce the results to the position of the optical axis is, therefore, $+0.12$ milligal.

ERRORS

Table IV gives a summary of those errors which could significantly influence the measured value of g. Additional comments are:

1. Rule calibration and plate reading errors are due chiefly to uncertainty of the primary calibration of the interval, and to a lesser extent to pointing

TABLE IV

		Probable maximum errors (e)
(1) Rule calibration and plate reading	Short interval	±0.62 mgal
	Long interval	±0.33
(2) Time	Short interval	±0.12
	Long interval	±0.10
(3) Temperature		±0.08
(4) Correction for thermal expansion		±0.03
(5) Levelling of optical axis		±0.08
(6) Tilt of cross hairs		+0.03*
(7) Residual gas pressure		−0.2 to 0.5
	Σe =	2.0
	$\sqrt{\Sigma e^2}$ =	0.9

*This applies for the Mk II rule; for the Mk I rule e was 0.18 milligal.

errors on the plates; these latter are presumably random and are averaged over a number of readings.

2. Errors in time measurement, as discussed earlier, may amount to 2×10^{-3} second.

3. Thermal shielding, thermal contact with the rule, thermistor power input (5 μwatt) and reading accuracy were such that rule temperature at the thermistors was known to better than ±0.003° C. The measuring circuit allowed monitoring for electrical leakages and no readings of any sort were taken when leakage could have contributed a significant error.

4. The error in the correction for thermal expansion arises from a ±1% uncertainty in the expansion coefficient, and will only be this large at the extreme temperatures encountered (19.7° C and 20.2° C).

5. The maximum tilt of the optical axis of ±3 minutes coupled with the greatest horizontal motion of the third scale is required to give the quoted ±0.08-milligal error.

6. The tilt error arises from lateral shifts of the scales with respect to the vertical cross hair as the rule drops, together with an uncertainty of about 3 minutes in the amount of tilt. The error is much greater for the Mk I rule because a substantial lateral shift (≈300 μ) was present throughout the drops.

7. The lower limit (−0.2 milligal) for the error of the residual gas correction has been set to coincide with the theoretical value at the operating pressure. The higher upper limit was selected as a result of the unsatisfactory agreement between theory and experiment.

A number of other factors that might affect the results were considered. These were either eliminated by appropriate design of the apparatus, or else measured and corrected for. Errors, after any appropriate correction has been applied, arising from the following sources are therefore considered to be negligible:

Dilation of the rule, vibration of the rule assembly, seismic vibrations, cosine corrections for tip and curvature of the rule, coriolis forces, diurnal variations of g, vertical gradient of g, asymmetry of the flash, flash lifetime, differential shrinkage of the photographic emulsion, and magnetic fields.

The sum of the probable maximum errors is about 2 milligal, not inconsistent with the difference between the results of the two rule assemblies. However, 0.5 milligal (the uncertainty in the pressure correction) is presumably in the same sense and of the same order of magnitude for each rule: in the light of this, the separation of the two sets of results seems fairly high. Taking this into consideration, we believe that we are justified in assigning a possible error of ± 1.5 milligal from the mean of the two sets of results.

DISCUSSION

The absolute gravity station at Ottawa is located in the subbasement of the National Research Council building, Sussex Drive, Ottawa, and is defined as the intersection of the optical axis and the geometric axis of the vacuum column. Its geographical co-ordinates are: latitude, 45° 26′ 18″.2, longitude, 75° 41′ 51″.3, altitude, 57.6 meters above mean sea level. The value of g at this point is 7.29 ± 0.03 milligal higher than the value of g at the national reference gravity station at the Dominion Observatory, Ottawa. The accepted best value of the reference station in the Potsdam system is 980.6196 cm sec^{-2} (Winter *et al.*). This gives a Potsdam value for the absolute gravity station of 980.6269 cm sec^{-2}. Our measured value of 980.6132 cm sec^{-2}, the mean of the two definitive sets of drops, is therefore 13.7 milligal below the Potsdam system. The uncertainty in the gravity ties is in the order of ± 0.5 milligal. From the above considerations we conclude that the correction to the Potsdam system required to bring it to absolute gravity units is $(-13.7 \pm 2.0) \times 10^{-3}$ cm sec^{-2}.

ACKNOWLEDGMENTS

The authors wish to express their appreciation to Dr. L. E. Howlett, Director of the Applied Physics Division, and Dr. J. T. Henderson, head of the Electricity and Mechanics Section, for their interest in this work. We also acknowledge the very substantial technical contributions which have been made by Mr. M. Grimm during the construction of the apparatus, Messrs. A. Clark, J. Hamel, G. West, and A. Gendron in the calibration of the rule and reading of the plates, and Mr. C. G. M. Kirby during the development of the discharge and timing circuits and the carrying out of the experiments. We should also like to mention that this project was initiated by Mr. R. H. Field shortly before his retirement in 1954.

APPENDIX I

Time Ratios

We require the ratio of the time intervals t_2 and t_1 such that the error in g arising from errors of measurement of S_1, S_2, t_1, and t_2 is a minimum.

Under uniform acceleration g the intervals S_1, S_2, t_1, t_2 are related by equation (3), i.e.:

$$g = \frac{2(S_2 t_1 - S_1 t_2)}{t_1 t_2 (t_2 - t_1)}.$$

Where δS_1, δS_2, δt_1, δt_2 are the uncertainties of measurement, the uncertainty in g is given by:

$$\tfrac{1}{2}\delta g = \delta S_1 \frac{-t_2}{t_1 t_2(t_2-t_1)} + \delta S_2 \frac{t_1}{t_1 t_2(t_2-t_1)} + \delta t_1 \frac{S_2 - g t_2(t_2-2t_1)}{t_1 t_2(t_2-t_1)} - \delta t_2 \frac{S_1 - g t_1(t_1-2t_2)}{t_1 t_2(t_2-t_1)}. \tag{13}$$

δg is a maximum when $\delta S = -\delta S_1 = \alpha \delta S_2$ and $\delta t = \delta t_1 = -\delta t_2$,* where α is determined from experimental conditions.

If $Kt_1 = t_2$, the above equation reduces to

$$\tfrac{1}{2}\delta g = \delta S \frac{\alpha K+1}{t_1^2 K(K-1)} + \delta t \frac{v_0 + (v_0+2gt_1)K}{t_1^2 K(K-1)} \tag{14}$$

where v_0 is the velocity at time $t = 0$.

In practice, the contribution of the second term in the above equation is small, and the optimum may be determined from the first term only by making $(\partial/\partial K)\ \delta g = 0$. This gives

$$K = \frac{1+\sqrt{\alpha+1}}{\alpha} \tag{15}$$

or $t_2 = 3\ t_1$ when $\alpha = 0.6$.

Gravitational Gradient

In general $g = g_0 + \beta X$ where β is a constant and X is a vertical displacement. If we define the position of the center of gravity as

$$X = \frac{g_0}{2}(t+\Delta t)^2 - X_0 \tag{16}$$

where Δt is the time interval between the release of the rule and the first flash (at $t = 0$), the equation of motion is given by:

$$\frac{d^2X}{dt^2} = g = g_0 + \frac{\beta g_0}{2}(t+\Delta t)^2 - \beta X_0. \tag{17}$$

A double integration of this equation gives

$$X = g_0\left\{\frac{t^2}{2} + \beta\left[\frac{t^4}{24} + \frac{t^3\Delta t}{6} + \frac{t^2(\Delta t)^2}{4}\right]\right\} + v_0 t - \frac{\beta X_0 t^2}{2} \tag{18}$$

where v_0 is the velocity at time $t = 0$. Rewriting equation (18) in terms of the distances S_1 and S_2 and time intervals t_1 and t_2 we obtain:

$$g_0 = \frac{2(S_2 t_1 - S_1 t_2)}{t_1 t_2(t_2-t_1)}\left\{1 - \beta\left[\frac{t_2^3 - t_1^3}{12(t_2-t_1)} + \frac{\Delta t}{6}(2t_2+2t_1+3\Delta t) - \frac{X_0}{g_0}\right]\right\}. \tag{19}$$

The second term within the brackets therefore gives the fractional correction

*Assumption of equal magnitudes for the time errors is consistent with the conditions of our experiments.

to be applied to the value determined from equation (3) if g is to be referred to the position of the center of gravity at $t = 0$. For the constants of our experiment ($\Delta t = 0.04$ sec, $X_0 = 0.8$ cm, $\beta = 2.6\times10^{-6}$ sec^{-2}, $t_1 = 0.2$ sec, $t_2 = 0.6$ sec) the expression in the bracket has the value $(1-1.4\times10^{-7})$.

Force Proportional to Velocity

A retarding force proportional to the velocity of the rule arises from the action of the residual gas in the vacuum chamber. For such a force we have $F = Kv$, and since $v \simeq g\,(t+\Delta t)$, the equation of motion may be written as

$$\frac{d^2X}{dt^2} = g\left[1-\frac{K}{m}(t+\Delta t)\right] \tag{20}$$

where m is the mass of the rule. Then we have

$$X = \tfrac{1}{2}gt^2\left[1-\frac{K}{m}\left(\frac{t}{3}+\Delta t\right)\right]+v_0t \tag{21}$$

and as in the previous case we can write:

$$g = \frac{2(S_2t_1-S_1t_2)}{t_1t_2(t_2-t_1)}\left[1+\frac{K}{m}\left(\frac{t_2+t_1}{3}+\Delta t\right)\right] \tag{22}$$

For our case, $\delta g = 0.3\,K/m$.

APPENDIX II

Pressure Effect

The forces exerted on the rule by the residual gases in the column can be divided into 'static' and 'streaming' effects. At pressures below 1 μ of Hg only 'molecular flow' of the gas need be considered. The static effect then arises from the average momentum imparted by the moving rule to the randomly directed molecules striking it. If, as is probable, the coefficient of slip of the molecules is zero, that is to say that the direction of departure of a molecule from the rule is independent of its original direction of approach, then the net force on the rule is given by:

$$F = AP\sqrt{\frac{M}{2\pi R_0T}}\cdot v = Kv \tag{23}$$

where A is the superficial area of the rule assembly, P is the pressure, v is the velocity of the rule, M is the average molecular weight, and R_0 and T have their usual significance. The effect on the measured value of g of a force that is proportional to the rule velocity is for our case, see Appendix I, given by:

$$\delta g = 0.3\,K/m$$

where m is the mass of the rule assembly.

This can be rewritten, using equation (23), as:

$$\delta g = 2.4\times10^{-7}\,P \text{ cm sec}^{-2}$$

where P is in dyne cm^{-2}.

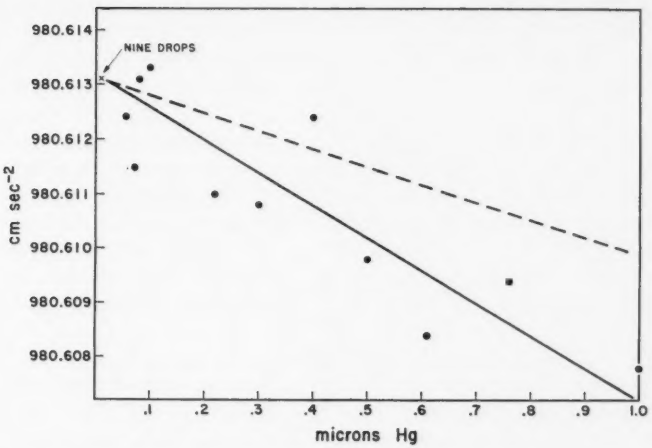

FIG. 10. Pressure–acceleration curve between 0.01 and 1.0 μ of Hg. The cross is the average value of nine drops at this pressure. The dotted line gives the theoretical slope for the molecular flow region of 'static' air.

The dotted line in Fig. 10 has this pressure dependence. The solid line of Fig. 10 is a closer fit to the experimental points of a series of drops at various pressures. These drops were made after the definitive series, and with less attention paid to the quality of the plates, attitude of the rule, accuracy of reading, etc. Their scatter, therefore, is greater than that of the definitive drops.

The departure of the results shown in Fig. 10 from the theoretical line suggests that a systematic departure from "static air" conditions at the given pressure exists. This may consist of: inaccuracies of a factor of 2 in the pressure measurement; heavier than air molecules in quantities sufficient to increase M by a factor of 4; or streaming effects.

To take these in order:

The ionization gauge used was calibrated *in situ* against a Knudsen (thermo molecular) gauge and found to be accurate except at the lowest pressures ($\approx$0.01 μ) where the ion gauge read high ($\approx$0.02 μ), presumably due to the presence of hydrocarbon molecules.

It is probable that the pressure in the column was due to air molecules both during the definitive drops and during the drops taken to determine the pressure effect; in the first case an inadvertent and in the second case a deliberate air leak was present, while the accuracy of the ionization gauge in both cases strongly suggests that it was measuring air molecules.

The known position and size of the leaks involved and of the pumping orifice make it possible to estimate the effect of a stream of gas. This is given by equation (23) where v is now the velocity of the gas stream relative to the rule and A is the area, not necessarily the total superficial area of the rule

assembly, on which the stream acts. Taking the position of the two leaks into account it does not seem possible that streaming would affect the result by more than 0.1 milligal at a pressure of 1 dyne cm^{-2}, while such effect as is estimated to exist would increase rather than diminish the slope of the curve in Fig. 10.

In an attempt to resolve this discrepancy between theoretical and experimental slope a series of drops were made at higher pressures. In the pressure region between 1 μ and 200 μ we expect to observe an effect compounded of molecular flow and viscous drag; at still higher pressures the inertial drag of the entrained air, the pumping effect of the rule, and similar effects will enter the picture. In the intermediate region the dependence of g on pressure was about four times as great as theory (c.f., for example, Dushman (1949)) indicates.

In these rather unsatisfactory circumstances it appears that the proper correction for the pressure effect is that taken from the slope of the curve of Fig. 10; this amounts, for the operating pressure of 0.07 μ of Hg, to 0.5 milligal. It is a matter of regret to the authors that the experiment was not conducted at a pressure of the order of 0.01 μ of Hg.

REFERENCES

AGALETZKI, P. N. and EGOROV, K. N. 1956. Izmeritelnaya Tekh. i Poverochnoe Delo, **6**, 29.

BAGLIETTO, E. E. 1957. International Union of Geodesy and Geophysics Study Group No. 5 Report; also *in* Bulletin géodesique (in press).

CLARK, J. S. 1939. Trans. Roy. Soc. A, **238**, 65.

DUSHMAN, S. 1949. Scientific foundations of vacuum technique (John Wiley & Sons, Inc., New York), p. 39.

HEYL, P. R. and COOK, G. S. 1936. J. Research Natl. Bur. Standards, **17**, 805.

JEFFREYS, H. 1948. Monthly Notices Roy. Astron. Soc. London Geophys. Suppl. **5**, 219.

KÜHNEN, F. and FURTWÄNGLER, PH. 1906. Veröffentl. Kgl. Pr. Geod. Inst. Neue Folge, Nr **27**, Berlin.

MARTSINYAK, A. J. 1956. Izmeritelnaya Tekn. i Poverochnoe Delo, **5**, 11.

THULIN, Å. 1958. Compt. rend. acad. sci. **246**, 3322; Thesis, University of Paris, Paris France; Ann. géophys (in press).

VOLET, CH. 1946. Compt. rend. acad. sci. **222**, 373.

——— 1952. Compt. rend. acad. sci. **235**, 442.

WINTER, P. J., VALLIANT, H. D., and HAMILTON, A. C. Pendulum observations at Ottawa, Gander, Bad Harzburg, Rome, and Paris. In preparation.

THE WAVELENGTH DISPLACEMENTS OF SOME INFRARED LINES BETWEEN LIMB AND CENTER OF THE SUN. II[1]

LUISE HERZBERG[2]

ABSTRACT

The differences between the wavelengths at the solar limb and at the center of the disk have been measured for lines of Fe I, Si I, and Ca II in the λ8500 Å and λ8900 Å regions of the spectrum. The values of the limb–center displacements (in km/sec) of the Fe I lines in the two wavelength regions studied are found to be the same as those obtained by M. G. Adam for neutral metal lines at λ6100 Å. The limb–center displacements of the Si I lines are similar in magnitude and in the same direction as those of Fe I. Although the data are insufficient to decide the question as to term dependence of the solar wavelength shifts of Si I, any relation to the shifts observed in a laboratory light source can be excluded. For the Ca II lines at λ8500 Å and λ8900 Å, corresponding to two different transitions, the limb–center displacements differ from each other both in magnitude and in direction. The limb–center displacements of the λ8900 Å Ca II lines are smaller than those of the Fe I lines, while those of the λ8500 Å Ca II lines are significantly larger and in direction opposite to those observed for lines of Fe I.

Where possible, comparison has been made between the wavelengths observed at limb and center of the disk and the solar wavelengths predicted by General Relativity Theory. In all cases the wavelengths at the limb were found to be closer to the predicted values than the wavelengths measured at the center of the disk. While for the lines of Fe I the predicted solar wavelengths and those observed near the limb ($r/R = 0.982$) are in good agreement, the wavelengths close to the solar limb of the λ8500 Å Ca II lines are found to be significantly larger than those predicted by relativity theory.

A. INTRODUCTION

On the basis of General Relativity Theory all solar absorption lines are expected to be shifted to the red with respect to those of a terrestrial vacuum source by an amount of 2.1×10^{-6} times the wavelength λ. Measurement of this gravitational red shift constitutes one of the classical tests for the validity of Einstein's theory. Although spectroscopic techniques to measure wavelength differences of the required order have been available since before the problem first arose, there is as yet no definite answer to the question whether or not the solar lines show the predicted shift. The reason for this is that the relativitistic gravitational shift, if present, is masked by other effects whose origin is, so far, not understood, and whose influence on the total observed wavelength shift cannot be properly assessed.

There are two major observational facts, mutually interdependent, which make it obvious that the wavelength shifts of solar lines with respect to their terrestrial counterparts have a component (or components) other than the gravitational shift and the Doppler shifts due to solar rotation and relative motions of earth and sun. These observations are: (*a*) The differences between the wavelengths measured in the spectrum of the center of the solar disk and in the spectrum of a standard light source ($\lambda_c^{\odot}-\lambda^{lab}$) are not strictly proportional

[1]Manuscript received February 15, 1960.
Contribution from the Dominion Observatory, Department of Mines and Technical Surveys, Ottawa, Canada. Issued as Contribution No. 5, Vol. 4.
[2]Now at Radio Physics Laboratory, Defence Research Board, Ottawa, Canada.

to the wavelength. (*b*) For most lines the wavelength, properly corrected for the effect of solar rotation, varies along the radius of the solar disk, resulting in a difference $(\lambda_L^{\odot}-\lambda_C^{\odot}) \neq 0$ (limb–center displacement, limb shift).

Until fairly recently, mainly on the basis of work by St. John (1928), it was believed that the differences between the observed and predicted solar wavelengths could be accounted for as Doppler shifts due to radial motion of the photospheric gases. However, the very accurate data on solar and terrestrial wavelengths, now accumulated by M. G. Adam and co-workers at University Observatory, Oxford, show that the effect is much too complicated to be interpreted in such a straightforward manner. The new material has stimulated much theoretical work on the processes which cause the observed solar wavelength displacements. So far, however, no theoretical treatment of the subject has yielded results which are in satisfactory agreement with the observations.

The eventual identification of the physical processes causing the observed solar wavelength displacements depends largely on a knowledge of the latter's dependence on parameters other than the wavelengths, for instance, the intensity, the atomic energy levels involved in the transition, etc. It seems reasonable to expect that such relations will become more obvious as observations are extended to longer wavelengths, since the displacements due to any cause, in general, increase with wavelength. The Oxford data, so far, refer to lines in the visible region of the spectrum only. Observations in the photographic infrared could therefore be expected to yield useful results. A preliminary study in the λ10700 Å region, made at the Dominion Observatory (Herzberg 1957), showed systematic differences in the solar limb–center displacements of two groups of Si I lines, belonging, respectively, to two different multiplets.

The work was therefore continued with a survey of the limb–center displacements of suitable solar lines in the λ8500 Å region of the spectrum. When the results obtained for the Ca II lines proved to be of special interest, the λ8900 Å region was added in order to include in the investigation the intense Ca II lines at this wavelength. The results obtained for lines of Fe I, Si I, and Ca II are presented below.

B. OBSERVATIONS. REDUCTION OF PLATES

The observations were made during the summer months of 1958 and 1959. The equipment was the same as that used in the previous investigation: a horizontal telescope producing a solar image of 230 mm diameter; an image rotator which makes it possible to place a section of the solar image in any desired direction over the slit of the spectrograph; a 20-ft spectrograph with a 15,000 lines/inch plane grating.

A spectrum from a point near the solar limb and one from the center of the disk were always taken immediately after each other without disturbing the plate. In this way, by the use of suitable diaphragms over the spectrograph slit, "strips" were obtained in which the spectrum from a point near the limb is bracketed by the spectrum from the center (see Fig. 3). Pairs of such

strips from opposite limb points have been evaluated as units. They are referred to as "plates". Only those plates were accepted on which both strips had been obtained within a small time interval and with the same setting of the image rotator; in this way errors due to inaccuracy in the determination of the east–west direction and to variations in the size of the solar image are automatically excluded.

All exposures were made with the spectrograph slit perpendicular to the solar diameter along which the observations were made. In order to obtain the maximum difference between center and limb spectrum which is advantageous for accurate measurement (see below) the plates were in general taken along the east–west diameter. The guiding accuracy is estimated to have been ± 1 mm in limb distance and $\pm 2°$ in latitude angle.

The spectra were taken in the third order of the grating (dispersion 0.7 Å/mm) with a slit width of 70 microns. The exposure times were of the order 10 seconds and 5 minutes respectively, in the 8500 Å and 8900 Å regions (Kodak spectroscopic plates IN, not hypersensitized).

The plates were measured on a conventional measuring machine with a field of view large enough to accommodate the whole width of a strip of spectra. The cross hair was set successively on the center section (limb spectrum) and on the two outer sections (spectrum from center of disk). No difficulty was experienced in focusing attention on one spectrum at a time. It is therefore believed that no appreciable errors have been introduced in the measurements due to the simultaneous presence in the field of view of two different spectra. The wavelengths given by Babcock and Moore (1947) for lines at the center of the disk and for terrestrial lines were used to obtain the dispersion. This is sufficiently accurate to determine the small wavelength differences ($\ll 1$ Å) between center and limb spectra.

C. RESULTS

From every plate a pair of values

$$\Delta\lambda_E^\odot = \lambda_E^\odot - \lambda_C^\odot \qquad \text{and} \qquad \Delta\lambda_W^\odot = \lambda_W^\odot - \lambda_C^\odot$$

can be obtained for each solar line, corresponding to the total wavelength difference between the two opposite limb points, respectively, and the center of the disk. After the usual corrections for the motion of the earth have been made, simple addition or subtraction yields values for the limb–center displacement and the Doppler shift due to solar rotation respectively:

$$(\lambda_L^\odot - \lambda_C^\odot) = \frac{\Delta\lambda_W^\odot + \Delta\lambda_E^\odot}{2} \qquad \text{(limb–center displacement; limb shift)}$$

$$\Delta\lambda_{rot} = \frac{\Delta\lambda_W^\odot - \Delta\lambda_E^\odot}{2} \qquad \text{(Doppler shift due to solar rotation).}$$

The results obtained are presented in Tables I and II. The values tabulated are averages of results derived from measurements of a number of individual plates, as indicated. The slight fluctuation in the number of plates is due to

TABLE I

Limb–center displacements ($\lambda_L^{\odot}-\lambda_C^{\odot}$) and rotational Doppler shifts ($\Delta\lambda_{rot}$) of solar lines in the λ8600 Å region

Element	$\lambda^{\odot}$(Å)*	Int.*	$r/R = 0.982$ No. of plates	$\lambda_L^{\odot}-\lambda_C^{\odot}$ (Å)	$\Delta\lambda_{rot}$† (Å)	$r/R = 0.956$ No. of plates	$\lambda_L^{\odot}-\lambda_C^{\odot}$ (Å)	$\Delta\lambda_{rot}$† (Å)
Si	8443.975	3	5	+0.003	0.046	3	+0.005	0.053
Fe	8471.744	2	5	+0.009	0.044	3	+0.011	0.050
Fe	8496.994	2	5	+0.011	0.050	3	+0.010	0.044
Ca II	8498.062	20	5	−0.020	0.053	3	−0.010	0.046
Si	8501.553	1	5	+0.009	0.046	3	+0.003	0.046
Si	8502.228	3	5	+0.008	0.054	3	+0.008	0.057
Fe	8514.082	7	5	+0.011	0.055	3	+0.012	0.054
Fe	8515.122	5	5	+0.012	0.051	3	+0.010	0.050
Fe	8526.676	3	5	+0.012	0.059	3	+0.008	0.054
Si	8536.163	3N	5	+0.007	0.046	3	+0.004	0.048
Fe	8538.021	3	3	+0.006	0.050	3	+0.010	0.055
Ca II	8542.144	25	5	−0.018	0.054	3	−0.020	0.045
Si	8556.797	8N	5	+0.010	0.051	3	+0.006	0.052
Fe	8571.807	2	4	+0.009	0.052	3	+0.001	0.058
Fe	8582.271	6	5	+0.012	0.054	3	+0.011	0.052
Fe	8592.969	3N	5	+0.014	0.055	3	+0.013	0.048
Si	8595.968	3N	5	+0.008	0.048	3	+0.004	0.051
Si	8597.059	1N	5	+0.011	0.054	3	+0.007	0.048
Fe	8598.836	3	4	+0.010	0.048	3	+0.009	0.051
Fe	8611.812	7	5	+0.013	0.052	3	+0.012	0.052
Fe	8613.946	1	4	+0.011	0.051	3	+0.010	0.057
Fe	8616.284	2	4	+0.014	0.054	3	+0.007	0.053
Fe	8621.618	5	4	+0.014	0.052	3	+0.008	0.052
Si	8648.472	10N	4	+0.012	0.050	3	+0.006	0.055

NOTE: N, hazy.
*Center of solar disk, Babcock and Moore (1947).
†Reduced to $r/R = 1$.

TABLE II

Limb–center displacements ($\lambda_L^{\odot}-\lambda_C^{\odot}$) and rotational Doppler shifts ($\Delta\lambda_{rot}$) of solar lines in the λ8900 Å region

Element	$\lambda^{\odot}$(Å)*	Int.*	$r/R = 0.982$ No. of plates‡	$\lambda_L^{\odot}-\lambda_C^{\odot}$ (Å)	$\Delta\lambda_{rot}$† (Å)	$r/R = 0.956$ No. of plates‡	$\lambda_L^{\odot}-\lambda_C^{\odot}$ (Å)	$\Delta\lambda_{rot}$† (Å)
Fe	8824.234	10	6	+0.015	0.055	3	+0.012	0.062
Fe	8838.441	6	6	+0.016	0.051	3	+0.012	0.061
Fe	8846.750	3	6	+0.011	0.054	3	+0.008	0.058
Ni	8862.563	3	6	+0.010	0.054	3	+0.010	0.054
Fe	8866.943	9	6	+0.010	0.053	3	+0.014	0.057
Fe	8868.444	3	6	+0.011	0.055	3	+0.008	0.059
Si	8892.738	4	6	+0.012	0.057	3	+0.009	0.055
Ca II	8912.101	7	6	+0.006	0.057	3	+0.007	0.053
Fe	8920.036	3	6	+0.014	0.040	3	+0.009	0.051
Ca II	8927.392	7	6	+0.007	0.054	3	+0.006	0.060
Fe	8943.058	2	6	+0.012	0.058	3	+0.009	0.052
Fe	8945.198	5	6	+0.012	0.057	3	+0.010	0.062
Si	8949.06	2N	2	+0.019	0.064	3	+0.010	0.053

NOTE: N, hazy.
*Center of solar disk, Babcock and Moore (1947).
†Reduced to $r/R = 1$.
‡Results from one plate, taken at latitude ±30° (see text) not included in $\Delta\lambda_{rot}$.

the fact that occasionally, on an otherwise satisfactory spectrum taken near the limb, the contrast for certain lines was too low to make measurement possible.

The tables contain results obtained at two different disk positions, $r/R = 0.982$ and $r/R = 0.956$ (r, distance from center; R, radius of solar disk), corresponding to limb distances on the solar image of 2 mm and 5 mm respectively. The values at 5-mm limb distance had been obtained at an early stage in the work when observations were made at a series of different limb distances in the hope of determining for the different lines the wavelength variation along the solar radius. After it was recognized that the method was not suitable for this purpose, further work was restricted to 2-mm limb distance. However, the values obtained for 5-mm limb distance are recorded here with those for 2-mm limb distance because the degree of consistency between the two sets of data provides a measure for the reliability of the results in general.

As far as we know (Freundlich, v. Brunn, and Brück 1930; Herzberg 1957), the limb–center displacement of solar lines is independent of heliographic latitude. The observations were therefore not diversified as to position angle, but, for reasons explained above, were made along the east–west diameter. Results from two plates, taken at position angle $\pm 30°$ owing to an oversight, have been given full weight when forming the average values for the limb–center displacement ($\lambda_L^\odot - \lambda_C^\odot$) but, because of the uncertainty of the law of solar rotation they have been rejected in the computation of the rotational Doppler shift $\Delta\lambda_{rot}$.

No limits of error are indicated in the tables because there are not enough single measurements to compute the conventional m.s.e. values. The accuracy of the final results can be estimated from the scatter of the values obtained from individual plates, as plotted in Fig. 1 for some of the lines. This scatter is due to a combination of measuring error and guiding error. Since each of the values for the limb–center displacement or the rotational Doppler shift is derived from measurements on four different spectra, twice the error of the single measurement has to be allowed for.

Some of the variations in the values for the limb–center displacement of different lines are clearly outside the limits of accuracy. These will be discussed below. The fluctuation in the values for the rotational Doppler shift, however, does not seem to be significant, and mean values, taken over the different lines in the same wavelength region, have been used to determine the rotational velocity of the sun.

Values for the linear velocity v_0 at the equator due to rotation, have been computed both from the average rotational Doppler shifts of all lines and from those of the Fe I lines of intensity > 5. The results obtained are as follows:

$v_0 = 1.77$ km/sec and $v_0 = 1.80$ km/sec (λ8500 Å region)

$v_0 = 1.85$ km/sec and $v_0 = 1.91$ km/sec (λ8900 Å region).

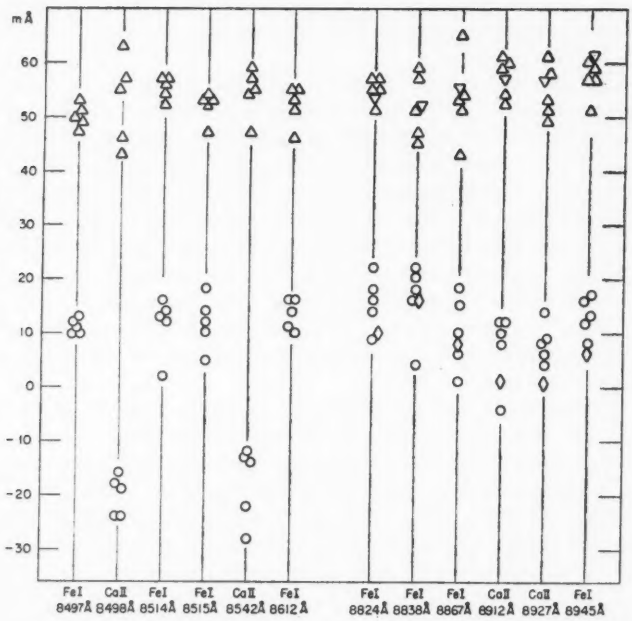

FIG. 1. Wavelength shifts due to solar rotation $\Delta\lambda_{rot}$ (triangles) and limb–center displacement ($\lambda_L^{\odot}-\lambda_C^{\odot}$) (circles and diamonds) for different solar lines obtained from measurement of individual plates. (Upright triangles and circles refer to measurements on the east–west diameter, inverted triangles and diamonds to measurements on a diameter of position angle ±30°.)

These values are within the range of other spectroscopically determined values of the solar rotational velocity, for instance

$$v_0 = 1.956 \text{ km/sec} \qquad (\lambda 6000 \text{ Å region (Hart 1954))}$$

and

$$v_0 = 1.85 \text{ km/sec} \qquad (\lambda 10800 \text{ Å region (Herzberg 1957))}.$$

D. DISCUSSION

(a) Lines of Neutral Iron, Fe I (and Nickel, Ni I)

The values for the limb–center displacements of the Fe I (and Ni I) lines at λ8500 Å and λ8900 Å show, within their respective wavelength regions, no noticeable variations with intensity, excitation potential, or other properties of the lines concerned. The average values for the two groups of lines can therefore be considered as fairly representative for their wavelength regions, and can be compared with the corresponding value for neutral lines (mostly Fe) at λ6100 Å (Adam 1948) in order to study the wavelength dependence of the effect.

Excluding infrared lines of intensity $\leqslant 2$ because of their lower accuracy, the average values for the limb–center displacements in the three regions of the spectrum are:

$$(\lambda_L^{\odot}-\lambda_C^{\odot}) = 0.0124\,\text{Å} \qquad \text{for } \lambda 8900\,\text{Å (mean of 8)},$$
$$(\lambda_L^{\odot}-\lambda_C^{\odot}) = 0.0113\,\text{Å} \qquad \text{for } \lambda 8500\,\text{Å (mean of 8)},$$
$$(\lambda_L^{\odot}-\lambda_C^{\odot}) = 0.0079\,\text{Å} \qquad \text{for } \lambda 6100\,\text{Å (mean of 14)}.$$

These three values, within the accuracy of guiding, refer to the same disk position ($r/R = 0.982$ for $\lambda 8500$ Å and $\lambda 8900$ Å; $r/R = 0.984$ for $\lambda 6100$ Å).

The wavelength displacements, expressed as "equivalent velocities" $v = \Delta\lambda c/\lambda$, are

$$(\lambda_L^{\odot}-\lambda_C^{\odot}) = +0.41_8\,\text{km/sec} \qquad \text{for } \lambda\ 8900\,\text{Å},$$
$$(\lambda_L^{\odot}-\lambda_C^{\odot}) = +0.39_6\,\text{km/sec} \qquad \text{for } \lambda\ 8500\,\text{Å},$$
$$(\lambda_L^{\odot}-\lambda_C^{\odot}) = +0.38_9\,\text{km/sec} \qquad \text{for } \lambda\ 6100\,\text{Å}.$$

The slight increase in these values with wavelength is only of the order of magnitude of the estimated error; 0.02 km/sec corresponds to 0.0004 Å at 6100 Å and to 0.0006 Å at 9000 Å. Within the limits of the present observational data therefore, the solar limb–center displacement of neutral metal lines is proportional to the wavelength.

This result makes it not unreasonable to expect a similar linear dependence on the wavelength to exist also for the solar–terrestrial line shifts and, therefore, for the differences between the observed solar wavelengths and those predicted by General Relativity Theory ($\lambda^{\text{pred}} = \lambda^{\text{lab}} + 2.1\times 10^{-6}\lambda$).

For the lines in the $\lambda 6100$ Å region, the relation between predicted and observed solar wavelength shifts has been investigated by Adam (1948), who has measured directly the wavelengths at different points across the disk and compared them with the wavelengths of a standard laboratory light source (vacuum arc). It was found that the average wavelength near the limb ($r/R = 0.984$) corresponded closely to that predicted by General Relativity Theory, while the average wavelength at the center of the disk was approximately halfway between the wavelengths measured at the limb and in the laboratory.

For the infrared solar lines, wavelengths at the center of the disk have been measured by Babcock and Moore (1947). From these the wavelengths at the solar limb can be obtained by adding the values for the limb–center displacements (Tables I and II). Unfortunately, corresponding wavelengths of a laboratory light source *in vacuo* are not available so far. However, for approximately half of the infrared lines considered, Meggers (1935) gives the wavelengths measured in the spectrum of an arc in air at atmospheric pressure, together with corrections to be applied to convert these wavelengths into those of a vacuum light source. If one accepts the wavelengths computed in this way as "standard" laboratory wavelengths, one obtains:

$$(\lambda_C^{\odot}-\lambda^{lab}) = +0.007\,\text{Å or } +0.23\,\text{km/sec}$$

for λ8500 Å (mean of 5)

$$(\lambda_L^{\odot}-\lambda^{lab}) = +0.019\,\text{Å or } +0.67\,\text{km/sec}$$

and

$$(\lambda_C^{\odot}-\lambda^{lab}) = +0.012\,\text{Å or } +0.41\,\text{km/sec}$$

for λ8900 Å (mean of 4)

$$(\lambda_L^{\odot}-\lambda^{lab}) = +0.025\,\text{Å or } +0.84\,\text{km/sec}$$

These values, together with the corresponding data for the λ6100 Å region are shown, to the left, in the diagram Fig. 2. The wavelength shifts are given in km/sec (see above). In these units

$$\Delta\lambda^{pred} = 0.63\,\text{km/sec.}$$

The vertical solid lines connecting the points for $(\lambda_L^{\odot}-\lambda^{lab})$ and $(\lambda_C^{\odot}-\lambda^{lab})$ represent the values of the limb–center displacements $(\lambda_L^{\odot}-\lambda_C^{\odot})$. The dotted

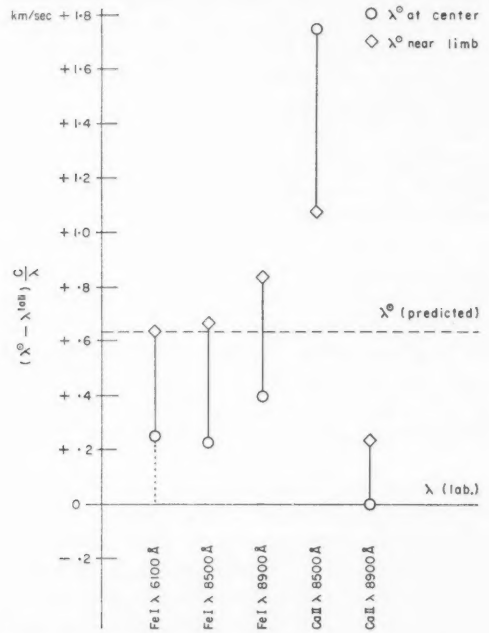

FIG. 2. Average shifts with respect to a standard laboratory light source of groups of solar lines (see text) at the center of the disk and at a point near the limb. (For the Ca II lines at 8900 Å, because of lack of good laboratory data, the shift between the wavelength at the center of the solar disk and in the laboratory has been arbitrarily assumed to be equal to zero.)

line connecting the point ($\lambda_C^{\odot} - \lambda^{lab}$) for λ6100 Å with the abscissa has been drawn in to stress the fact that, in this wavelength region, the difference between solar and terrestrial (vacuum arc) wavelength is known to the same accuracy as the value for the limb–center displacement.

A glance at the diagram shows that, for the Fe I lines in the λ8500 Å region, the solar wavelength shifts (in km/sec) are indeed practically identical with those observed at λ6100 Å. For the λ8900 Å lines the shifts between solar and laboratory wavelengths are larger. However, for this group of lines the laboratory wavelengths are so uncertain that the values obtained for the solar terrestrial displacements (different from those for the limb–center displacements) have too wide a margin of error to be relevant for the present discussion. The evidence obtained therefore favors the conclusion that for lines of iron and similar neutral metal atoms, in the infrared as well as in the λ6100 Å region, the solar wavelengths observed at a point near the limb are close to those predicted by General Relativity Theory.

(b) Lines of Neutral Silicon, Si I

Tables III and IV show the values obtained for the solar limb–center displacements of the Si I lines studied, together with the laboratory wavelengths and other relevant data, arranged according to multiplets.

The laboratory wavelengths of the Si I lines in the literature (Kiess 1938) have not been obtained under very good vacuum conditions and must be assumed to be affected by disturbing factors in the light source. They are therefore referred to as λ_p^{lab}. Moore (1956) has found that the wavelengths

TABLE III

Wavelength displacements of Si I lines

Part I

$\lambda^{\odot}$(Å)*	Int.*	$\lambda_L^{\odot} - \lambda_C^{\odot}$ (Å) $r/R = 0.982$	$r/R = .965$	$r/R = 0.956$	λ_p^{lab}(Å)†	Int.†	$\lambda^{\odot} - \lambda_p^{lab}$(Å)	Transition	Excitation potential (ev)
8892.738	4	+0.012		+0.009	8892.97	25w	−0.23		
8949.06	2N			+0.010	8949.33	15w	−0.27	$4p\ ^3D$–$6s\ ^3P^0$ (54)‡	6.0–7.3
8925.288	1				8925.55	8w	−0.26		
8766.417	−1				8766.68	3w	−0.26		
8883.68	0				8883.84	4w	−0.16		
10727.42	9		+0.013$_7$		10727.21	75w	+0.21		
10694.25	8		+0.008$_9$		10694.14	50w	+0.11	$4p\ ^1D$–$4d\ ^1F^0$ (53)‡	6.0–7.1
10689.71	8		+0.008$_6$		10689.52	20w	+0.19		
10882.84	3				10882.66	5w	+0.18		
10784.57	3				10784.33	5w	+0.24		
10827.14	12		+0.003$_0$		10827.09	100	+0.05		
10749.39	12		+0.005$_3$		10749.40	60	−0.01		
10979.34	4				10979.27	35	+0.07	$4s\ ^3P^0$–$4p\ ^3P$ (5)‡	4.9–6.1
10786.85	7		+0.004$_6$		10786.86	50	−0.01		
10603.426	10				10603.38	60	+0.05		
10660.99	10				10660.98	50	+0.01		

NOTE: N, n, hazy; w, widened, not sharp.
*Center of solar disk, Babcock and Moore (1947).
†Kiess (1938).
‡Multiplet No., assigned by Moore (1945).

TABLE IV

Wavelength displacements of Si I lines

Part II

$\lambda^{\odot}$ (Å)*	Int.*	$(\lambda_L^{\odot}-\lambda_C^{\odot})$ (Å) $r/R = 0.982$	$r/R = 0.956$	λ_p^{lab}(Å)†	Int.†	$\lambda^{\odot}-\lambda_p^{lab}$(Å)	Transition	Excitation potential (ev)
8556.797	8N	+0.010	+0.006	8556.64	100w	+0.16	$3d\,^1D^0$–$4f\,^1G$ (45)‡	5.9–7.3
8502.228	3	+0.008	+0.008	8502.38	30w	−0.15	$3d\,^1D^0$–$4f\,^1D$ (46)‡	5.9–7.3
8443.975	3	+0.003	+0.005	8444.00	15w	−0.02		
8444.377	−3			8444.48	3w	−0.10		
8501.553	1	+0.009	+0.003	8501.50	20w	+0.05	$3d\,^1D^0$–$4f\,^1D$ (47)‡	5.9–7.3
8595.968	3N	+0.008	+0.004	8596.02(P)				
8536.163	3N	+0.007	+0.004	8536.38	3w	−0.22	$3d\,^3F^0$–$5f\,^3G$ (80)‡	6.2–7.3
8597.059	1N	+0.011	+0.007	8597.00	2nl	+0.06		
8648.472	10N	+0.012	+0.006	8648.89	100nl	−0.42	Unclassified	

NOTE: N, n, hazy; w, widened, not sharp; l, unsymmetrically shaded to longer wavelengths; P, predicted.
*Center of solar disk, Babcock and Moore (1947).
†Kiess (1938).
‡Multiplet No., assigned by Moore (1945).

measured at the center of the solar disk provide a more consistent system of atomic energy levels than the present laboratory data and that therefore the solar wavelengths can be taken to be the better approximation to the wavelengths of a perfect vacuum laboratory light source. (The relativistic shift of solar lines is within the accuracy of the laboratory wavelengths.) The values $(\lambda^{\odot}-\lambda_p^{lab})$ can therefore be considered as a measure for the magnitudes of the wavelength shifts produced in the laboratory light source essentially by pressure effects.

If pressure effects had a noticeable influence on the wavelengths of solar (photospheric) lines one would expect the effect to be greater at the center of the disk than at the limb, because of the decrease of pressure with increasing height in the photosphere. The values $(\lambda_L^{\odot}-\lambda_C^{\odot})$ for the limb–center displacements would then be analogous to the differences $(\lambda^{\odot}-\lambda_p^{lab})$, and should, if pressure were the main governing factor, show a similar term dependence.

Results obtained in an earlier investigation (Herzberg 1957) on lines belonging to multiplets No. 5 and No. 53 (Moore's (1945) notation) seemed to give an indication that such an effect might exist. The results for these multiplets are included in Table III. As can be seen, the values for $(\lambda_L^{\odot}-\lambda_C^{\odot})$ as well as those for $(\lambda^{\odot}-\lambda_p^{lab})$ are consistently larger for multiplet No. 53 than for multiplet No. 5. In order to see whether or not this agreement is more than coincidence, special attention was given to Si I lines in the present investigation.

The best test object amongst the lines studied is provided by multiplet No. 54, although unfortunately only one of its lines is intense enough to be measured at disk position $r/R = 0.982$. The lines of this multiplet and those of multiplet No. 53 have the same lower energy levels, but their values for $(\lambda^{\odot}-\lambda_p^{lab})$ are in opposite directions. If the values for the limb–center dis-

placement were really related to the differences ($\lambda^{\odot}-\lambda_p^{lab}$), the lines of multiplet No. 54 should show very small, perhaps even negative values for ($\lambda_L^{\odot}-\lambda_C^{\odot}$). The results of observation (see Table III) show that this is not the case. The limb–center displacements measured for the lines of multiplet No. 54 are of the same order of magnitude and in the same direction as those of the lines belonging to multiplet No. 53.

Another case of interest in the present context is the unclassified line λ8648.472 Å (Table IV). This line has an exceptionally large shift ($\lambda^{\odot}-\lambda_p^{lab}$) in the same direction as the lines of multiplet No. 54 (negative); in addition it is asymmetrically broadened towards longer wavelengths. Even this line has been found to have a limb–center displacement of average magnitude and in the usual direction (positive).

Although the present data are not sufficient to exclude altogether the possibility that the limb–center displacements of the solar Si I lines are term dependent, they definitely show that there is no direct relation between these displacements and the (inferred) wavelength shifts observed in the laboratory light source.

(c) Lines of Singly Ionized Calcium, Ca II

The values obtained for the limb–center displacements of the Ca II lines are presented in Table V, together with other relevant data. Only for four

TABLE V

Wavelength displacements of Ca II lines

$\lambda^{\odot}$(Å)*	Int.*	$\lambda_L^{\odot}-\lambda_C^{\odot}$ (Å) $r/R=0.982$	$r/R=0.956$	λ^{lab}(Å)	Int.	$\lambda^{\odot}-\lambda^{lab}$(Å)	Transition	Excitation potential (ev)
8498.062	20	−0.020	−0.010	8498.018†	300	+0.044	$3\,^2D$–$4\,^2P^0$	1.7–3.1
8542.144	25	−0.018	−0.020	8542.089†	1500	+0.055		
8662.170	23			8662.140†	1000	+0.030		
8912.101	7	+0.006	+0.007	8912.10‡	15		$4\,^2D$–$4\,^2F^0$	7.0–8.4
8927.392	7	+0.007	+0.006	8927.34‡	20			

*Center of solar disk, Babcock and Moore (1947).
†Wagman (1937).
‡Shenstone (1946).

of the five Ca II lines on the plates has it been possible to derive a value for the limb–center displacement; the fifth line, λ8662.170 Å could not be measured in the spectrograms obtained at points near the solar limb because of blending with the Fe I line λ8661.97 Å (see Fig. 4).

The Ca II lines at λ8500 Å and λ8900 Å belong, respectively, to two different electronic transitions. The λ8500 Å lines have low excitation potential (1.7 ev) and are exceptionally intense and broad; the λ8900 Å lines have high excitation potential (7.0 ev), and their intensity and general appearance is that of an average line in the solar spectrum.

The differences between these two groups of lines are reflected in a remarkable manner in their limb–center displacements: the values obtained for the low excitation lines are more than twice as large as those for the high excita-

tion lines, and in the opposite direction. The good agreement between the results obtained from individual plates, as plotted in the diagram, Fig. 1, shows that this effect is definitely outside the limits of error. Inspection of the diagram and of Tables I and II shows further that the limb–center displacement of the high excitation lines is in the direction parallel to that observed for the lines of Fe I and Si I, while the limb–center displacement of the low excitation lines is "reversed".

Although the very broad Ca II lines at λ8500 Å are not easy to measure, no asymmetry should have been introduced by the measuring process, because all spectra have been measured both in the direction of increasing and of decreasing wavelengths. Actually the behavior of the low excitation Ca II lines is sufficiently different from that of the average solar lines that it can be noticed by inspection of the plates (see Figs. 3 and 4).

For the low excitation lines of Ca II, standard laboratory wavelengths have been provided by Wagman (1937). From these, together with Babcock and Moore's (1947) wavelengths for the center of the solar disk and the values for the limb–center displacements given in Table V, one obtains the following average wavelength shifts for the Ca II lines λ8498.062 Å and λ8542.144 Å:

$$(\lambda_C^{\odot} - \lambda^{lab}) = +0.050 \text{ Å or } +1.76 \text{ km/sec}$$

$$(\lambda_L^{\odot} - \lambda^{lab}) = +0.031 \text{ Å or } +1.09 \text{ km/sec}$$

The corresponding values for the high excitation lines of Ca II cannot be determined, due to lack of reliable laboratory data.

In the diagram Fig. 2, the results obtained for Ca II are shown side by side with those for Fe I. (The value $(\lambda_C^{\odot} - \lambda^{lab})$ for the high excitation lines of Ca II has been arbitrarily set equal to zero.)

It is seen that the magnitude of the (average) limb–center displacement, given by the length of the solid vertical lines, is relatively large for the low excitation, relatively small for the high excitation lines of Ca II. It appears significant that the low excitation Ca II lines, in addition to the reversal of the sign of the limb shift, show shifts between the wavelengths at the center of the solar disk and in the laboratory which are considerably greater than those predicted by relativity theory. Therefore, for these lines as well as for the "normal" Fe I lines, the solar wavelengths measured at the limb are closer to the predicted wavelengths than those measured at the center of the disk. However in the case of the Ca II lines, different from that of the Fe I lines, even close to the limb ($r/R = 0.982$) the solar wavelengths are considerably larger than the predicted wavelengths.

The only case of a large "reversed" limb shift that has been observed previously seems to be that of the central absorption (K_3) of the doubly self-reversed Ca II resonance line at λ3933.684 Å (St. John 1910). This line and the lines at λ8500 Å have the upper energy level in common. In addition, all three lines are exceptionally intense in the solar spectrum, and must

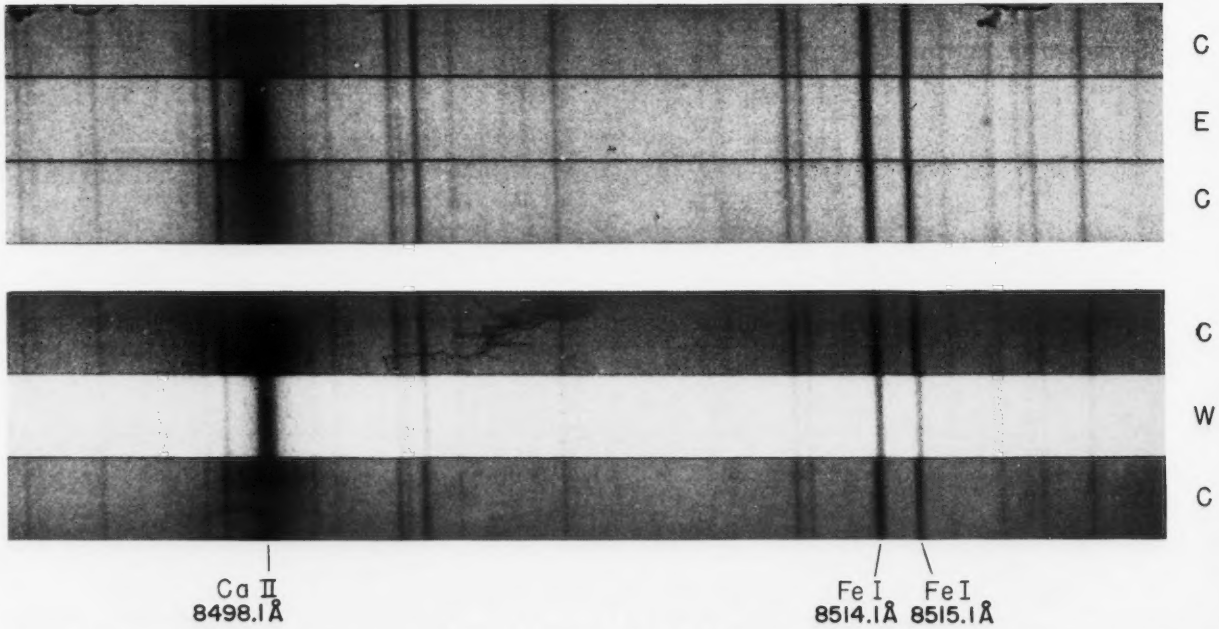

FIG. 3. Solar spectrum at 8500 Å at east and west points of the limb and at the center of the disk. For the two Fe I lines marked the shift to longer wavelengths at the west limb is greater than the shift to shorter wavelengths at the east limb, showing the effect of a limb shift to longer wavelengths. For the Ca II line marked this asymmetry is in the opposite direction, due to a limb shift towards shorter wavelengths. (Because of the great width of the Ca II line the effect does not come out well in the reproduction, though it can be clearly seen on the original plates.)

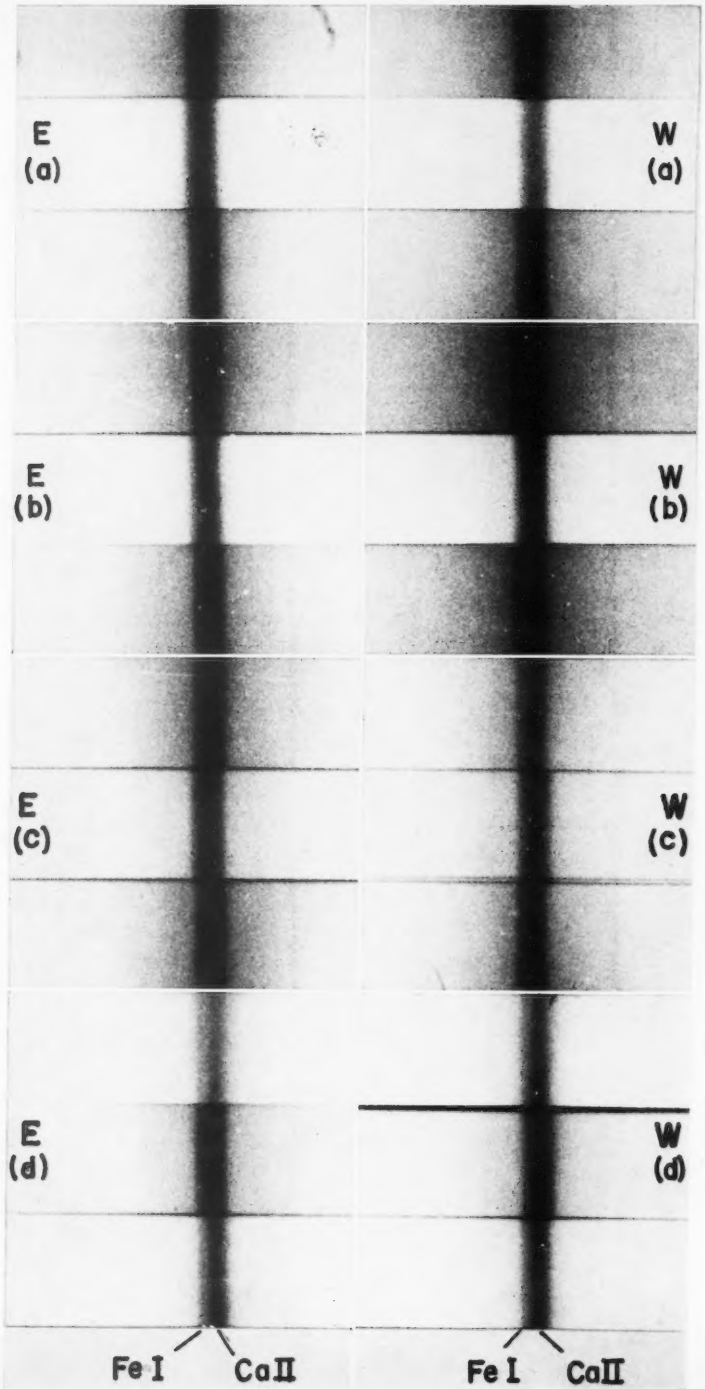
E
(a)
W
(a)
E
(b)
W
(b)
E
(c)
W
(c)
E
(d)
W
(d)
Fe I
Ca II
Fe I
Ca II

therefore be formed high in the solar atmosphere. Further observational data will be needed to decide which of the foregoing facts are relevant to explain the similar and exceptional solar wavelength shifts of these lines.

ACKNOWLEDGMENTS

The author would like to express her sincere thanks to Dr. C. S. Beals for his continued support of her work and much valuable advice. She also wishes to thank Dr. M. G. Adam and Dr. C. E. Moore for profitable discussions and suggestions. She is greatly indebted to members of the Observatory Staff, especially Dr. V. Gaizauskas, for their generous help in many phases of the work.

REFERENCES

ADAM, M. G. 1948. Monthly Notices Roy. Astron. Soc. **108**, 446.
BABCOCK, H. D. and MOORE, C. E. 1947. The solar spectrum, λ6600 to λ13495. Carnegie Institution of Washington Publication 579, Washington, D.C.
FREUNDLICH, E. F., BRUNN, A. v., and BRÜCK, H. 1930. Z. Astrophys. **1**, 43.
HART, A. B. 1954. Monthly Notices Roy. Astron. Soc. **114**, 17.
HERZBERG, L. 1957. Can. J. Phys. **35**, 766.
KIESS, C. C. 1938. Natl. Bur. Standards J. Research, **21**, 185.
MEGGERS, W. F. 1935. Natl. Bur. Standards J. Research, **14**, 33.
MOORE, C. E. 1945. A multiplet table of astrophysical interest. Observatory Publication, Princeton, N.J.
——— 1949. Atomic energy levels as derived from the analysis of optical spectra. Vol. I. Circular of the Natl. Bur. of Standards 467. Washington, D.C.
——— 1956. Discussion, Am. Astron. Soc. Meeting, Columbus, Ohio.
SHENSTONE, A. G. 1946. Unpublished. *Quoted by* C. E. Moore (1949).
ST. JOHN, C. E. 1910. Astrophys. J. **32**, 36.
——— 1928. Astrophys. J. **67**, 196.
WAGMAN, N. E. 1937. Univ. of Pittsburgh Bull. **34**, 1. *Quoted by* C. E. Moore (1945).

FIG. 4. The solar absorption lines λ8661.97 Å of Fe I and λ8662.170 Å of Ca II at different distances from the east and west limb and at the center of the sun. The two lines, seen well separated in the spectrum at the center of the disk, merge at close approach to the limb. This effect is very likely due to the fact that the limb shifts of the two lines are in opposite directions. The unmarked spectra are from the center of the disk, those marked E and W from east and west limb respectively. (*a*) $r/R = 0.982$. (*b*) $r/R = 0.956$. (*c*) $r/R = 0.912$. (*d*) $r/R = 0.825$.

GAMMA RADIATION IN THE DECAY OF Ag^{113}

A. KJELBERG, H. TANIGUCHI, AND L. YAFFE

Gamma rays have been reported recently in the decay of 5.3-hour Ag^{113}. Alexander *et al.* (1958) found a gamma ray of 0.31 Mev in low abundance. Workers at the Ames Laboratory (1959) observed 0.27- and 0.30-Mev γ-rays in coincidence.

Coulomb excitation studies by Wall (1954), Mark *et al.* (1955), Temmer and Heydenburg (1955), Paulissen and Mark (1955), and McGowan and Stelson (1958) have established excited states in Cd^{113} at 0.300, 0.582, and 0.675 Mev, together with transitions of 0.282 and 0.375 Mev. Alexander *et al.* (1958) observed γ-rays in reasonable agreement with these in the decay of 1.2-minute Ag^{113m}, together with 0.14- and 0.56-Mev γ-rays in coincidence.

Recent work in this laboratory has indicated that the decay of Ag^{113} is more complex than indicated by previous investigators.

Ag^{113} was produced as a fission product by bombarding thorium metal in the McGill synchrocyclotron with 45-Mev protons for a period of 10 minutes.

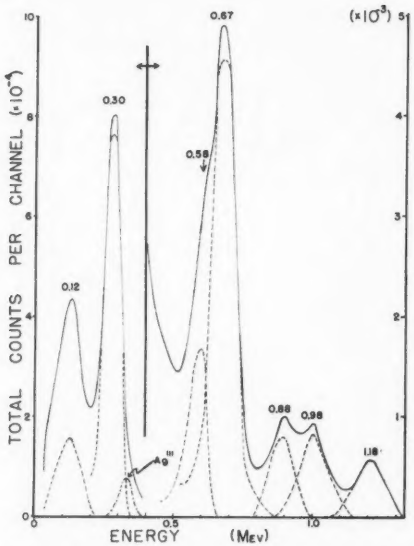

FIG. 1. Gamma spectrum of Ag^{113} obtained with a 3 in. × 3 in. NaI crystal. ——— Raw data. - - - Photopeaks. —·—·— Ag^{111} contribution.

Silver was separated radiochemically by a method essentially due to Glendenin (1951). The use of short bombardment times and rapid chemical separations, followed by a decay period of up to 36 hours, gave samples of Ag^{113} essentially free of 3.2-hour Ag^{112} (which is semishielded by its parent 21-hour Pd^{112}). The gamma spectrum was obtained with a 3 in. × 3 in. NaI(Tl) crystal feeding into a 100-channel pulse height analyzer.

In Fig. 1 is shown a typical spectrum obtained in this manner. The solid line indicates the raw data obtained after a small correction for background had been made. The Compton contribution and amount of backscattered γ-radiation were determined using well-known γ-standards under conditions identical with those in the original measurement. The photopeaks which resulted are indicated by the dotted lines in the figure. All γ-peaks decayed with a 5.3-hour half-life. A small contribution ($\sim 10\%$) in the neighborhood of the 0.30-Mev peak, due to 7.5-day Ag^{111}, was measured after the decay of Ag^{113} and corrections were made as indicated.

The results, corrected for crystal efficiencies according to Heath (1957), are given in Table I.

TABLE I

Gamma rays arising from the decay of Ag^{113}

Energy (Mev)	Relative abundance
0.12±0.03	10±3
0.30±0.01	100
0.58±0.02	5±1
0.67±0.01	17±1
0.88±0.02	4±1
0.98±0.02	5±1
1.18±0.02	4±1

The γ-energies observed are essentially in agreement with those observed for transitions between levels in Cd^{113}, except for the three highest energies which previously have not been found. There were also indications of a 0.27-Mev γ-ray in low abundance. This has been included in the 0.30-Mev peak for intensity calculations. The 0.38-Mev γ-ray reported by Alexander *et al.* (1958) in the decay of Ag^{113m} and McGowan and Stelson (1958) in Cd^{113} was not observed. The latter found that 16% of the transitions proceed from the 0.675-Mev level through the 0.300-Mev level, giving a 0.375-Mev transition. This intensity was just outside the limit of detection in the present experiment.

No gamma rays with energies above 1.18 Mev were observed. These would have been detected, if present, to about 1% of the 0.300-Mev γ-ray.

A tentative decay scheme for Ag^{113}, using all presently available data, is given in Fig. 2. This preliminary work has not established whether the 0.88 Mev γ-ray arises from a level at 0.88 Mev or whether it represents a transition between the 1.18- and 0.30-Mev levels. Since the necessary spectrometer and coincidence equipment are not available in our laboratory at the moment to proceed on the further elucidation of this scheme, these data are now being published.

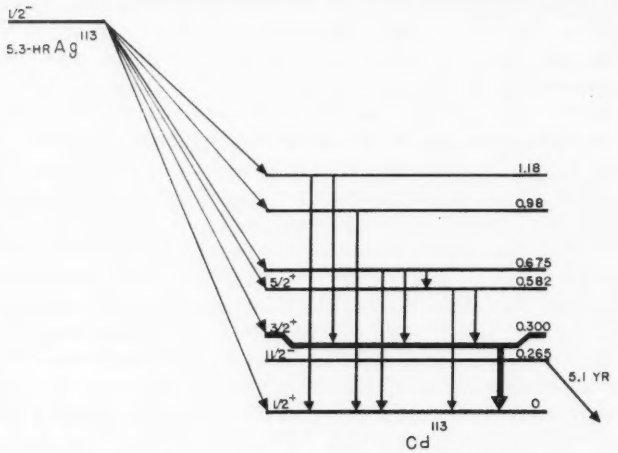

FIG. 2. Tentative decay scheme for Ag^{113}.

ALEXANDER, J. M., SCHINDEWOLF, U., and CORYELL, C. D. 1958. Phys. Rev. **111**, 228.
AMES LABORATORY, AMES, IOWA. 1959. Semi-Annual Summary Research Report in Physics for July–December 1958, ISC-1115.
GLENDENIN, L. E. 1951. *In* Radiochemical studies. The fission products, *edited by* C. D. Coryell and N. Sugarman. Paper 267, National Nuclear Energy Series, Plutonium Project Record, Vol. 9, Div. IV (McGraw-Hill Book Company, Inc., New York).
HEATH, R. L. 1957. U.S. Atomic Energy Commission IDO-16408.
MCGOWAN, F. K. and STELSON, P. H. 1958. Phys. Rev. **109**, 901.
MARK, H., MCCLELLAND, C., and GOODMAN, C. 1955. Phys. Rev. **98**, 1245.
PAULISSEN, G. and MARK, H. 1955. Phys. Rev. **99**, 617.
TEMMER, G. M. and HEYDENBURG, N. P. 1955. Phys. Rev. **98**, 1308.
——— 1955. Phys. Rev. **99**, 617.
WALL, N. S. 1954. Phys. Rev. **96**, 664.

RECEIVED FEBRUARY 8, 1960.
RADIOCHEMISTRY LABORATORY,
DEPARTMENT OF CHEMISTRY,
MCGILL UNIVERSITY,
MONTREAL, QUE.

NOTE ON THE HYPERFINE STRUCTURE OF THE $2s^2 2p\ ^2P_{\frac{1}{2}}$ STATE OF BORON 10 AND 11*

H. LEW AND R. S. TITLE†

In an attempt to detect a "hyperfine structure anomaly" for boron 10 and 11 the hyperfine structure of the $2s^2 2p\ ^2P_{\frac{1}{2}}$ ground states of this pair of isotopes has been measured by the atomic beam magnetic resonance method. Preliminary measurements (Title 1957 quoted in Brouwer and Petch 1958)

*Issued as N.R.C. No. 5651.
†National Research Laboratories Postdoctorate Fellow. Now at IBM Research Laboratories, Poughkeepsie, N.Y.

suggested that an appreciable anomaly existed. If true, this would contradict theoretical expectations. The present, more precise measurements show, however, that the anomaly is zero to within 2 parts in 10^5.

The apparatus and techniques used were essentially the same as those described by Wessel and Lew (1953) but with certain improvements in instrumentation to facilitate more precise measurements. The oven was, as in the case of silver and gold, a graphite tube directly heated by a high current to a temperature of about 2000° C to 2100° C. However, it was found impractical and unnecessary to use a thoria crucible to contain the boron.

For the study of boron 11 lines, the naturally occurring isotopic mixture was used. For the study of the boron 10 lines, the separated isotope was used.

Of the numerous Zeeman lines that were observable, three lines of each isotope were chosen for careful measurement. These were, in the (F, m_F) designation:

for boron 11 ($J = \frac{1}{2}$, $I = \frac{3}{2}$, neglecting g_I in comparison with g_J)

$$(2,0)-(1,0) = \Delta\nu+\frac{1}{2}\frac{g_J^2\mu_0^2H^2}{\Delta\nu},$$

$$\left.\begin{matrix}(2,1)-(1,0)\\(2,0)-(1,1)\end{matrix}\right\} = \Delta\nu+\frac{1}{4}g_J\mu_0H+\frac{7}{16}\frac{g_J^2\mu_0^2H^2}{\Delta\nu},$$

$$\left.\begin{matrix}(2,0)-(1,-1)\\(2,-1)-(1,0)\end{matrix}\right\} = \Delta\nu-\frac{1}{4}g_J\mu_0H+\frac{7}{16}\frac{g_J^2\mu_0^2H^2}{\Delta\nu};$$

for boron 10 ($J = \frac{1}{2}$, $I = 3$)

$$\left.\begin{matrix}\left(\frac{7}{2},\frac{1}{2}\right)-\left(\frac{5}{2},-\frac{1}{2}\right)\\\left(\frac{7}{2},-\frac{1}{2}\right)-\left(\frac{5}{2},\frac{1}{2}\right)\end{matrix}\right\} = \Delta\nu+\frac{24}{49}\frac{g_J^2\mu_0^2H^2}{\Delta\nu},$$

$$\left.\begin{matrix}\left(\frac{7}{2},\frac{1}{2}\right)-\left(\frac{5}{2},\frac{3}{2}\right)\\\left(\frac{7}{2},\frac{3}{2}\right)-\left(\frac{5}{2},\frac{1}{2}\right)\end{matrix}\right\} = \Delta\nu+\frac{2}{7}g_J\mu_0H+\frac{22}{49}\frac{g_J^2\mu_0^2H^2}{\Delta\nu},$$

$$\left.\begin{matrix}\left(\frac{7}{2},-\frac{1}{2}\right)-\left(\frac{5}{2},-\frac{3}{2}\right)\\\left(\frac{7}{2},-\frac{3}{2}\right)-\left(\frac{5}{2},-\frac{1}{2}\right)\end{matrix}\right\} = \Delta\nu-\frac{2}{7}g_J\mu_0H+\frac{22}{49}\frac{g_J^2\mu_0^2H^2}{\Delta\nu}.$$

It is seen from these relations that the first line of each group is field-independent to first order and that the other two lines have equal and opposite field dependences to the same degree of approximation. Thus the average of the latter two gives $\Delta\nu$ directly except for a small second-order correction. At fields of the order of 1 gauss, the second-order correction is of the order of

.0005 Mc/sec for B^{11} and .001 Mc/sec for B^{10}. Hence it is not necessary to know g_J accurately to obtain an accurate value of $\Delta\nu$ from the observations.

The majority of the measurements of the h.f.s. intervals were made at fields of less than 5 gauss. The widths of the lines observed were from 0.040 Mc/sec to 0.050 Mc/sec. The signal-to-noise ratio ranged from 3 to 1 to 15 to 1.

For the determination of g_J, only B^{11} was studied. A series of measurements were made at a field of nominally 48 gauss. The Na^{23} low frequency line was measured alternately with the $^2P_{\frac{1}{2}}$ low frequency line of B^{11}. The line widths were about 0.070 Mc/sec. The magnetic field was calculated from the Na frequency using the constants of Na as given in Kusch and Hughes (1959), viz. $\Delta\nu(\mathrm{Na}) = 1771.6262$ Mc/sec, $g_J = 2.002309$. The nuclear magnetic moment used was the diamagnetically corrected value tabulated in Walchli (1953) $\mu = +2.217529$ nuclear magnetons. These measurements could be summarized in the pair of corresponding frequencies, $\nu_{LF}(\mathrm{Na}) = 35.694 \pm 0.005$ Mc/sec, $\nu_{LF}(B^{11}, {}^2P_{\frac{1}{2}}) = 11.703 \pm 0.005$ Mc/sec. These correspond to a field of 48.145 ± 0.007 gauss.

The results of the observations are as follows:

$$\Delta\nu(B^{11}, {}^2P_{\frac{1}{2}}) = 732.153 \pm .003 \text{ Mc/sec},$$

$$\Delta\nu(B^{10}, {}^2P_{\frac{1}{2}}) = 429.048 \pm .003 \text{ Mc/sec},$$

$$g_J(B^{11}, {}^2P_{\frac{1}{2}}) = 0.6656 \pm .0004.$$

The $\Delta\nu$ of B^{11} disagrees with the earlier preliminary measurement of Wessel (1953), who obtained a value of 732.4 ± 0.1 Mc/sec. The observed value of g_J agrees with the theoretically expected one of 0.66589 for pure Russell–Saunders coupling with the anomalous magnetic moment of the electron taken into account.

The ratio of the magnetic dipole interaction constants is

$$\frac{a_{11}}{a_{10}} = \frac{\Delta\nu_{11}}{2} \cdot \frac{7/2}{\Delta\nu_{10}} = 2.98630 \pm .00003.$$

This is to be compared with the ratio of the nuclear g-factors as found by Brouwer and Petch (1958)

$$g_{11}/g_{10} = 2.98629 \pm .00002.$$

Thus the "h.f.s. anomaly" δ as defined by

$$a_{11}/a_{10} = (g_{11}/g_{10})(1+\delta)$$

is zero to within 2 parts in 10^5. Actually a contribution to δ of $+1.5 \times 10^{-5}$ is expected from the reduced mass correction to "a" but this is beyond the accuracy of the measurements.

BROUWER, W. and PETCH, H. E. 1958. Can. J. Phys. **36**, 632.
KUSCH, P. and HUGHES, V. W. 1959. Handbuch der Physik, Vol. XXXVII/1 (Springer-Verlag, Berlin).
TITLE, R. S. 1957. *Quoted in* Brouwer and Petch 1958.

WALCHLI, H. E. 1953. A table of nuclear moment data, United States Atomic Energy Commission, ORNL-1469.
WESSEL, G. 1953. Phys. Rev. **92**, 1581.
WESSEL, G. and LEW, H. 1953. Phys. Rev. **92**, 641.

RECEIVED FEBRUARY 24, 1960.
DIVISION OF PURE PHYSICS,
NATIONAL RESEARCH COUNCIL,
OTTAWA, CANADA.

INTERNAL PAIR ANGULAR CORRELATION SPECTROMETER FOR DETERMINATION OF γ-RAY MULTIPOLARITIES*

G. A. BARTHOLOMEW

The angular correlation between the positive and negative electrons produced by γ-ray internal pair conversion is an index of the multipolarity of the γ-ray transition. It is the purpose of this note to point out the possible advantages possessed by a certain design of a 180° flat field pair spectrometer for measuring this correlation under conditions of good energy resolution (of the order of 1%).

Direct measurements of angular correlations of internal pair electrons, with electron counters but without energy analysis, have been employed by Devons and Goldring (1954) for determining multipolarities of isolated γ-rays. Similar measurements have been made by Gorodetsky *et al.* (1956), who achieved some energy resolution by using scintillation detectors and summing the voltage pulses for coincident electrons and positrons. Internal pair angular correlations have also been measured with the aid of a cloud chamber by Harries (1954).

The 'type-3' slits described by Bartholomew, Campion, and Robinson (1960) effectively define conical acceptance solid angles for the electrons and positrons transmitted to the detectors from the source which, in Fig. 1, is assumed for simplicity to be localized at a point midway between the detectors. The acceptance solid angle for each detector is approximately $2\pi\delta$ steradians where δ is the ratio of the aperture gap width, in the plane of symmetry (the plane of the page, Fig. 1), to the distance from the inner jaw of the slit to the source. The line profile obtained with these apertures is determined largely by the geometry of the apertures and source and only to a small extent by the electron pair distribution. For a point source the theoretical base width of the line is equal to δ in units of the γ-ray energy, and the resolution (full width of a line at half maximum intensity) is approximately equal to $\delta/2$. Clearly by rotating the detectors about the source, it is possible to record the coincidence counting rate between the detectors as a function of the angle χ between the principal axes of the acceptance cones.

In order to estimate the degree of discrimination, for different multipoles, of the electron angular correlations observed with an arrangement such as

*Issued as A.E.C.L. No. 1008.

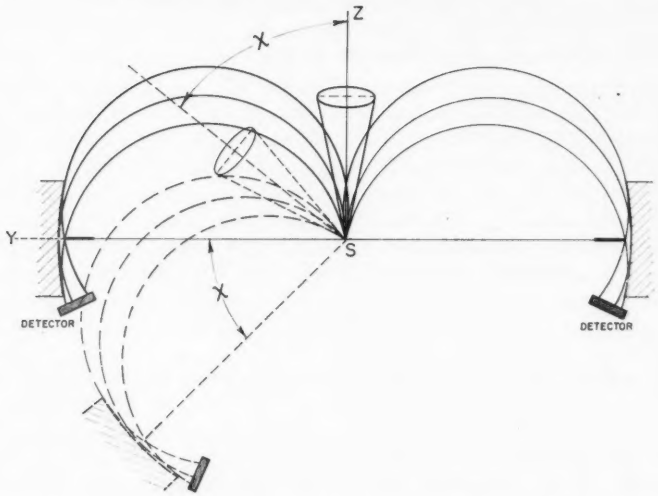

FIG. 1. Schematic geometry of the spectrometer. The 'type-3' detector apertures are shown in section in the plane of symmetry. They define conical acceptance solid angles for particles transmitted from the source S to the detectors. The magnetic field is normal to the plane of the paper. By rotating the detectors about the source, the variation of the coincidence counting rate as a function of the angle χ between the acceptance cones may be obtained.

shown in Fig. 1, we use the theoretical expressions given by Rose (1949). We compute, for each multipole n, the intensity, $I_n(\Theta)\, d\cos\Theta\, d\, W_+$, of pairs per quantum with the angle between the directions of emission of the particles equal to Θ, and equal positron and electron total energies, $W_+ = W_-$. The ratio, $R_n = I_n(0)/I_n(\Theta')$ is then a first-approximation estimate of the angular correlation to be observed by detecting pair coincidences at counter angles $\chi = 0$ and $\chi = \Theta'$. (For simplicity the assumption is made that the emission angles of all pairs transmitted at the counter angle χ are equal to χ. An exact calculation of the correlation would include an integration over all values of Θ allowed by the acceptance solid angles.) The ratios R_{E1}, R_{M1}, R_{E2}, and R_{M2} for various Θ' are plotted as a function of γ-ray energy in Fig. 2. The ratios, $F_n = R_n/R_{E1}$, which compare the angular correlations for $M1$, $E2$, and $M2$ radiation with that for $E1$ radiation are nearly independent of energy; values of these ratios at 6 Mev are plotted as a function of Θ' in Fig. 3. It is clear from Figs. 2 and 3 that an experimental determination of R for a given γ-ray should provide a practical method of discriminating between the various multipoles provided the maximum counter angle is not too small. In practice, the finite acceptance solid angles presented by the detector apertures, the finite area of the source, and the scattering of the pairs in the source would all tend to blur the angular correlation so that the ratios R_n would be less than shown in Fig. 2 and the discrimination between multipoles would probably not be as pronounced as shown in Fig. 3. However, it is not expected that

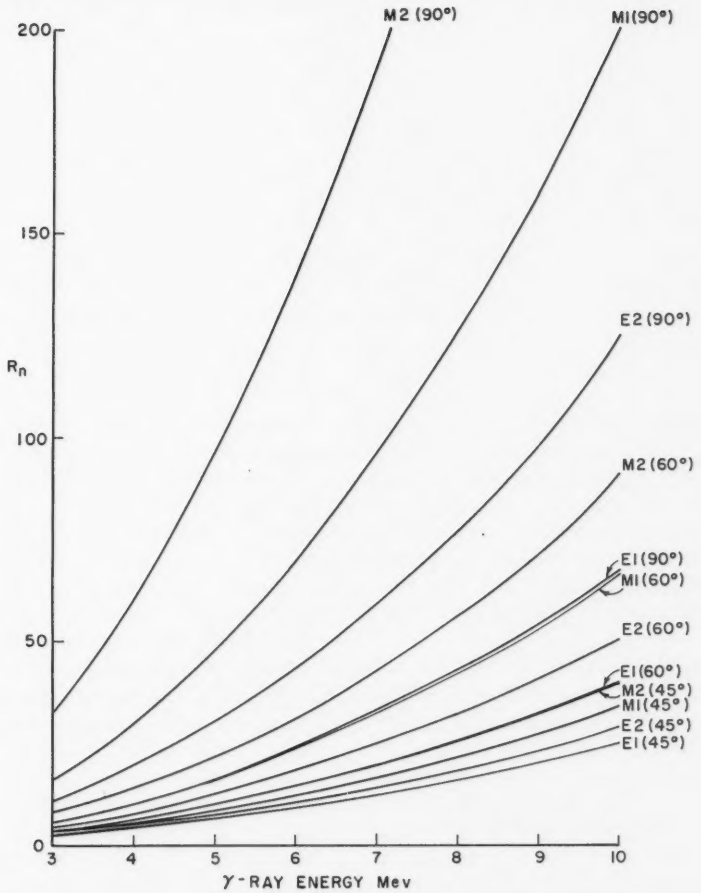

FIG. 2. The ratio of the number of pairs with emission angle $\Theta = 0$ to the number with $\Theta = \Theta'$ as a function of γ-ray energy for $E1$, $M1$, $E2$, and $M2$ radiation and $\Theta' = 90°$, 60°, and 45°. The multipole order and maximum emission angle are given on the curves.

these effects will be so large as to entirely vitiate the method. It remains to be shown that such a spectrometer would have an acceptable counting efficiency near 1% resolution.

In order to compute the absolute efficiency of the spectrometer for $\chi = 0$ we require the angular correlation function for the internal pair particles with respect to axes fixed in the spectrometer. Using equations 7 and 8 in the paper by Rose (1949), a transformation of angle variables followed by integration over the azimuthal angles leads to the following expressions for the number of pairs, with $W_+ = W_-$, per quantum of energy km_0c^2 in the interval $d \cos \theta^+$

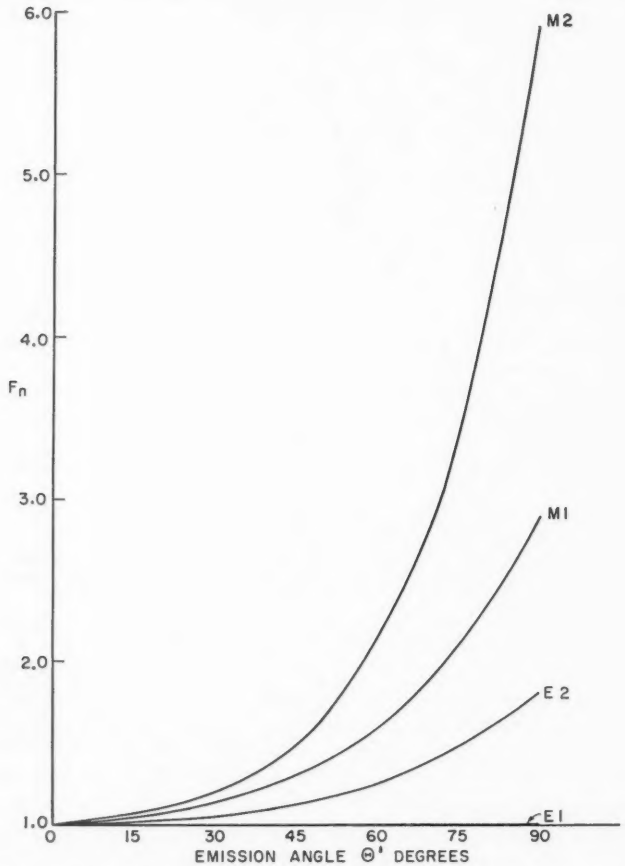

FIG. 3. The discrimination factor, $F_n = R_n/R_{E1}$, for various multipoles as a function of emission angle, Θ'.

$d\cos\theta_- d W_+$, where θ_+ and θ_- are the positron and electron polar angles measured with respect to the Z-axis of Fig. 1. For $M1$ radiation:

$$(1)\quad N(M1)d\cos\theta_+ d\cos\theta_- d W_+ = \frac{\alpha(k^2-4)}{16\pi k^3}\left[\frac{(\rho^2-\sigma^2)(k^2-4)+4\rho k^2}{(\rho^2-\sigma^2)^{3/2}}-1\right] \times d\cos\theta_+ d\cos\theta_- d W_+,$$

and for $E1$ radiation:

$$(2)\quad N(E1)d\cos\theta_+ d\cos\theta_- d W_+ = \frac{\alpha(k^2-4)}{16\pi k^3}\left[\frac{(\rho^2-\sigma^2)k^2+4\rho k^2}{(\rho^2-\sigma^2)^{3/2}}+1\right] \times d\cos\theta_+ d\cos\theta_- d W_+$$

where

$$\sigma = \frac{(k^2-4)}{2} \sin\theta_+ \sin\theta_-,$$

$$\rho = k^2 - \frac{(k^2-4)}{2}(1+\cos\theta_+ \cos\theta_-),$$

and

$$\alpha = 1/137.$$

Following Bartholomew *et al.* (1960) the line profile (pair counts per γ-quantum vs. strength of magnetic field) produced by the type-3 apertures at a given value of δ may be obtained from the expressions:

$$(3) \qquad P(k,\omega,\delta) = 2\int_0^{\zeta}\int_{1-\omega+z}^{1}\int_{1-\omega-z}^{1} \frac{(k^2-4)}{2k} N\, d\cos\theta_+\, d\cos\theta_-\, dz$$

where the momentum parameter, $z = |p_0 - p_\pm|/p_0$, measures the departure of the momentum of either particle from p_0 the momentum at equal energy division;* the magnetic field parameter, $\omega = (H_0-H)/H_0$, measures the difference between the magnetic field, H, and the maximum field at which coincidences can occur, H_0; and where ζ is the lesser of ω and $\delta-\omega$. By computing the line profiles for various values of k, the peak counting efficiency curves shown in Fig. 4 are obtained. At 6 Mev and 1% resolution these efficiencies are comparable to those obtained experimentally with the internal pair spectrometer of lens type (Alburger 1956).†

The line profiles for $\chi \neq 0$ cannot be so easily computed. However, as shown by Bartholomew *et al.* (1960), the line profile depends strongly on the aperture geometry and only weakly on the electron angular distribution. Therefore, there seems to be no reason to expect that the line shape for $\chi \neq 0$ would differ radically from that for $\chi = 0$. Moreover, the position of the high-field end point of the line, H_0, should suffer no appreciable shift as χ is varied. Two causes of such a shift are (*a*) the recoil energy imparted to the nucleus varies with χ, and (*b*) for a source of finite area and $\chi \neq 0$, the sum of the distances from the point of origin of a pair to the detector apertures depends on the Y-co-ordinate (Fig. 1) of the point of origin and, in general, is greater than that for $\chi = 0$. Since the momentum imparted to the nucleus is of the order of m_0c the first effect is negligible even for light nuclei. The second effect may be shown to produce a change in the end point of less than 0.1% (and may therefore also be ignored at 1% resolution) if the source width is less than about one tenth of the distance separating the detectors. As shown by Bartholomew *et al.* (1960), restriction of the source to small dimensions is also necessary to obtain good resolution with apertures of this type.

*It is assumed that the distribution function N, which holds for $p_+ = p_-$, is a close approximation to the true distribution over the range of momentum division implied by the limits of integration for z.

†Alburger's efficiencies are expressed as counts per transition for the 6.06 Mev O^{16} nuclear pair line. To compare with the present efficiencies his efficiencies must be multiplied by the internal pair conversion coefficient (Rose 1949).

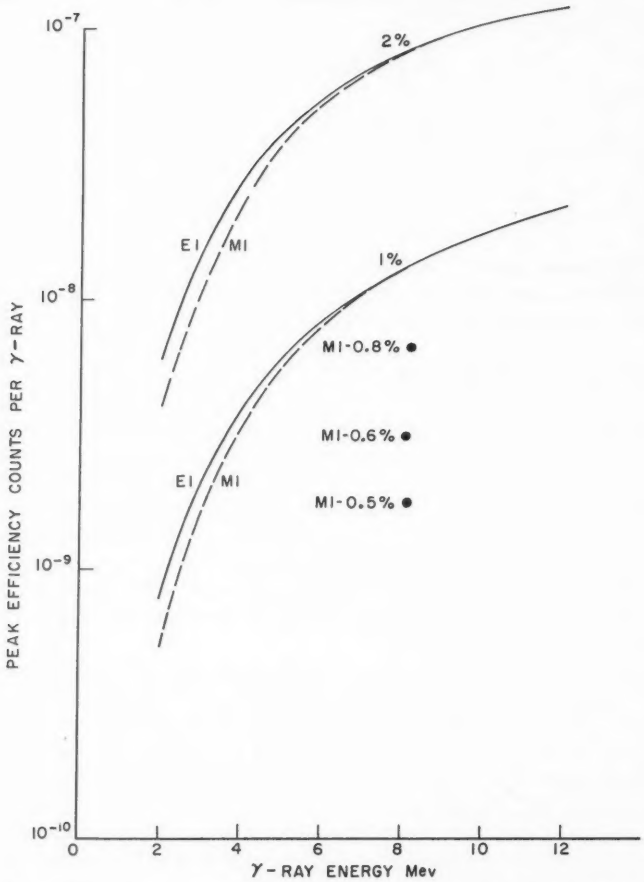

FIG. 4. Theoretical peak counting efficiency as a function of energy at $\chi = 0$ for various values of the resolution. Curves for both $E1$ and $M1$ radiation at 1% and 2% resolution and three points for $M1$ radiation at higher resolutions are shown.

The present note is intended only to demonstrate the feasibility of this method of measuring γ-ray multipolarities. As mentioned above, no account has been taken of the effects of finite solid angle, finite source area, and scattering of electrons and positrons in the source, and no attempt has been made to calculate the exact line profile and peak intensity for $\chi \neq 0$. To the uncertainties in the expected values of the correlations (Figs. 2 and 3) resulting from neglect of these effects must be added the uncertainty arising from approximations in the theory of internal pair production (Rose 1949). Further investigation of the practicability of the technique and an empirical calibration of the correlations, using transitions of known multipolarity, can be

carried out experimentally. Modifications of an existing pair spectrometer (Kinsey and Bartholomew 1953) are presently being made for this purpose. These modifications include the installation of a mechanism for changing the angle between the detectors and the introduction of shielding between the source and detectors to prevent detection of γ-rays emitted by the source.

It is a pleasure to acknowledge the help of Mrs. R. W. Attree, J. M. Kennedy, G. E. Lee-Whiting, and T. D. Newton, who assisted with the theoretical calculations appearing in this report.

ALBURGER, D. E. 1956. Rev. Sci. Instr. **27**, 991.
BARTHOLOMEW, G. A., CAMPION, P. J., and ROBINSON, K. 1960. Can. J. Phys. **38**, 194.
DEVONS, S. and GOLDRING, G. 1954. Proc. Phys. Soc. (London), A, **67**, 413.
GORODETSKY, S., ARMBRUSTER, R., and CHEVALLIER, P. 1956. J. phys. radium, **17**, 548.
HARRIES, G. 1954. Proc. Phys. Soc. (London), A, **67**, 153.
KINSEY, B. B. and BARTHOLOMEW, G. A. 1953. Can. J. Phys. **31**, 537.
ROSE, M. E. 1949. Phys. Rev. **76**, 678.

RECEIVED MARCH 9, 1960.
PHYSICS DIVISION,
ATOMIC ENERGY OF CANADA LIMITED,
CHALK RIVER, ONTARIO.

A NOTE ON THE DECAY OF Cs^{132}

G. N. WHYTE, BALRAJ SHARMA, and H. W. TAYLOR

Cs^{132} decays to Xe^{132} principally by orbital-electron capture followed by the emission of a single γ-ray with an energy of about 0.67 Mev (Wapstra *et al.* 1953; Robinson and Fink 1955; Bhatki *et al.* 1956). A number of other γ-rays have been observed, but their intensities are less than 1% of that of the 0.67-Mev radiation (Bhatki *et al.* 1956). The half-life of Cs^{132} has been measured to be 6.2 ± 0.2 days (Robinson and Fink 1955) and 7.1 days (Camac 1944).

Because the energy of the intense γ-ray lies very close to that of the accurately known 0.6616-Mev γ-ray of Cs^{137}, it lends itself to precise determination by the relatively simple techniques of scintillation spectroscopy. At the same time, the predominance of this line in the spectrum provides a means of measuring the half-life of Cs^{132} without interference from possible impurities. In the work reported here these two measurements have been combined.

Ten grams of high-purity (99.99%) cesium chloride were irradiated for 10 hours with 30-Mev X rays from the Queen's University synchrotron. At this bombarding energy the principal reaction in cesium is Cs^{133} (γ,n) Cs^{132}. Thirty-three-minute Cl^{34} is also produced and must be given time to decay away before measurements are started.

The source was placed in a jig which located it at a reproducible distance (6 in.) from a 3 in.$\times$3 in. NaI (Tl) crystal mounted on a DuMont 3-in. photo-

multiplier tube. The resolution of the counter at 0.662 Mev was 8.6%. The pulses from the counter were amplified and fed into a Baird-Atomic 20-channel analyzer. The gain of the spectrometer was adjusted so that the photopeak of the 0.67-Mev γ-ray was distributed over about 15 channels, and the counting rates were determined to better than 1% at the peak. A Cs^{137} source of comparable activity was counted alternately with the Cs^{132}. A sequence of measurements consisted of two groups of three, arranged to minimize the effects of drift: 132–137–132; 137–132–137. Between the two groups the 0.84-Mev photopeak from Mn^{54} was scanned with the spectrometer to give a second point for the energy calibration of the bias control. The above sequence was repeated at approximately 2-day intervals over a period of almost three half-lives.

For the half-life determination the relative activity of the source at the time of each sequence of measurements was obtained by comparing the areas under the Cs^{132} photopeaks with those under the Cs^{137} photopeaks. (Since the half-life of Cs^{137} is about 30 years, it provides an effectively constant reference peak.) The ratio of the mean area for the three Cs^{132} runs to the mean area for the three Cs^{137} runs gave a point on the decay curve corresponding to the mean time of the observations. The decay curve (Fig. 1) shows no departure from an exponential variation with time. A least-squares fit to the data gave a half-life of 6.48 ± 0.03 days.

The energy of the γ-ray was derived from the same measurements. For each sequence of measurements the difference between the average pulse heights for the Cs^{132} and Cs^{137} photopeaks was determined and compared with the difference between the Mn^{54} and Cs^{137} peaks. (Since the Cs^{132}–Mn^{54} energy difference is about 30 times the Cs^{132}–Cs^{137} difference, it is not necessary to know the energy of the Mn^{54} γ-ray as accurately as the Cs^{137} energy.) The two most precise determinations of the Cs^{137} γ-ray energy are 0.66160 ± 0.00014 Mev (Muller *et al.* 1952) and 0.66165 ± 0.00015 Mev (Lindstrom *et al.* 1953). A mean value of 0.66162 ± 0.00010 Mev was assumed for the purposes of the present experiment. The best published values for the energy of the Mn^{54} γ-ray are 0.840 ± 0.007 (Maeder *et al.* 1954) and 0.835 ± 0.015 Mev (Deutsch and Elliott 1944). The same transition follows the decay of V^{54}, and the energy in this case has been measured to be 0.835 ± 0.009 Mev (Schardt and Dropesky 1956). The mean value used here is 0.838 ± 0.005 Mev. On the basis of the Cs^{137} and Mn^{54} energies, the energy of the Cs^{132} photopeak was found to exceed that of the Cs^{137} photopeak by 0.00623 ± 0.00019 Mev. (This is the average of nine determinations, each based on three measurements of each peak.) This energy difference will be sensitive to the presence of weak photopeaks lying under the main Cs^{132} peak, which could shift the observed position of the latter. A coincidence investigation of this energy region revealed the presence of a line at 0.62 Mev with an intensity between 0.5 and 1% of that of the main line. The superposition of these two peaks leads to a downward energy shift of 0.0001 Mev in the apparent position of the main Cs^{132} peak. The energy difference between the Cs^{132} and Cs^{137} γ-rays is therefore 0.0063 ± 0.0003 Mev. The resulting energy for the Cs^{132} γ-ray is 0.6679 ± 0.0004 Mev.

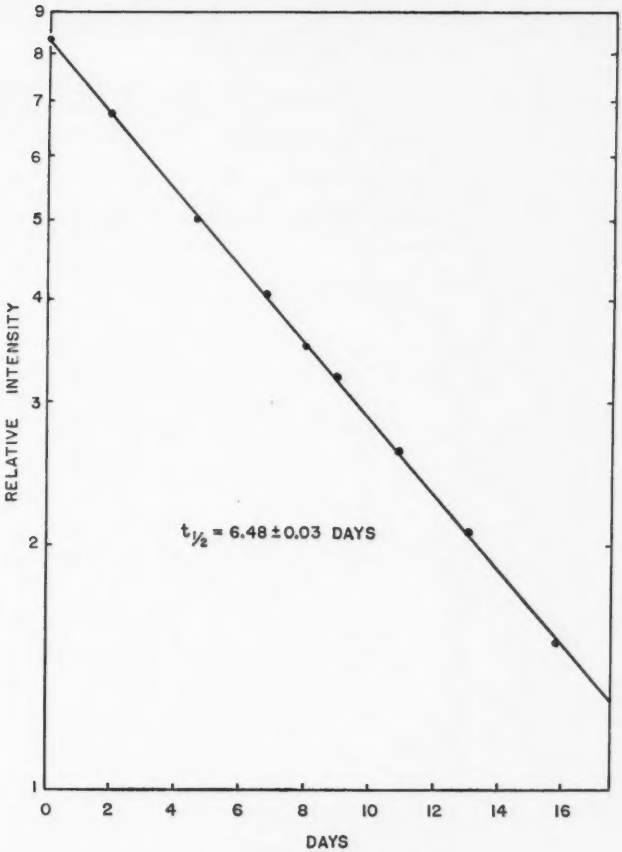

FIG. 1. Decay curve for Cs^{132}.

Previous measurements have yielded 0.685±0.010 Mev (Wapstra *et al.* 1953), 0.673±0.006 Mev (Finston and Bernstein 1954), and 0.669±0.003 Mev (Robinson and Fink 1955).

A practical matter connected with Cs^{132} may be worth noting. In view of the probable use of large CsI (Tl) crystals for the measurement of high-energy γ-rays, experimenters may find that they have produced this radioisotope within the crystal volume. The energy of the observed line in this case will include that of the X rays following the electron capture process. In the case of *K*-capture this will add another 0.0346 Mev, and the observed photopeak will occur at 0.702 Mev.

The authors wish to thank the National Research Council and the Atomic Energy Control Board for financial support.

BHATKI, K. S., GUPTA, R. K., and JHA, S. 1956. Nuovo cimento, **4**, 1519.
CAMAC, M. 1944. Metallurgical Laboratory Report CC-2409.
DEUTSCH, M. and ELLIOTT, L. G. 1944. Phys. Rev. **65**, 211.
FINSTON, H. L. and BERNSTEIN, W. 1954. Phys. Rev. **96**, 71.
LINDSTROM, G., SIEGBAHN, K., and WAPSTRA, A. H. 1953. Proc. Phys. Soc. B, **66**, 54.
MAEDER, D., WAPSTRA, A. H., NIJGH, G. J., and ORNSTEIN, L. Th.M. 1954. Physica, **20**, 521.
MULLER, D. E., HOYT, H. C., KLEIN, D. J., and DUMOND, J. W. 1952. Phys. Rev. **88**, 775.
ROBINSON, B. L. and FINK, R. W. 1955. Phys. Rev. **98**, 231A.
SCHARDT, A. W. and DROPESKY, B. J. 1956. Bull. Am. Phys. Soc. Ser. II, **1**, 162.
WAPSTRA, A. H., VERSTER, N. F., and BOELHOUWER, M. 1953. Physica, **19**, 138.

RECEIVED MARCH 15, 1960.
PHYSICS DEPARTMENT,
QUEEN'S UNIVERSITY,
KINGSTON, ONTARIO.

LETTERS TO THE EDITOR

Under this heading brief reports of important discoveries in physics may be published. These reports should not exceed 600 words and, for any issue, should be submitted not later than six weeks previous to the first day of the month of issue. No proof will be sent to the authors.

Frequency Measurement of Standard Frequency Transmissions[1, 2]

Measurements are made at Ottawa, Canada, using N.R.C. caesium-beam frequency resonator as reference standard (with an assumed frequency of 9 192 631 770 c.p.s.). Frequency deviations from nominal are quoted in parts per 10^{10}. A negative sign indicates that the frequency is below nominal.

Date, March 1960	MSF, 60 kc/s	GBR, 16 kc/s		WWVB† 60 kc/s
		6-hour average*	24-hour average	
1	−184	−174	−174	−78
2	−181	−174	−176	−78
3	−187	−175	−179	−30
4	N.M.	−176	−178	−84
5	−179	−176	−177	N.M.
6	−179	−178	−179	N.M.
7	−170	−178	−178	−78
8	−190	−180	N.M.	−90
9	−184	N.M.	N.M.	−79
10	N.M.	−183	N.M.	N.M.
11	−188	N.M.	N.M.	−82
12	−188	−189	−187	N.M.
13	−190	−189	−188	N.M.
14	−186	−192	−187	−80
15	−185	−191	−187	−83
16	N.M.	−188	−188	−80
17	−193	−191	−191	−80
18	−166	−161	−163	−81
19	−159	−162	−160	N.M.
20	−158	−159	−158	N.M.
21	−159	−161	−157	−82
22	−152	−157	−155	−81
23	−148	−154	−153	−82
24	−145	−154	−152	−80
25	−154	−151	−151	−84
26	−152	−152	−149	N.M.
27	−129	−149	−145	N.M.
28	−135	−148	−141	−77
29	N.M.	−145	−143	−82
30	−143	−139	−146	−84
31	N.M.	−161	−156	−78
Midmonthly mean	−168	−169	−168	−79
Midmonthly mean of WWV	−151			

NOTE: N.M. No measurement.
*Time of observations: 00.00 to 06.00 U.T.
†Call signals for station KK2XEI have been changed to WWVB.

RECEIVED APRIL 14, 1960.
S. N. KALRA
DIVISION OF APPLIED PHYSICS,
NATIONAL RESEARCH COUNCIL,
OTTAWA, CANADA.

[1]Issued as N.R.C. No. 5695.
[2]Cf. Kalra, S.N. 1959. Can. J. Phys. 37, 1328.

Measurements of the Last Few Periods of Sputnik III by a Radio Direction Finder*

A direction finder at Ottawa was used to track Sputnik III during the last 2 weeks of its life. The frequency of the transmission from the satellite was 20.0045 megacycles per second. The tracking data were primarily used for another experiment and also to provide immediate information on the position of the satellite to aid in possible visual sightings. Data of this nature, however, could be used with the more accurate but fewer visual observations to give a fuller picture of the falling-in process.

Observations were made automatically on a facsimile recorder (McLeish 1958) and processed to give the time (T_0), bearing (B_0), and distance (d_0) at nearest approach (Wolfe 1958). The time of crossing the 45th parallel (T_{45}) was calculated by plotting the tracks on a map. The mean period T was derived from the T_{45} values of successive 16th crossings.

The initial values of d_0 and T_{45} were derived by assuming the eccentricity $e = 0$ and the period $T = 90.0$ minutes for all crossings. The distance at nearest approach was therefore recalculated using the approximation that the angular velocity of the satellite in its orbit is $\omega = (2\pi/T)(1+e\cos\theta)$ where θ is the angular distance (in the orbital plane) between the satellite and the position of perigee.

The values of e and θ were derived from data published by the Smithsonian Observatory. The first estimates of T were used to get ω, which differed from 4 deg/min by only +1.5% on March 23 and +3% on April 5.

New values of T_{45} were derived in the same manner as before and are listed in Table I along with the time of nearest approach to Ottawa (45°.21′N., 75°.34′W.). All of the observed crossings were from the north to the south.

TABLE I

Date	T_0 (U.T.)	T_{45} (U.T.)
March 23	1810.0	1808.5
24	1507.0	1509.6
24	1639.7	1639.5
24	1810.4	1809.0
25	1639.3	1638.7
26	1505.4	1506.9
26	1637.7	1636.8
27	1502.5	1503.3
27	1633.9	1633.0
28	1457.6	1458.2
29	1450.9	1451.3
30	1442.5	1442.6
31	1431.4	1431.5
April 2	1400.3	1400.1
3	1339.3	1339.2
4	1314.7	1314.7
5	1244.9	1245.1

No observation was made on April 1 because of equipment maintenance.

The calculated mean periods and the corresponding times are given in Table II.

TABLE II

Date	Time (U.T.)	Mean period
March 24	0610	90.03
25	0440	89.95
25	1510	89.92
26	0440	89.88
27	0305	89.77
27	0435	89.76
28	0300	89.68
29	0255	89.57
30	0245	89.46
31	0235	89.31
April 1	1415	89.02
3	0150	88.69
4	0125	88.47
5	0100	88.15

The estimated accuracy of the time measurements in Table I is ±3 seconds for T_0 and ±5 seconds for T_{45}.

McLeish, C. W. 1958. Electronic and Radio Eng. **35** (10), 386.
Wolfe, J. L. 1958. J. Atmospheric and Terrest. Phys. **13**, 155.

Received April 26, 1960.
Division of Radio and Electrical Engineering,
National Research Council,
Ottawa, Canada.

J. L. Wolfe

*Issued as N.R.C. No. 5707.

Can. J. Phys. Vol. 38 (1960)

An Apparent Solar Periodicity in Radio Star Scintillation

From the beginning of December 1957 to the end of November 1958, the radio sources Cassiopeia-A, Cygnus-A, Taurus-A, and Virgo-A were observed at upper culmination from the Radio Observatory of Queen's University, Kingston, Ontario. The scintillation characteristics of each of the sources were studied at 50 Mc/s and significant correlations were obtained with local magnetic indices.

It is generally accepted that the geomagnetic field exhibits cyclic changes which are related to the period of rotation of the photosphere (Chapman 1940). The high correlation between scintillation and magnetic activity obtained by the authors and others (Dagg 1957) would suggest a similar periodicity in scintillation data. In an attempt to discover if such periodicity exists in the present records, an autocorrelation function was calculated for the scintillation index for Cygnus-A, the source showing highest correlation with magnetic activity. The scintillation index used was a measure of both amplitude and rate of scintillation.

This function is shown in the accompanying figure, for intervals up to 33 sidereal days. The limits shown are probable errors based solely on the number of observations. The solid

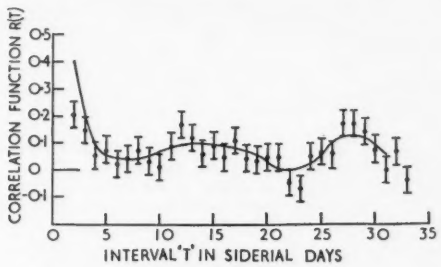

FIG. 1.

line is a 5-day running mean to indicate the trend of the data. It can be seen that a significant correlation is obtained after about 27 days. A quasi-period of 27.6 sidereal days has been estimated from the running mean, but this is subject to considerable error.

These results strongly suggest that solar activity contributes directly to the ionospheric processes responsible for the scintillation of radio stars, at least at locations in or near the auroral zone.

CHAPMAN, S. 1940. Geomagnetism, Vol. I (Clarendon Press, Oxford), pp. 370–384.
DAGG, M. 1957. J. Atmospheric and Terrest. Phys. **10**, 194.

RECEIVED APRIL 19, 1960.
W. D. RYAN* AND G. A. HARROWER
ASTRONOMY GROUP,
QUEEN'S UNIVERSITY,
KINGSTON, ONTARIO.

*Now at Queen's University, Belfast, N. Ireland.

Observations of Macromosaic Substructures in Lead

Previous investigations on macromosaic substructures called "striations" (Teghtsoonian and Chalmers 1951, 1952; Atwater and Chalmers 1957) have illustrated the effects of freezing velocity, impurity type and content, and crystal orientation upon the formation and characteristics of these dislocation arrays. The present investigation illustrates the effects produced by the temperature distribution in the liquid and solid at the interface.

Single crystals of lead and lead–silver alloys in the range 10^{-4}–10^{-2} at.% Ag were grown horizontally in graphite-coated lavite boats by the zone-melting technique illustrated in Fig. 1. The unique feature of this study is that the crystals were grown under varying ambient temperatures as illustrated. By varying the ambient temperature, T_A, relative to the melting temperature, T_m, the effect of the temperature distribution on array formation could be studied.

Two sizes of crystals were grown, each $\frac{3}{4}$ in. wide and 7 in. long, some $\frac{1}{4}$ in. deep and others $\frac{5}{8}$ in. deep. The thicker crystals were solidified with the solid–liquid interface perpendicular

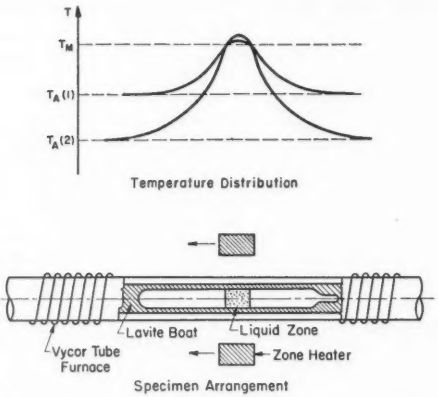

FIG. 1. Zone melting apparatus and temperature distribution throughout specimen.

to the crystal axis, whereas it was not always possible to maintain this interface orientation for the thinner crystals at the highest ambient temperature.

The main body of experiments were carried out at a freezing velocity, v, of 2 mm/min and the results are presented in Table I. At each ambient temperature two crystals were grown.

TABLE I
Striation formation

Conditions		Purity				Alloy concentration at.% Ag					
ΔT_{max}, °C	Size	Z.R.*		99.9999		10^{-4}		10^{-3}		10^{-2}	
13	Small					−	−	(+)	−	−	−
32	Large	−	−	+	+	−	−	−	−	−	−
40	Small					+	+	+	−	−	−
60	Large					+	+	+	+	−	−
100	Small					+	+	+	+	+	+
102	Large					+	+	+	+	+	+

NOTE: − indicates no striations visible; + indicates striations visible.
*This lead was zone-refined from a starting material of 99.9999% quoted purity.

An additional experiment was performed with $C_0 = 10^{-3}$ at.% Ag and $\Delta T = 100°$ C using various v. Two crystals were grown at $v = 8$ mm/min yielding visible arrays but much narrower striations than at $v = 2$ mm/min. Two crystals were grown at $v = 20$ mm/min and no striation arrays were evident even though a well-developed cellular substructure (Rutter and Chalmers 1953) was visible.

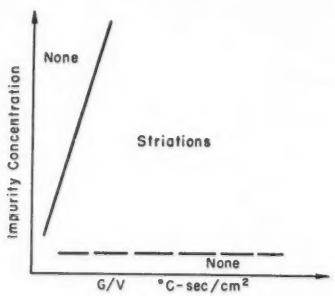

FIG. 2. Schematic illustration of the dependence of striation formation on the solute concentration, C_0, and the ratio of temperature gradient, G, to growth velocity, v.

Since decreasing ΔT decreases the temperature gradient in the solid at the interface and consequently the gradient in the liquid at the interface, G, the results of Table I can be illustrated schematically as in Fig. 2. With very pure material no striations are produced even with low G, whereas, for crystals containing some measurable solute concentration, striation formation is inhibited only under extremes of high v or low G. However, it was noted that under such extremes a well-developed cellular substructure was observed in the crystals.

It was also observed that (i) the incubation distance for striations, i.e. the amount of crystal grown before striation arrays appear, increased as G decreased, (ii) the width of the striations decreased as G/v decreased, and (iii) the misorientation decreased as G/v decreased.

These results suggest that, in high purity lead, insufficient dislocations were grown into the crystals to cause array formation and in lead–silver alloys, if the cellular substructure is well developed, the solute segregation decreases the mobility of dislocations to the point that array formation cannot occur.

ATWATER, H. A. and CHALMERS, B. 1957. Can. J. Phys. **35**, 208.
RUTTER, J. W. and CHALMERS, B. 1953. Can. J. Phys. **31**, 15.
TEGHTSOONIAN, E. and CHALMERS, B. 1951. Can. J. Phys. **29**, 370.
——— 1952. Can. J. Phys. **30**, 388.

RECEIVED APRIL 13, 1960.
R. F. SEKERKA, G. F. BOLLING, AND W. A. TILLER
CRYSTALLOGENIC SECTION,
METALLURGY DEPARTMENT,
WESTINGHOUSE ELECTRIC CORP.,
BEULAH ROAD, CHURCHILL BORO,
PITTSBURGH 35, PA.

NOTES TO CONTRIBUTORS

Canadian Journal of Physics

MANUSCRIPTS

General.—Manuscripts, in English or French, should be typewritten, double spaced, on paper 8½×11 in. **The original and one copy are to be submitted.** Tables and captions for the figures should be placed at the end of the manuscript. Every sheet of the manuscript should be numbered. Style, arrangement, spelling, and abbreviations should conform to the usage of recent numbers of this journal. Greek letters or unusual signs should be written plainly or explained by marginal notes. Characters to be set in boldface type should be indicated by a wavy line below each character. Superscripts and subscripts must be legible and carefully placed. Manuscripts and illustrations should be carefully checked before they are submitted. Authors will be charged for unnecessary deviations from the usual format and for changes made in the proof that are considered excessive or unnecessary.

Abstract.—An abstract of not more than about 200 words, indicating the scope of the work and the principal findings, is required, except in Notes.

References.—References should be listed **alphabetically by authors' names,** unnumbered, and typed after the text. The form of the citations should be that used in current issues of this journal; in references to papers in periodicals, titles should not be given and only initial page numbers are required. The names of periodicals should be abbreviated in the form given in the most recent *List of Periodicals Abstracted by Chemical Abstracts.* All citations should be checked with the original articles and each one referred to in the text by the authors' names and the year.

Tables.—Tables should be numbered in roman numerals and each table referred to in the text. Titles should always be given but should be brief; column headings should be brief and descriptive matter in the tables confined to a minimum. Vertical rules should not be used. Numerous small tables should be avoided.

ILLUSTRATIONS

General.—All figures (including each figure of the plates) should be numbered consecutively from 1 up, in arabic numerals, and each figure referred to in the text. The author's name, title of the paper, and figure number should be written in the lower left corner of the sheets on which the illustrations appear. Captions should not be written on the illustrations.

Line drawings.—Drawings should be carefully made with India ink on white drawing paper, blue tracing linen, or co-ordinate paper ruled in blue only; any co-ordinate lines that are to appear in the reproduction should be ruled in black ink. Paper ruled in green, yellow, or red should not be used. All lines must be of sufficient thickness to reproduce well. Decimal points, periods, and stippled dots must be solid black circles large enough to be reduced if necessary. Letters and numerals should be neatly made, preferably with a stencil (**do NOT use typewriting**) and be of such size that the smallest lettering will be not less than 1 mm high when the figure is reduced to a suitable size. Many drawings are made too large; originals should not be more than 2 or 3 times the size of the desired reproduction. Whenever possible two or more drawings should be grouped to reduce the number of cuts required. In such groups of drawings, or in large drawings, full use of the space available should be made; the ratio of height to width should conform to that of a journal page (4¾×7½ in.), but allowance must be made for the captions. **The original drawings and one set of clear copies (e.g. small photographs) are to be submitted.**

Photographs.—Prints should be made on glossy paper, with strong contrasts. They should be trimmed so that essential features only are shown and mounted carefully, with rubber cement, on white cardboard, with no space between those arranged in groups. In mounting, full use of the space available should be made. **Photographs are to be submitted in duplicate;** if they are to be reproduced in groups one set should be mounted, the duplicate set unmounted.

REPRINTS

A total of 100 reprints of each paper, without covers, are supplied free. Additional reprints, with or without covers, may be purchased at the time of publication.

Charges for reprints are based on the number of printed pages, which may be calculated approximately by multiplying by 0.6 the number of manuscript pages (double-spaced typewritten sheets, 8½×11 in.) and including the space occupied by illustrations. Prices and instructions for ordering reprints are sent out with the galley proof.

Contents

Printed in Canada *by* University of Toronto Press